SAFETY IN MINES RESEARCH ADVISORY COMMITTEE

SIMRAC

Final Project Report

Title: DEVELOP GUIDELINES FOR THE DESIGN OF
PILLAR SYSTEMS FOR SHALLOW AND
INTERMEDIATE DEPTH, TABULAR, HARD ROCK
MINES AND PROVIDE A METHODOLOGY FOR
ASSESSING HANGINGWALL STABILITY AND
SUPPORT REQUIREMENTS FOR THE PANELS
BETWEEN PILLARS

Part 2: Appendices D - E (E1 and E2)

Author/s: A T Haile and A J Jager

Research
Agency: CSIR: Division of Mining Technology

Project No: GAP024/OTH002

Date: December 1995

Appendix D

In situ Pillar Monitoring at Impala Platinum Mines

SUMMARY.

The overall view of the research being conducted at Impala Platinum was to improve pillar design techniques through a rock testing programme, underground instrumentation and back analysis. Figure (68) in Appendix (6) shows the overall view and how it fits together.

The laboratory rock testing programme has provided a useful insight into pillar behaviour showing that even at a width to height ratio around 5, the pillar can have a negative post failure characteristic. Using Flac to reproduce the laboratory stress strain curves for the width to height tests has, so far, not proved to be successful.

Data collected from underground instrumentation suggests that the pillars are punching into the footwall. Closure meter and extensometer results indicate that stope closure is occurring primarily as a result of footwall lifting.

Minsim back analysis of the underground instrumentation results is needed before a meaningful interpretation can be made.

LIST OF CONTENTS.

PAGE.

APPENDIX (1)   General information.

Figure (1)   :   1:2500 scale plan illustrating the project site and the areas of
                         instrumentation that have been enlarged to 1 in 1000 scale.

Figure (2)   :   1:1000 scale plan showing the instrumentation and face
                         positions in the vicinity of the 15 - 107 raise line.

Figure (3)   :   1:1000 scale plan showing the instrumentation and face
                         positions in the vicinity of the 16 - 108 raise line.

Figure (4)   :   1:1000 scale plan showing the instrumentation and face
                         positions in the vicinity of the 16 - 109 and 108 raise lines.

Figure (5)   :   A generalised stratigraphic section from hangingwall 1 to
                         footwall 16.

APPENDIX (2)   Uniaxial and Triaxial tests.

Figure (6)   :   Uniaxial and Triaxial test results for pyroxenite.

Figure (7)   :   Uniaxial and Triaxial test results for footwall 1 (mottled).

Figure (8)   :   Uniaxial and Triaxial test results for pyroxenite and footwall 1
                         (mottled).

Figure (9)   :   Uniaxial and Triaxial test results for footwall 1 (spotted).

1. INTRODUCTION.

This report details work undertaken by Gencor Rock Engineering at Impala Platinum, as a collaborative researcher to Miningtek, for the period January 1994 till November 1995. The contribution from Gencor Rock Engineering was confined to Enabling outputs 4.3 and 4.4 as defined by GAP 024 research proposal.

2. DESCRIPTION OF THE PROJECT SITE AND GEOLOGY.

The project site is located at 12 shaft, Bafokeng North Mine at a depth of between 593 metres and 644 metres below surface. On reef instrumentation was concentrated in the 108 and 109 stopes between 15 and 16 levels. Off reef instrumentation on 15 level was extended upto the 106 raise line as stoping progressed during the time of the project.

This area was chosen for the project because it appeared to be relatively free of geological losses giving a percentage extraction of about 88 percent with only planned pillars being left insitu. This was considered important if the pillars were to be loaded beyond their strength. The mining layout consists of 27 metre long panels with a system of 3 metre wide by 6 metre long pillars running parallel to the strike gullies. Regional support is provided by 20 metre wide barrier pillars orientated on dip. Permission was granted to mine out the barrier next to the 107 raise line in order to create a larger span in the project stope.

Figure (1) in Appendix (1) is a 1 in 2500 scale plan showing the project site and illustrating the three areas of instrumentation that have been enlarged to a 1 in 1000 scale, see figures (2) to (4) in Appendix (1).

In the project area the Merensky reef lies on footwall 1 and is referred to as "A" reef.

Figure (5) in Appendix (1) is a generalised geological section for 12 shaft showing the rock types on either side of the Merensky reef.

3. PROGRESS.

3.1 Miningtek enabling output 4.3 - To validate the strain softening option for the Flac computer code as a suitable numerical model for pillar stress - strain behaviour.

To achieve this a rock testing programme was undertaken consisting of three set of tests to be conducted on the two rock types that constitute the Merensky

reef pillars, namely Anorthositic norite and pyroxenite. The objectives of these tests were the following :

- to obtain the strain softening parameters required by Flac.

- to obtain stress - strain curves for laboratory specimens with a range of width to height ratios.

- to obtain stress - strain curves for punch tests using a range of width to height ratios for the punch. This would also gain an insight into the likely behaviour of pillars underground having different width to height ratios.

- use Flac to duplicate the abovementioned laboratory stress - strain curves for the width to height ratio tests and the punch tests using the strain softening parameters derived from the uniaxial and triaxial tests. If this could be achieved it would result in a predictive tool capable of producing stress strain curves for different width to height pillars.

3.1.1   Uniaxial and Triaxial tests.

Each of the two rock types was tested individually as well as a combination of both rock types in the same proportion as they occur in the pillars underground, namely the top 20 % being pyroxenite and the remaining 80 % being anorthositic norite.

Photograph (1) in Appendix (7) shows an example of a triaxial test specimen. By studying photograph (9) in Appendix (7), the two different rock types present in the pillar can clearly be distinguished. The darker rock is the hangingwall pyroxenite and the lighter rock is the anorthositic norite. It also appears as if the 20% - 80% split is incorrect. This is caused when the siding on the downdip side of the gully is cut in horizontally rather than on the dip of the reef.

3.1.2 Width to height tests.

The relationship between width to height ratio and pillar strength increase was investigated by testing the combined rock types in the following manner.

80 millimetre diameter core was used for these tests with the height of the sample being cut such that width to height ratios of 1:1, 3:1 and 5:1 were created. As with the tests described in the previous section, the height dimension of each core was divided to create a 20 % - 80 % split of pyroxenite and anorthositic norite.

Photograph (2) in Appendix (7) illustrates the appearance of three prepared specimens.

3.1.3 Punch tests.

These tests consisted of two sections. Firstly a "punch" manufactured from 25 millimetre core of anorthositic norite and made up to width to height ratios of 1:1, 3:1 and 5:1. Secondly a "foundation" manufactured from 80 millimetre diameter core of anorthositic norite, cut to a height of 80 millimetres and confined in a steel jacket.

The "punch" represents the pillar and the "foundation" the footwall beneath the pillar. The "punch" was placed centrally ontop of the "foundation", placed into the press and loaded.

Photographs (3) and (4) in Appendix (7) show examples of tested specimens.

3.1.4 Flac modelling.

One of the constituitive models offered in Flac is the strain softening option. This allows the user to model non linear behaviour and is considered ideal for the study of brittle failure. It was decided that this option presented the most realistic approach to reproducing the laboratory test data, and as such would shed light on the behaviour of yield pillars.

An axisymmetric geometry was chosen in order to represent the three dimensional condition depicted by a piece of core being compressed in

a testing machine. The dimensions of the model were identical to those of the core with a one quarter symmetry condition being applied. Loading of the model was achieved by applying a downward velocity to the nodes along the top boundary. The rate of this loading was calculated to achieve a strain rate of one millimetre per metre per one thousand steps which was considered low enough not to cause any abnormal effects.

A fish function was included in each data set that calculated the average stress and strain across the model. This allowed a stress - strain plot to be made and compared directly with the laboratory plot.

3.1.5 Results from the rock testing programme.

3.1.5.1 Uniaxial and Triaxial tests.

Figures (6) to (14) in Appendix (2) contains the results obtained from the uniaxial and triaxial tests, for the individual as well as the combined rock types, in terms of their peak strength, confining stress, Young's modulus and Poisson's ratio. Averages and standard deviations are also given.

Equations are presented that link the peak strength to the uniaxial strength, the confining stress and the rate of strength increase.

A comparison of the combined rock types shows that the pyroxenite/footwall 1 (mottled) is the weakest, followed by pyroxenite/footwall 3 with pyroxenite/footwall 1 (spotted) being the strongest.

The internal angle of friction varied from 42 to 47 degrees.

3.1.5.2 Width to height tests.

Figures (15) to (17) in Appendix (3) contains the results of three width to height tests that were conducted by Miningtek. The post failure part of the curve could not be plotted accurately enough and it was therefore decided to carry out the

remainder of these tests in the stiff testing machine at the University of the Witwatersrand.

The equation developed by Obert and Duvall linking strength to width to height ratio predicts strengths of 231 MPa and 302 MPa for width to height ratios of 3 to 1 and 5 to 1 respectively. It can be seen that the test results gave 210 MPa and 250 MPa. Although these are lower than the predicted values they are based on three tests only and any conclusions must wait until the remaining tests have been completed.

3.1.5.3 Punch tests.

Figures (18) to (23) in Appendix (4) contains the results from six of ten punch tests that were conducted by Miningtek. The following table is a summary of the peak and residual strengths of the various width to height ratios for footwalls 1 and 3.

Width to height	Peak strength (MPa)	Residual strength (MPa)	Residual to Peak %
FOOTWALL 1			
5.1 : 1	471.5	217.5	46.1
3.3 : 1	392.0	29.1	7.4
1 : 1	248.5	6.9	2.8
FOOTWALL 3			
5.1 : 1	465.5	140.9	30.3
3.4 : 1	308.0	9.9	3.2
1 : 1	248.5	3.1	1.3

Table 1: Average values for the punch tests.

The residual strengths for both footwall rock types show a dramatic drop off as the width to height ratio decreases from 5.1 : 1 to 3.3 : 1, then flattens off as it reaches 1 : 1.

Figure (24) in Appendix (4) is a plot of width to height ratio versus the ratio between the compressive strengths of a

specimen with $\frac{w}{h} \neq 1$ and $\frac{w}{h} = 1$. This illustrates a good agreement between the laboratory results and Obert and Duvall's equation.

Figure (25) in Appendix (4) illustrates the effect of width to height ratio on post failure behaviour. The curved line suggests that at a width to height ratio of 5:1, the post failure curve is flat. In other words there is no load shedding. The results of the punch tests on the footwalls 1 and 3 rock types indicate two points :

- Load shedding does occur in these rock types at a width to height ratio of 5:1.

- Load shedding at a width to height ratio of 3:1 is slightly more than that shown by the curved line.

3.1.6 Results from the flac modelling.

The Flac modelling exercise was an attempt to duplicate the three width to height tests described in section 3.1.5.2 using strain softening parameters derived from the tests described in section 3.1.5.1. It was realised that only having one test per width to height ratio represented insufficient data, however the idea was to establish a methodology for duplicating laboratory tests using Flac's non linear modelling capabilities.

Appendix (5) contain the results of the Flac modelling.

The objective was to create one table of strain softening parameters that would be applied to each width to height model. The idea being that the different geometries of the width to height models would be responsible for the changing stress strain curves and not the strain softening parameters of the host rock.

On completion of the initial Flac runs it became apparent that the strain softening parameters would have to be derated in order to come close to duplicating the laboratory results. Figures (26) to (28) show the Flac generated stress - strain curves for width to height ratios of 5:1,

3:1 and 1:1 using the derated strain softening values give in figure (29). In figure (29) it must be noted that the value of friction was dropped from 39 degrees for the width to height ratio of 1:1 to 26 degrees for the width to height ratios of 3:1 and 5:1. This was necessary in order to reproduce the different peak strengths of the laboratory tests. The post peak part of the curve has proved very difficult to manipulate.

A number of comparative runs were undertaken to understand the following relationships :

- An axisymmetrical configuration versus a two dimensional geometry.

- An axisymmetrical configuration versus a three dimensional geometry.

- The effect of the number of zones on the results.

Findings from these comparative runs are as follows.

3.1.6.1 Axisymmetrical configuration.

A comparison of the axisymmetrical stress - strain curves, see figures (30) to (32), show that as the number of zones increase, so the peak strength decreases.

There is not a great deal of difference in the residual strengths, however the 24 by 8 grid has a slightly higher value than the other grids.

In all these grids there is at least one zone that develops a tensile value for horizontal stress.

The number of zones with a tensile value increases as the number of zones increases.

3.1.6.2 Two dimensional rib configuration.

These stress - strain curves, see figures (33) to (35) show an identical trend to those of the axisymmetrical geometry in that the peak strength decreases as the number of zones increases.

The actual values of the peak strength and residual strength are all higher than those for the axisymmetrical geometries.

In all these grids there is at least one zone that develops a tensile value for horizontal stress.

The number of zones with a tensile value increases as the number of zones increase.

In addition the 12 by 4 and 24 by 8 grids also develop tensile vertical stresses in some of their zones. This is not a desirable state of affairs. In the model there are large values of plastic strain in the top third of the model at the edge, the remaining two thirds has virtually no damage. From this it would appear that the zones at the top of the model, at the edge, fails thus protecting the remaining zones. As a result the failed zones are squeezed laterally dragging the unfailed zones with them. This action may induce tensile horizontal stresses which may in turn induce some tensile vertical stresses.

3.1.6.3 Three dimensional geometry.

A three dimensional geometry was run as a direct comparison to the 6 by 2 grid two dimensional axisymmetrical grid.

The results, see figure (36), show good agreement between the two geometries.

3.2 Miningtek enabling output 4.4 - Determine the extent of fracture propagation into pillars.

To achieve this it was initially planned to drill holes over, through and under selected pillars in order to conduct petroscope observations of the pillars and their foundations. The instrumentation for this section was expanded to enable other data to be collected that was considered necessary in determining insitu pillar behaviour.

The following sections are a description of each instrumented site.

ON - REEF INSTRUMENTATION.

3.2.1 Pillar A.

This pillar is located in gully 2 south of the 16 - 109 stope. The pillar contains three BX boreholes. One drilled into the pyroxenite above the pillar and two drilled into the anorthositic norite, one at the mid height of the pillar and the other into the footwall foundation under the pillar. The purpose of these holes is to enable petroscope observations to be made at different locations in the pillar cross-section.

A horizontal EX borehole was drilled into the pyroxenite above the pillar. Two vibrating wire hard rock stress meters were installed into the hole. The first at 1.5 metres and the second at 0.5 metres as measured from the collar of the hole. Both stress meters have been orientated to measure the vertical stress increase.

A total of seven closure meters were installed, four on the updip side and three on the down dip side of the pillar.

3.2.2 Pillar B.

This pillar is located in gully 2 south of the 16 - 109 stope. The pillar contains three BX boreholes. One drilled into the pyroxenite above the pillar and two drilled into the anorthositic norite, one at the mid height of the pillar and the other into the footwall foundation under the pillar. The purpose of these holes is to enable petroscope observations to be made at different locations in the pillar cross-section.

A horizontal EX borehole was drilled into the pyroxenite above the pillar. Three vibrating wire hard rock stress meters were installed into the hole. The first at 1.5 metres and the second at 0.5 metres as measured from the collar of the hole. Both stress meters have been orientated to measure the vertical stress increase. The third at 1.3 metres is orientated to measure horizontal stress increase.

A total of seven closure meters were installed, four on the updip side and three on the down dip side of the pillar.

A vertical, sixteen metre long hangingwall extensometer hole equipped with four anchor was installed in the gully adjacent to the pillar.

3.2.3 **Pillar C.**

This pillar is located in gully 12 south of the 16 - 109 stope. The pillar contains three BX boreholes. One drilled into the pyroxenite above the pillar and two drilled into the anorthositic norite, one at the mid height of the pillar and the other into the footwall foundation under the pillar. The purpose of these holes is to enable petroscope observations to be made at different locations in the pillar cross-section.

A total of eight closure meters were installed, five on the updip side and three on the down dip side of the pillar.

3.2.4 **Pillar D.**

This pillar is located in gully 20 south of the 15 - 108 stope. The pillar contains three BX boreholes. One drilled into the pyroxenite above the pillar and two drilled into the anorthositic norite, one at the mid height of the pillar and the other into the footwall foundation under the pillar. The purpose of these holes is to enable petroscope observations to be made at different locations in the pillar cross-section.

A horizontal EX borehole was drilled into the pyroxenite above the pillar. One vibrating wire hard rock stress meters was installed into the hole at a distance of 1.5 metres from the collar of the hole. The stress meter was orientated to measure the vertical stress increase.

A total of eight closure meters were installed, four on the updip side and three on the down dip side of the pillar.

3.2.5 **Pillar E.**

This pillar is located in gully 14 south of the 16 - 108 stope.

A horizontal EX borehole was drilled into the pyroxenite above the pillar. Two vibrating wire hard rock stress meters were installed into the hole. One stress meters was orientated to measure the vertical stress increase, the other to measure horizontal stress increase .

A total of three closure meters were installed on the down dip side of the pillar.

A vertical, sixteen metre long hangingwall extensometer hole equipped with four anchor was installed in the centre gully adjacent to the pillar.

The purpose of this instrumentation was as follows :

- To relate vertical stress increase to the progression of fracturing into the pillar.

- To relate vertical stress increase to the closure immediately next to the pillar and produce a rough stress strain curve.

- To measure closure in the panels on either side of the instrumented pillar.

- To monitor any inelastic movement that may occur in the hangingwall, with specific reference to the bastard Merensky parting which is a sheared contact.

OFF - REEF INSTRUMENTATION.

3.2.6   Vibrating wire stress meters.

In April and May 1994 two insitu stress measurement were completed, one in the 15 - 107 laybye and the other in the 16 south drive close to the 109 raise line. The vertical stress from this measurement has enabled the absolute vertical stress to be calculated for the vibrating wire stress meters on 15 and 16 level.. This was achieved by adding the measured vertical stress to the stress changes measured by the vibrating wire stress meters.

It must be emphasised that the readings from the vibrating wire stress meters are to be confirmed through a series of laboratory calibration tests. Therefore the results and graphs can only be considered as preliminary.

Vibrating wire stress meters were installed at the following locations :

- 15 south drive between the 108 and 107 raise lines.

- 15 - 107 laybye.

- 15 south drive between the 107 and 106 raise lines.

- 15 - 106 laybye.
- 16 south drive.

3.2.7 Extensometer.

A vertical, twenty three metre long extensometer hole equipped with four anchors was drilled from the 16 south drive at a position mid way between the 109 and 108 raise lines. The hole stops approximately one metre below the reef at a point half way between the pillars of panel 18 south in the 16 - 109 stope.

3.2.8 Results of the underground instrumentation.

Appendix (6) contains the results from the underground instrumentation.

ON REEF INSTRUMENTATION.

3.2.8.1 Pillar A.

Figure (37) shows the absolute vertical stress change that has occurred 1.5 metres into the pillar since March 1994.

Figure (38) shows the period of oscillation reading for the vibrating wire stress meter which is located 0.5 metres into the pillar.

When the reading drops below 2000 it is not possible to use the conversion tables to calculate the stress.

It is anticipated that the planned calibration tests will rectify this situation.

Figure (39) is a quarterly plot of the closure profile in the panels on either side of pillar A.

Figure (40) is a plot of the progressive closure of the individual meters adjacent to pillar A.

Photographs (5) and (6) in Appendix (7) are snap shots of pillar A taken 18 months apart. Of interest to note is the jointing that runs through this pillar. The closure meter (A4) immediately next to the pillar has registered 58 millimetres of closure during

this period which is reflected by the one broken stick in photograph (6).

Photographs (7) and (8) in Appendix (7) shoe the increase in closure (109 millimetres) that has occurred on the updip side of the gully over a 12 month period. The stable unchanging nature of the hangingwall should be noted.

3.2.8.2 Pillar B.

An insitu stress measurement was completed next to this pillar in June 1994, when it was a solid abutment. The results of this measurement are shown in Figure (41). As can be seen an interpolation was necessary to determine the vertical stress at 1.5 metres into the pillar. Figure (42) is a plot of the absolute vertical stress change that has occurred 1.5 metres into the pillar since March 1994.

Figure (43) shows the vertical stress change at a point 0.5 metres in from the pillar edge. No absolute vertical stress change has been presented as it was felt that the interpolation could not be continued so close to the edge of the pillar.

Figure (44) is a plot of the absolute horizontal stress at a point 1.3 metres in from the pillar edge.

A common feature to figures (42, 43, 44) is the build up in stress from September to October and the sharp reversal of this trend during the following month.

The only explanation for this observation is that a seismic event was recorded in the area on 9th November 1994 measuring 0.5 in magnitude.

Damage occurred to pillar B in that about 30 centimetres of the pillar skin was ejected. No damage was observed in the other pillars in the area and it was concluded that pillar B was somehow involved in the seismic event.

Figure (45) is a quarterly plot of the closure profile in the panels on either side of pillar B.

Figure (46) is a plot of the progressive closure of the individual meters adjacent to pillar B.

Figure (48) shows the absolute vertical stress change recorded at a vibrating wire stress meter located 29 metres in the footwall.

Photographs (9) and (10) in Appendix (7) are snap shots of pillar B taken 18 months apart. In contrast to pillar A, pillar B contains virtually no jointing at all. The closure meter (B4) immediately next to the pillar has registered 53 millimetres of closure during this period.

On the 9 November 1994 a magnitude 1.5 seismic event was registered in the 16 - 109 stope. The only damage that could be found was to pillar B and the pillars on either side.

Photographs (11) and (12) in Appendix (7) illustrate the degree of damage. The difference between the slabbing on the downdip side and the more fragmented nature of the updip side is interesting to note. The most likely explanation for this difference is that the updip side of the pillar is more confined as the siding was cut in horizontally. Hence the height of the updip side of the pillar is less than that on the downdip side.

3.2.8.3 Pillar C.

Figure (47) is a quarterly plot of the closure profile in the panels on either side of pillar C.

Figure (48) is a plot of the progressive closure of the individual meters adjacent to pillar C.

Photographs (13) and (14) in Appendix (7) shows the increase in closure (77 millimetres) that has occurred on the updip side of the gully adjacent to pillar C.

3.2.8.4 Pillar D.

Figure (49) is a quarterly plot of the closure profile in the panels on either side of pillar D.

Figure (50) is a plot of the progressive closure of the individual meters adjacent to pillar D.

3.2.8.5 Pillar E.

Figure (51) is a quarterly plot of the closure profile in the panels on either side of pillar E.

Figure (52) is a plot of the progressive closure of the individual meters adjacent to pillar E.

Photographs (17) and (18) in Appendix (7) show the amount of scaling that has occurred on pillar E during a 12 month period.

Photographs (19) and (20) in Appendix (7) illustrate the amount of closure (52 millimetres) that has taken place over the same time period.

3.2.8.6 Extensometer next to pillar B.

Figure (53) is a plot of the progressive movement occurring between anchors.

3.2.8.7 Extensometer in the 16 - 108 centre gully next to pillar E.

Figure (54) is a plot of the progressive movement occurring between anchors.

Figure (55) is a plot of the progressive stope closure occurring next to the extensometer.

3.2.8.8 Petroscope observations in pillar A, B and D.

Figures (62) and (63) show the increase in fracturing across pillar A during a four month period. The increase in fracturing, especially towards the end of the holes, can be attributed to the mining of the panel on the downdip side of pillar A past the petroscope position

Figures (64) and (65) show the changes that occurred in pillar B during a six month period. At the end of this period the panel mining on the downdip side of the pillar was almost in line with the petroscope location - see Figure (4) in Appendix (1). What is of particular interest is the occurrence of "dog earing" in the middle and lower holes with only a slight increase in the fracture density. The fracturing and "dog earing" in the top hole remains virtually unchanged.

Figures (66) and (67) show the changes that occurred in pillar D that occurred during a one month period.

The petroscope boreholes were drilled at a diameter of about 60 millimetres which is only slightly larger than the diameter of the petroscope itself. This situation works well until the downdip panel mines past the petroscope location, then excessive crushing takes place in the pillar and it is no longer possible to fit the petroscope into the hole.

Because useful information was coming from the petroscope holes it was decided to enlarge the holes to 102 millimetres so that observations could be continued with.

Unfortunately, up until the present day the drilling contractors have been unable, or unwilling, to under take this.

OFF - REEF INSTRUMENTATION.

3.2.8.9 Vibrating wire stress meter in 15 south drive between the 108 and 107 raise lines.

Figure (56) shows the absolute vertical stress change that has occurred monthly since May 1994. The build up in stress to the September 1994 peak is attributed to the advancing faces, see Figure (2) in Appendix (1). Overstoping of the vibrating wire

stress meter resulted in a stress drop which has stabilised over the past three months since March 1995.

3.2.8.10 Vibrating wire stress meter in 15 - 107 laybye.

Figure (57) shows the build up in the absolute vertical stress that peaks at day 283 (February 1995) prior to the site being overstoped.

3.2.8.11 Vibrating wire stress meter in 15 south drive refuge bay.

Figure (58) shows the steady decline in the absolute vertical stress since its installation at day 0 (February 1995) up until day 102 (June 1995) when it flattened out.

3.2.8.12 Vibrating wire stress meter in 15 - 106 laybye.

Figure (59) shows the steady decline in the absolute vertical stress since its installation at day 0 (February 1995) up until day 53 (April 1995) when it flattened out.

3.2.8.13 Vibrating wire stress meter in 16 south drive between the 109 and 108 raise lines.

Figure (60) shows the steady decline in the absolute vertical stress from day 67 (July 1994) until day 218 (December 1994). During this period two panels were being mined in the immediate vicinity, see figure (4) in Appendix (1).

3.2.8.14 Extensometer in 16 south drive between the 109 and 108 raise lines.

Figure (61) shows the movement between anchors. It is very noticeable that there is an opening up between anchor 1 and 2. This corresponds to a prominent geological feature known as the footwall 4 unit which is a cohesionless mud parting in this particular area of the mine.

In March 1995 (day 282) no reading could be taken for

anchor 1 as the wire had corroded through and broke.

4.   CONCLUSIONS.

4.1   Rock testing programme.

4.1.1   Figure (24) in appendix (4) shows that the rock types tested do conform to an accepted strength relationship.

4.1.2   Figure (25) in appendix (4) shows that the rock types tested exhibit load shedding even when the width to height is slightly in excess of 5:1. This demonstrates that pillars having width to height ratios around 5:1 have a seismic potential.

4.1.3   The internal angle of friction of the rock types tested is around 45 degrees.

4.1.4   The strength of the hangingwall pyroxenite exceeds that of the footwall anorthositic norite. This confirms underground observations where fracturing of the footwall occurs but not the hangingwall.

4.2   Flac analysis.

4.2.1   The fact that the rib geometries attain higher peak and residual values makes sense in terms of their 2 - dimensional nature as opposed to the simulated 3 - dimensional nature of the axisymmetrical geometries.

4.2.2   It appears acceptable to use the axisymmetrical option to approximate the 3 - dimensional geometry of a core sample.

4.2.3   Of concern is the large discrepancy between the laboratory determined strain softening parameters for Flac and those used in Flac to duplicate the laboratory width to height tests.

4.2.4   Although some success has been achieved in trying to duplicate laboratory results there appear to be major obstacles to overcome before it can be applied reliably.

4.3 Underground instrumentation.

4.3.1 It must be emphasised that all the vibrating wire stress meter results are subject to adjustment pending the outcome of the laboratory calibration tests.

4.3.3 The pillars appear to be failing by punching into the footwall.

4.3.2 A majority of the stope closure is occurring as footwall lifting. Visual observations have indicated an upward bulging of the footwall as well as opening up of joints in the footwall of the stope. This is confirmed by the results from the wire extensometers that clearly indicate negligible inelastic movement in the hangingwall and definite upward movement of the footwall. An explanation for this is that loading of the pillars induces higher horizontal stress in the footwall between the pillars. This stress causes the footwall to move upwards into the stope. The footwall 4 contact, being a cohesionless mud parting, is able to open up and thereby amplify the amount of upward movement into the stope. Photographs (15) and (16) in Appendix (7) illustrate the observed phenomena of footwall lifting due to the opening of joints and upward bulging of the footwall.

5. RECOMMENDATIONS FOR FURTHER WORK.

5.1 The remaining laboratory test work on the width to height samples needs to be completed at the University of the Witwatersrand.

5.2 The punch test samples need to be cut in half to allow an examination of the fracturing in the footwall foundation of the punch.

5.3 Laboratory work must be continued in order to calibrate the vibrating wire stress meters thus permitting the interpretation of underground readings.

5.4 Minsim back analyses need to be conducted to interpret the result of all the underground instrumentation programme.

D.Spencer.

APPENDIX (1)

General information.

LEGEND
x ---- VIBRATING WIRE STRESS METERS
△ ---- CLOSURE METERS

INSTRUMENTATION IN THE
VICINITY OF THE 107 RAISE LINE

SCALE 1 : 1 000

Figure (2).

LEGEND

x ------- VIBRATING WIRE STRESS METRES
△ ------- CLOSURE METRES
⊙ ------- WIRE EXTENSOMETRE

INSTRUMENTATION IN THE
VICINITY OF THE 108 RAISE LINE
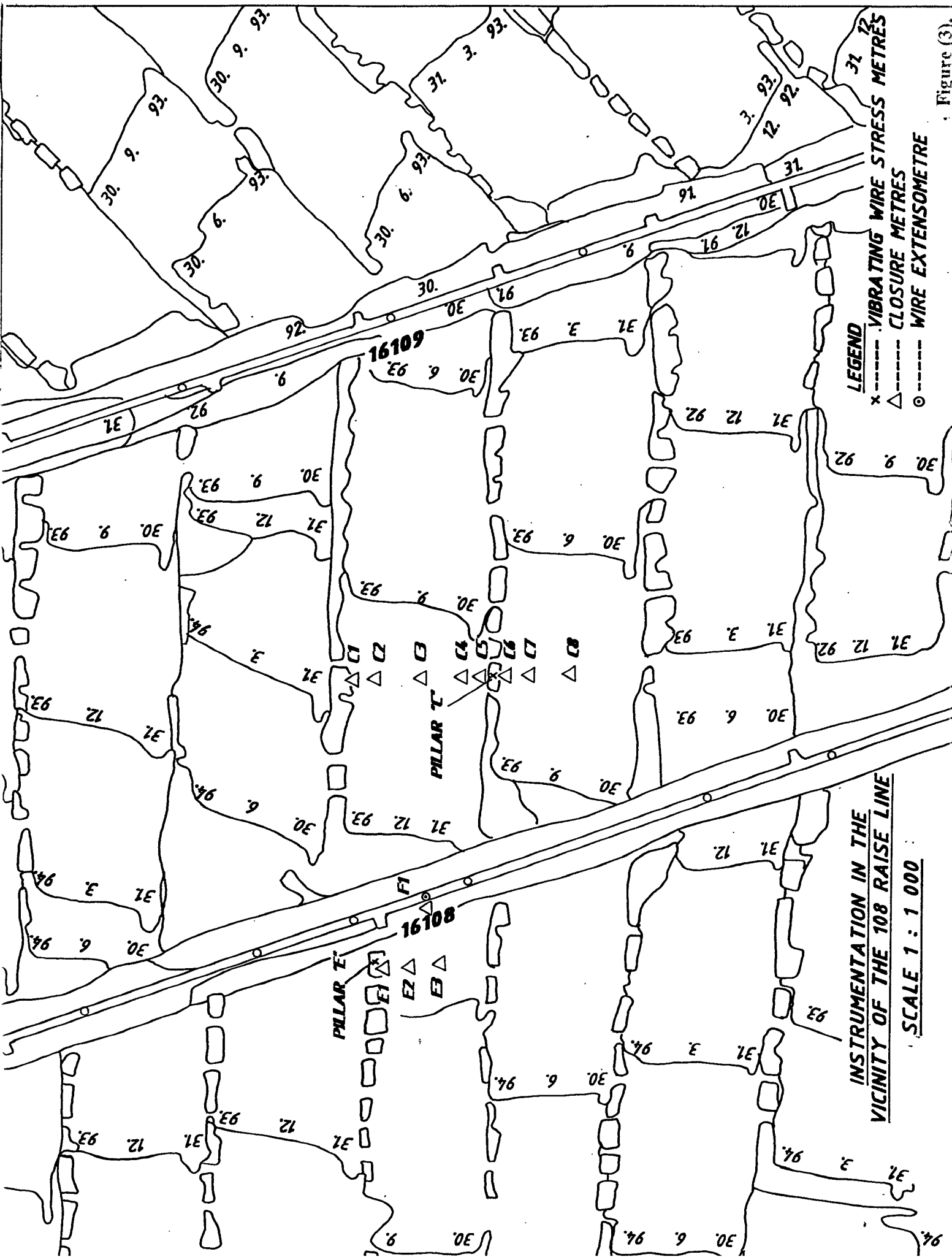
SCALE 1 : 1 000

Figure (3).
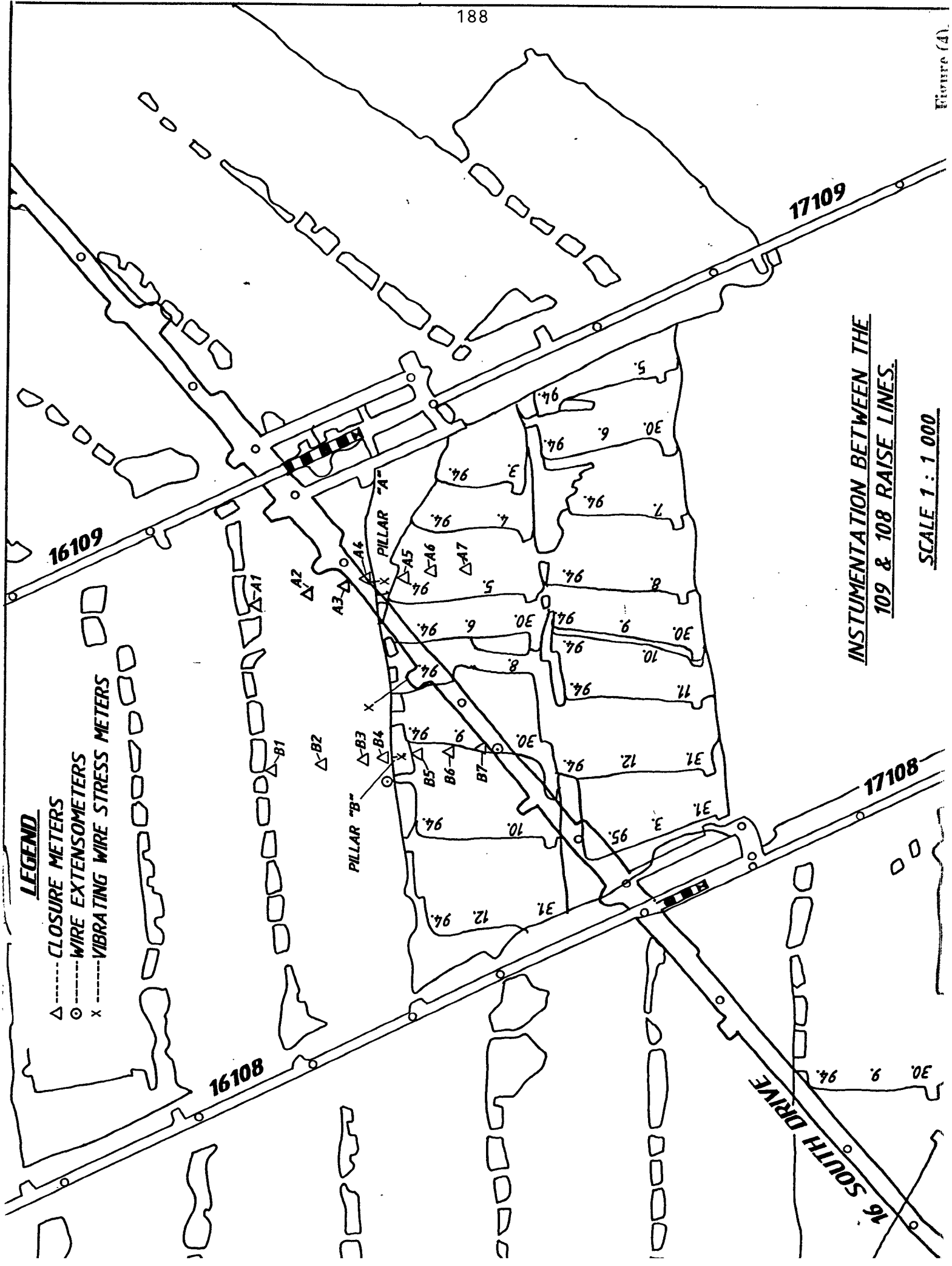
LEGEND

△ ----- CLOSURE METERS
⊙ ----- WIRE EXTENSOMETERS
✕ ----- VIBRATING WIRE STRESS METERS

INSTUMENTATION BETWEEN THE
109 & 108 RAISE LINES.

SCALE 1 : 1 000

Figure (4)

Depth (m)	Unit	Rock Type
0	HANGINGWALL 1 (5-9m)	NORITE
	BASTARD PYROXENITE (2-3m)	PYROXENITE
10	MIDDLING 3 (3m)	MOTTLED ANORTHOSITE
	MIDDLING 2 (6m)	SPOTTED ANORTHOSITE
	MIDDLING 1 (0.2-0.8m)	NORITE
20	MERENSKY PYROXENITE (1.5m)	PYROXENITE
	MERENSKY PEGMATOID (0,1-0,5m)	PEGMATOID
	FOOTWALL 1 (3-5m)	NORITE
	FOOTWALL 2 (0,02-0,25m)	CYCLIC UNIT
30	FOOTWALL 3-5 (3,5-7m) / FOOTWALL 4 (0,02-0,5m)	NORITE
	FOOTWALL 6 (0,1-4m)	MOTTLED ANORTHOSITE
40		
50	FOOTWALL 7 (30-60m)	NORITE
60		
70		
	FOOTWALL 8 (1-3m)	SPOTTED ANORTHOSITE
	FOOTWALL 9 (1,5-3m)	MOTTLED ANORTHOSITE
80	FOOTWALL 10 (0,1-0,3m)	HARZBURGITE
	FOOTWALL 11 (3-7m)	SPOTTED ANORTHOSITE
90	FOOTWALL 12 (8-12m)	MOTTLED ANORTHOSITE
100	UG2 PYROXENITE (4-10m)	
	LEADER CHROMITITE LAYERS	
	UG2 CHROMITITE (0,5-1,8m)	
	UG2 PEGMATOID (0-1,5m)	
110	FOOTWALL 13 (8-10m) SPOTTED ANORTHOSITE	
	UG1 PYROXENITE (6-9m)	
120	UG1 CHROMITITE (0,5-3,5m)	
	CHROMITITE STRINGERS	
	FOOTWALL 16 MOTTLED ANORTHOSITE TO NORITE	

— FIG. 2

GEOLOGY DEPARTMENT
IMPALA OPERATIONS AND PROJECTS

IMPALA PLATINUM LIMITED

BAFOKENG NORTH MINE

GENERALISED STRATIGRAPHIC
SECTION FROM
HANGINGWALL 1 TO FOOTWALL 16

SCALE 1 : 500

APPENDIX (2)

Uniaxial and Triaxial tests.

UNIAXIAL AND TRIAXIAL TEST RESULTS FOR :

PYROXENITE.

Confining Stress (MPa).	Peak Strength		Young's Modulus (GPa).	Poissons Ratio
	Individual specimens	Average		
0	184.40		116.80	
0	196.60	190.50	118.70	
10	241.50		130.30	0.14
10	299.80	270.65	120.40	0.14
20	332.60		127.30	0.15
20	333.40	333.00	119.10	0.19
40	387.60		125.00	0.15
40	399.20	393.40	120.40	0.16
		Average values	122.25	0.16
		Standard Deviation	4.18	0.02

PYROXENITE.
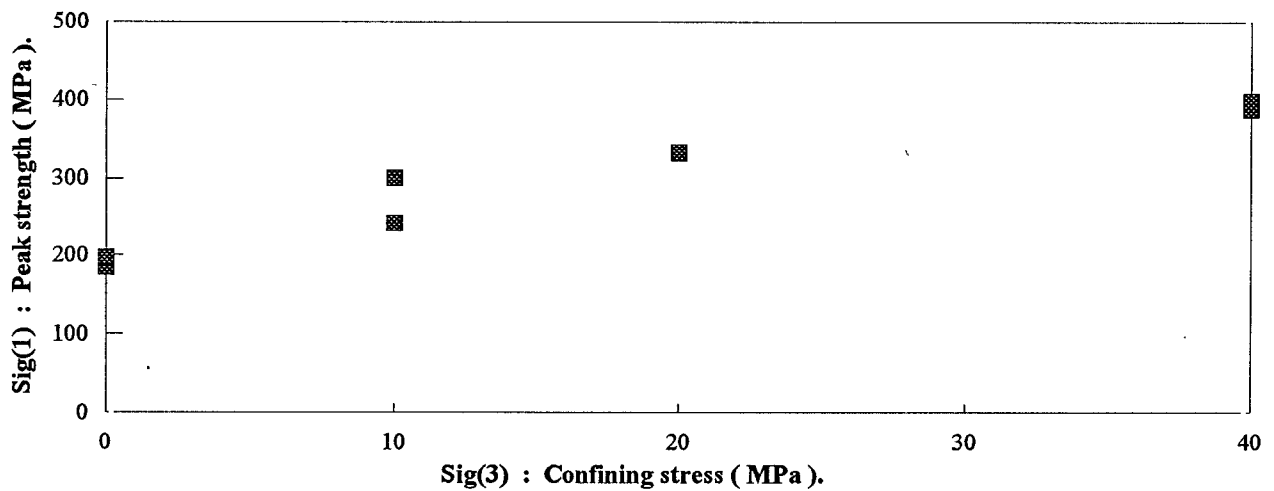
Sig(1) = 211 + 4.94{Sig(3)}.
Angle of internal friction = 42

UNIAXIAL AND TRIAXIAL TEST RESULTS FOR :

FOOTWALL 1. (Mottled).

Confining Stress (MPa).	Peak Strength		Young's Modulus (GPa).	Poissons Ratio
	Individual specimens	Average		
0	144.10		71.80	
10	236.00		75.40	0.28
20	288.50		80.70	0.25
40	383.80		88.20	0.21
		Average values	79.03	0.25
		Standard Deviation	6.17	0.03
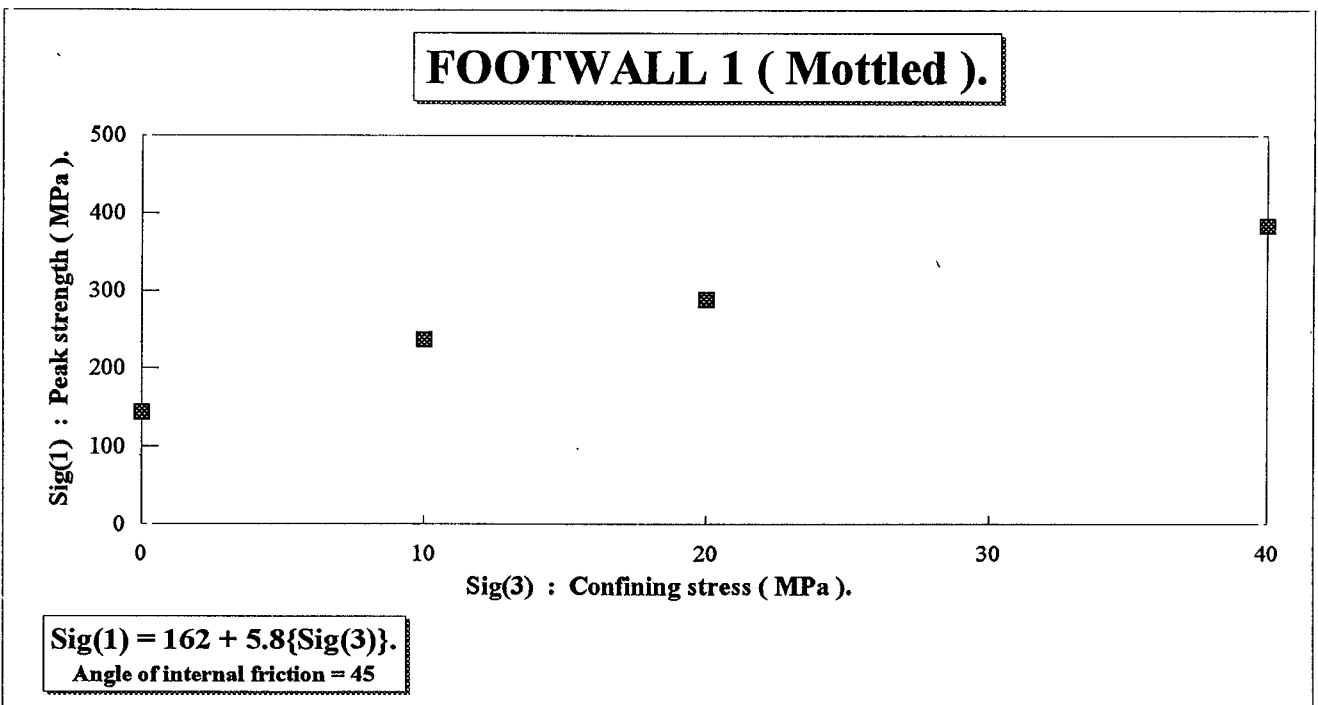
FOOTWALL 1 (Mottled).

Sig(1) : Peak strength (MPa). vs Sig(3) : Confining stress (MPa).

Sig(1) = 162 + 5.8{Sig(3)}.
Angle of internal friction = 45

UNIAXIAL AND TRIAXIAL TEST RESULTS FOR :

PYROXENITE and FOOTWALL 1 (mottled).

Confining Stress (MPa).	Peak Strength		Young's Modulus (GPa).	Poissons Ratio
	Individual specimens	Average		
0	113.20		67.30	
0	129.40	121.30	77.90	
10	181.30		73.40	0.21
20	263.90		88.10	0.22
40	353.00		85.60	0.20
		Average values	78.46	0.21
		Standard Deviation	7.67	0.01

PYROXENITE and FOOTWALL 1 (Mottled).

Sig(1) = 125 + 5.94{Sig(3)}.

Angle of internal friction = 45

UNIAXIAL AND TRIAXIAL TEST RESULTS FOR :

FOOTWALL 1 (Spotted)

Confining Stress (MPa).	Peak Strength		Young's Modulus (GPa).	Poissons Ratio
	Individual specimens	Average		
0	167.30		94.00	
0	170.90	169.10	96.60	
10	242.80		92.10	0.22
20	314.60		95.30	0.23
40	410.10		97.00	0.21
		Average values	95.00	0.22
		Standard Deviation	1.79	0.01

FOOTWALL 1 (spotted).

$$Sig(1) = 176 + 6.11\{Sig(3)\}.$$
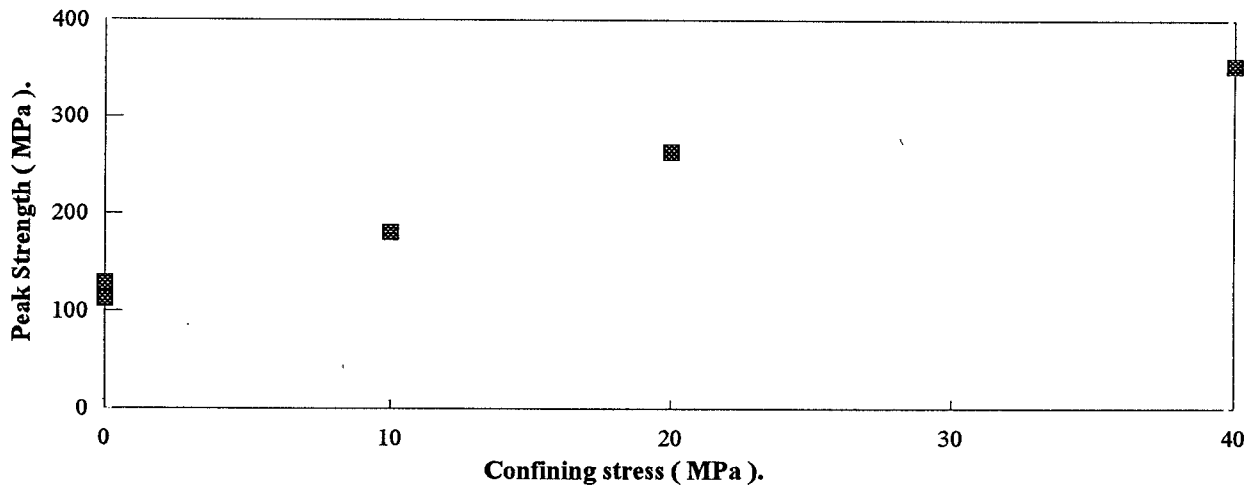
Angle of internal friction = 46

UNIAXIAL AND TRIAXIAL TEST RESULTS FOR :

PYROXENITE and FOOTWALL 1 (spotted).

Confining Stress (MPa).	Peak Strength		Young's Modulus (GPa).	Poissons Ratio
	Individual specimens	Average		
0	191.30		92.30	
0	197.60	194.45	89.40	
10	274.90		92.60	0.25
20	331.60		89.10	0.24
40	455.00		95.60	0.22
		Average values	91.80	0.24
		Standard Deviation	2.38	0.01

PYROXENITE and FOOTWALL 1 (spotted).

$Sig(1) = 199 + 6.5\{Sig(3)\}$.

Angle of internal friction = 47

UNIAXIAL AND TRIAXIAL TEST RESULTS FOR :

FOOTWALL 3

Confining Stress (MPa).	Peak Strength		Young's Modulus (GPa).	Poissons Ratio
	Individual specimens	Average		
0	173.10		102.00	
0	181.80		103.5	
0	183.50	179.47	105.50	
10	245.80		99.00	0.18
10	265.10	255.45	97.50	0.20
20	291.20		103.70	0.17
20	325.60	308.40	98.70	0.20
40	428.80		105.40	0.18
40	438.20	433.50	105.40	0.18
		Average values	102.30	0.19
		Standard Deviation	2.83	0.01

FOOTWALL 3.

Sig(1) = 184 + 6.29{Sig(3)}.
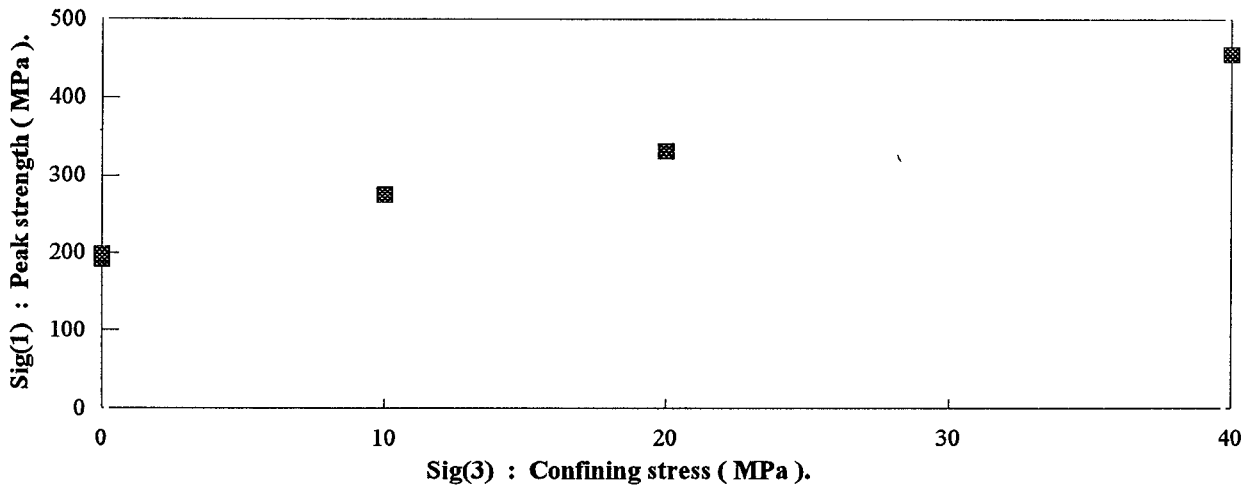Angle of internal friction = 47
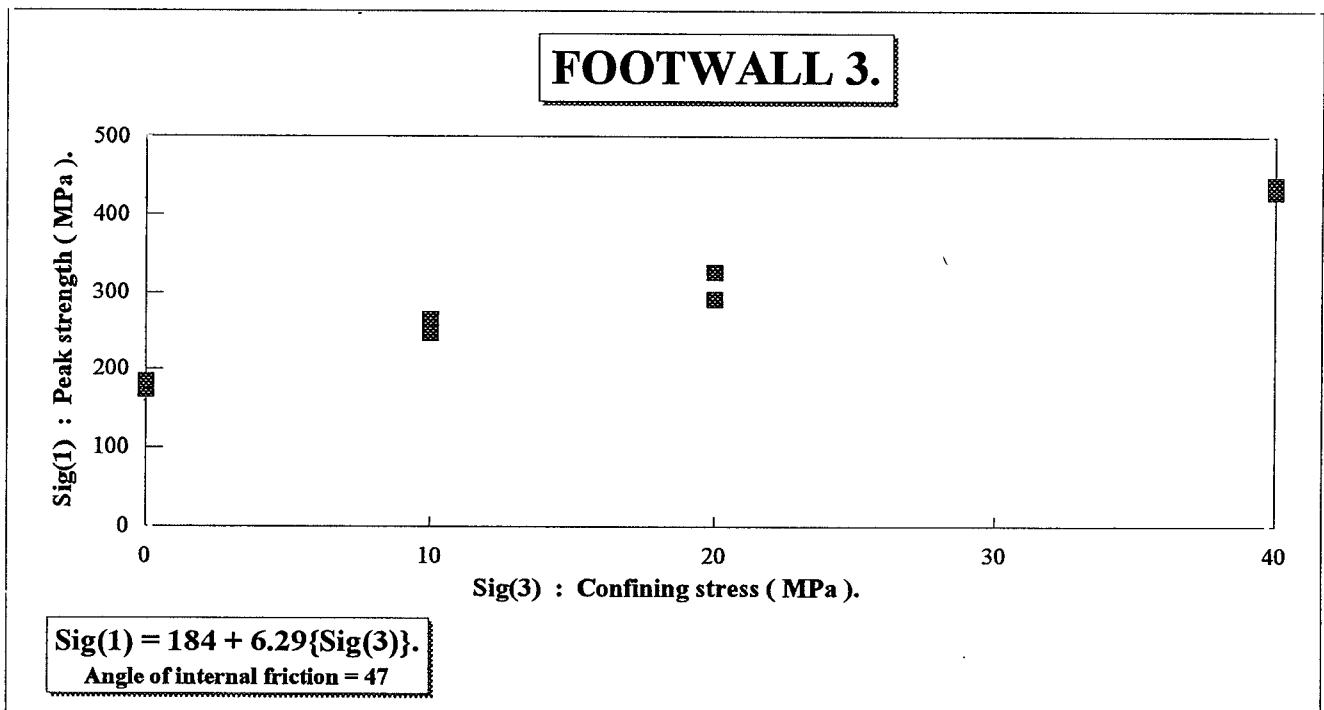
UNIAXIAL AND TRIAXIAL TEST RESULTS FOR :

PYROXENITE and FOOTWALL 3.

Confining Stress (MPa).	Peak Strength		Young's Modulus (GPa).	Poissons Ratio
	Individual specimens	Average		
0	157.10		83.20	
0	169.00		92.50	
0	176.10	167.40	88.50	
10	299.80		99.30	0.19
20	314.20		100.80	0.19
20	320.90	317.55	96.70	0.18
40	358.90		105.20	
40	419.30	389.10	101.20	0.19
		Average values	95.93	0.19
		Standard Deviation	6.48	0.00

PYROXENITE and FOOTWALL 3.

Sig(1) = 179 + 5.61{Sig(3)}.
Angle of internal friction = 44
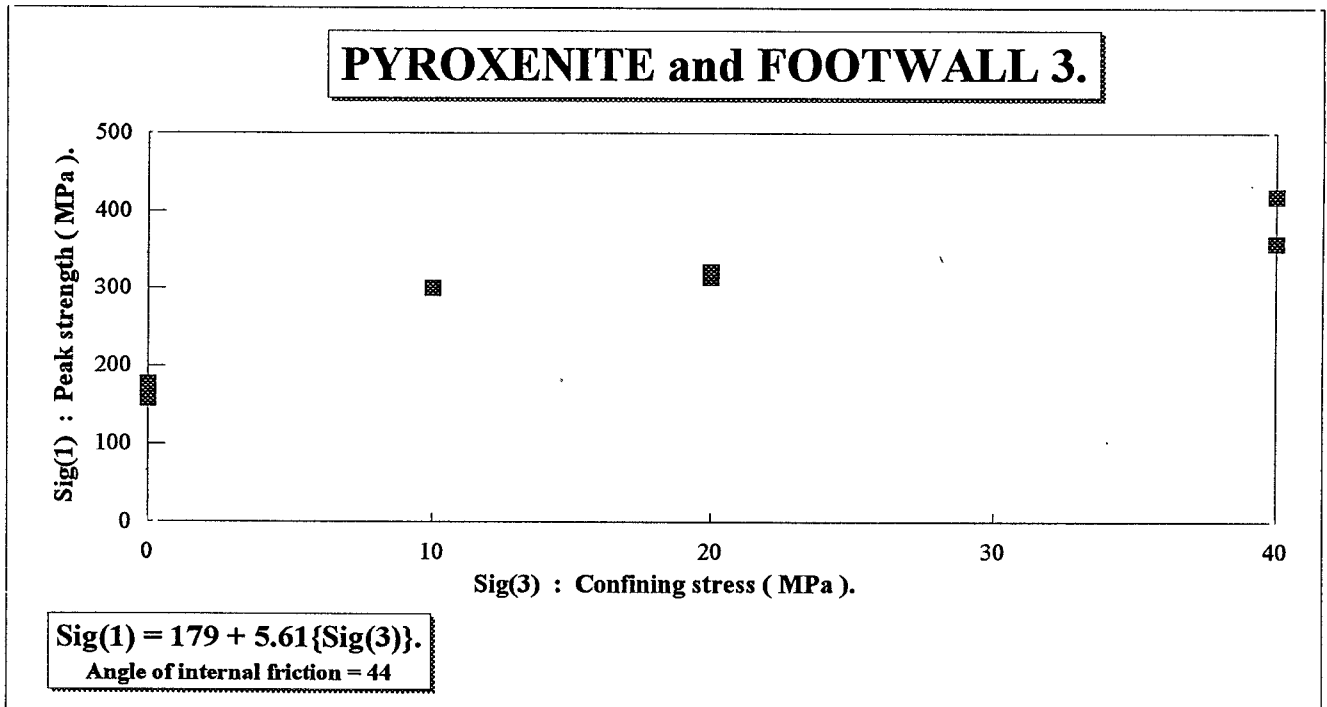
COMPARISON OF THE COMBINED ROCK TYPES.

Confining Stress (MPa).	Peak strength (MPa). Pyrox + FW1(mot)	Peak strength (MPa). Pyrox + FW1(spot)	Peak strength (MPa). Pyrox + FW3
0	125.00	199.00	179.00
10	184.40	264.00	235.10
20	243.80	329.00	291.20
30	303.20	394.00	347.30
40	362.60	459.00	403.40

COMPARISON OF THE THREE COMBINED ROCK TYPE
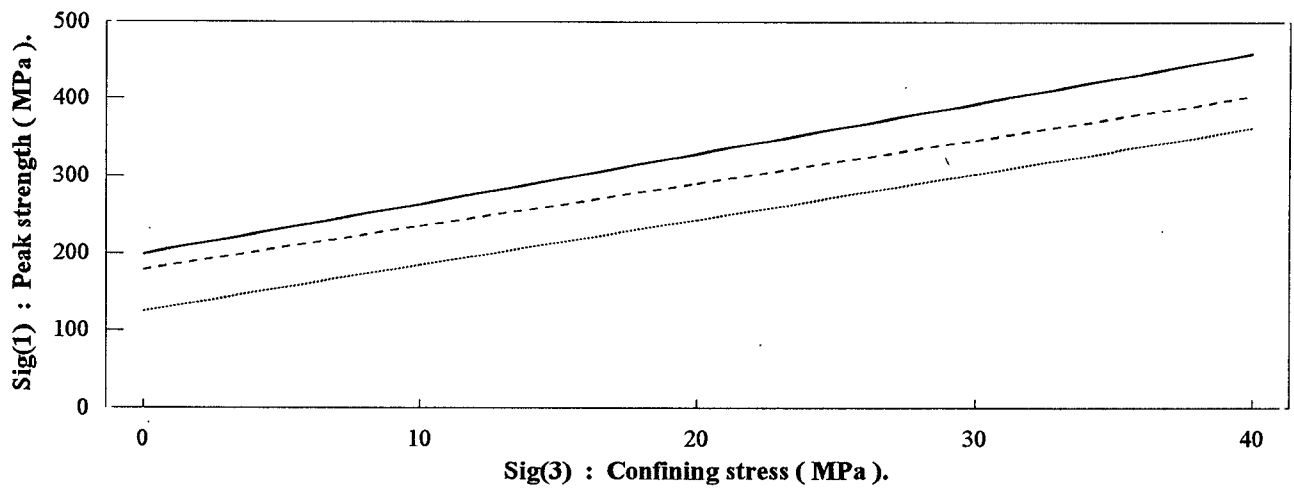
...... Pyroxenite and Footwall 1 (mottled).   —— Pyroxenite and Footwall 1 (spotted).
-- Pyroxenite and Footwall 3.

Table of laboratory based strain softening values for Flac modelling.

Strain (mm/metre)	Friction (degrees)	Strain (mm/metre)	Dilation (degrees)	Strain (mm/metre)	Cohesion (MPa)
0.0000	13.2	0.0000	0.0	0.0000	60.0
0.0050	29.2	0.0005	27.6	0.0025	38.0
0.0015	37.6	0.0050	27.6	0.0050	18.0
0.0025	42.4	0.0140	3.2	0.0065	8.0
0.0035	44.8			0.0080	2.0
0.0050	47.2				

APPENDIX (3)

<u>Width to height.</u>

UPF1−5−1

(diameter=77,8 mm, height=15,3 mm)
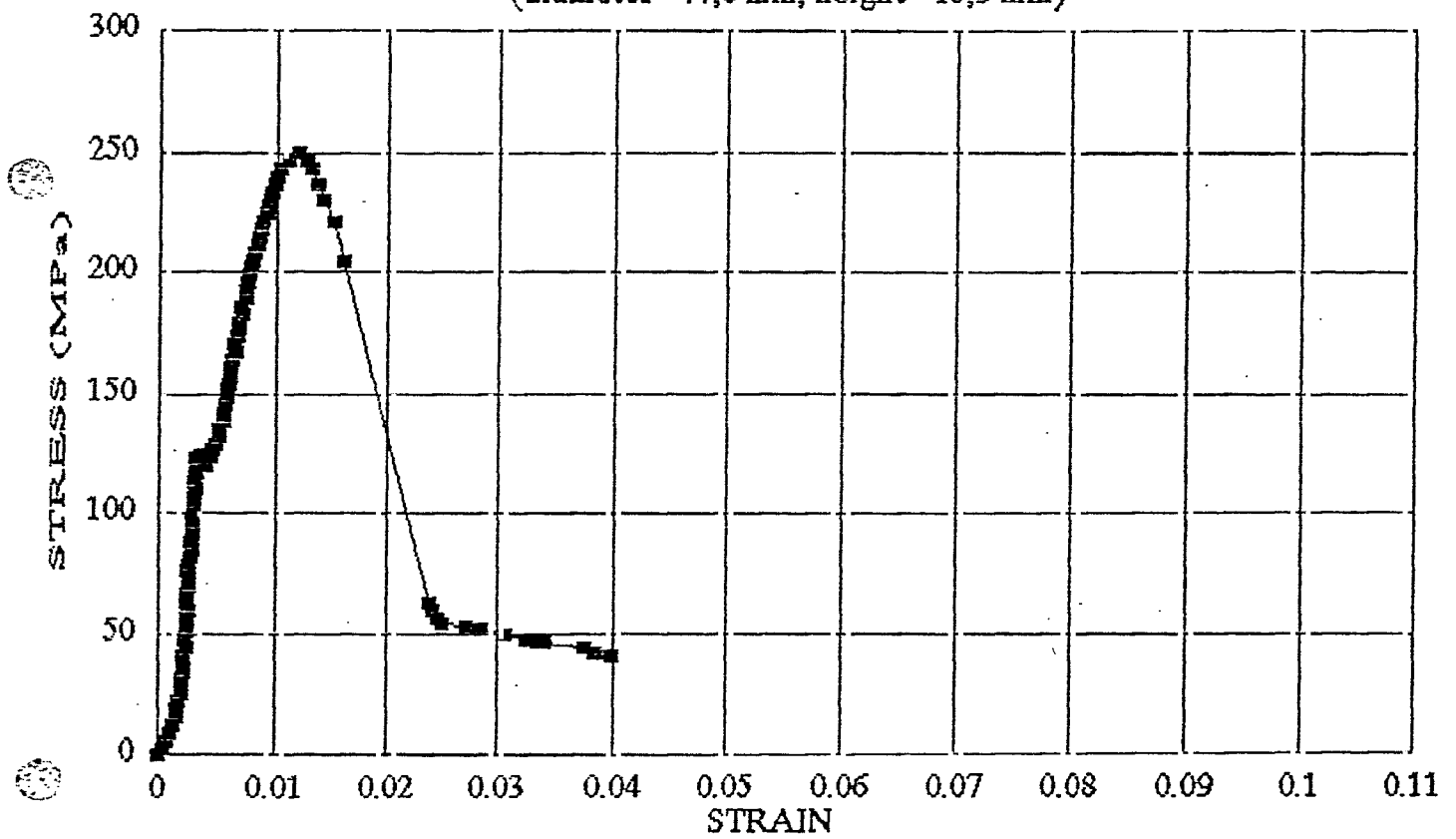
top piece: diameter=78,8 mm, height=3,1 mm
bottom piece: diameter=77,8 mm, height=12,2 mm

UPF1−3−1

(diameter=77,9 mm, height=25,8 mm)
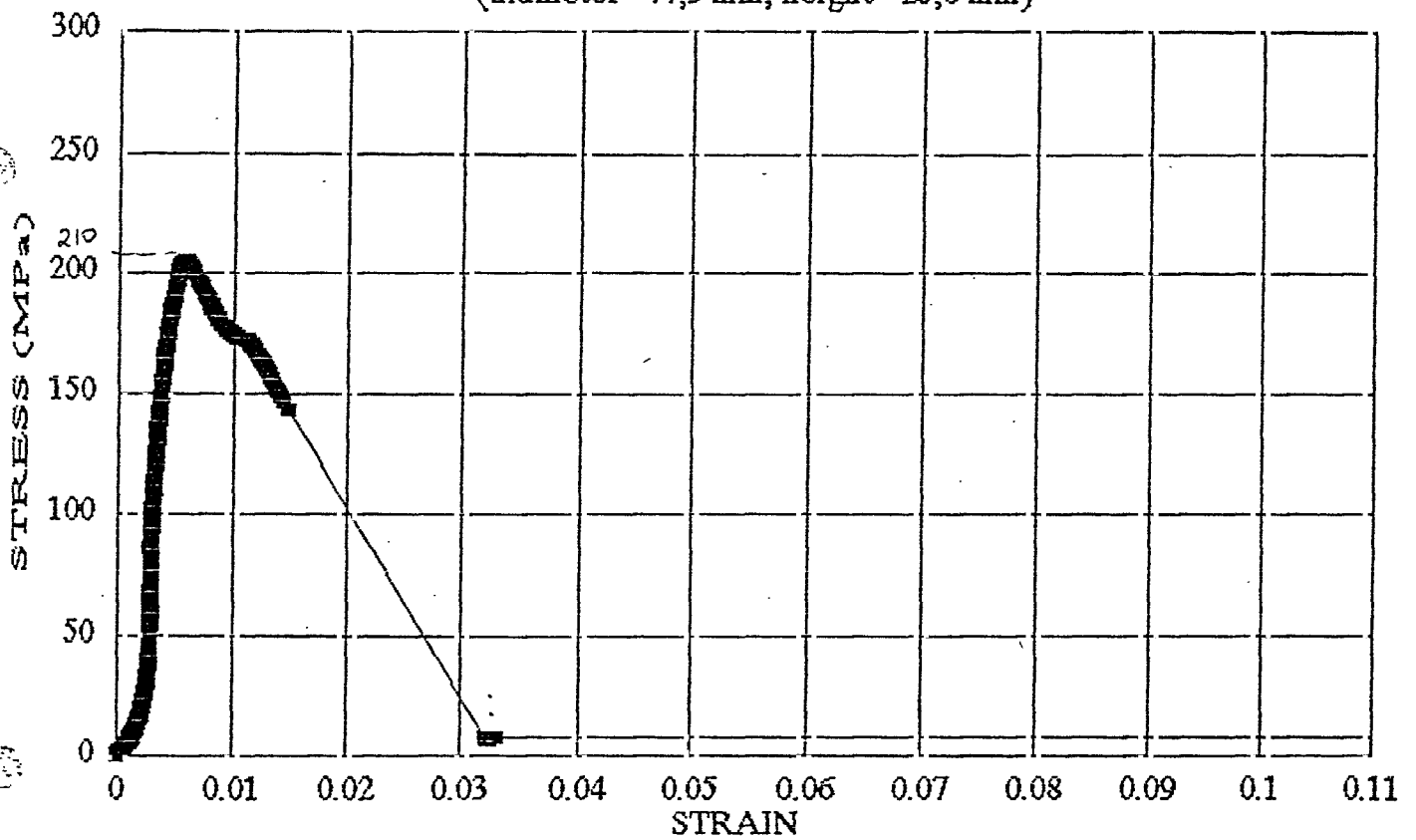
top piece: diameter=77,9 mm, height=5,0 mm
bottom piece: diameter=77,9, height=20,8 mm

UPF1−1−1

(diameter=77,9 mm, height=77,9 mm)
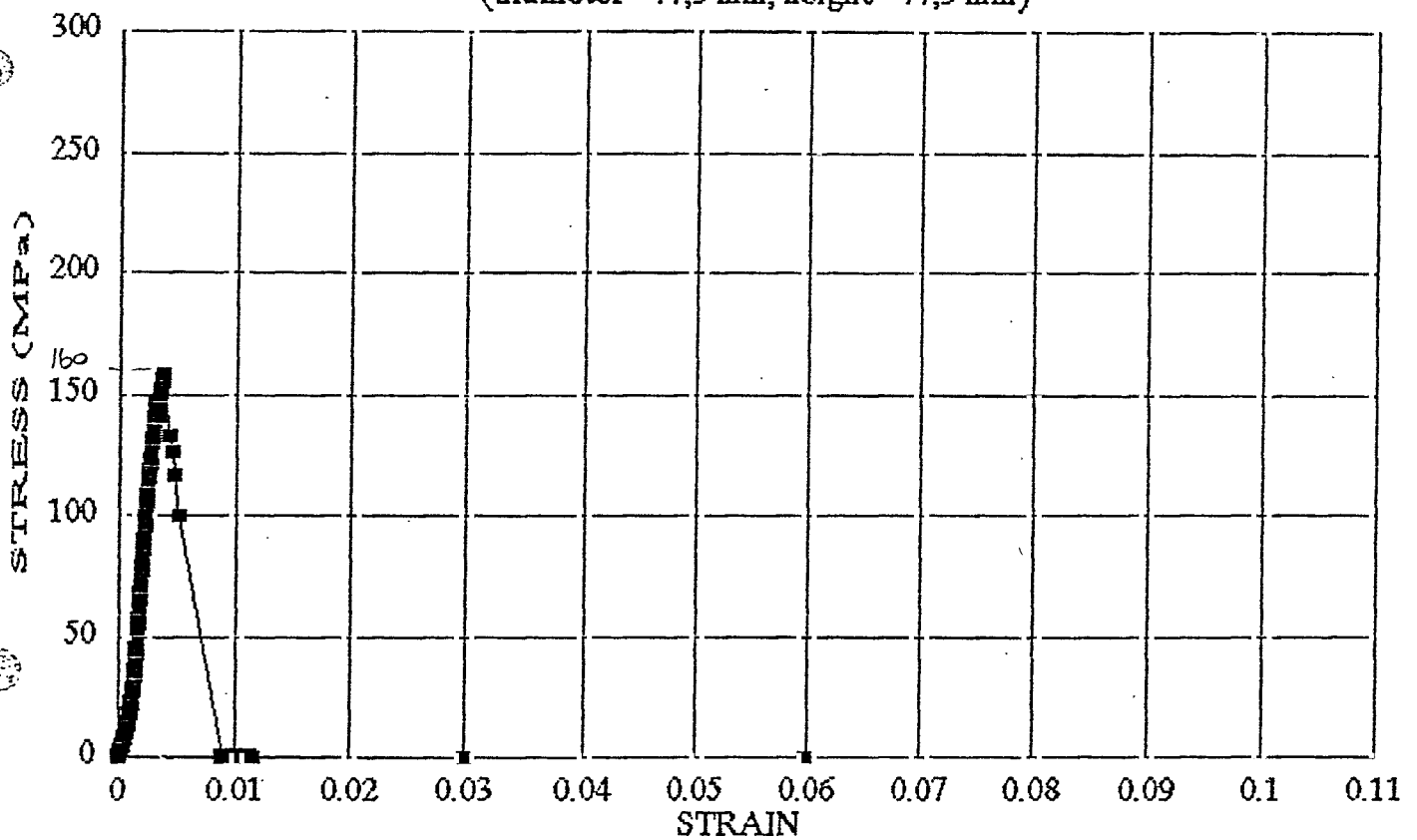
top piece: diameter=77,9 mm, height=15,5 mm
bottom piece: diameter=77,9 mm, height=62,4 mm

APPENDIX (4)

Punch tests.

GENMIN R.M.DEPT. - STAMP TEST - SAMPLE PFW1-2
FW1 MAT NO.2 - FW1 PUNCH 5:1 RATIO 25.35mm DIAM

GENMIN R.M.DEPT. - STAMP TEST - SAMPLE PFW1-3
FW1 MAT NO.3 - FW1 PUNCH 3:1 RATIO 25.34mm DIAM

GENMIN R.M.DEPT. - STAMP TEST - SAMPLE PFW1-6A
FW1 MAT NO.6 - FW1 PUNCH 1:1 RATIO 25.34mm DIAM
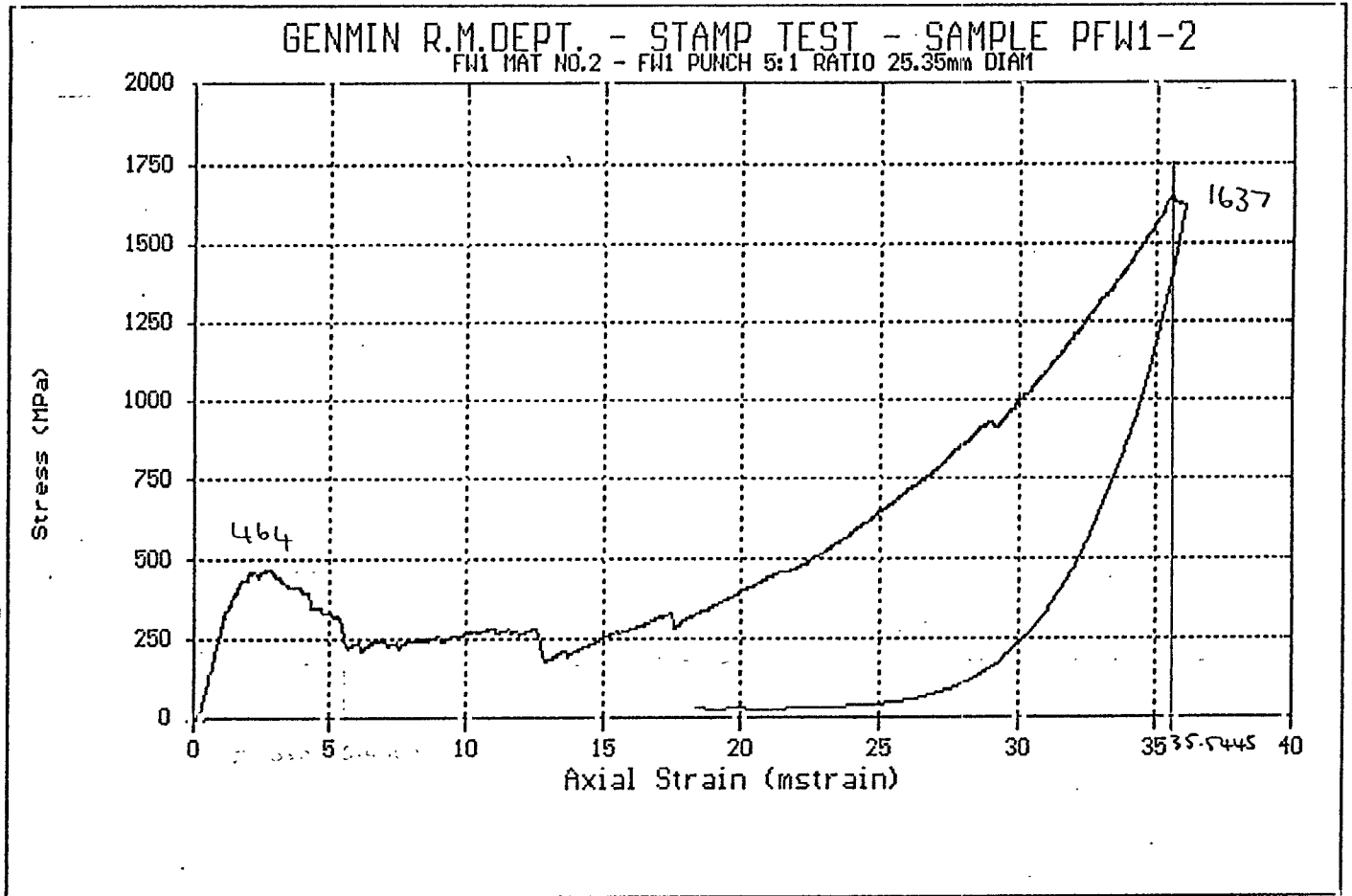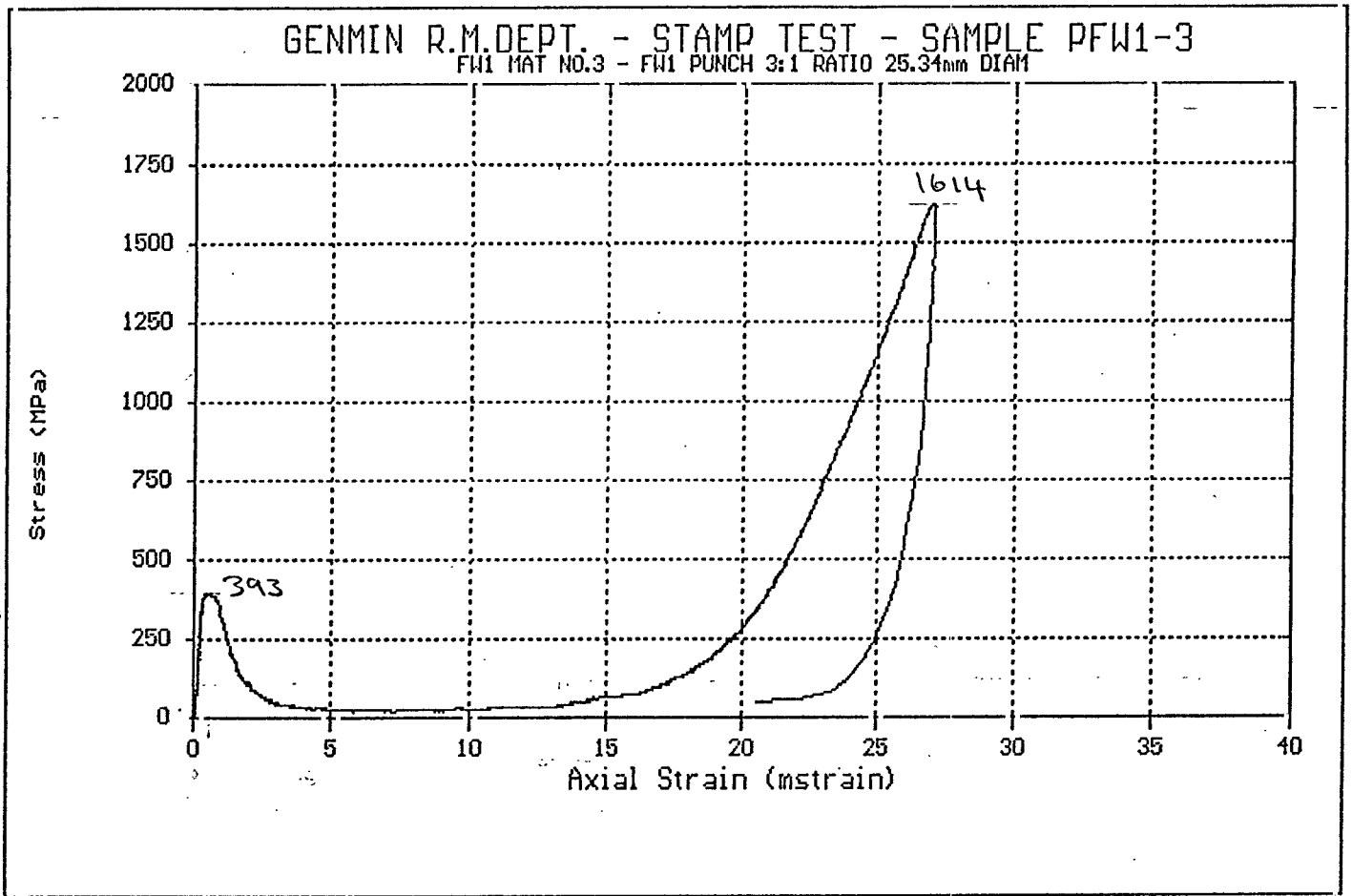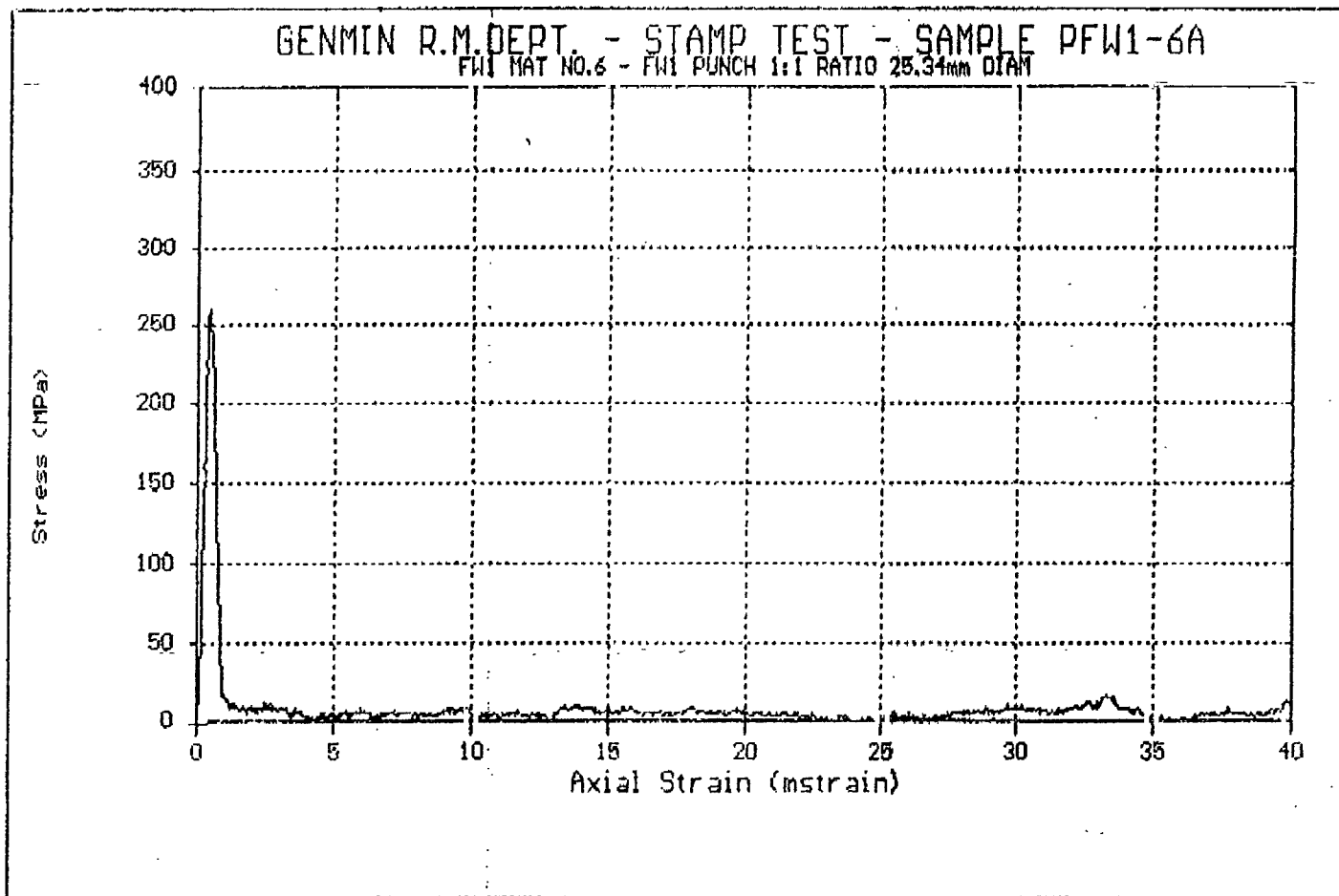
GENMIN R.M.DEPT. – STAMP TEST – SAMPLE PFW3-1B

FW3 MATERIAL NO.1 – FW3 PUNCH 5:1 RAT. 25.37mm DIAM

Stress (MPa) — vertical axis: 0, 250, 500, 750, 1000, 1250, 1500, 1750, 2000

Axial Strain (mstrain) — horizontal axis: 0, 5, 10, 15, 20, 25, 30, 35, 40

404

556
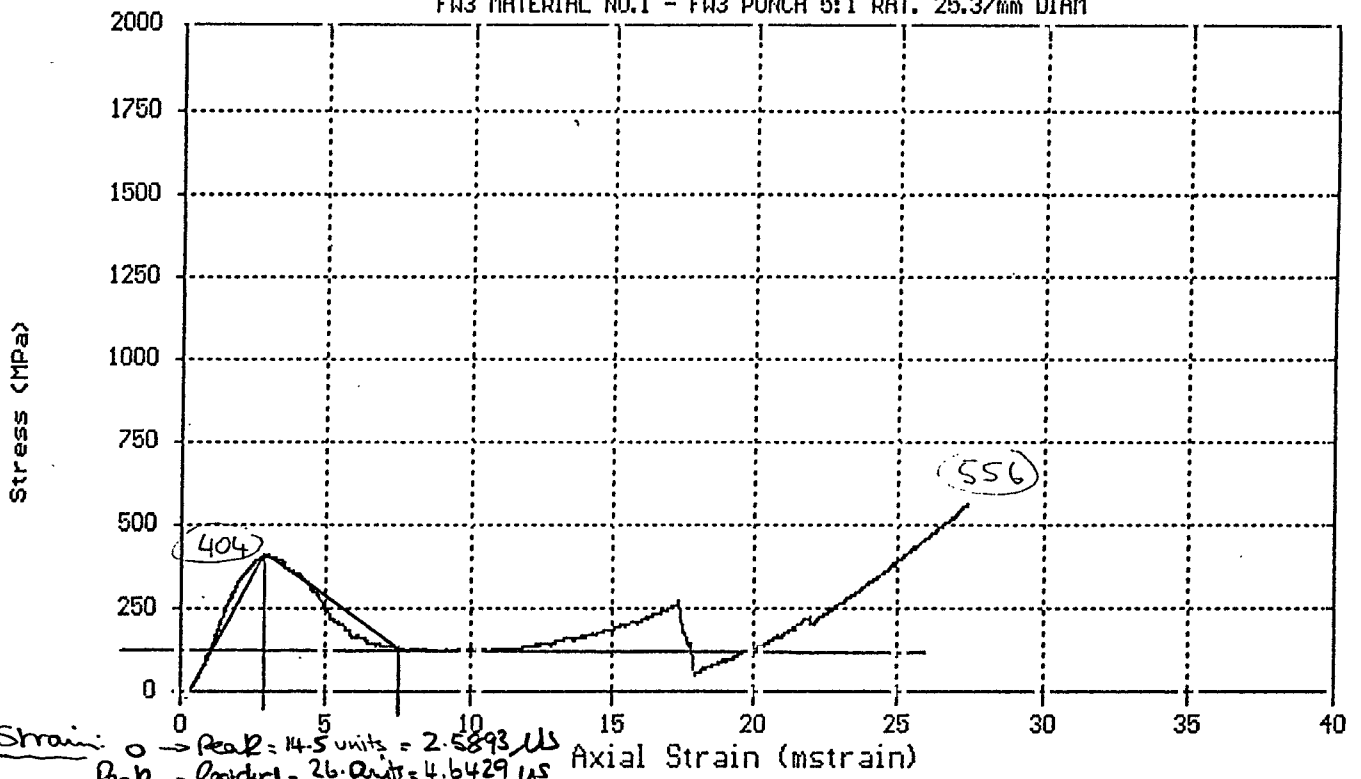
Strain: 0 → Peak = 14.5 units = 2.6893 µs

Peak → Residual = 26.0 units = 4.6429 µs

Stress: Residual = 2.7 units × $\frac{250}{5.5}$ = 122.7 MPa .

GENMIN R.M.DEPT. - STAMP TEST - SAMPLE PFW3-3
FW3 MAT NO.3 - FW3 PUNCH 3:1 RATIO 25.37mm DIAM

GENMIN R.M.DEPT. - STAMP TEST - SAMPLE PFW3-6A
FW3 MAT NO.5 - FW3 PUNCH 1:1 RATIO 25.34mm DIAM
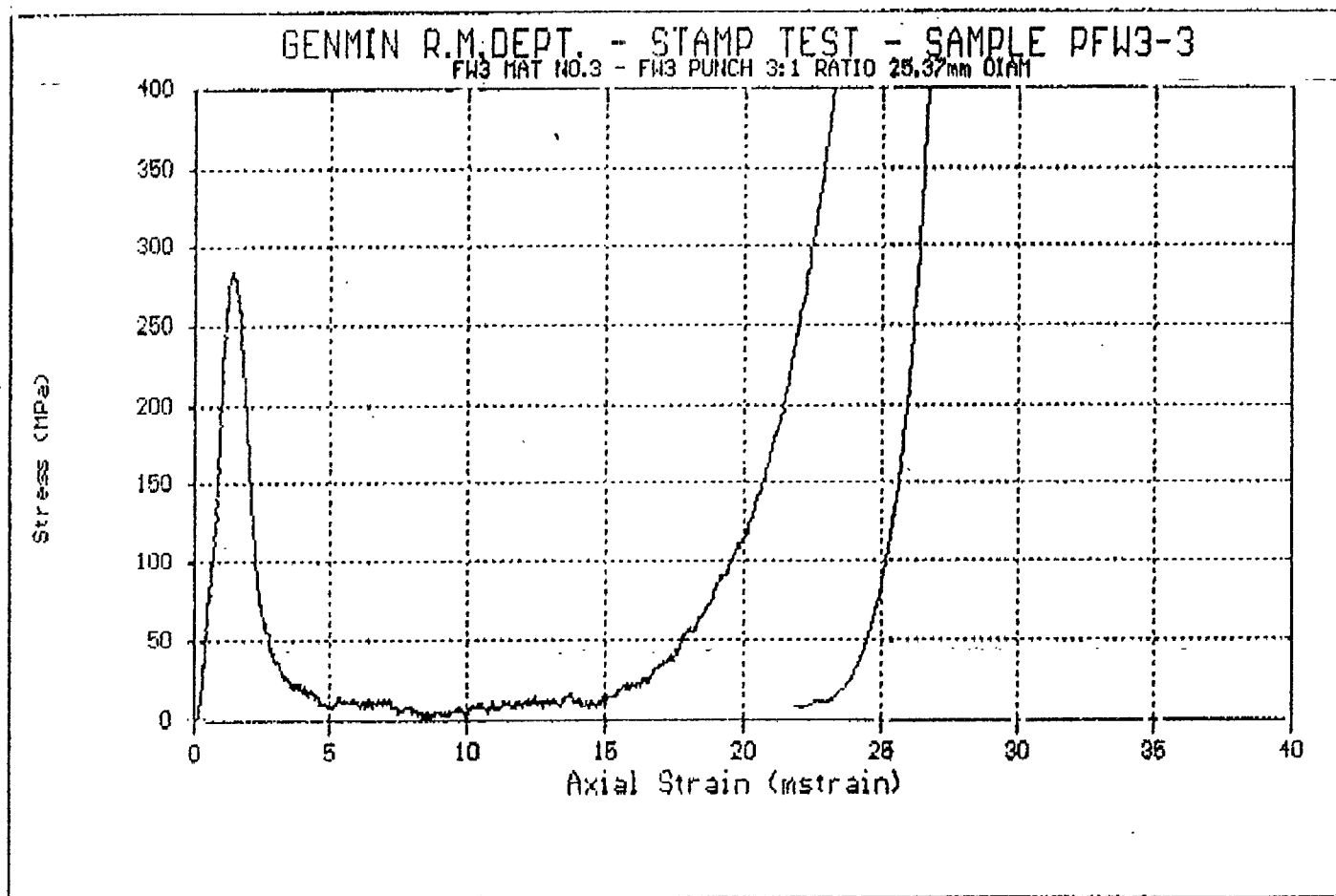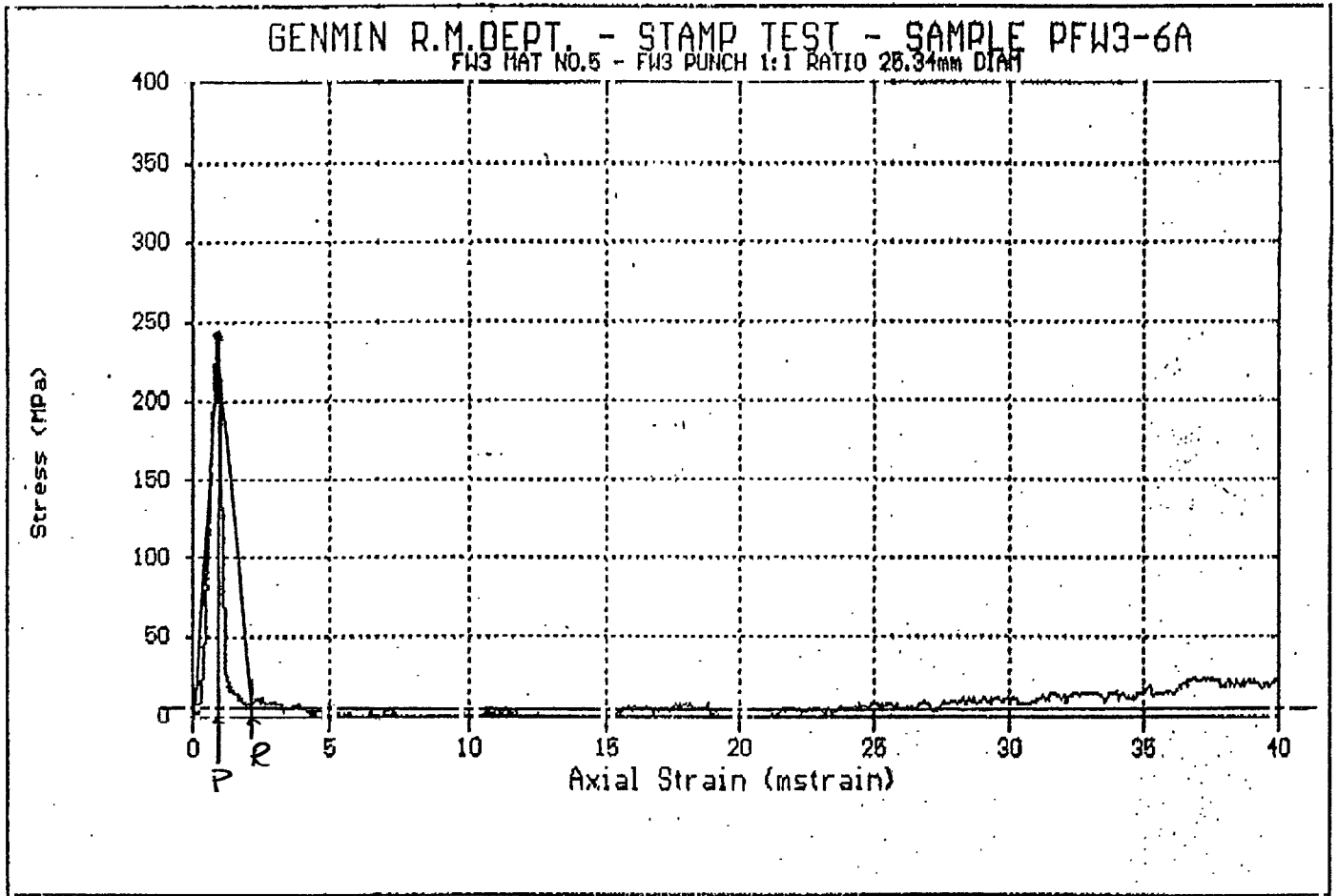
EFFECT OF WIDTH TO HEIGHT RATIO ON PILLAR STRENGTH.

— Obert and Duvall.
··· Footwall 1.
— Footwall 3.

Pillar strength to cube strength.

2

1.5

1

0.5

0.33 1.33 2.33 3.33 4.33 5.33

Width to height ratio.
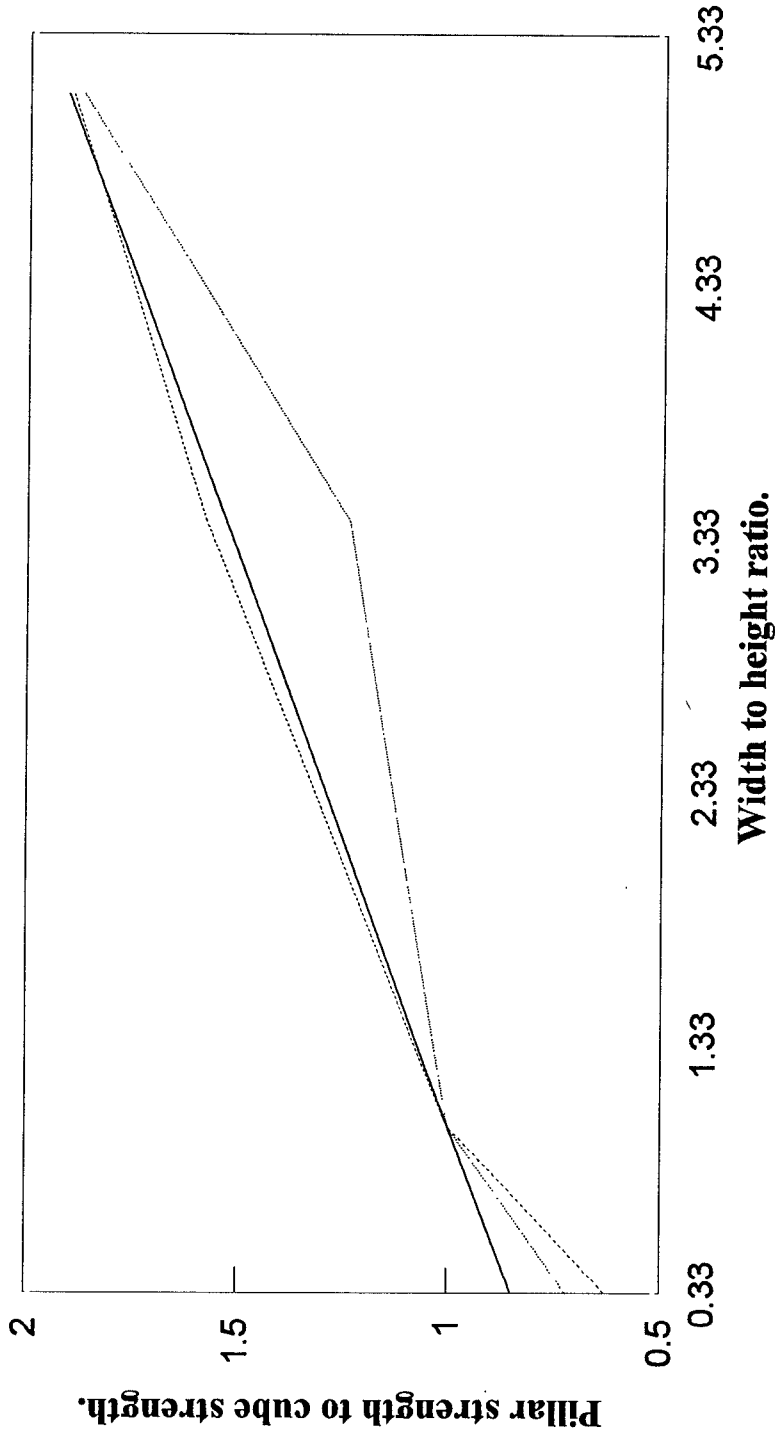
$$Ps = Cs \{ 0.778 + 0.222 \, (w/h) \}$$

EFFECT OF WIDTH TO HEIGHT RATIO ON POST FAILURE BEHAVIOUR.

Width to height ratio.

Post failure modulus / Elastic modulus.

— $Ep/E= 0.23\{[5/(w/h) - 1]\}$ After Ozbay.
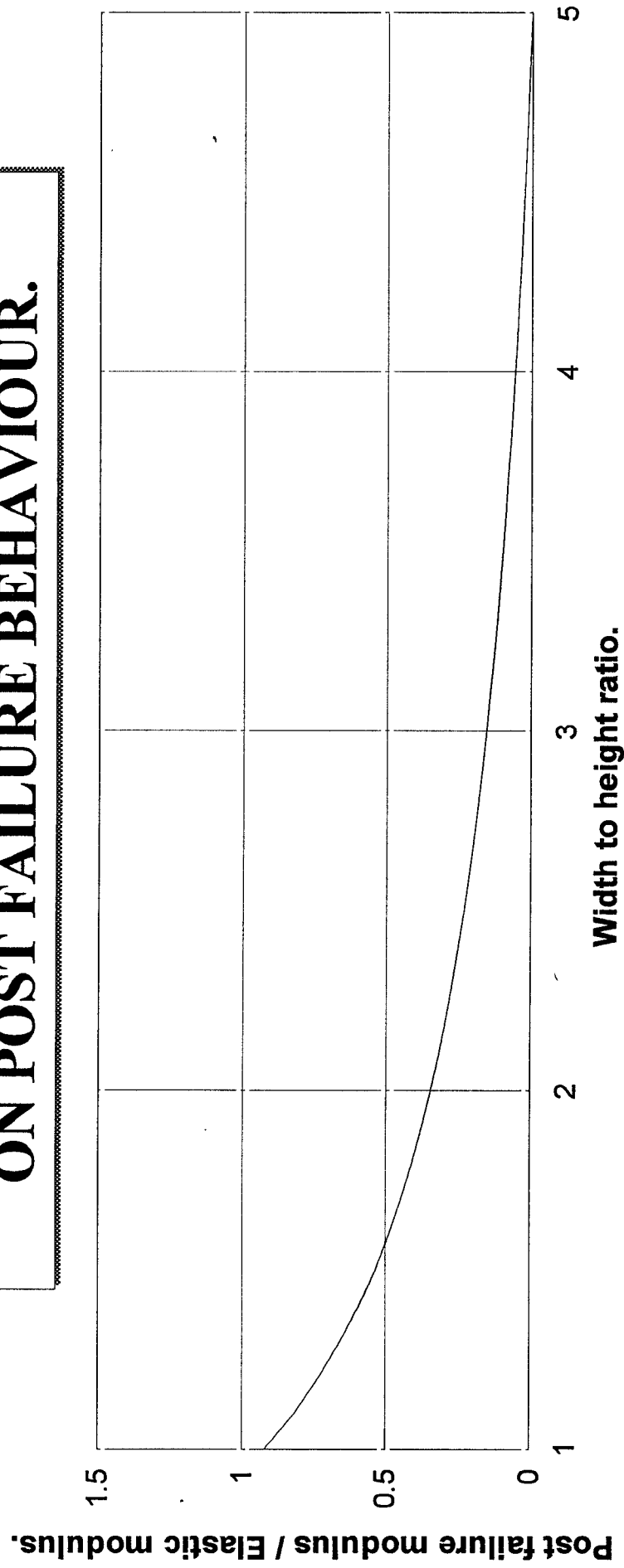
APPENDIX (5)

<u>Flac modelling.</u>

B TITLE : Width to height = 5 to 1. Axisymmetrical configuration. *Derated Values.*

FLAC (Version 3.04)

LEGEND

8/12/1994 12:10
tep 20000

STORY PLOT
Y-axis :
v_average_stress (FISH)
X-axis :
v_strain   (FISH)
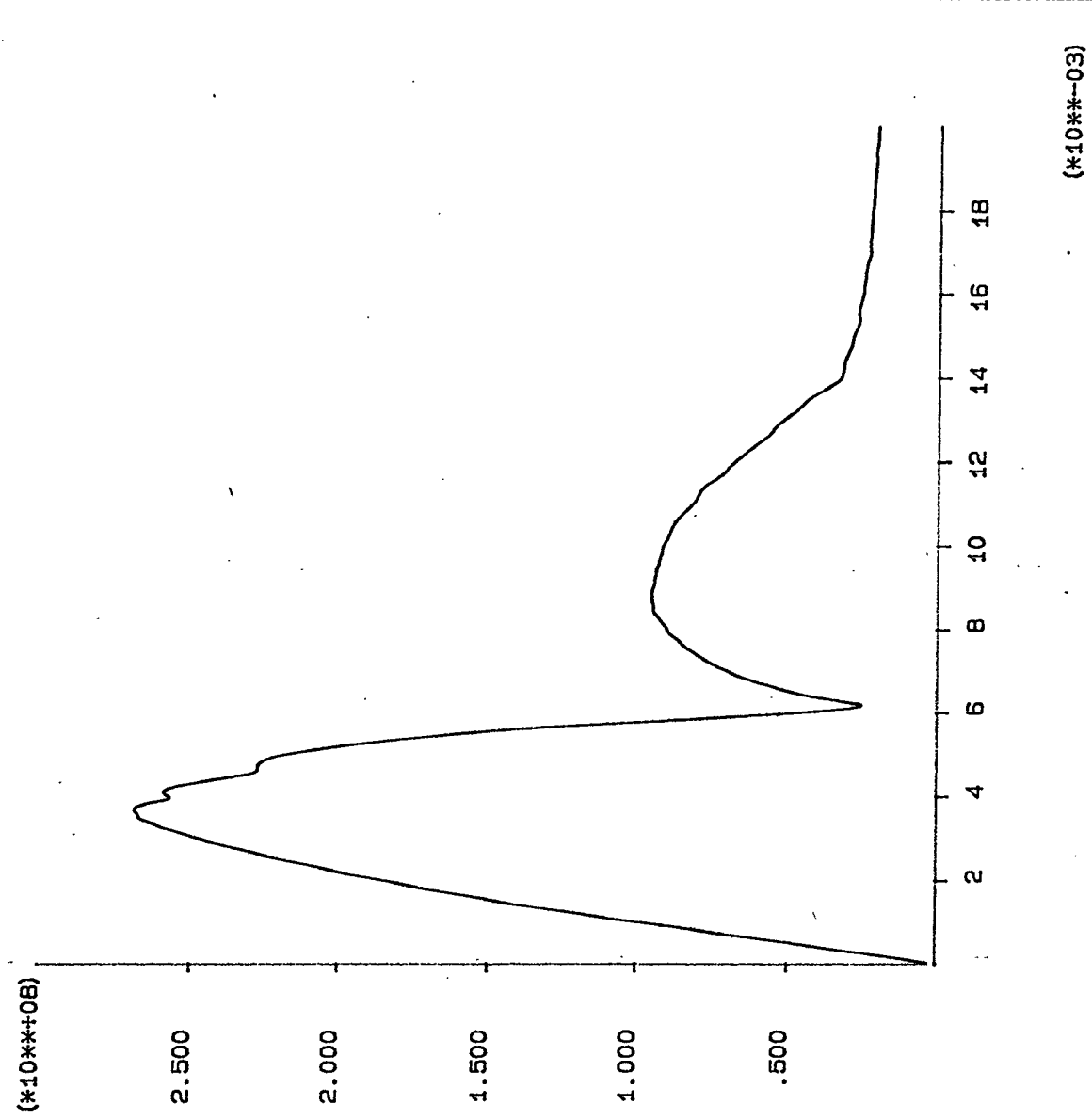
MIN Rock Engineering Dept. #2
v/Bag 82279, Rustenburg 0300

JOB TITLE : Width to height = 3 to 1. Axisymmetrical configuration. Derated value.

FLAC (Version 3.04)

LEGEND

8/12/1994 08:53
step 40000

HISTORY PLOT
    Y-axis :
Rev_average_stress (FISH)
    X-axis :
Rev_strain   (FISH)
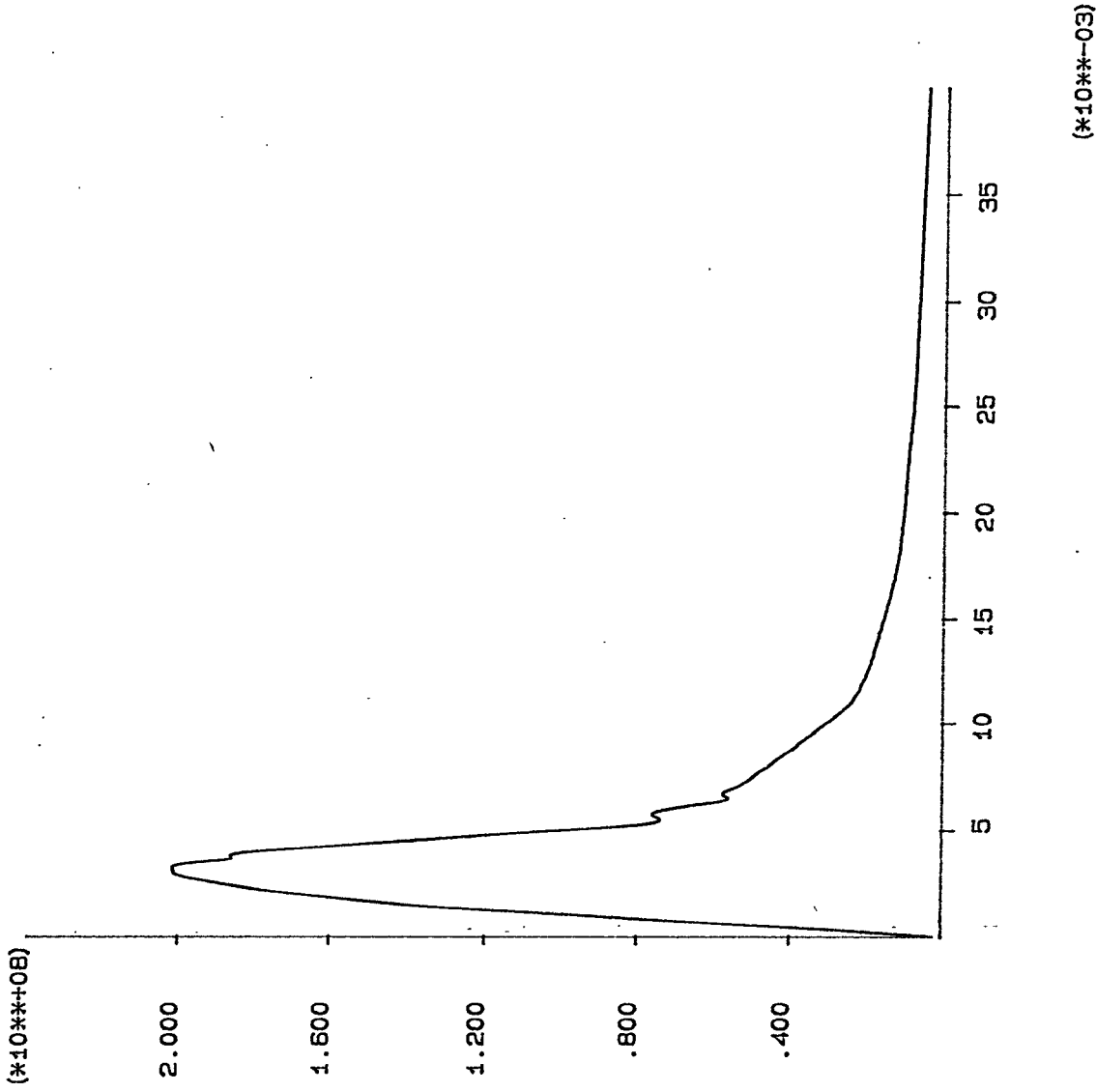
ENMIN Rock Engineering Dept. #2
riv/Bag 82279, Rustenburg 0300

OB TITLE : Width to height = 1 to 1. Axisymmetrical configuration. Derated values.

FLAC (Version 3.04)

LEGEND

9/12/1994 11:06
step 20000

ISTORY PLOT
  Y-axis :
av_average_stress (FISH)
  X-axis :
ev_strain   (FISH)

(*10**+08)

1.600

1.400

1.200

1.000

.800

.600

.400

.200

(*10**-03)

2   4   6   8   10   12   14   16   18

WMIN Rock Engineering Dept. #2
lv/Bag 82279, Rustenburg 0300

Table of derated strain softening values for Flac modelling.

Width to height of 1:1

Strain (mm/metre)	Friction (degrees)	Strain (mm/metre)	Dilation (degrees)	Strain (mm/metre)	Cohesion (MPa)
0.0000	39.0	0.0000	20.0	0.0000	36.0
0.0600	39.0	0.0300	0.0	0.0100	7.0
				0.0300	0.2

Width to height of 5:1 and 3:1

Strain (mm/metre)	Friction (degrees)	Strain (mm/metre)	Dilation (degrees)	Strain (mm/metre)	Cohesion (MPa)
0.0000	26.0	0.0000	20.0	0.0000	36.0
0.0600	26.0	0.0300	0.0	0.0100	7.0
				0.0300	0.2

B TITLE : Width to height = 3 to 1. Axisymmetrical configuration. (8*2 grid).

FLAC (Version 3.22)

LEGEND

9/05/1995 11:59
tep 40000

STORY PLOT
 Y-axis :
v_average_stress (FISH)
 X-axis :
v_strain   (FISH)

(*10**+08)

2.000

1.600

1.200

.800

.400

                    5   10   15   20   25   30   35

                                              (*10**-03)

COR Rock Engineering
82279, Rustenburg 0300, RSA

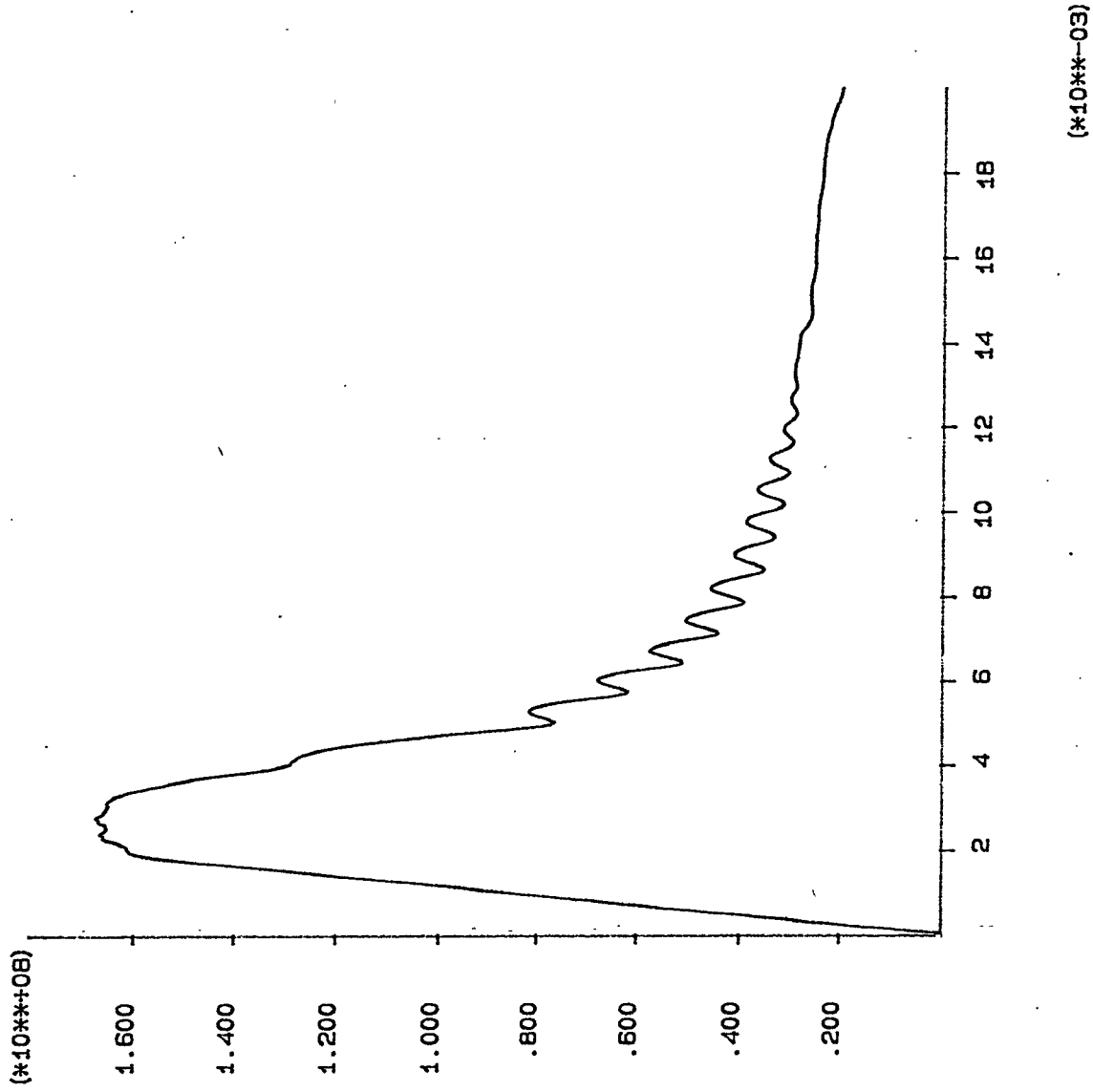B TITLE : Width to height = 3 to 1. Axisymmetrical configuration. Derated values. (12×4)

FLAC (Version 3.22)

(*10**+08)

2.000

1.600

1.200

.800

.400

5   10   15   20   25   30   35

(*10**-03)

LEGEND

9/05/1995 12:35
ep 40000

STORY PLOT
Y-axis :
  _average_stress (FISH)
X-axis :
  _strain   (FISH)

OR Rock Engineering
82279, Rustenburg 0300, RSA

OB TITLE : Width to height = 3 to 1. Axisymmetrical configuration. (24*8 grid).
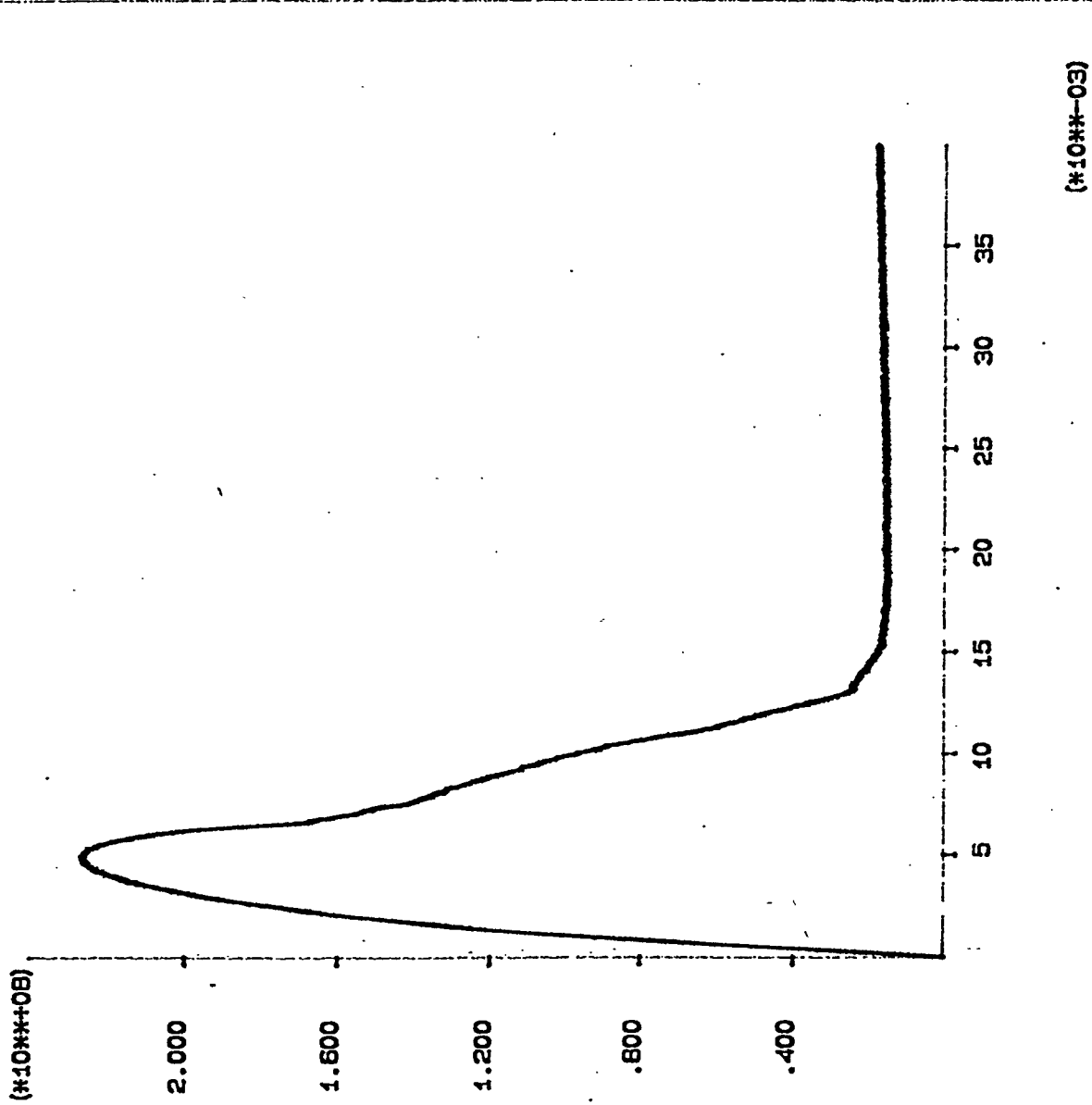
FLAC (Version 3.22)

LEGEND

9/05/1995 14:22
step 40000

ISTORY PLOT
  Y-axis :
av_average_stress (FISH)
  X-axis :
av_strain   (FISH)

ICOR Rock Engineering
82279, Rustenburg 0300, RSA

(*10**+08)

1.800
1.600
1.400
1.200
1.000
.800
.600
.400
.200

5 10 15 20 25 30 35

(*10**-03)

OB TITLE : Width to height = 3 to 1. 2D rib configuration. (BM2 grid).

FLAC (Version 3.22)

(*10**+08)

3.000

2.500

2.000

1.500

1.000

.500

(*10**-03)

35

30

25

20

15

10

5

LEGEND

29/05/1995 14:42
step 40000

ISTORY PLOT
Y-axis :
ev_average_stress (FISH)
X-axis :
ev_strain (FISH)
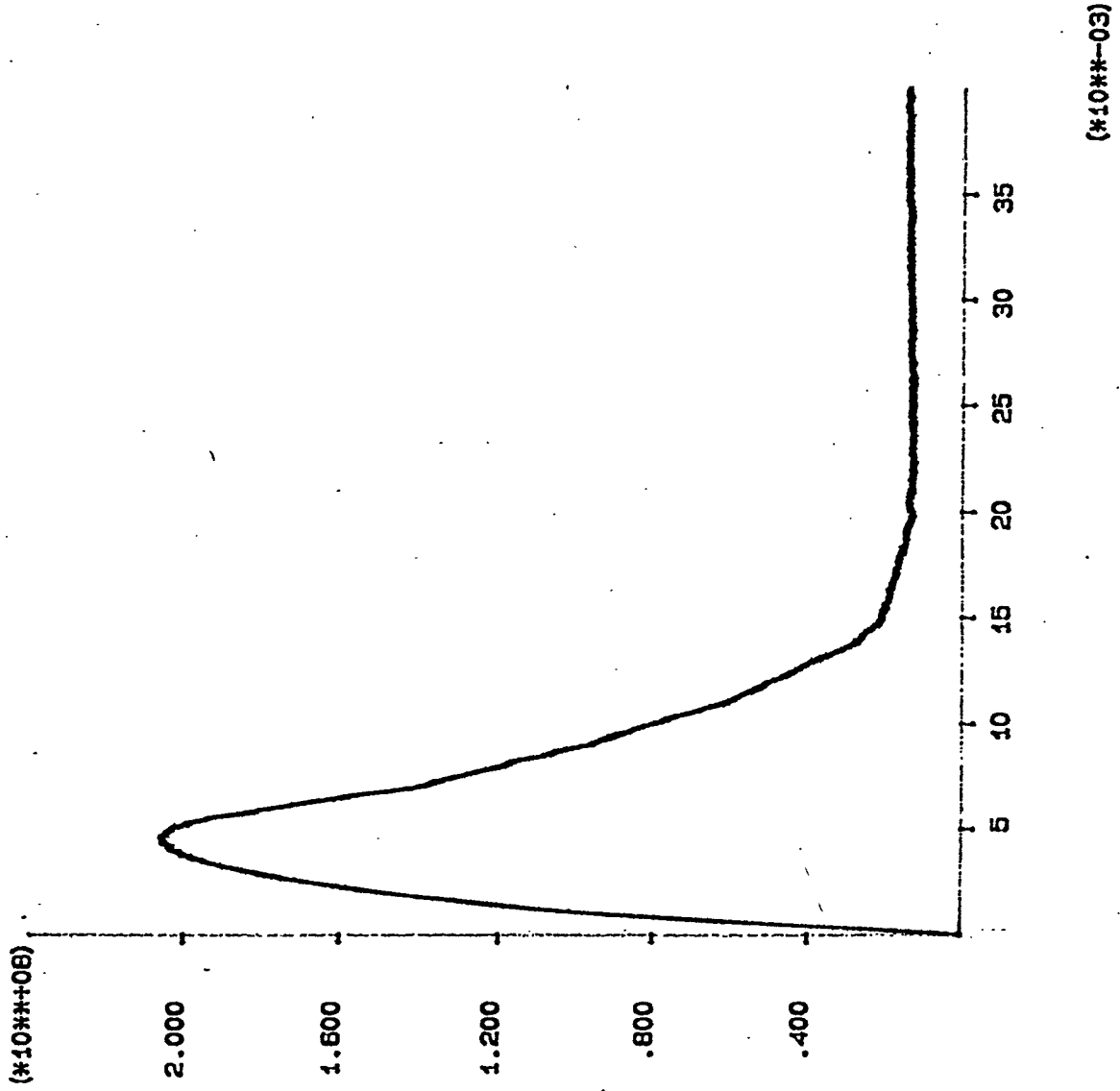
NCOR-Rock Engineering
B 82279, Rustenburg 0300, RSA

B TITLE : Width to height = 3 to 1. 2D rib configuration. (12x4)

FLAC (Version 3.22)
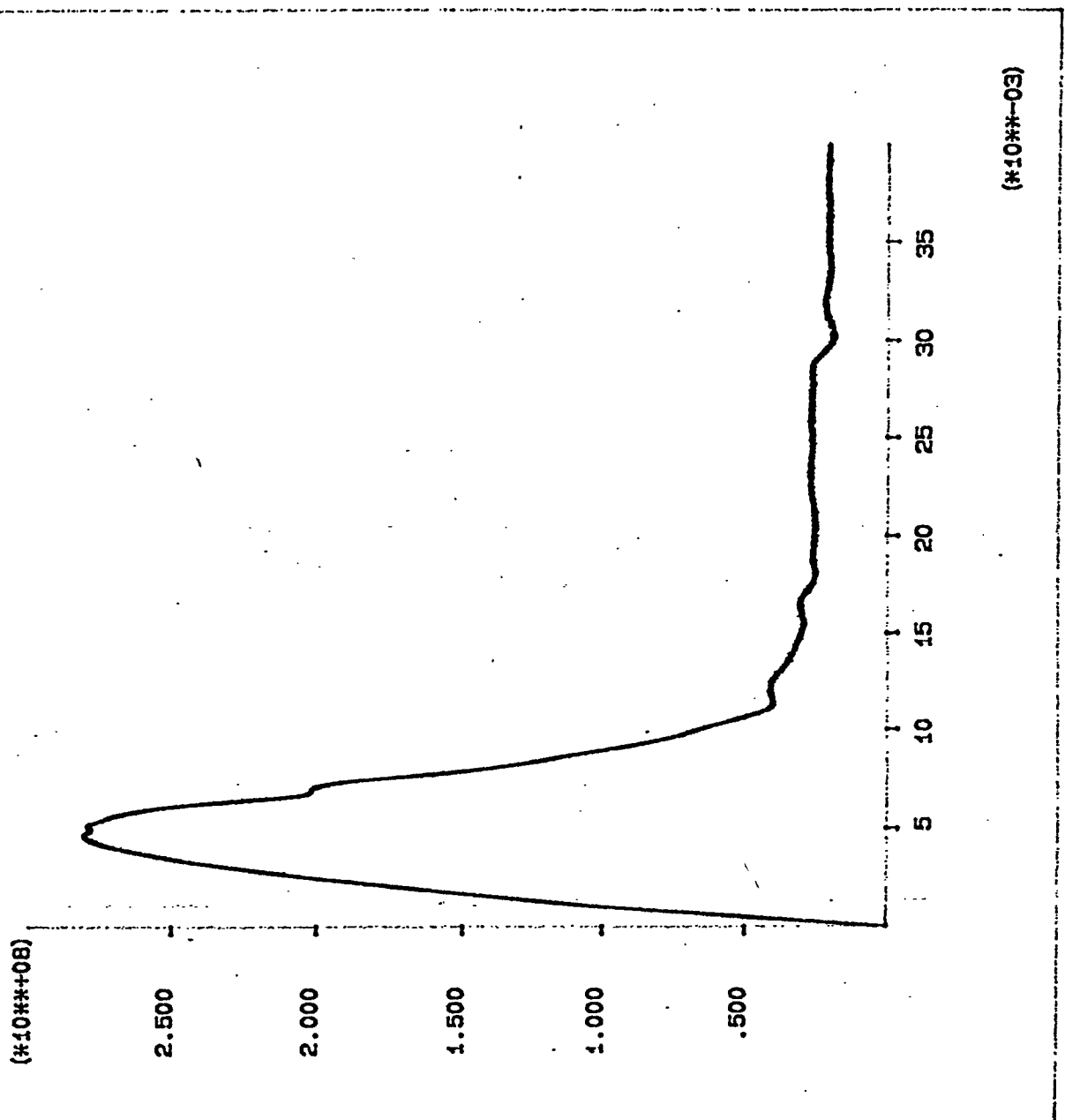
LEGEND

0/05/1995 07:26
tep 40000

STORY PLOT
Y-axis :
v_average_stress (FISH)
X-axis :
v_strain   (FISH)
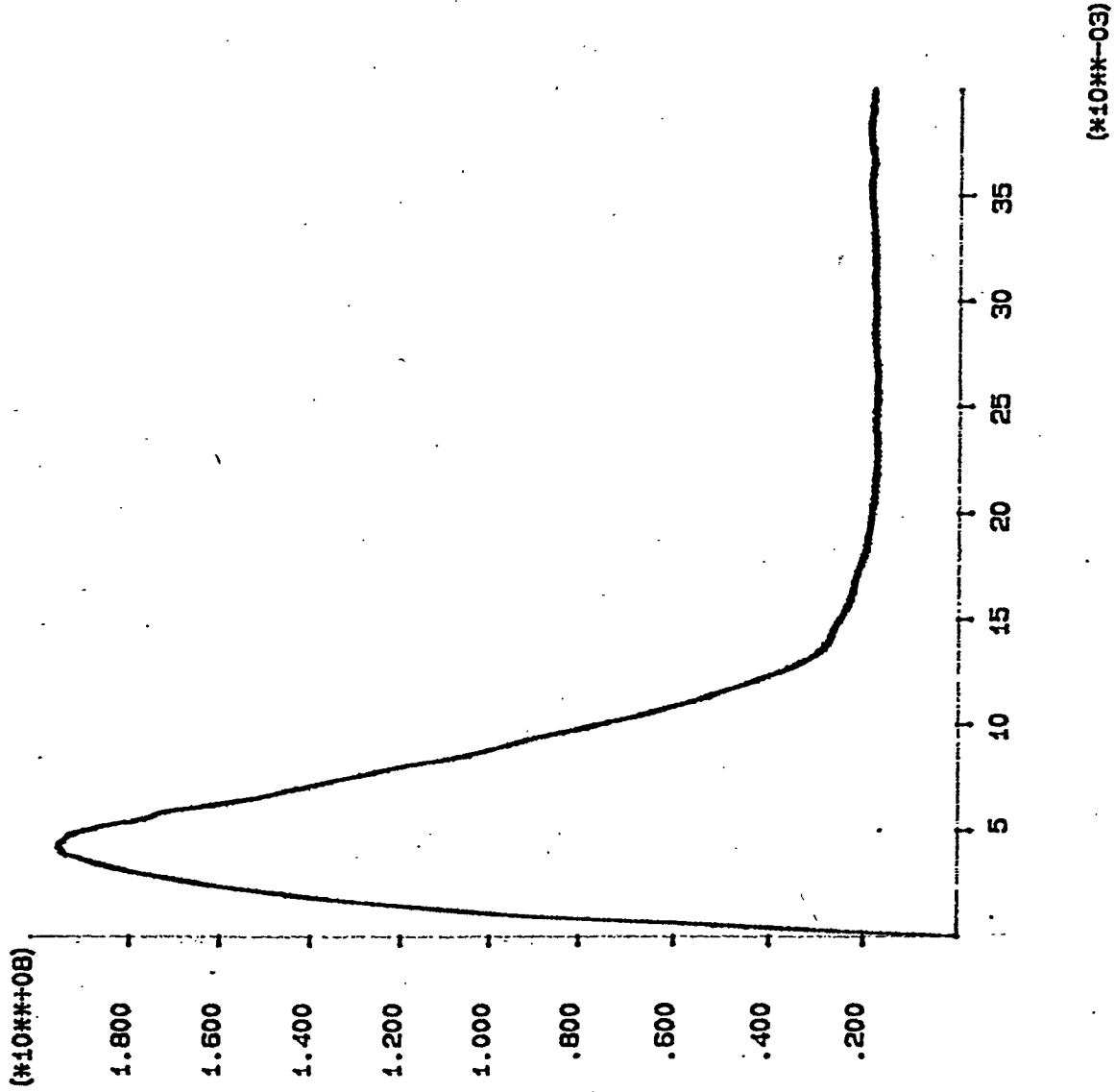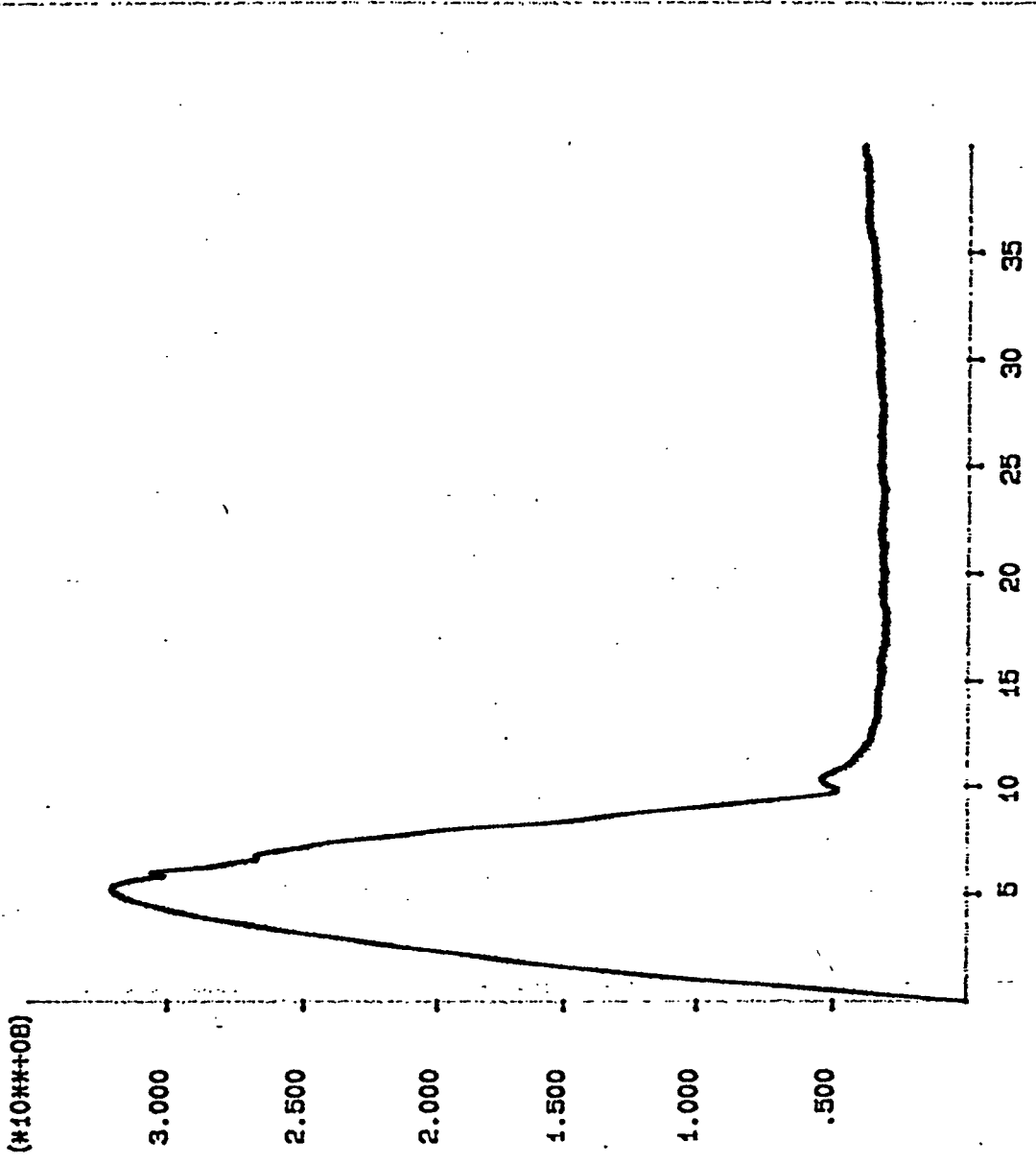
0R Rock Engineering
82279, Rustenburg 0300, RSA

B TITLE : Width to height = 3 to 1. 2D rib configuration. (24*8 grid). Yooh~20/04/2010).

FLAC (Version 3.22)

(*10**+08)

2.500

2.000

1.500

1.000

.500

(*10**-03)

5   10   15   20   25   30

LEGEND

0/05/1995 10:26
tep 30600

STORY PLOT
Y-axis :
v_average_stress (FISH)
X-axis :
v_strain   (FISH)
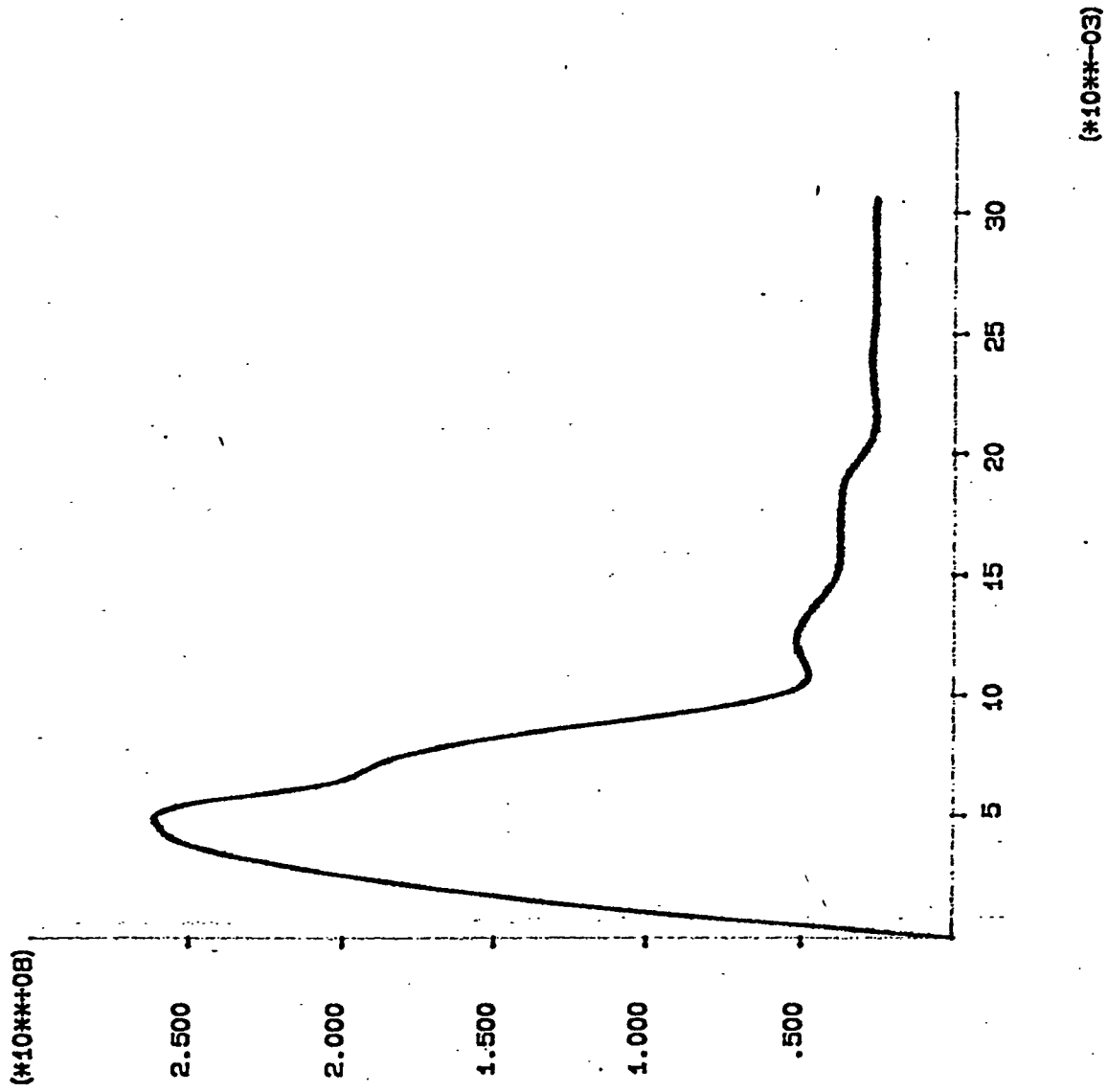
OR Rock Engineering
82279, Rustenburg 0300, RSA

Comparison between FLAC3d and FLAC2d
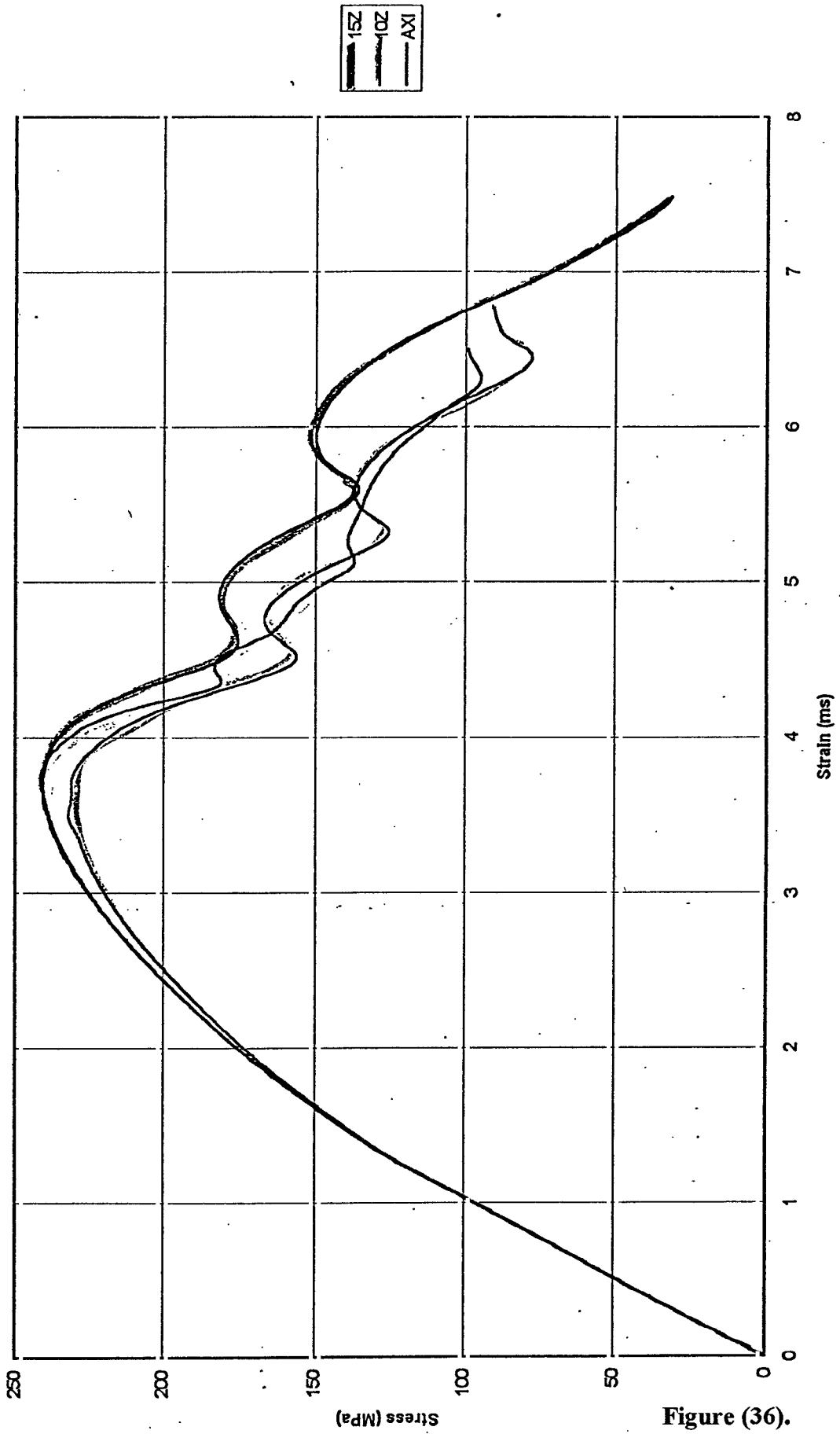
Figure (36).

APPENDIX (6)

Underground instrumentation.

VERTICAL STRESS CHANGE VERSUS TIME.
16 - 109 STOPE, PILLAR "A".
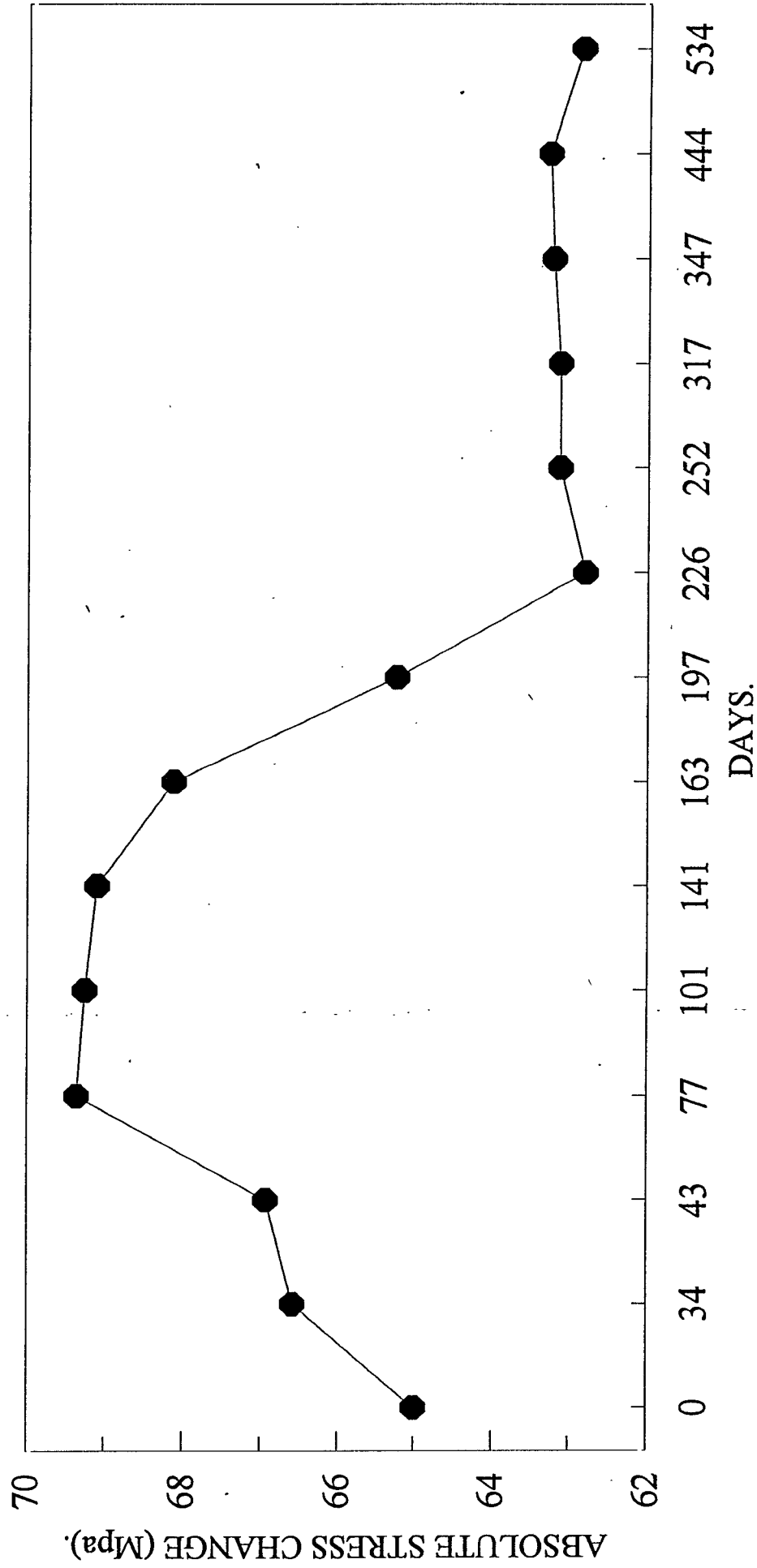
METER LOCATED 1.5m FROM PILLAR EDGE.

FREQUENCY READING VERSUS TIME.

16-109 STOPE, PILLAR "A".

METER LOCATED 0.5m FROM PILLAR EDGE.

FREQUENCY READING.

DAYS.
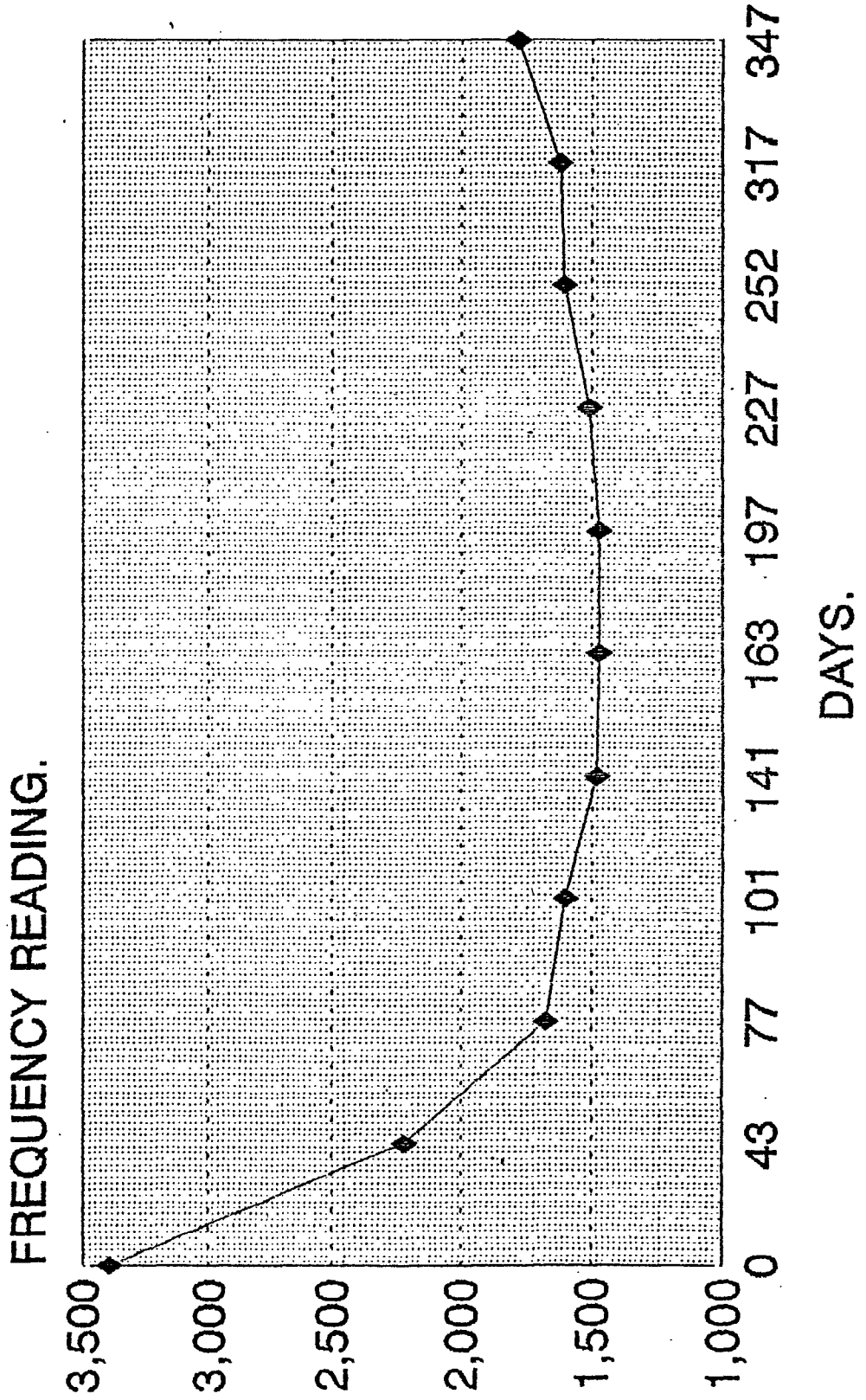
Figure (38)

A DECREASE IS COMPRESSIVE

QUARTERLY CLOSURE PROFILE ADJACENT TO PILLAR "A".

(CLOSURE PROFILE AT 02-03-94 IS AN ESTIMATE AT THE TIME OF CLOSURE METER INSTALLATION.)

Closure in millimetres.
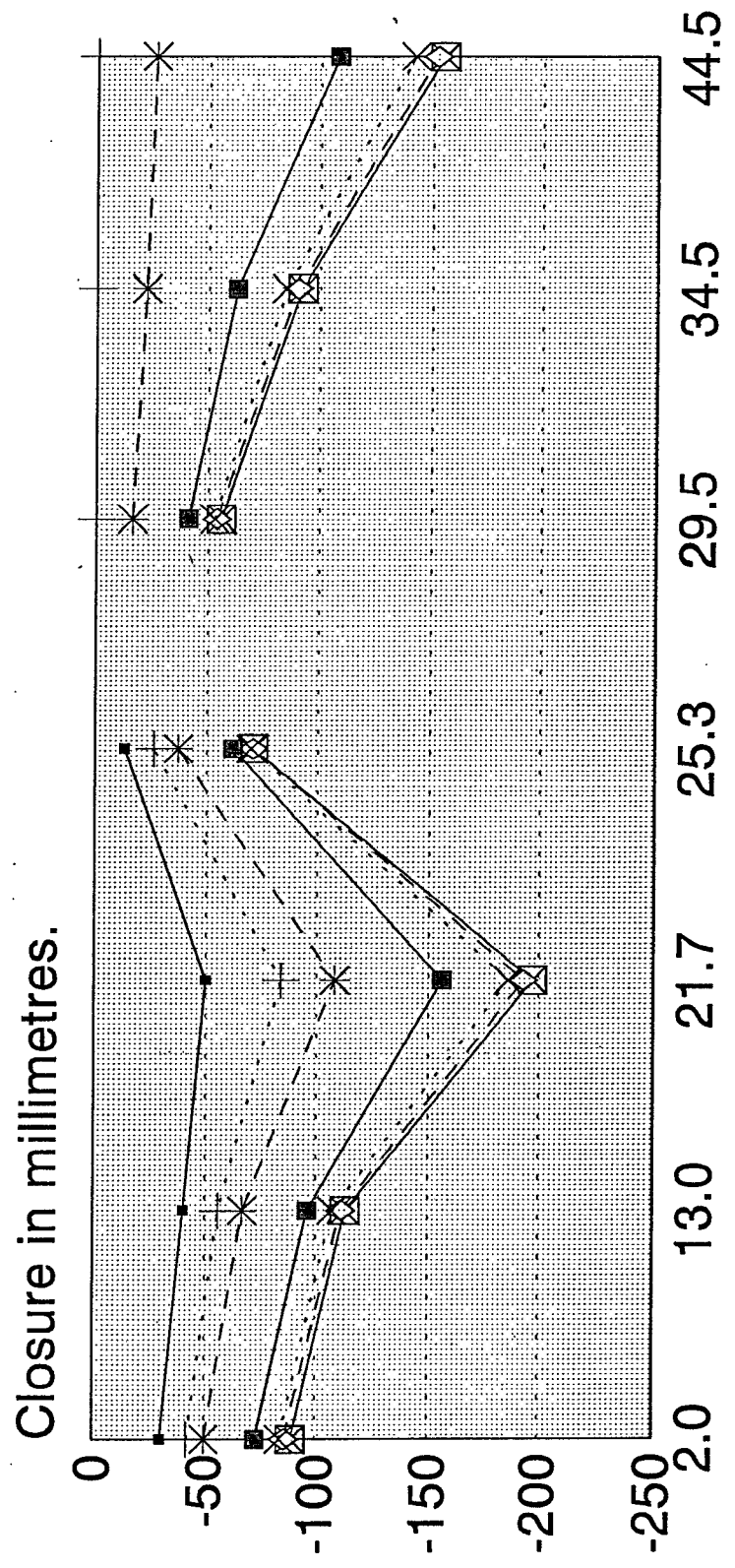
Distance from pillar at top of panel 2 south.

- 02-03-94.Panel 2s.   + 14-06-94.Panel 2s.   + 14-06-94.Panel 18s.   ✳ 07-09-94.Panel 18s.
✳ 07-09-94.Panel 2s.   06-12-94.Panel 2s.   06-12-94.Panel 18s.   ✖ 15-03-95.Panel 2s.
✖ 15-03-95.Panel 18s.   ◇ 15-06-95.Panel 2s.   15-06-95.Panel 18s.   13-09-95.Panel 2s.
13-09-95.Panel 18s.

PROGRESSIVE CLOSURE OF METERS ADJACENT TO PILLAR "A".

Millimetres.

Days.
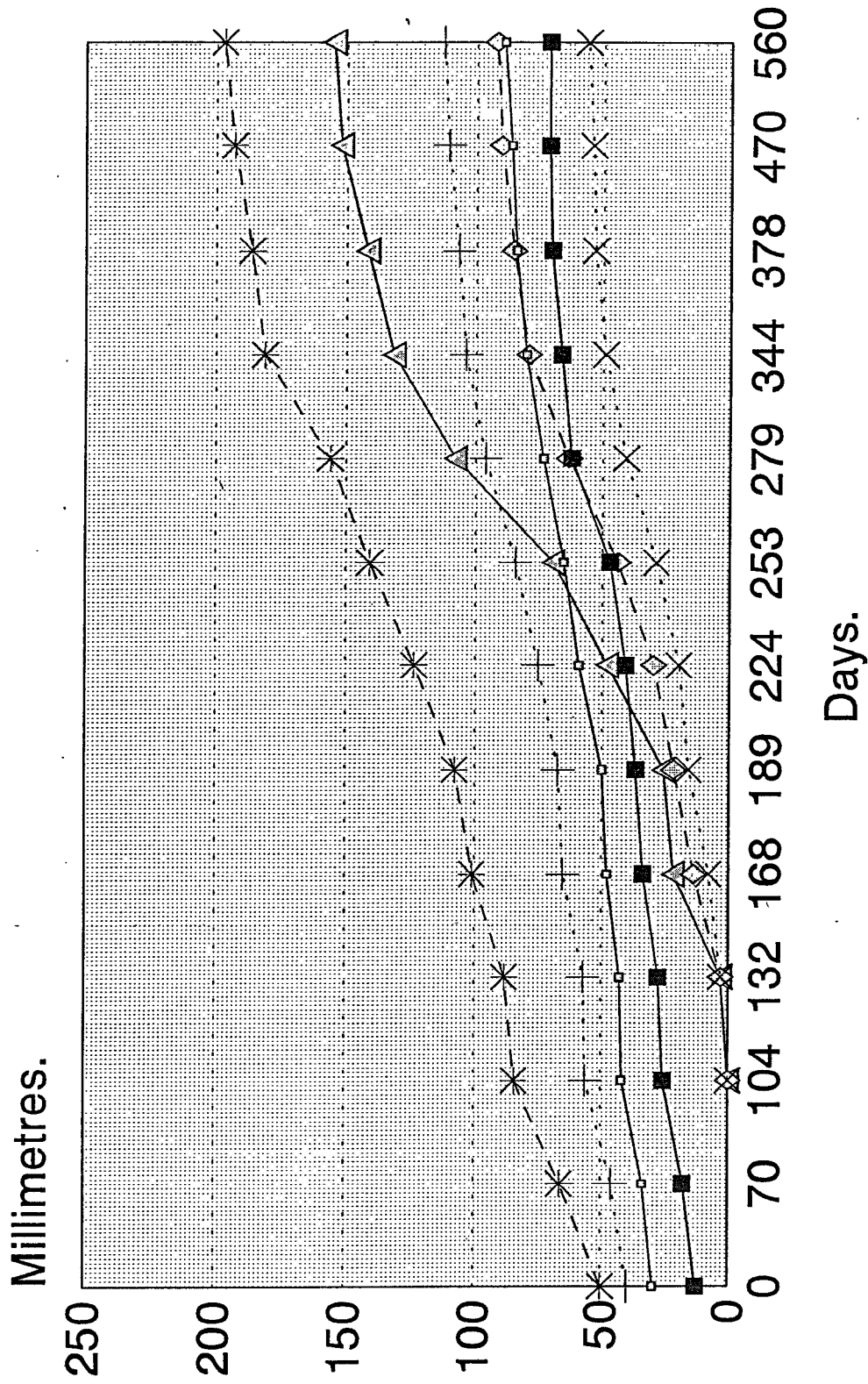
- Meter A1.   + Meter A2.   * Meter A3.   - Meter A4.
- Meter A5.   - Meter A6.   - Meter A7.

MEASURED VERTICAL AND HORIZONTAL STRESS
IN THE ABUTMENT NEXT TO PILLAR B.

ESTIMATE OF σ_V AT 1.5m INTO ABUTMENT.

ESTIMATE OF σ_H AT 1.5m INTO ABUTMENT.
(INSTEAD)
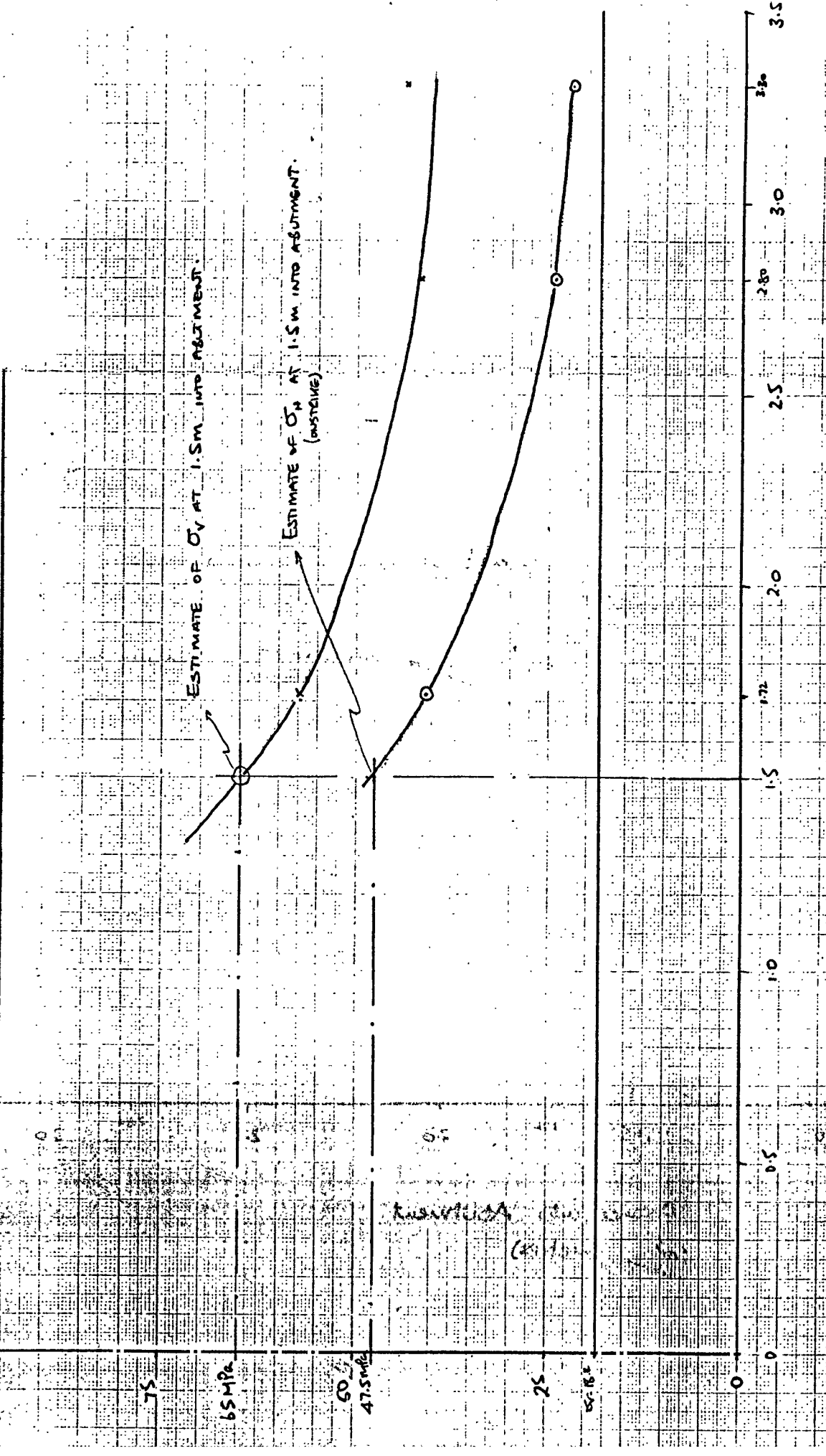
Distance into Abutment
(metres)

Figure (41).

ABSOLUTE VERTICAL STRESS CHANGE VERSUS TIME.
16 - 109 STOPE, PILLAR "B".
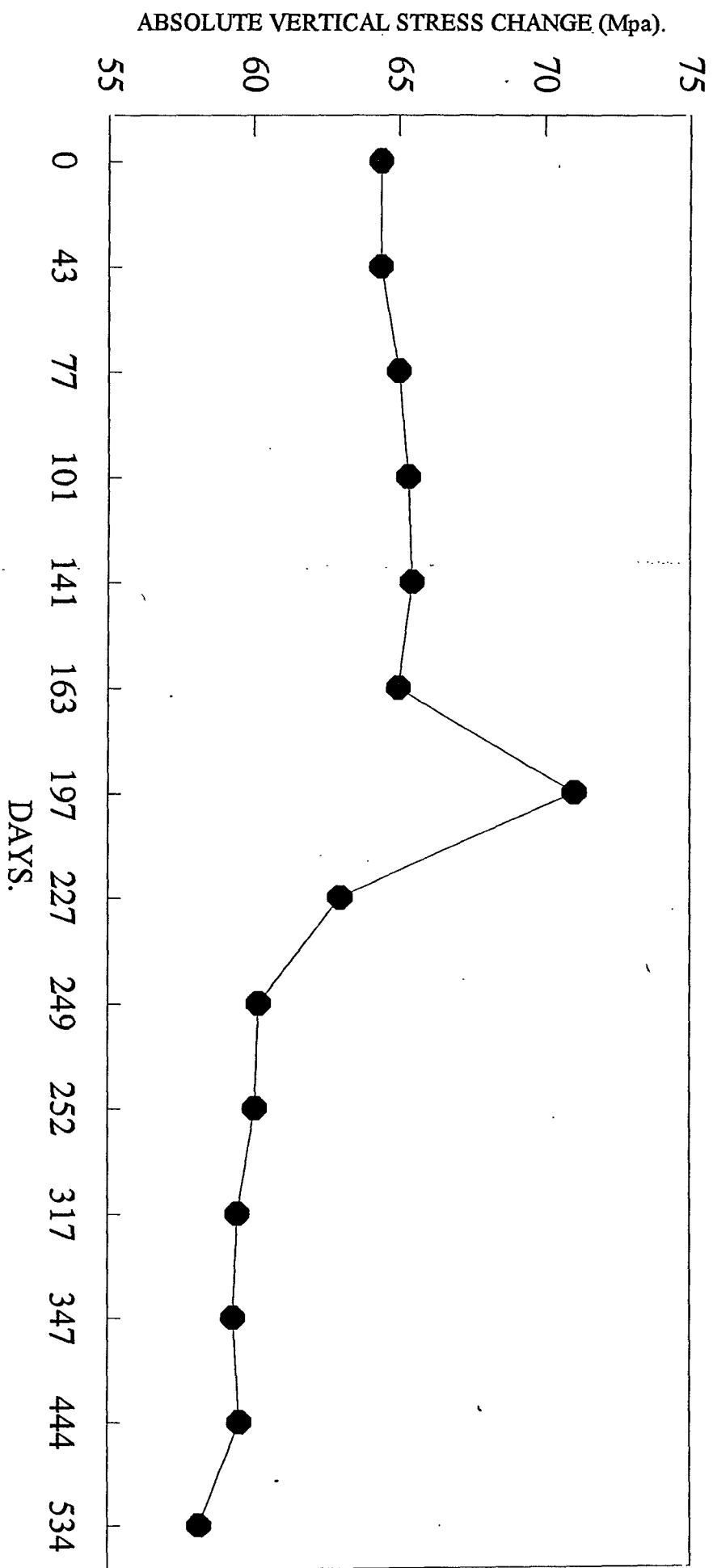
METER LOCATED 1.5m FROM PILLAR EDGE.

Figure (42).

231

ABSOLUTE VERTICAL STRESS CHANGE VERSUS TIME.
16 - 109 STOPE, PILLAR "B".
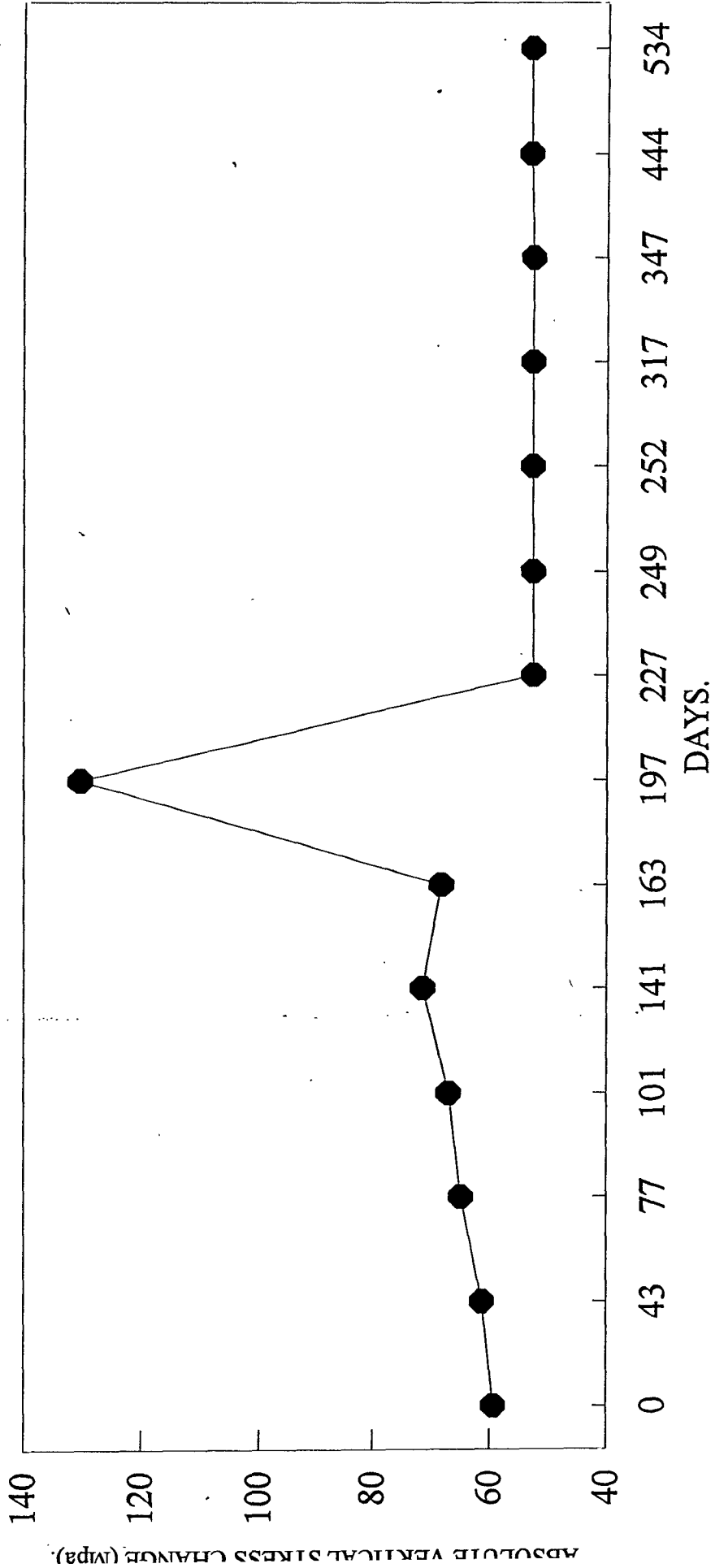
METER LOCATED 0.5m FROM PILLAR EDGE.

ABSOLUTE VERTICAL STRESS CHANGE (MPa).

140
120
100
80
60
40

0   43   77   101   141   163   197   227   249   252   317   347   444   534

DAYS.

232

ABSOLUTE HORIZONTAL STRESS CHANGE VERSUS TIME.
16 - 109 STOPE, PILLAR "B".
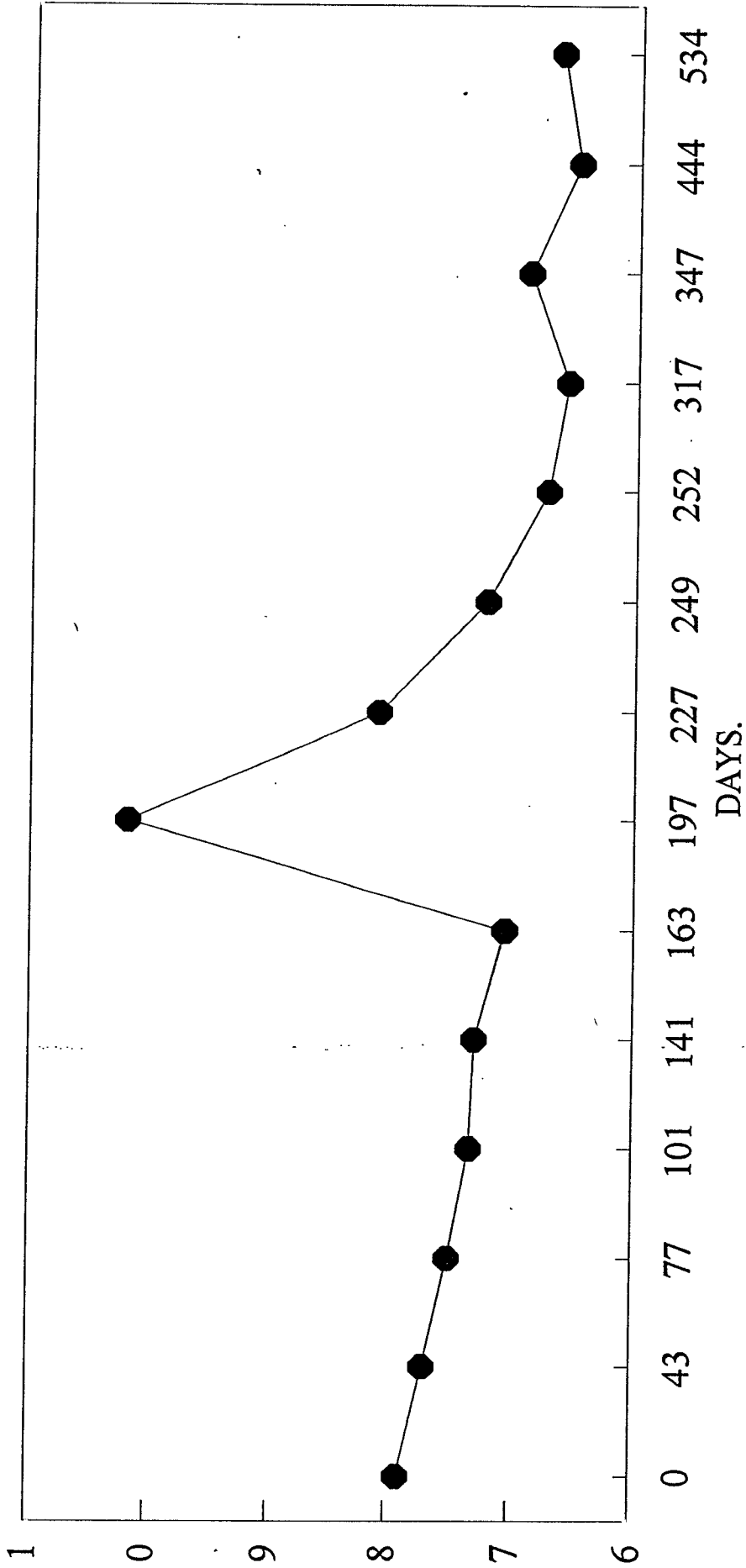
METER LOCATED 1.3m FROM PILLAR EDGE.

234

QUARTERLY CLOSURE PROFILE ADJACENT TO PILLAR "B".

QUARTERLY CLOSURE.

(CLOSURE PROFILE AT 02-03-94 IS AN ESTIMATE AT THE TIME OF CLOSURE METER INSTALLATION.)

Closure in millimetres.

Distance from pillar at top of panel 2 south.

Legend:
- 02-03-94.Panel 2S.
- 07-09-94.Panel 18s.
- 15-03-95.Panel 2s.
- 15-06-95.Panel 18s.
- + 14-06-94.Panel 2S.
- 06-12-94.Panel 2s.
- X 15-03-95.Panel 18s.
- 13-09-95.Panel 2s.
- ✳ 07-09-94.Panel 2s.
- 06-12-94.Panel 18s.
- 15-06-95.Panel 2s.
- △ 13-09-95.Panel 18s.

# PROGRESSIVE CLOSURE OF METERS ADJACENT TO PILLAR "B".

Millimetres.

Days.

- Meter B1.   + Meter B2.   ✳ Meter B3.   ▪ Meter B4.
✕ Meter B5.   ◇ Meter B6.   ◁ Meter B7.

QUARTERLY CLOSURE PROFILE ADJACENT TO PILLAR "C".

(CLOSURE PROFILE AT 15-03-94 IS AN ESTIMATE AT THE TIME OF CLOSURE METER INSTALLATION.)

Closure in millimetres.
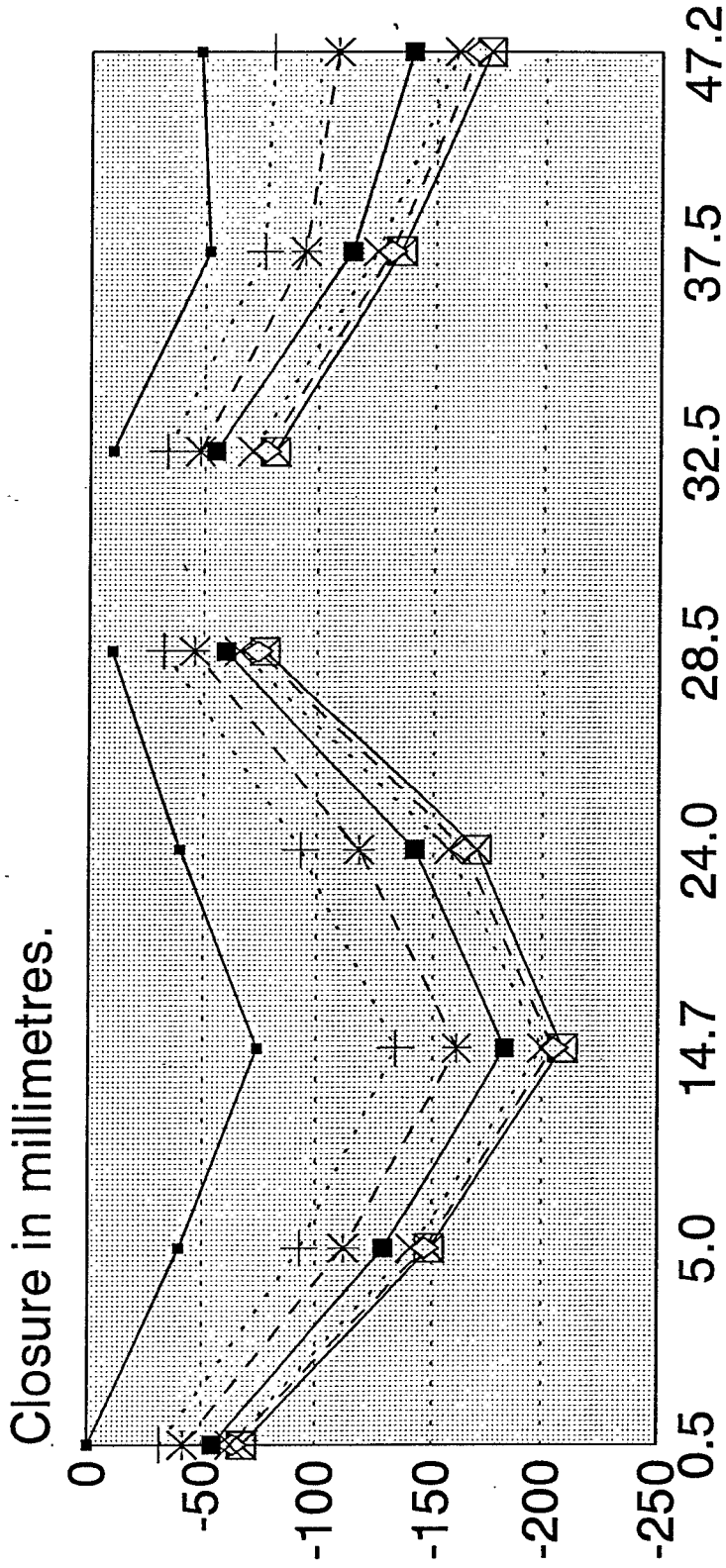
Distance from pillar at top of panel 12 south.

Legend:
- ━ 15-03-94.Panel 12s
- ━ 15-03-94.Panel 10s
- ＋ 14-06-94.Panel 10S.
- ＋ 15-03-94.Panel 12S.
- ＊ 07-09-94.Panel 12s.
- ＊ 07-09-94.Panel 10s.
- ■ 06-12-94.Panel 12s.
- ■ 06-12-94.Panel 10s.
- ✕ 10-03-95.Panel 12s.
- ✕ 10-03-95.Panel 10s.
- ◇ 09-06-95.Panel 10s.
- ◇ 09-06-95.Panel 12s.
- ⊠ 11-09-95.Panel 10s.
- ⊠ 11-09-95.Panel 12s.

PROGRESSIVE CLOSURE OF METERS ADJACENT TO PILLAR "C".

Millimetres.

Days.
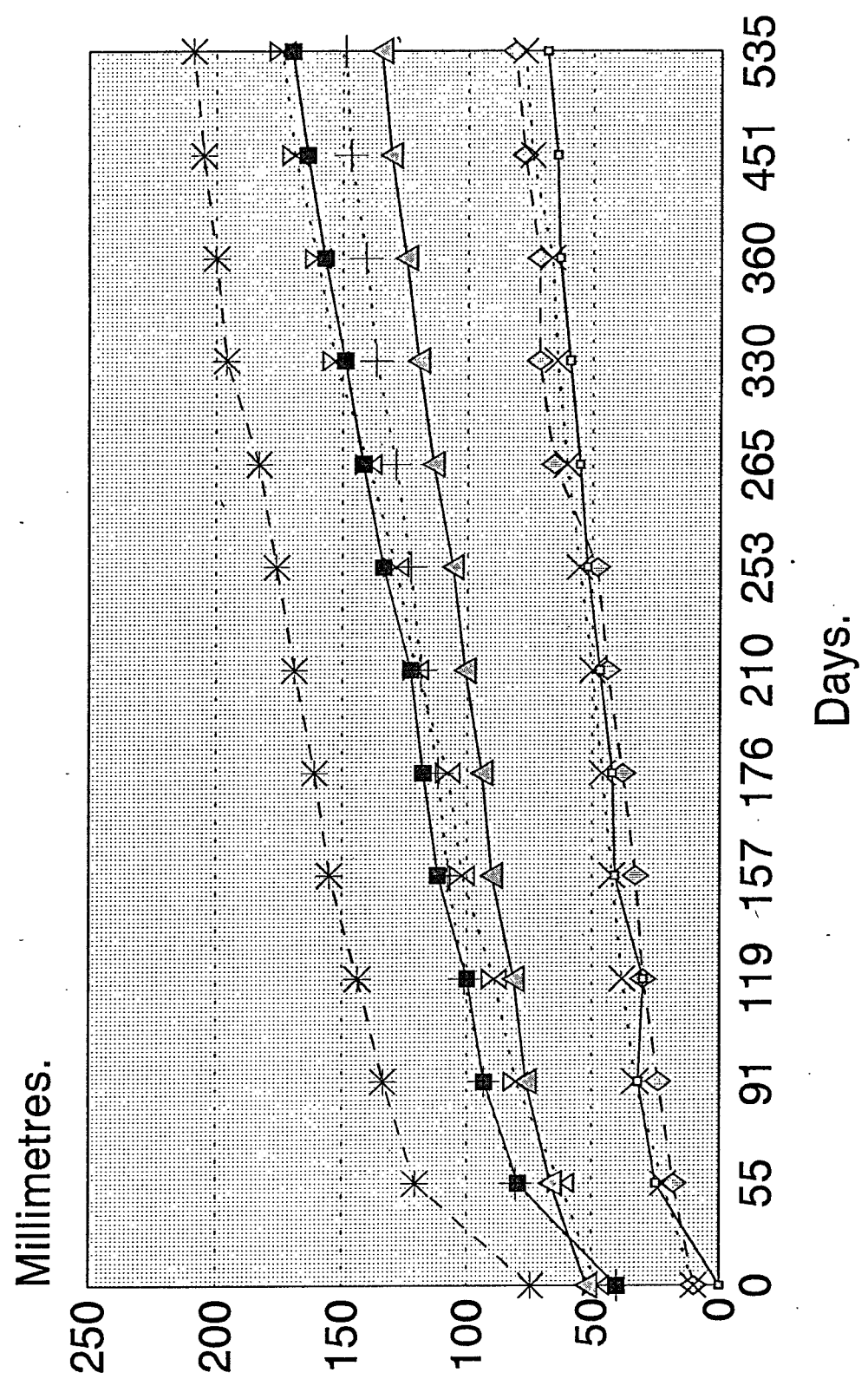
- □ - Meter C1. + Meter C2. ✳ Meter C3. ■ Meter C4.
- ✕ - Meter C5. ◇ Meter C6. ◁ Meter C7. ⊠ - Meter C8.
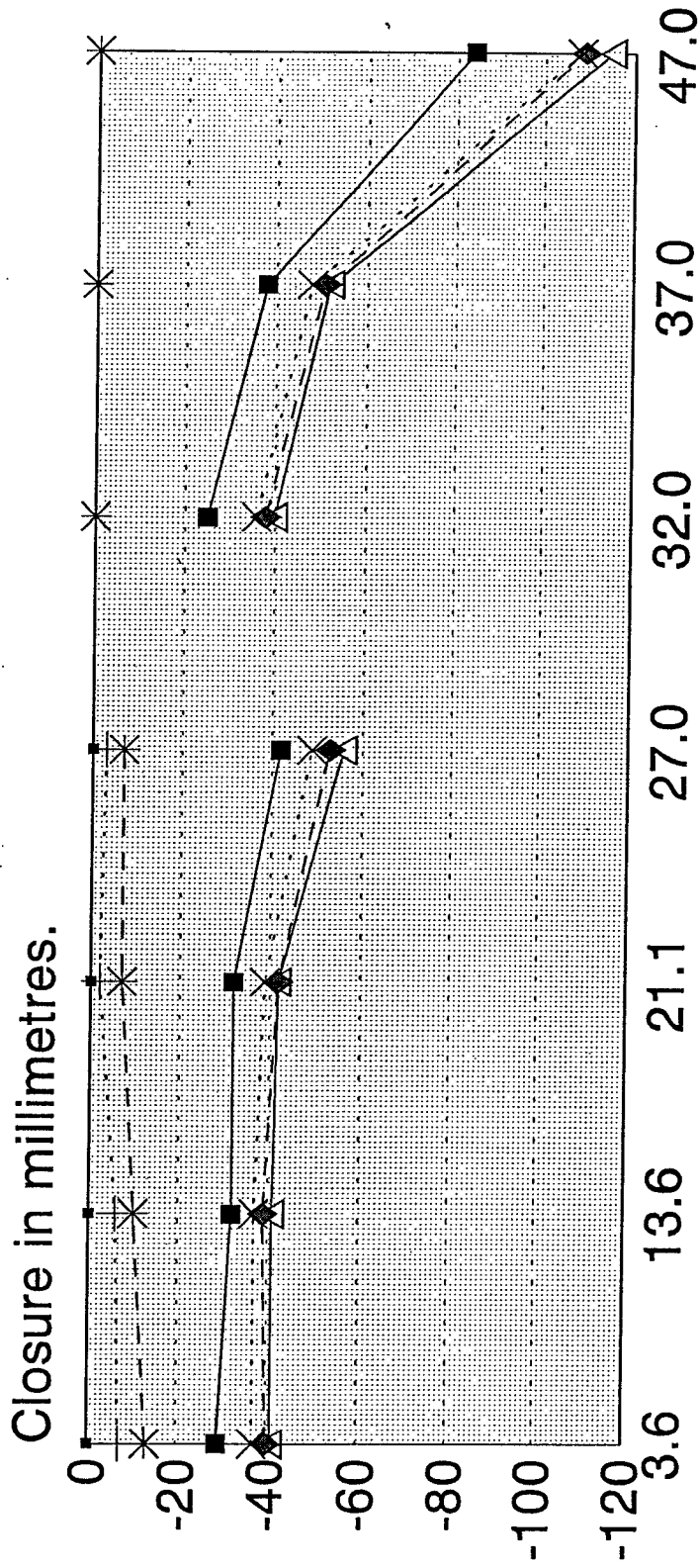
QUARTERLY CLOSURE PROFILE ADJACENT TO PILLAR "D".

QUARTERLY CLOSURE.

(CLOSURE PROFILE AT 20-04-94 IS AN ESTIMATE AT THE TIME OF CLOSURE METER INSTALLATION.)

238

Closure in millimetres.
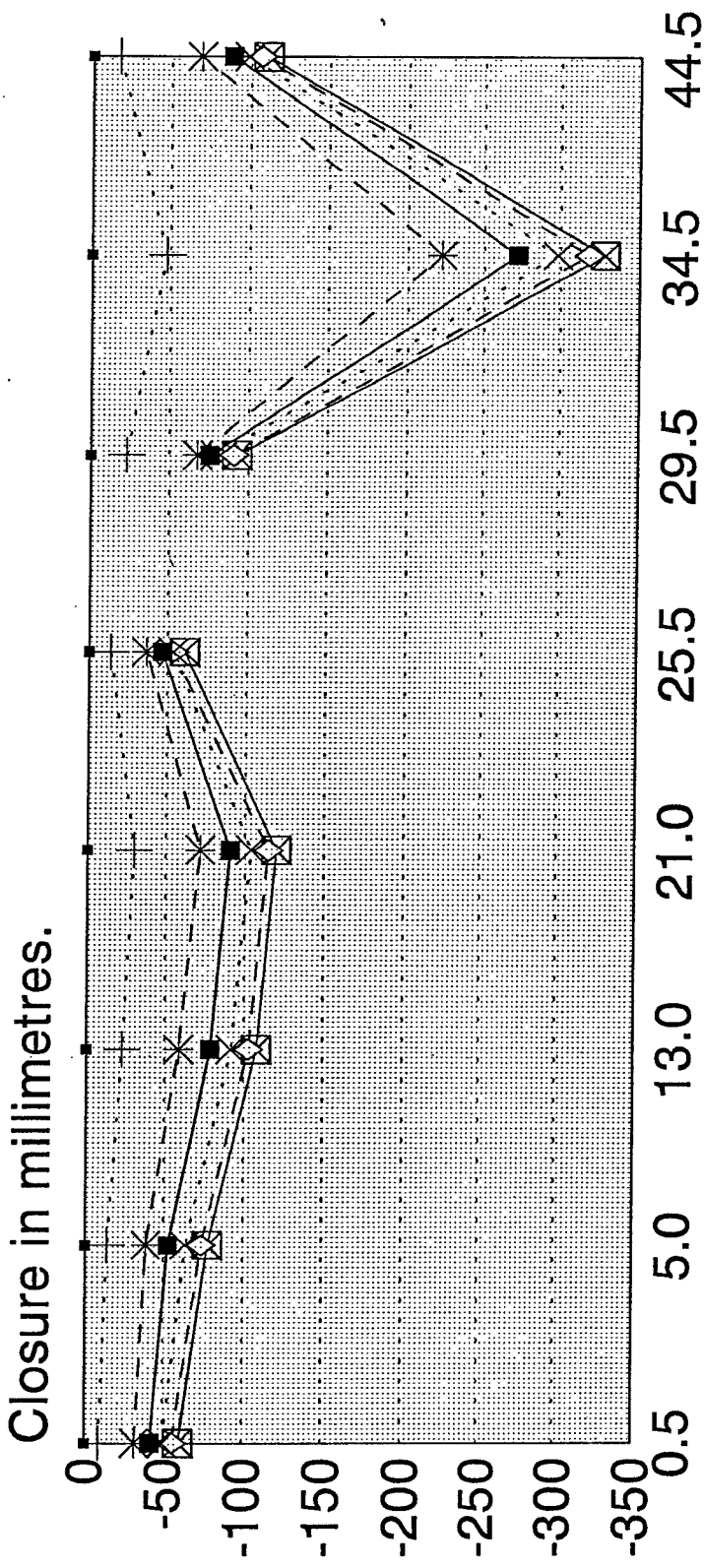
Distance from pillar at top of panel 20 south.

- 20-04-94.Panel 22s
- 20-04-94.Panel 20s
- + 14-06-94.Panel 22s.
- + 14-06-94.Panel 20s.
- ✳ 07-09-94.Panel 22s.
- ✳ 07-09-94.Panel 20s.
- ▪ 05-12-94.Panel 22s.
- ▪ 05-12-94.Panel 20s.
- ✕ 10-03-95.Panel 22s.
- ✕ 10-03-95.Panel 20s.
- ◇ 09-06-95.Panel 22s.
- ◇ 09-06-95.Panel 20s.
- ⊠ 11-09-95.Panel 20s.
- ⊠ 11-09-95.Panel 22s.

PROGRESSIVE CLOSURE OF METERS ADJACENT TO PILLAR "D".

Millimetres.

Days.
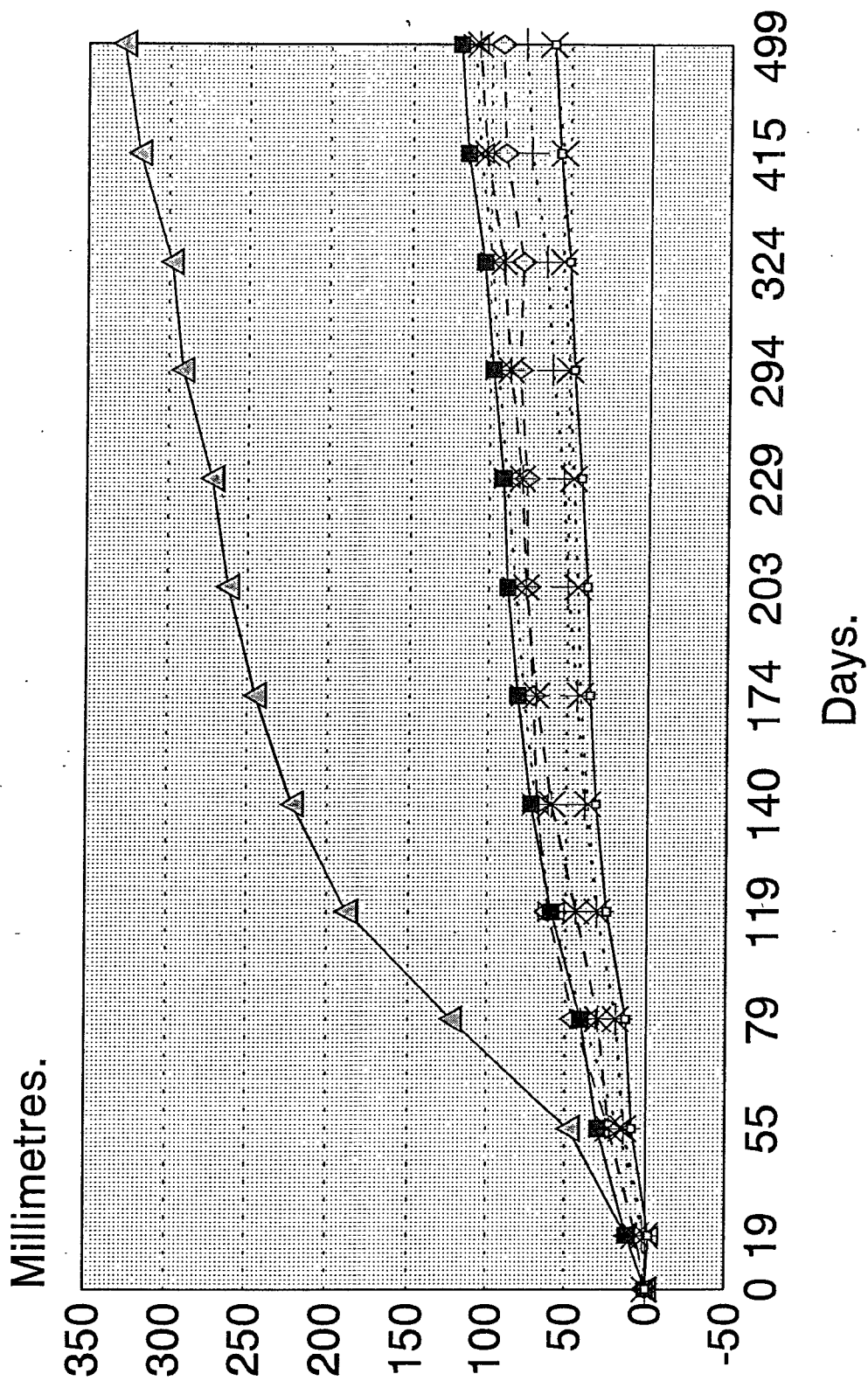
Meter D1.　+ Meter D2.　✳ Meter D3.　■ Meter D4.
✕ Meter D5.　◇ Meter D6.　△ Meter D7.　✕ Meter D8.

QUARTERLY CLOSURE PROFILE ADJACENT TO PILLAR "E".

240

QUARTERLY CLOSURE.

(CLOSURE PROFILE AT 21-06-94 IS AN ESTIMATE AT THE TIME OF CLOSURE METER INSTALLATION.)

Closure in millimetres.
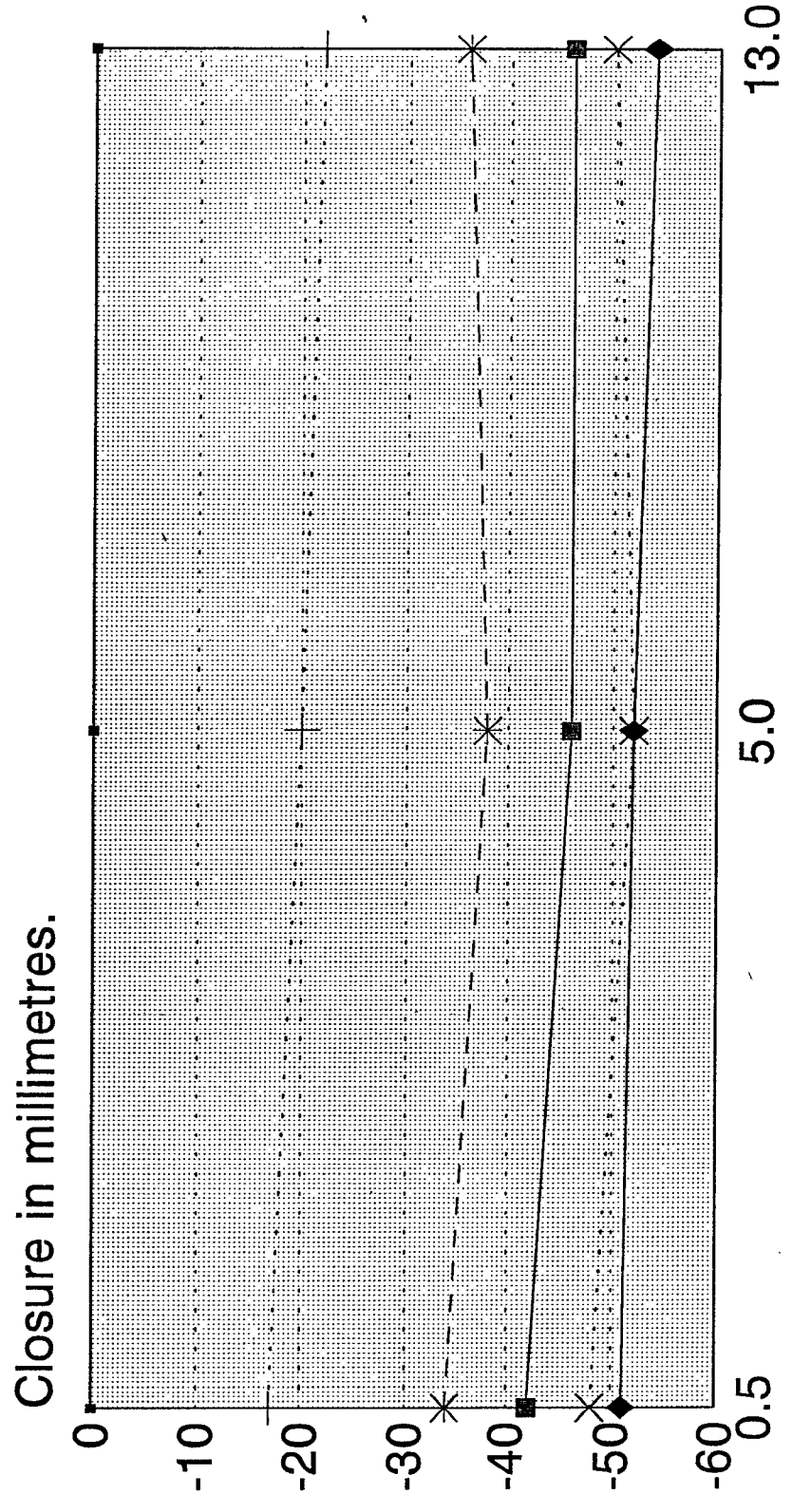
Distance from pillar at top of panel 14 south.

- 21-06-94.Panel 14s.   + 07-09-94.Panel 14s.   * 05-12-94.Panel 14s.   ◆ 11-09-95.Panel 14s.
- 10-03-95.Panel 14s.   ✕ 09-06-95.Panel 14s.

PROGRESSIVE CLOSURE OF METERS ADJACENT TO PILLAR "E".

Millimetres.

Days.
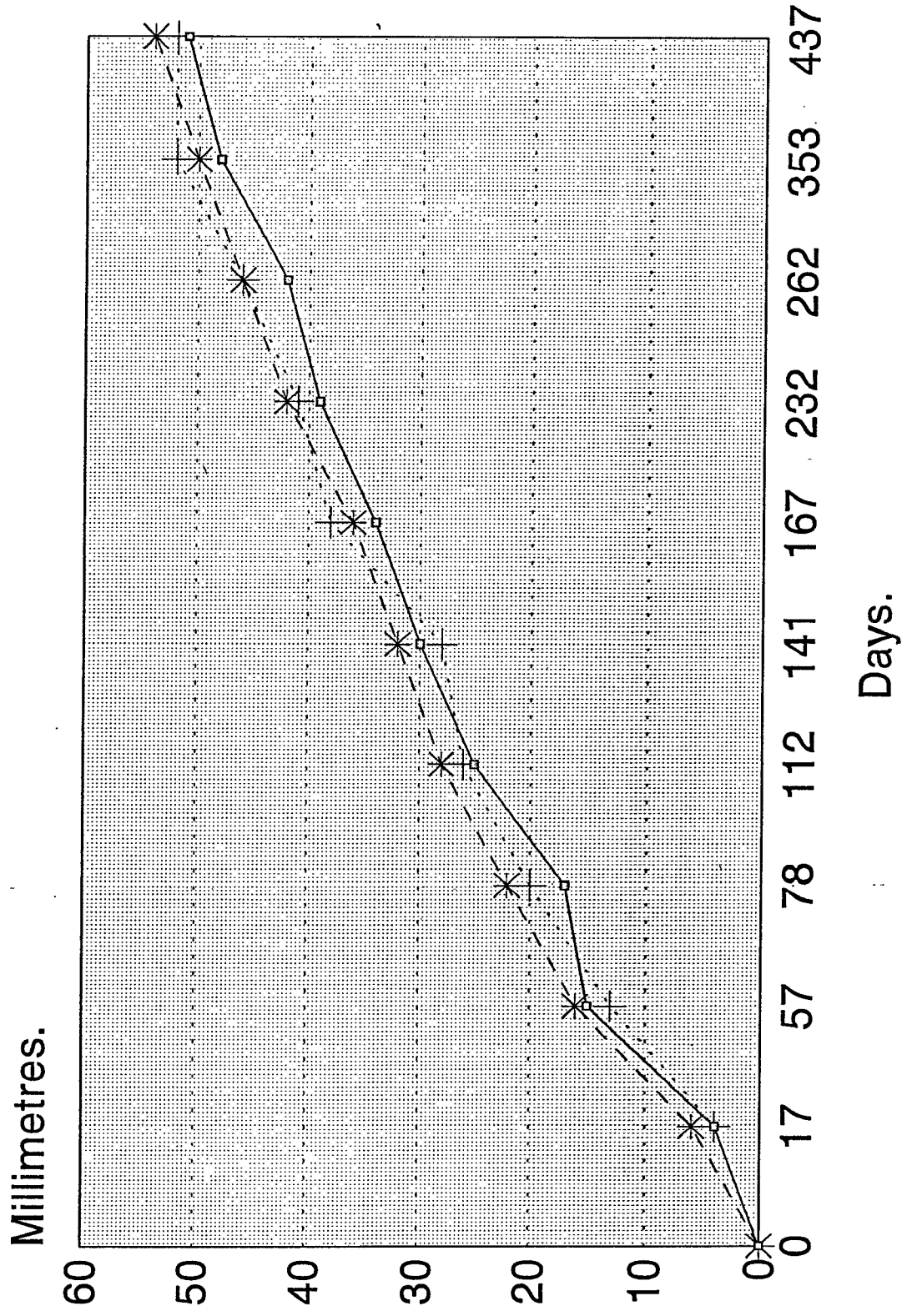
-□- Meter E3. + Meter E4. ∗ Meter E5.

HANGINGWALL EXTENSOMETER ADJACENT TO PILLAR "B".
(MOVEMENT BETWEEN ANCHORS).

Legend:
- ✳ Anchor 1 - 2.
- ◆ Anchor 2 - 3.
- ▲ Anchor 3 - 4.
- ⊕ Anchor 4.

MOVEMENT (mm).

DAYS.
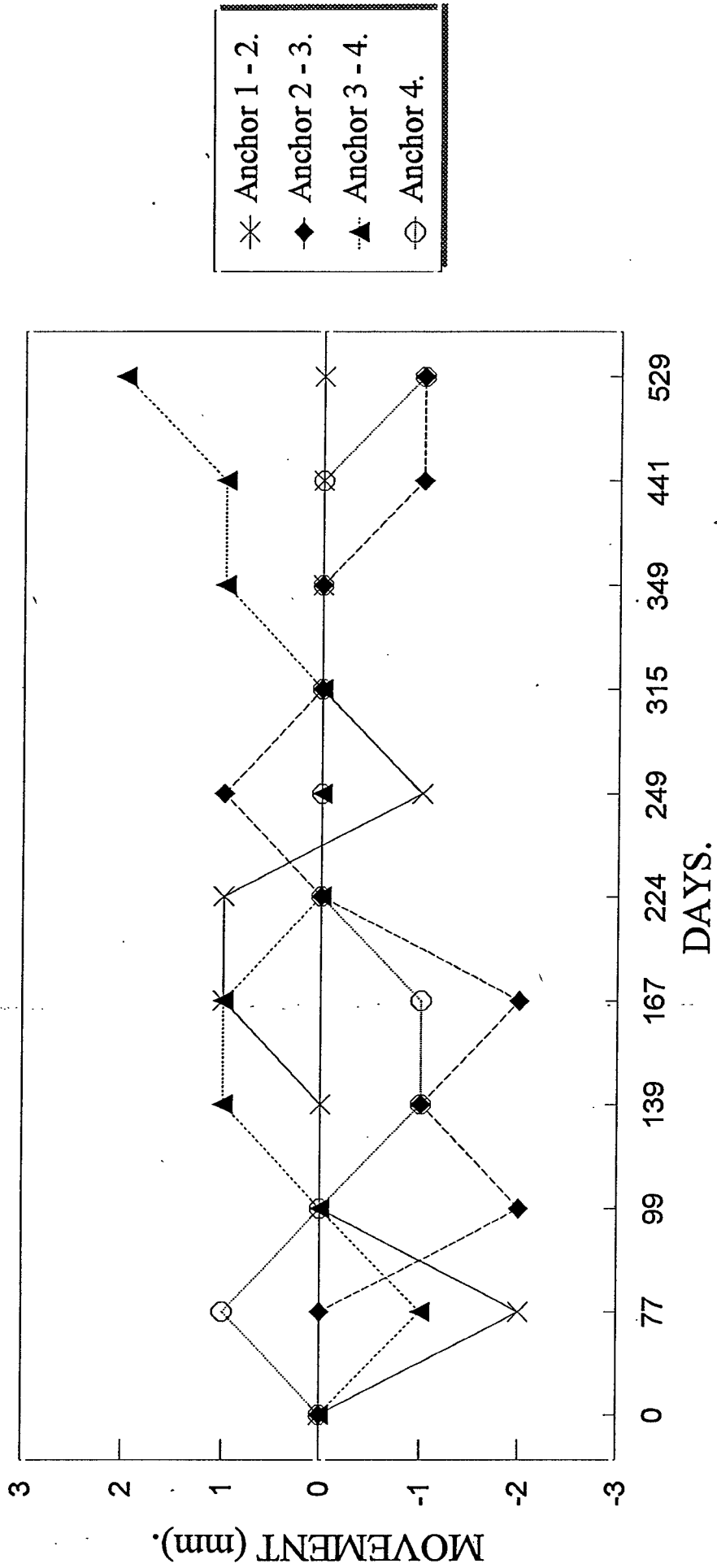
HANGINGWALL EXTENSOMETER ADJACENT TO PILLAR E. (MOVEMENT BETWEEN ANCHORS).
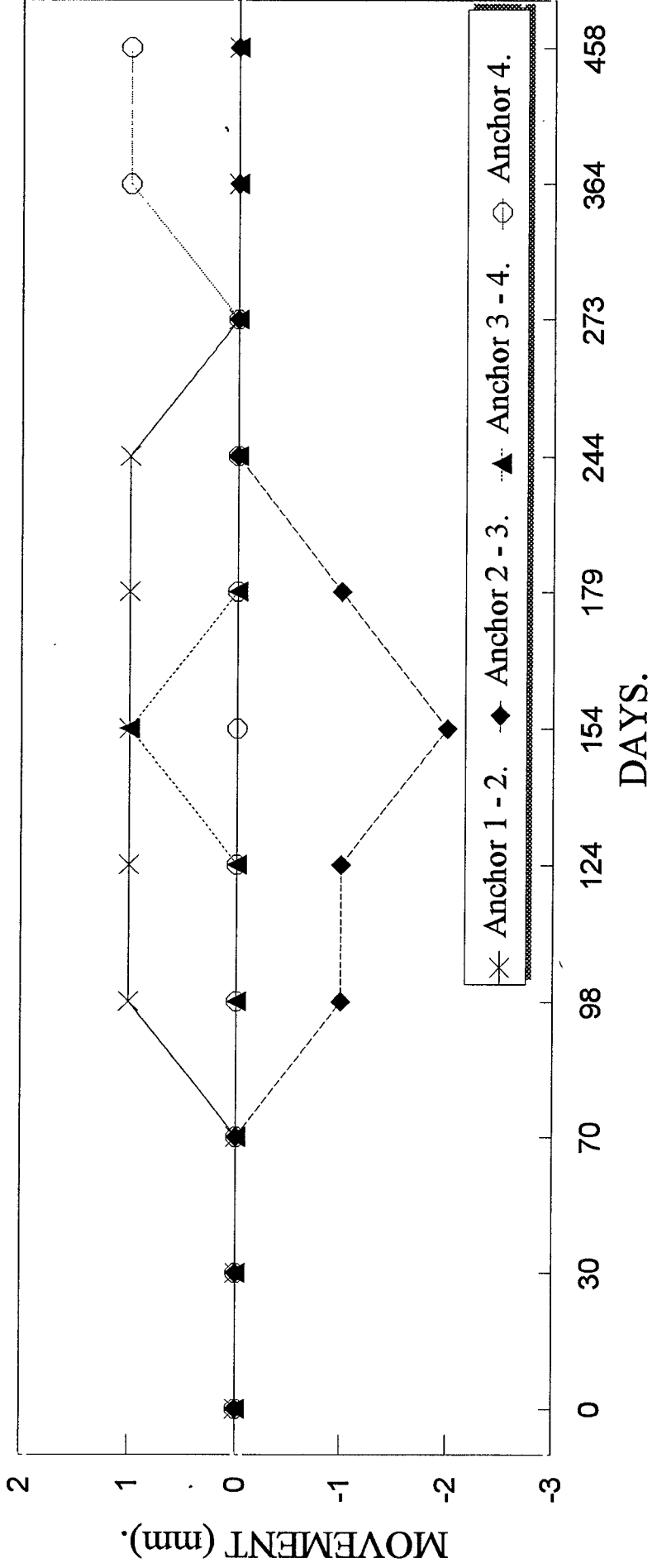
Legend: — Anchor 1 - 2.   ◆ Anchor 2 - 3.   ▲ Anchor 3 - 4.   ⊕ Anchor 4.

A negative movement denotes a shortening.
A positive movement denotes an opening up.

MOVEMENT (mm). — y-axis: 2, 1, 0, -1, -2, -3

DAYS. — x-axis: 0, 30, 70, 98, 124, 154, 179, 244, 273, 364, 458

PLOT OF PROGRESSIVE CLOSURE OCCURRING ADJACENT TO EXTENSOMETER IN 16-108 CENTRE GULLY.

Vertical closure (mm).

Days.
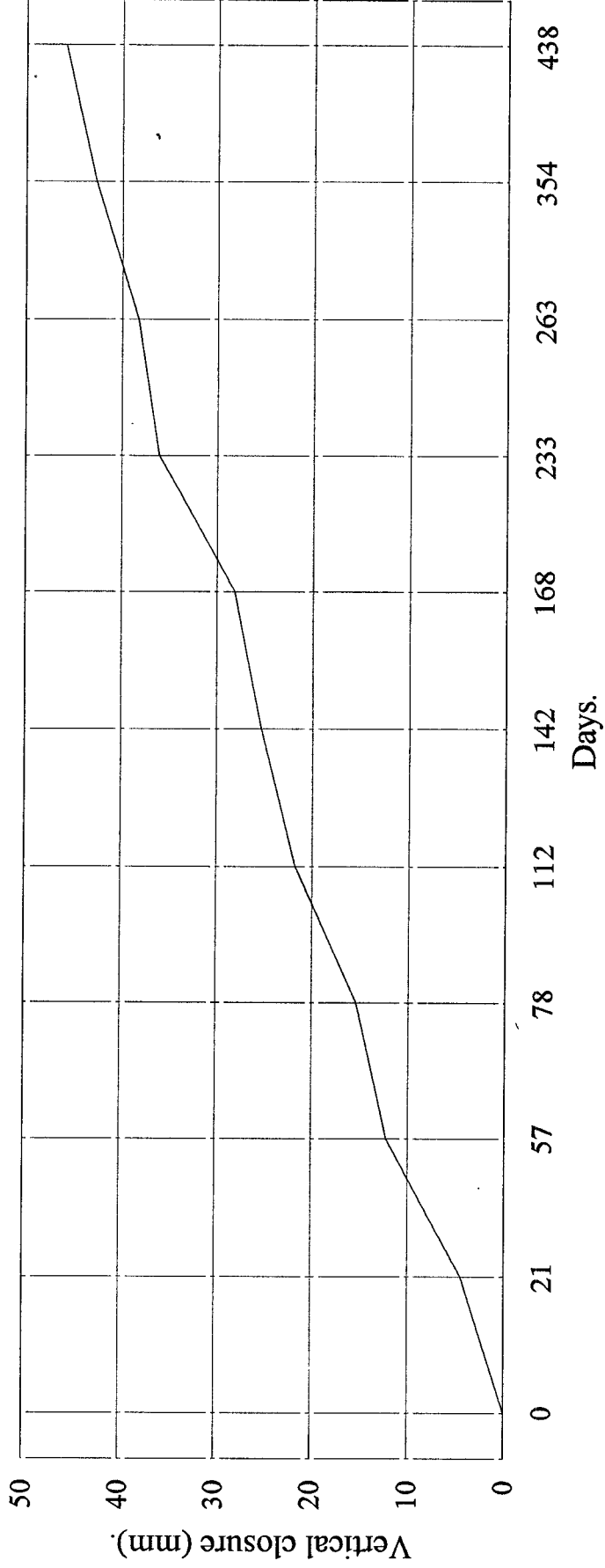
— Meter F1.

ABSOLUTE VERTICAL STRESS CHANGE VERSUS TIME.
CUBBY BETWEEN 15-108 AND 15-107.

245
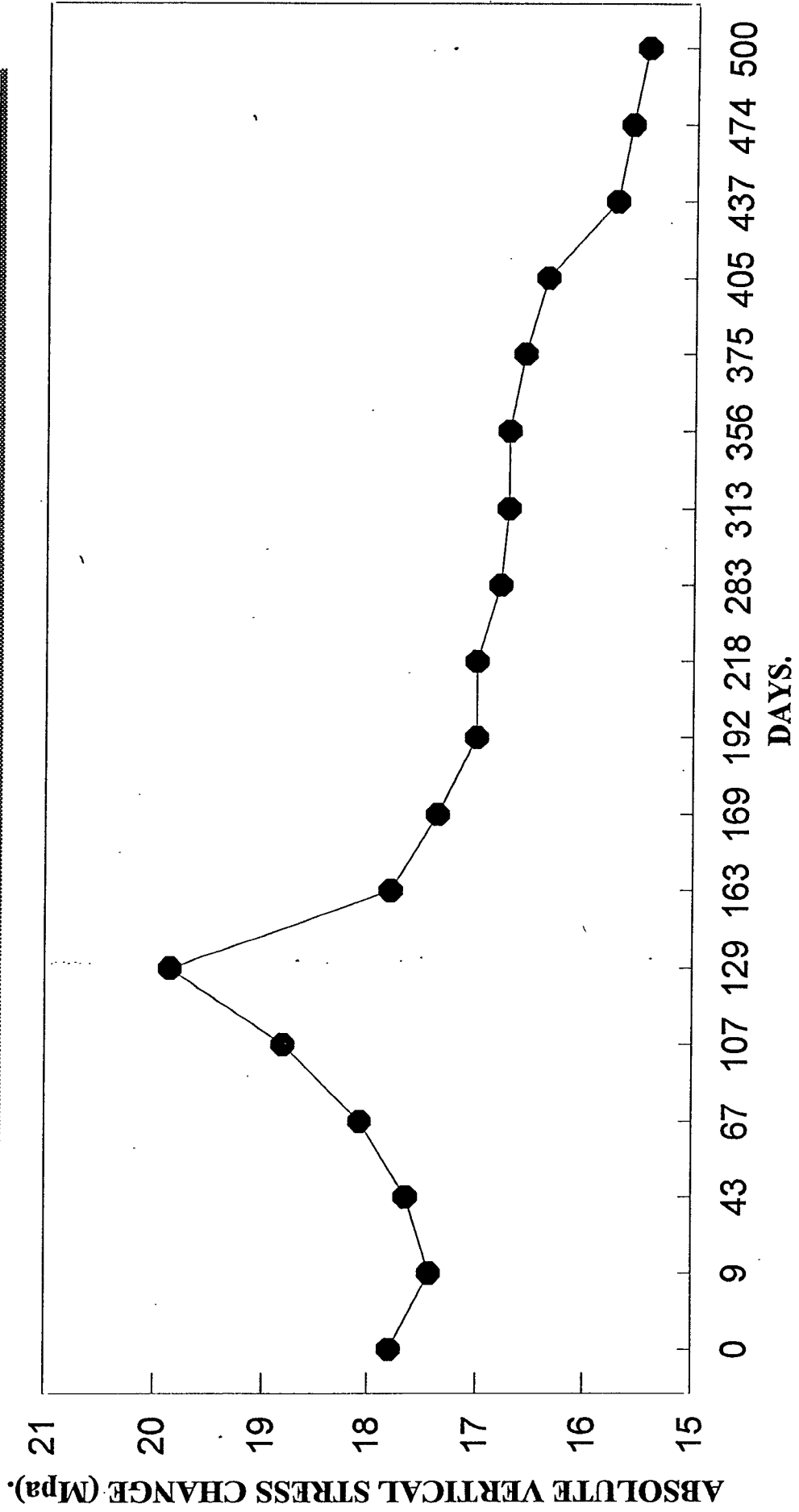
ABSOLUTE VERTICAL STRESS CHANGE VERSUS TIME.
15-107 LAYBYE.
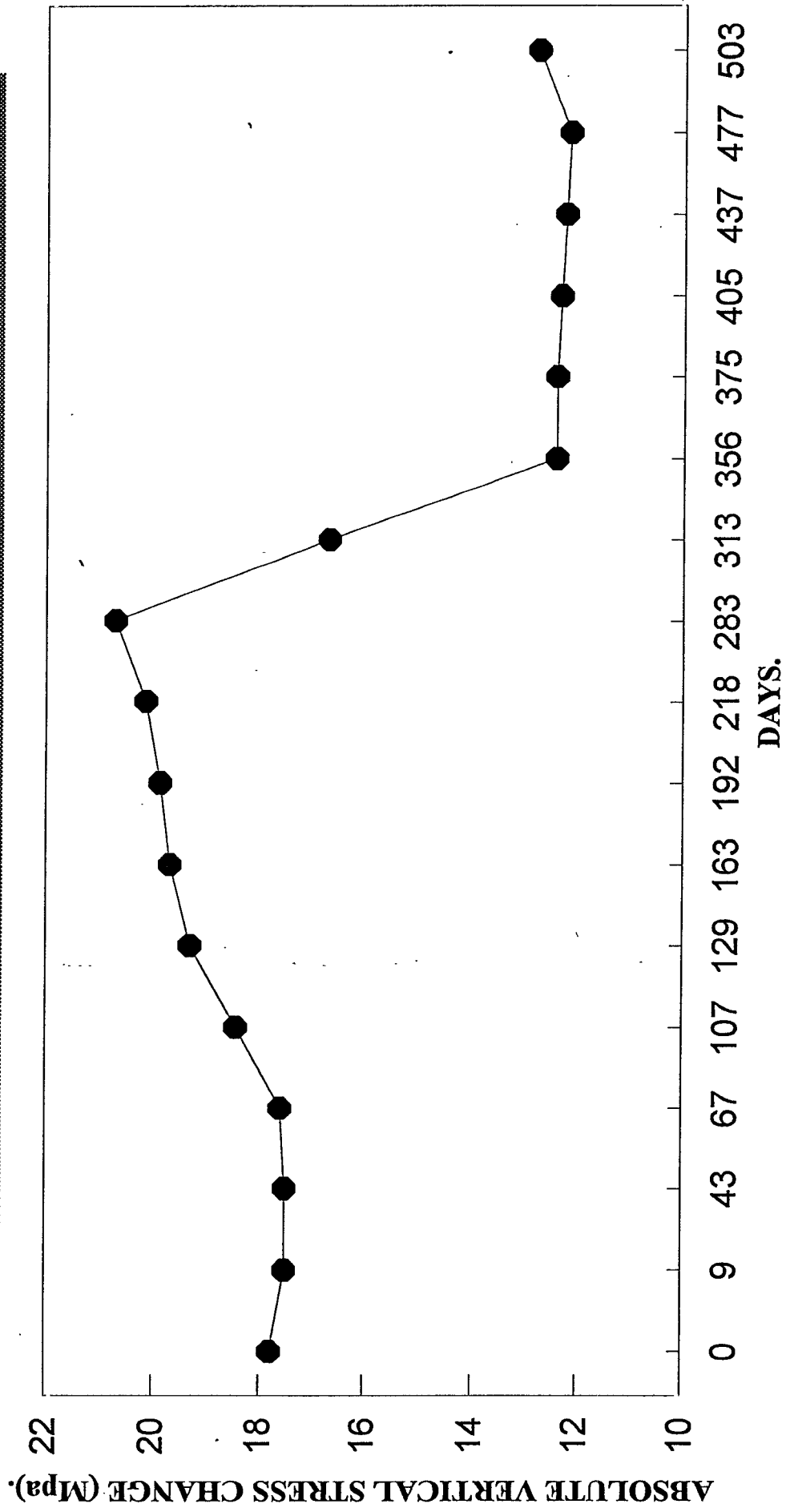
ABSOLUTE VERTICAL STRESS CHANGE VERSUS TIME.
15 SOUTH DRIVE REFUGE BAY.

Chart: Absolute Vertical Stress Change (MPa) versus Days. The y-axis ranges from 10 to 20 MPa; the x-axis shows days at 0, 11, 53, 72, 102, 134, 174, 200.
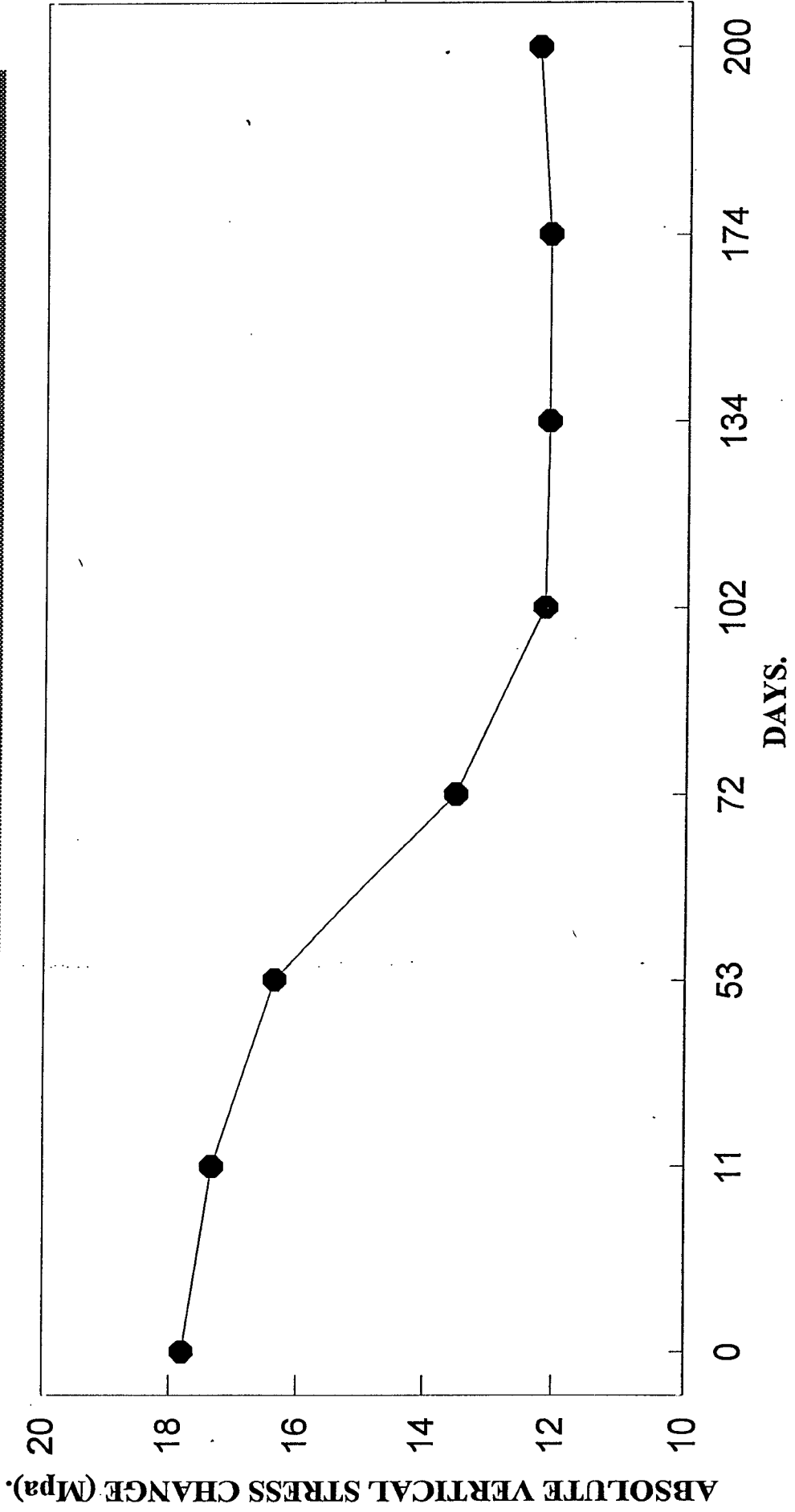
ABSOLUTE VERTICAL STRESS CHANGE VERSUS TIME.
15 - 106 LAYBYE.

248

X-axis: DAYS. (0, 11, 53, 72, 102, 134, 174, 200)

Y-axis: ABSOLUTE VERTICAL STRESS CHANGE (Mpa). (10, 12, 14, 16, 18, 20)
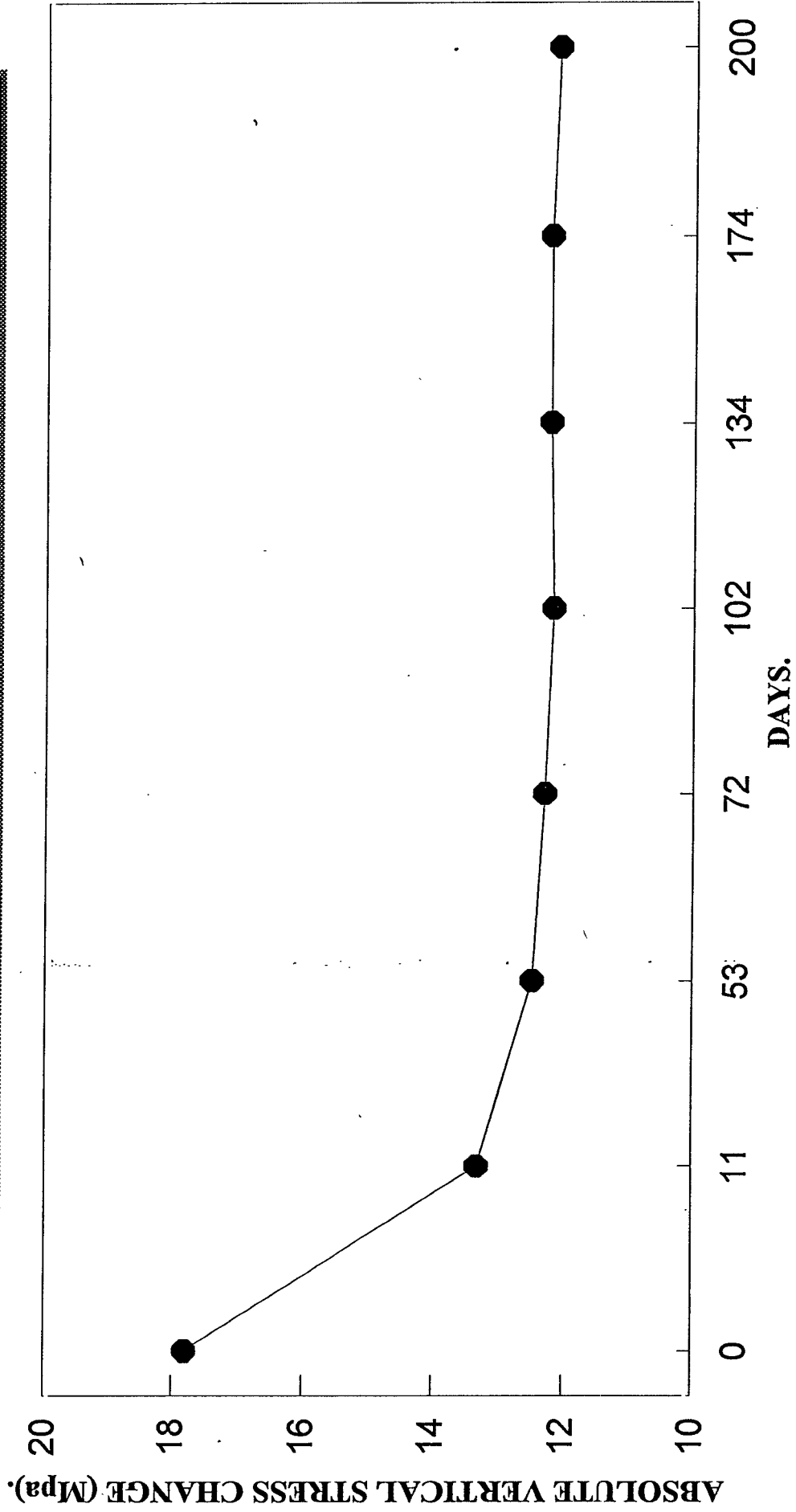
ABSOLUTE VERTICAL STRESS CHANGE VERSUS TIME.

16 SOUTH DRIVE.

ABSOLUTE VERTICAL STRESS CHANGE (Mpa).

DAYS.

250
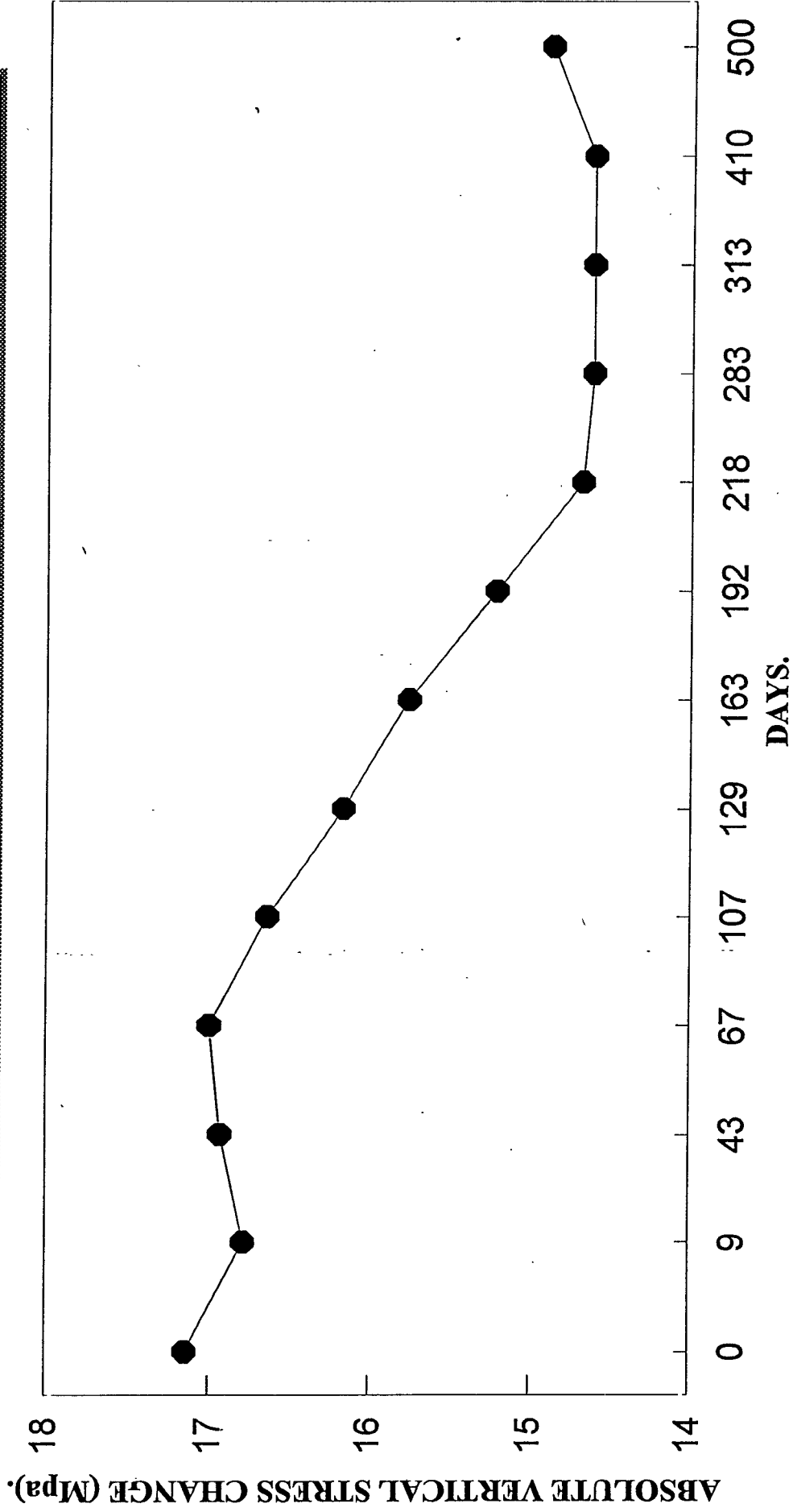
FOOTWALL EXTENSOMETER ON 16 SOUTH DRIVE BETWEEN THE 109 AND 108 RAISE LINES.. (MOVEMENT BETWEEN ANCHORS).
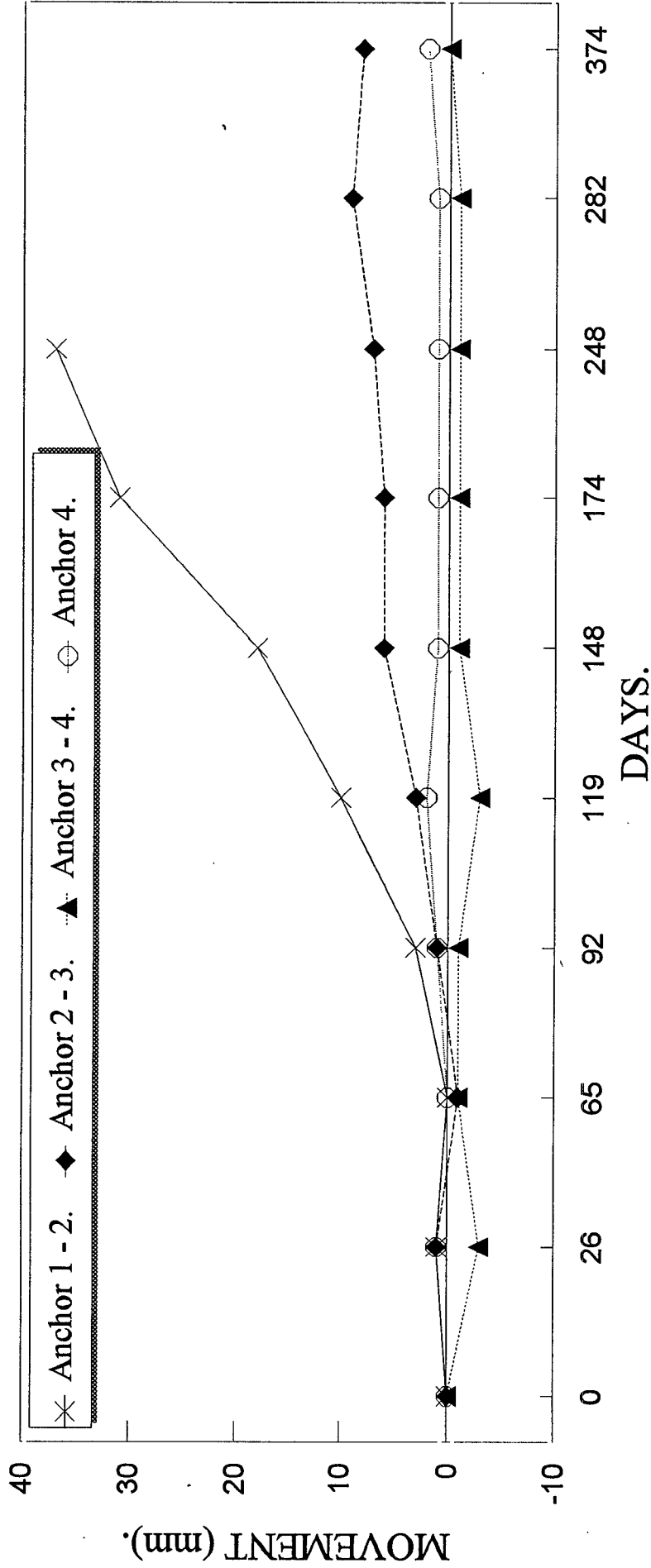
A negative movement denotes a shortening.
A positive movement denotes an opening up.

Legend:
✳ Anchor 1 - 2.   ◆ Anchor 2 - 3.   ▲ Anchor 3 - 4.   ⊙ Anchor 4.

X-axis: DAYS (0, 26, 65, 92, 119, 148, 174, 248, 282, 374)
Y-axis: MOVEMENT (mm) (-10, 0, 10, 20, 30, 40)

SCOPE OBSERVATIONS FOR PILLAR A: (GULLY 2s, 16-109 SLOPE):

22/3/94 — INITIAL OBSERVATIONS.
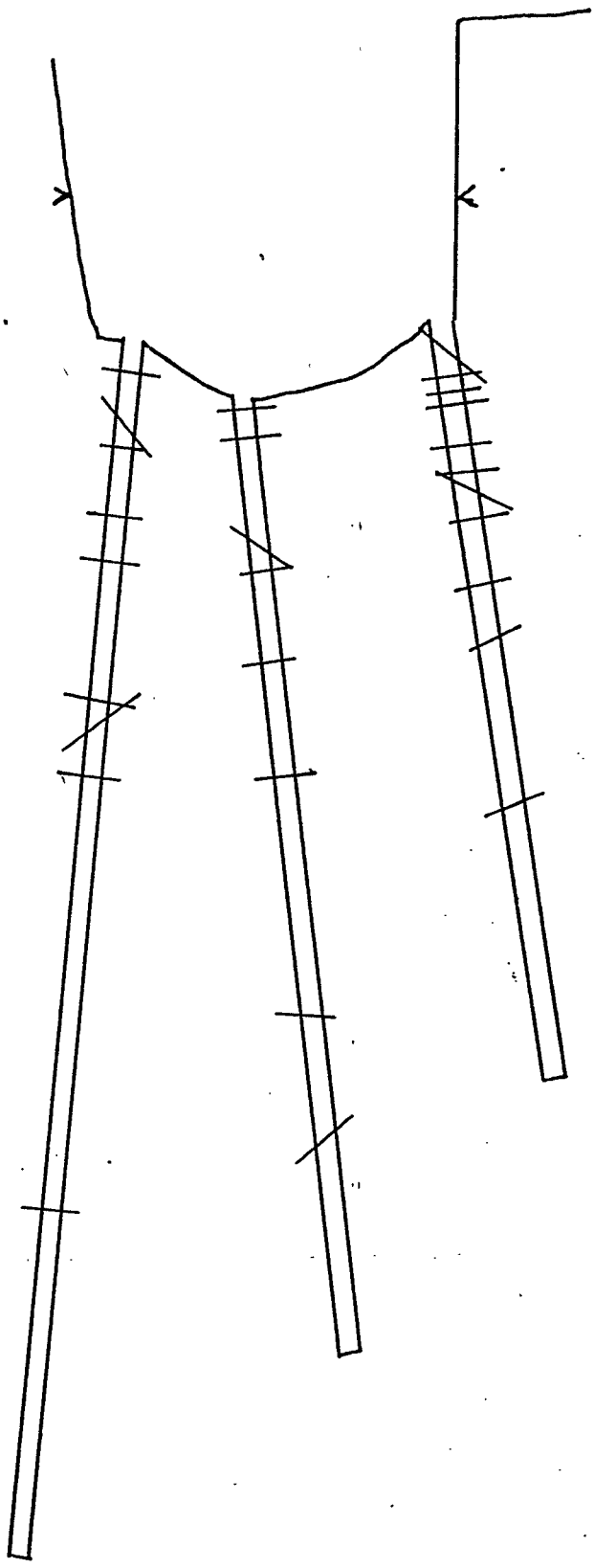
SCOPE OBSERVATIONS FOR PILLAR A : (GULLY 2S, 16-109 S   E):

13/7/94 - 4ᵗʰ OBSERVATIONS.
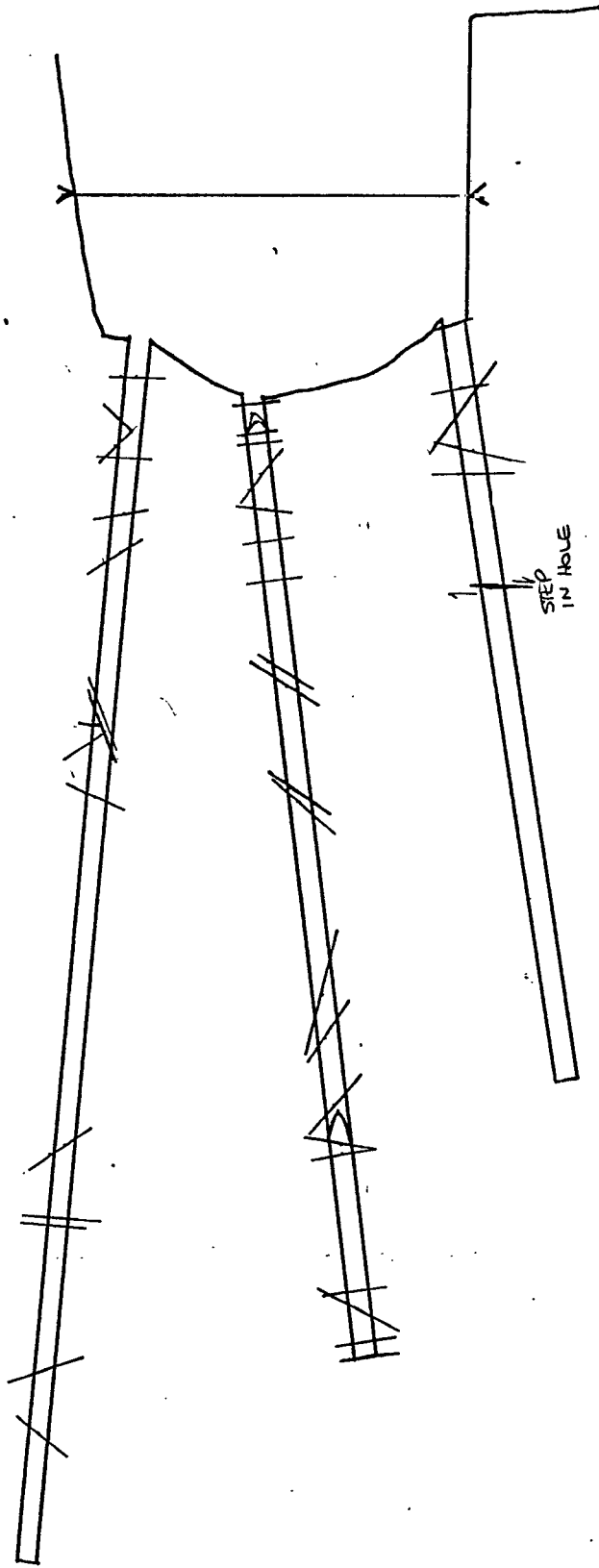
STEP
IN HOLE

SCOPE OBSERVATIONS FOR PILLAR 4 (GULLY 2S, 16-109 STOPE)

23/3/94 - INITIAL OBSERVATIONS.

SCOPE OBSERVATIONS FOR PILLAR F (GULLY 2S, 16-109 STOPE)

16/9/94 (1st READING).

OPEN
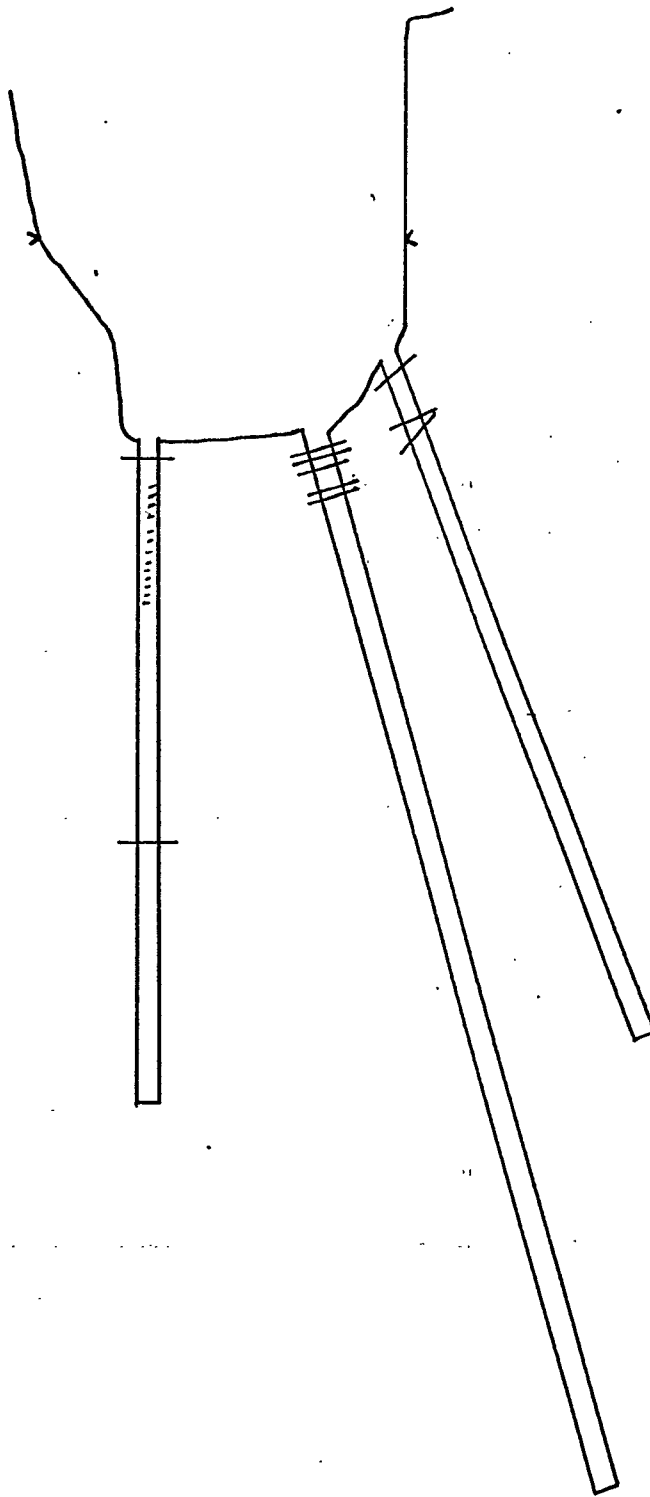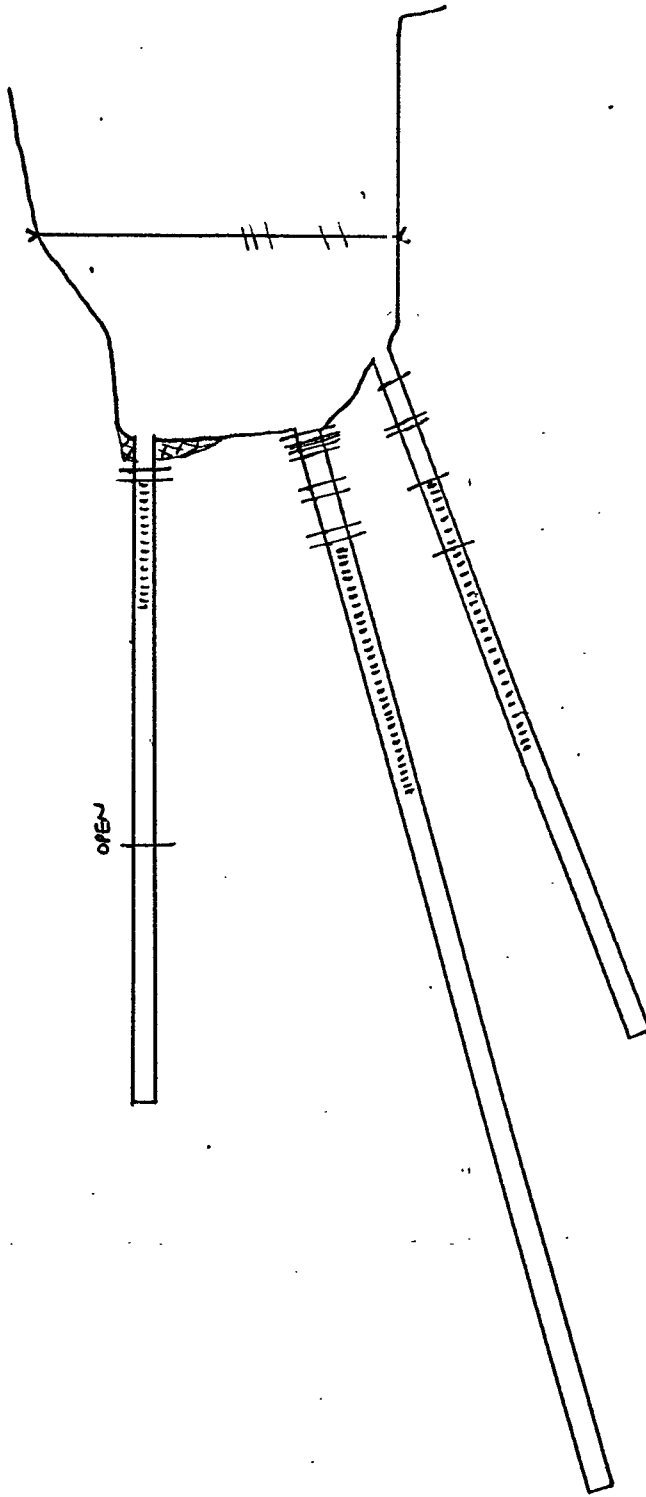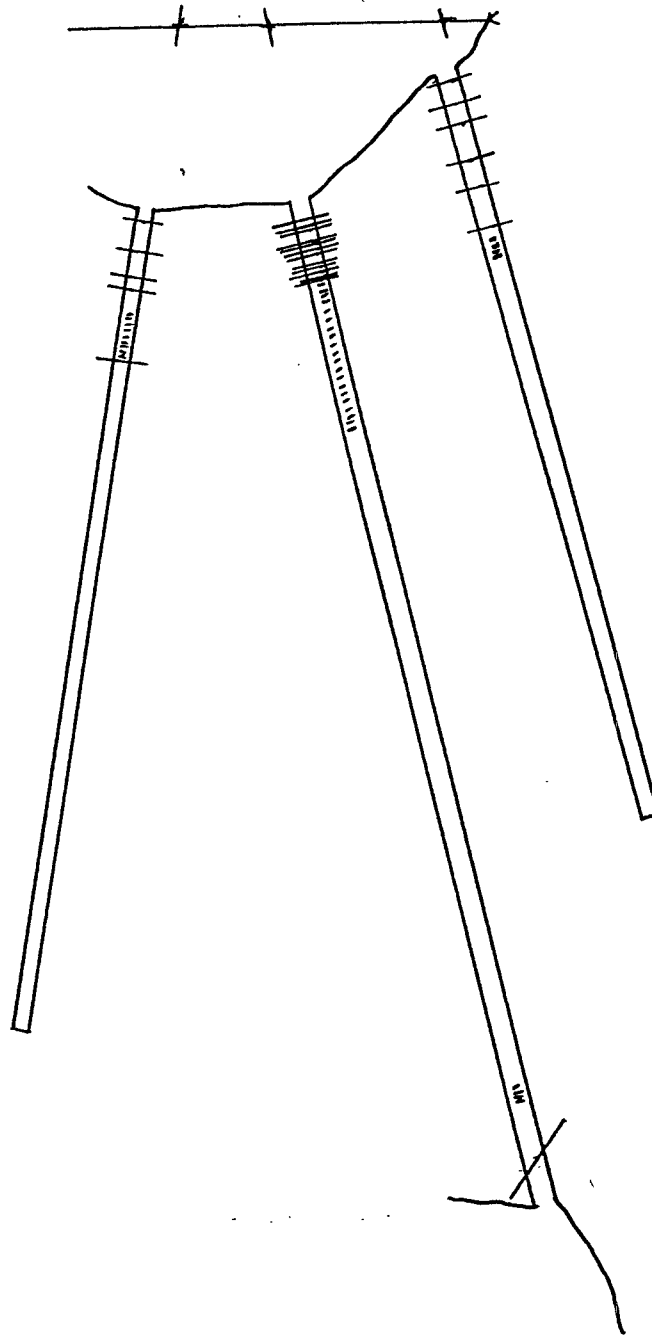
re: 3/5/94 - INITIAL READINGS.

SCALED OUT

STOPIN HOLE

STOPE HOLE (ANTI GAS) PERCED PASSED

MAJOR STOPIN HOLE GAS (ANT GAS) PERCED PASSED

HOLE CLEARED FROM BOTTOM SIDE

DATE: 13/6/94 - 2ND OBSERVATIONS.
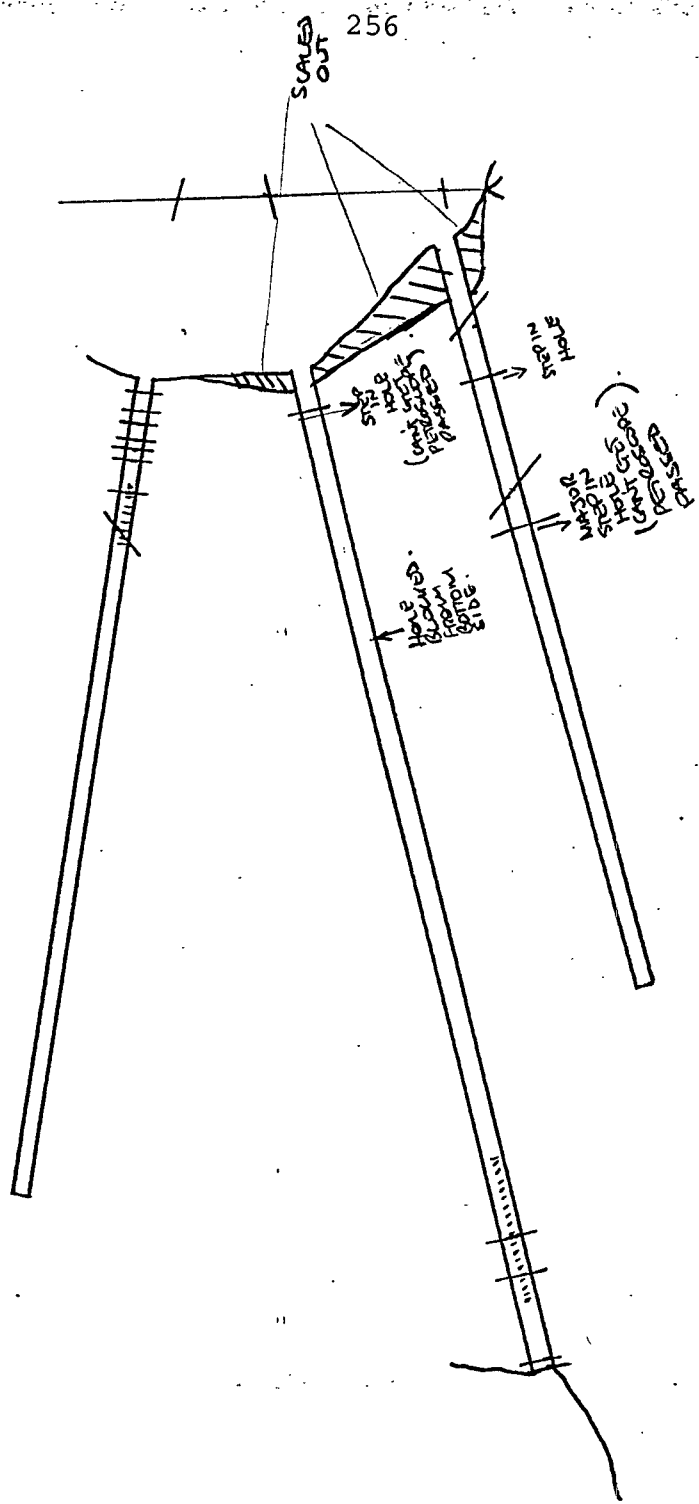
OVERALL VIEW OF RESEARCH APPROACH
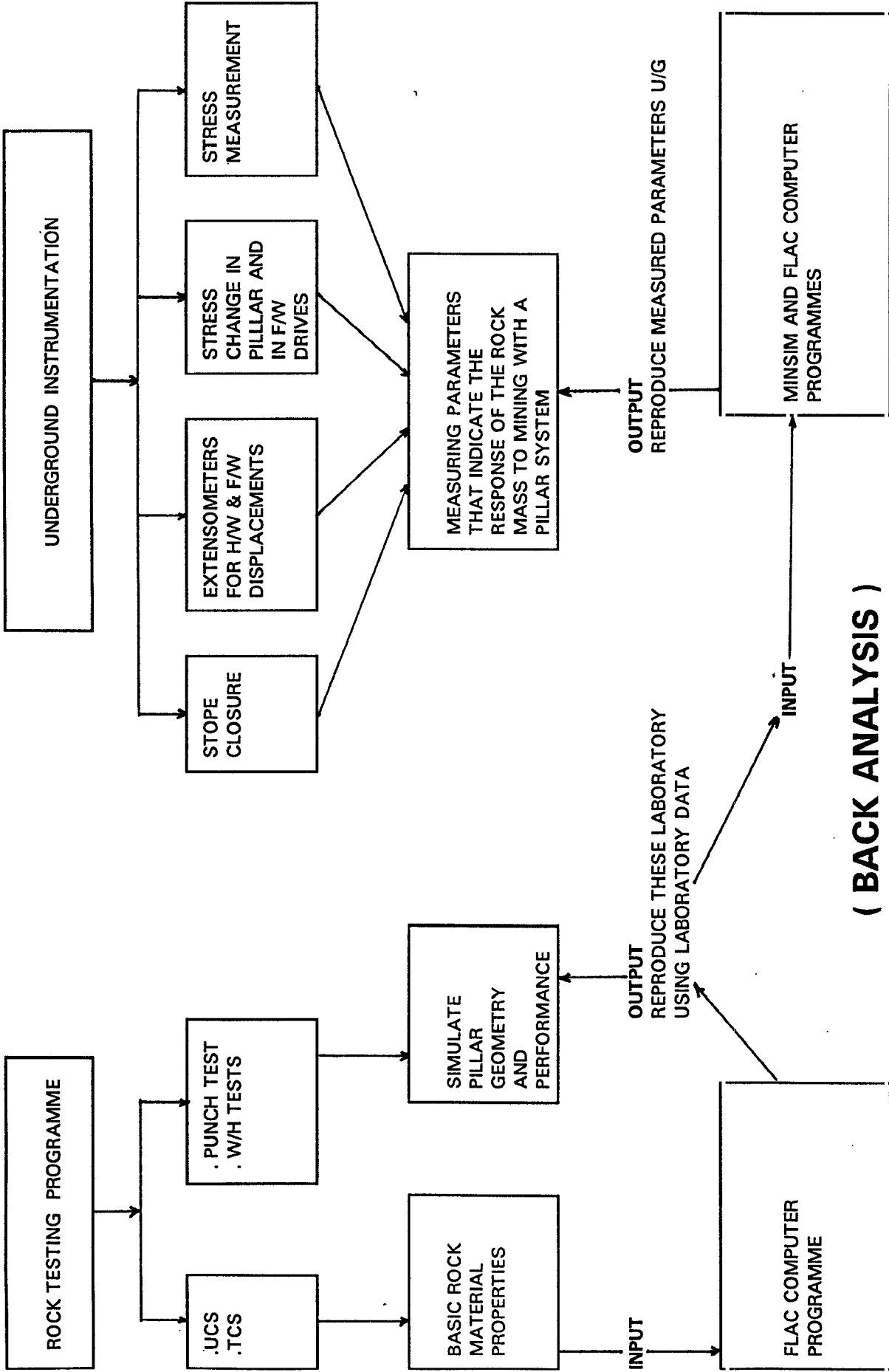
IMPROVED PILLAR DESIGN TECHNIQUES

(BACK ANALYSIS)

APPENDIX (7)

Photographs.

Photograph 1 : Example of a triaxial test specimen.
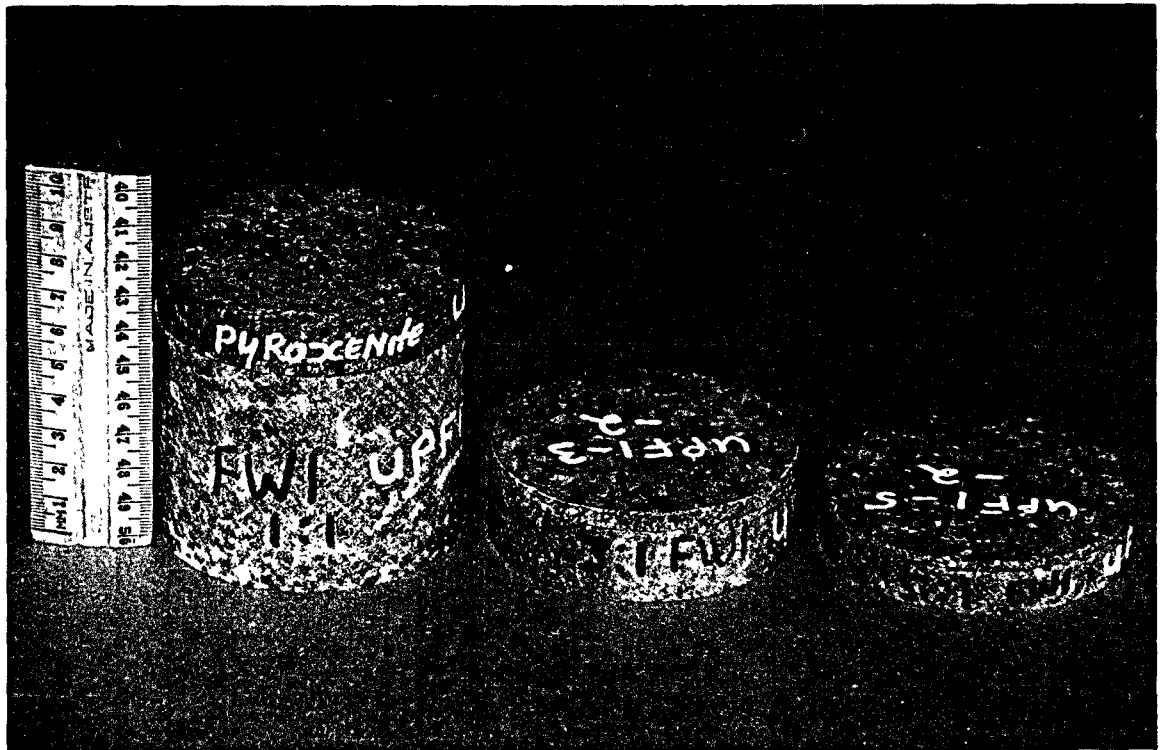
Photograph 2 : Example of three width to height ratio test specimens.
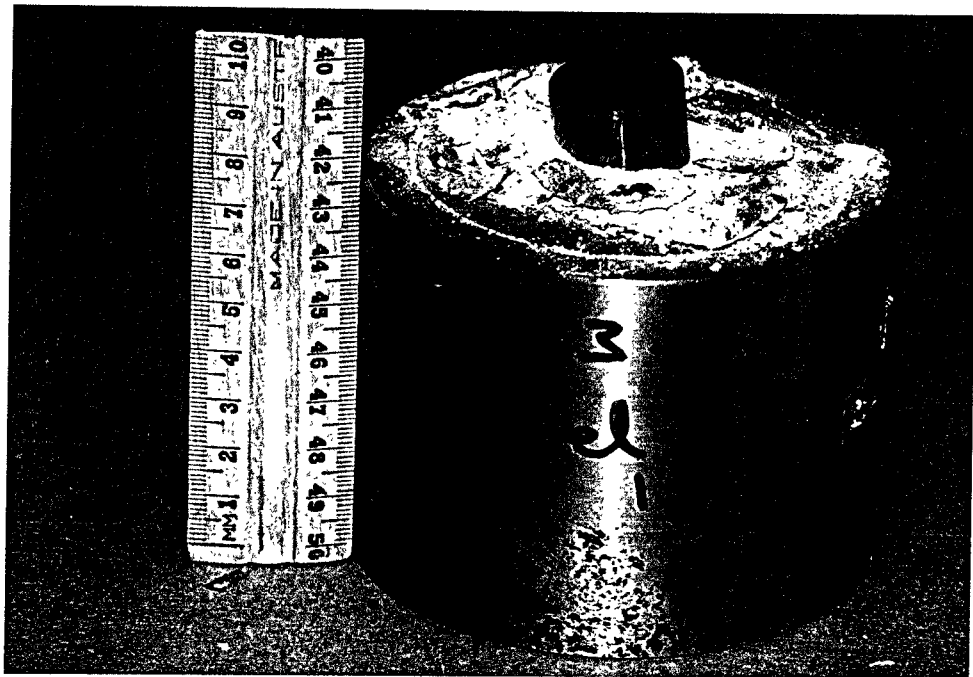
Photograph 3 :   Example of a punch test showing the penetration of the steel punch into the confined footwall rock type.
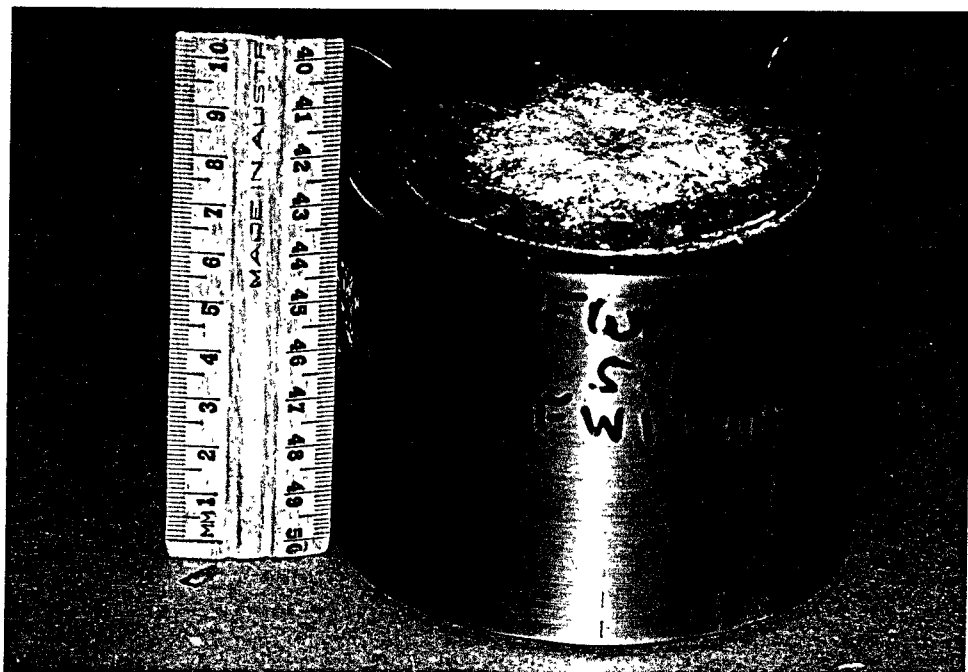
Photograph 4 :   Example of a punch test showing the results of a footwall 1 punch at a width to height ratio of 5:1.
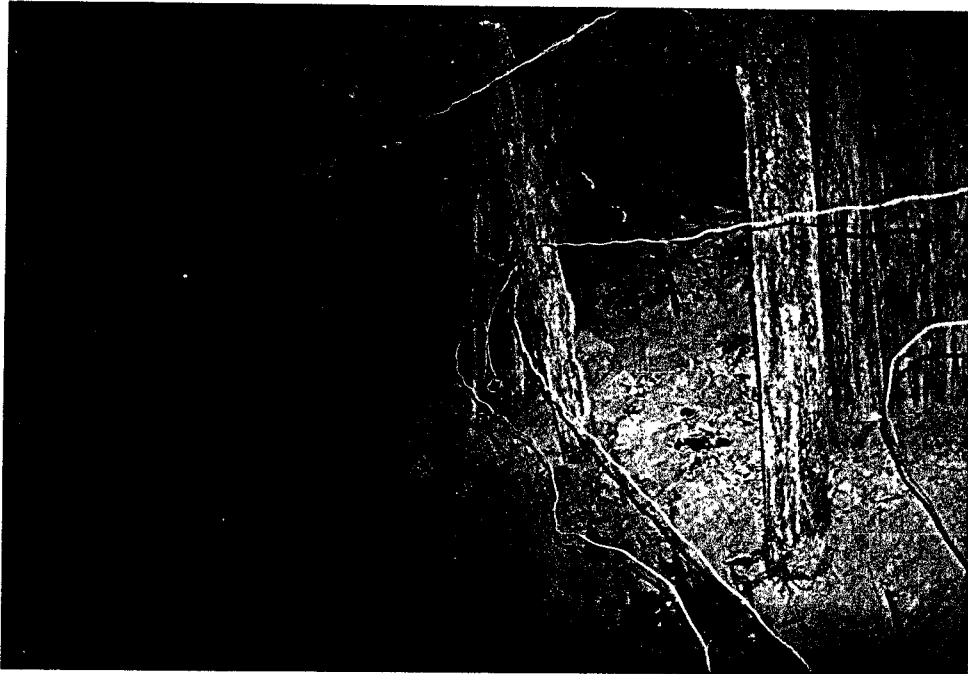
Photograph 5 :   View of pillar A in March 1994.
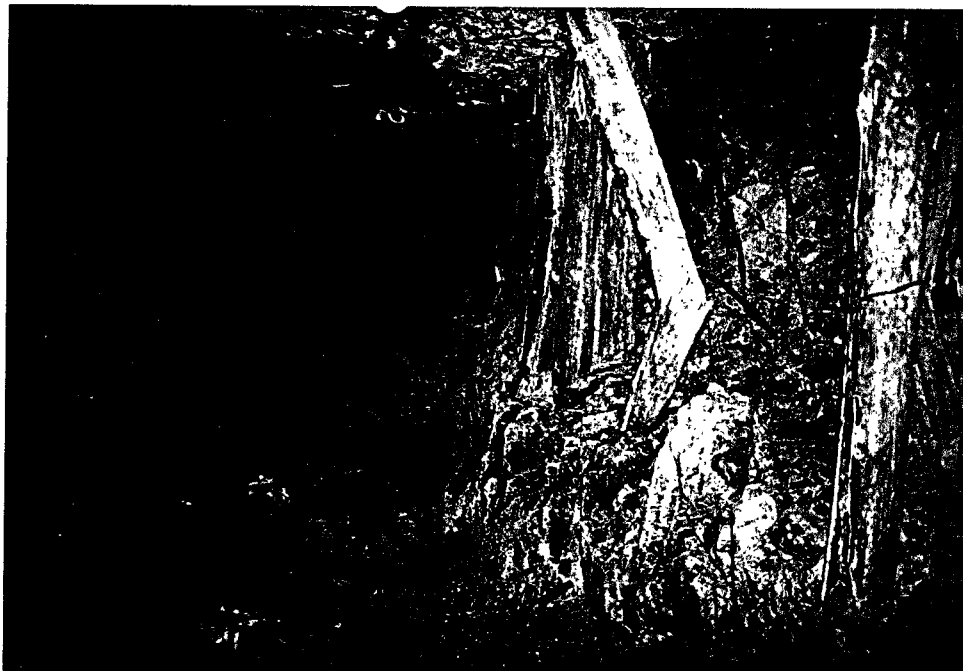
Photograph 6 :   View of pillar A in June 1995.

Photograph 7 :   View of closure adjacent to pillar A in June 1994.
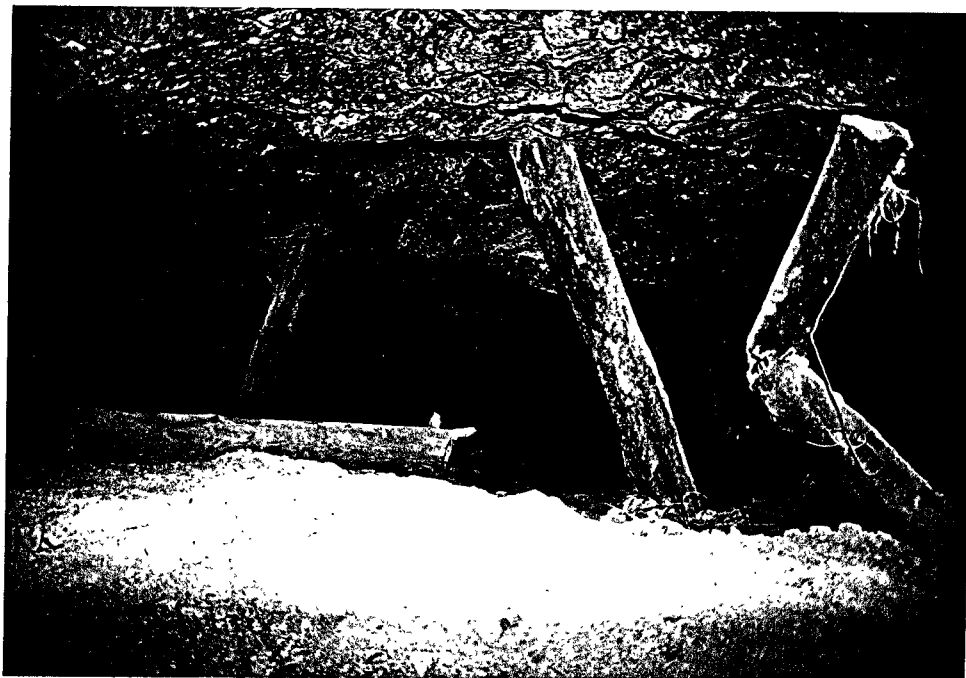
Photograph 8 :   View of closure adjacent to pillar A in June 1995.

Photograph 9 :   **View of pillar B in March 1994.**

Photograph 10 :   **View of pillar B in June 1995.**
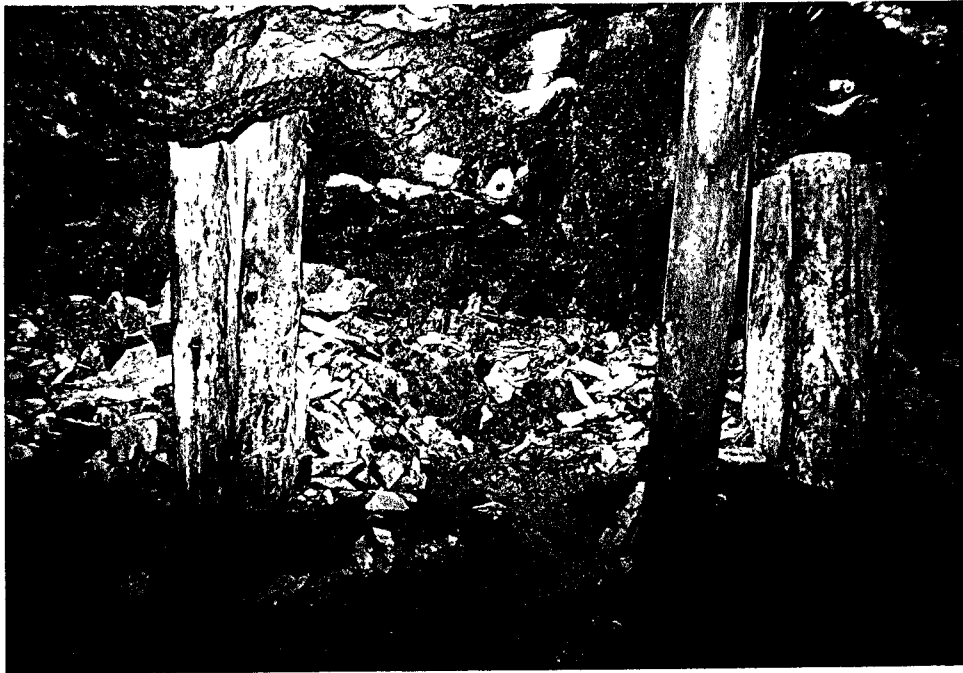
Photograph 11 :   Damage to the updip side of pillar B following a

seismic event on 09/11/94.

Photograph 12 :   Damage to the downdip side of pillar B following a

seismic event on 09/11/94.
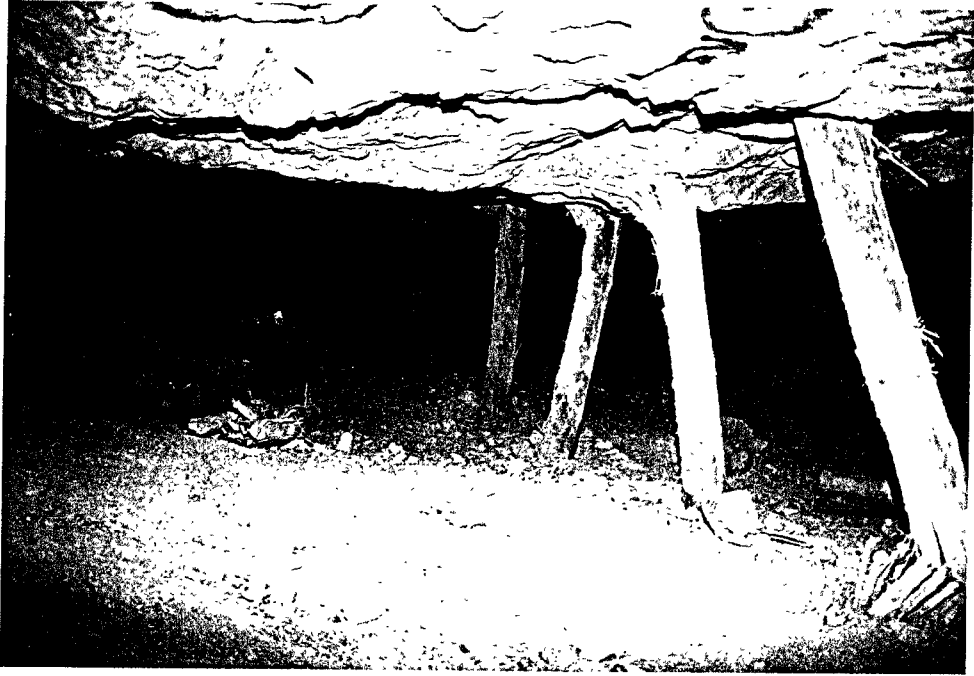
Photograph 13 : View of closure adjacent to pillar C in June 1994.
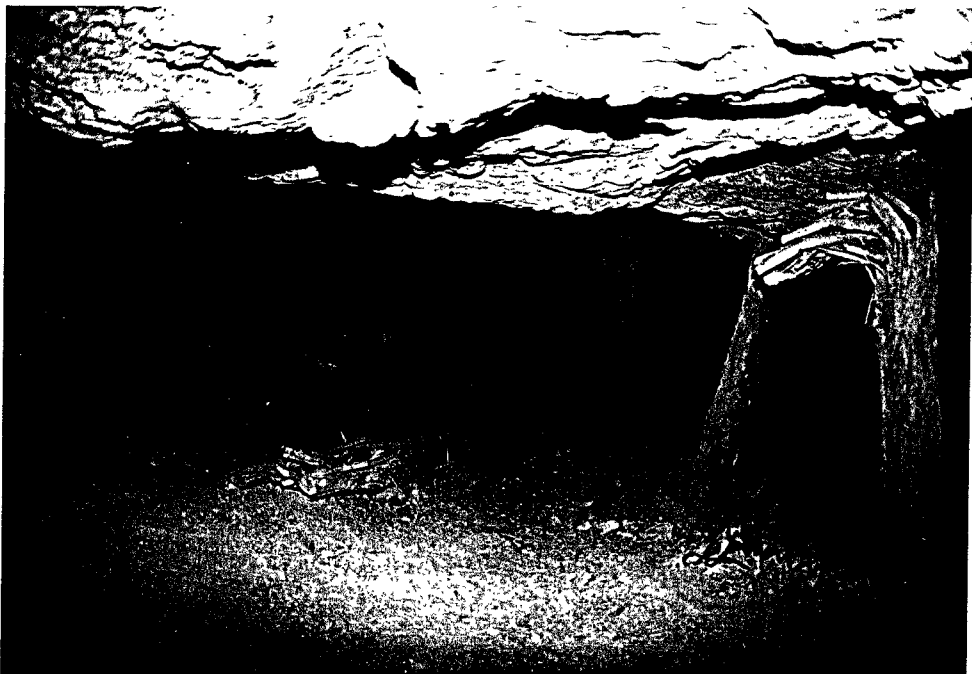
Photograph 14 : View of closure adjacent to pillar C in June 1995.

Photograph 15 :   Joint opening on the down dip side of pillar D.
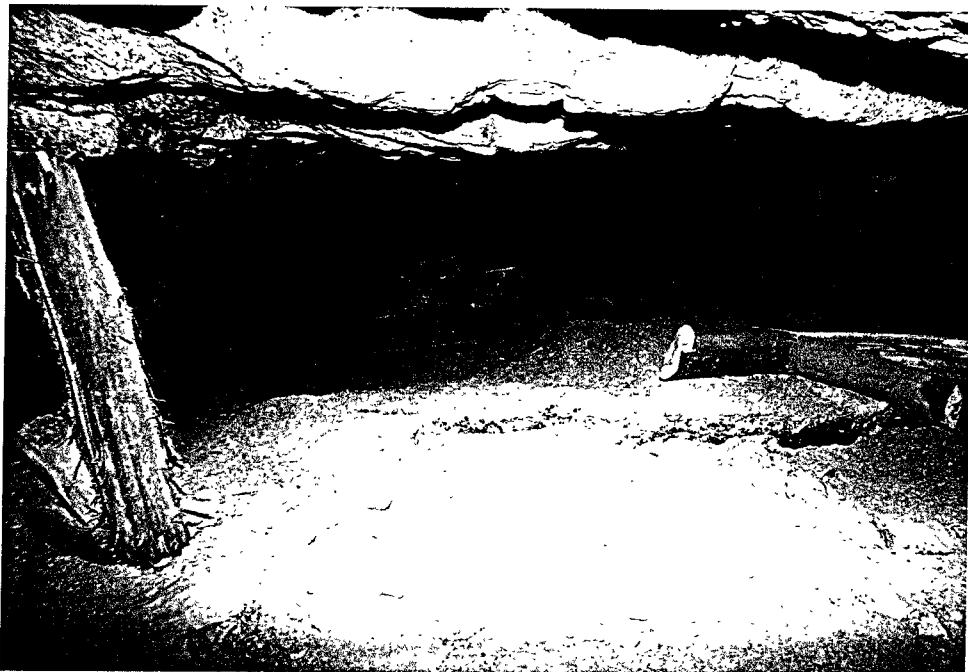
Photograph 16 :   Typical view of footwall lifting into the stope.
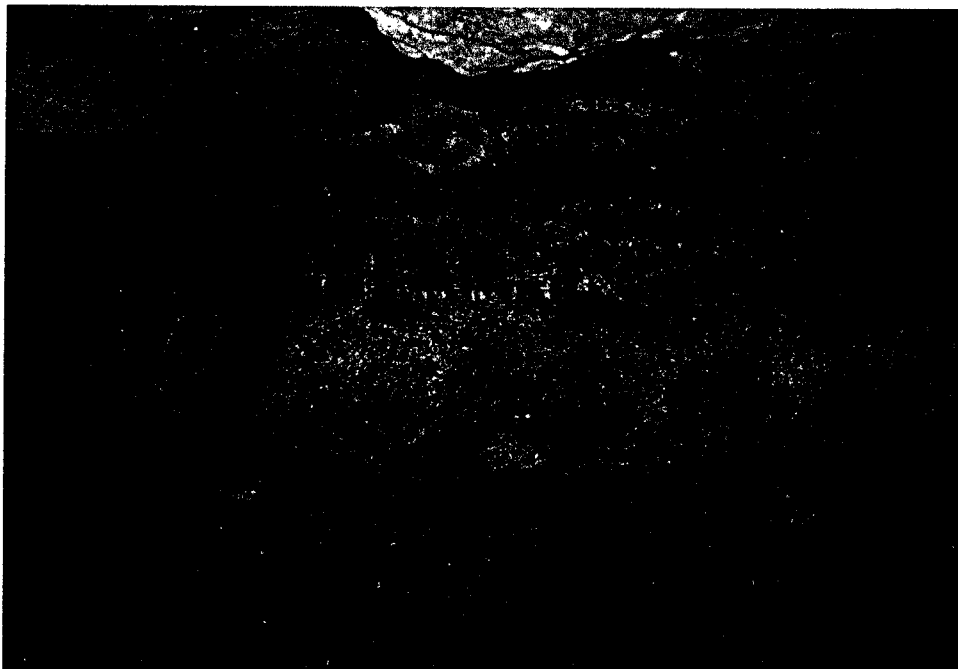
Photograph 17 : View of pillar E in June 1994.
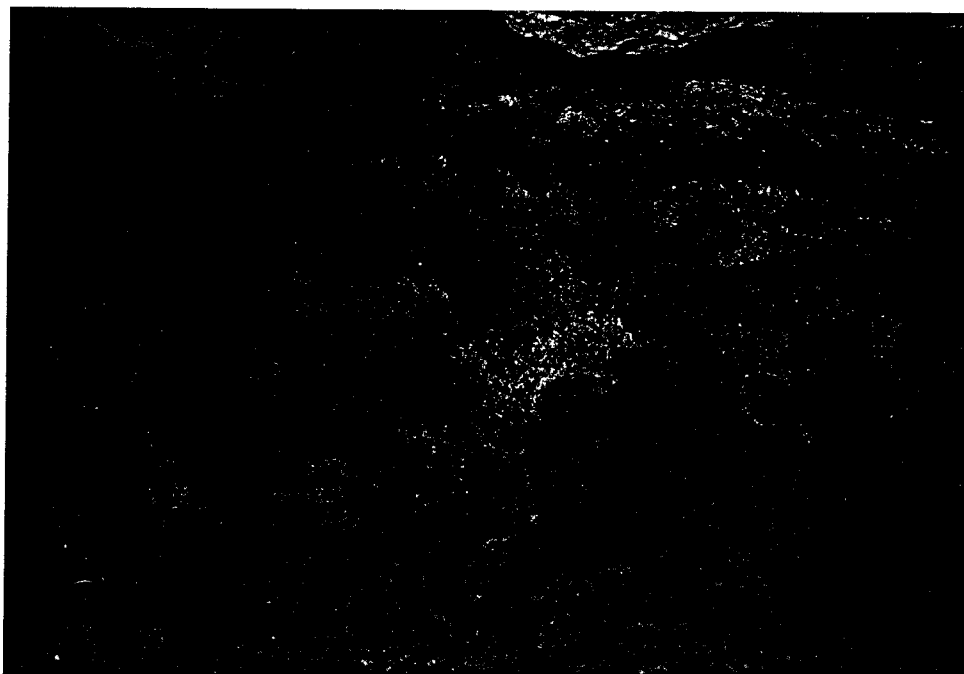
Photograph 18 : View of pillar E in June 1995.

.

Appendix E1

Definition of Key Block Failure at RPM Union Section

i

Table of Contents

J

1 Introduction

The Union Section site has been found to have certain lithologically and structurally based geotechnical characteristics to which can be attributed most of the excavations behaviour in terms of ground stability. It has been found moreover on examining other sites at Union as well as a number of areas on Western and Eastern Platinum that these too have lithologically and structurally based criteria that characterise the areas geotechnically with respect to ground stability. In places a stress criterion is also relevant.

It can be said that a number of litho-structural facies can be identified within which the geotechnical characteristics can be predicted.

What is significant is that the structural elements within the litho-sructural facies at Union Section have been found mostly to be reasonably continuous and van be projected from the primary development, ledged raise or pre-developed gully stage. The elements have been found to occur associated in a number of ways, the structural associations too being projectable. These structural associations have block stability and areal stability characteristics that can be used to define certain support requirements, most that are standard but several that seem likely to require innovative measures.

2 The litho-structural facies of the Union Section site.

2.1 The lithological component of the facies

Lithologically the pyroxenitic and melanoritic rocks comprise the minerals pyroxene and lesser feldspar. As igneous crystalline rocks they are in themselves competent rocks. At the Union Section 22/8 stope they have been widely serpentinised.

Serpentinisation

Serpentinisation is a process of low-temperature hydrothermal metamorphism that alters pyroxenes and olivines to very weak, soft (it can be readily scratched with the fingernail) serpentine. Serpentinisation occurs particularly along the joints that transect the rocks as well as on some patches of bedding-parallel jointing. A few joints contain calcite as well as serpentine. Some serpentinisation within the rock itself has been observed in particular around and in the cleavage planes of some of the pyroxene grains. This seems to be on a minor scale and probably does not significantly influence the rock strength of the body of the rock away from the immediate proximity of some of the joints. On the joints the serpentinisation, while almost always present, appears to occur more thickly and consistently on the steeply down-dip dipping subset of the predominant strike joint set. This would imply that while the formation of all the joint sets preceded the serpentinisation process, this subset was the major conduit of serpentinising fluids.

The parallelism between this joint subset and a major fault that occurs several levels down dip and has an associated zone, several metres wide, of intense country-rock chloritization (chloritization is similar to serpentinization, the mineral compositions grading into one another) and serpentinization along it suggests a structural and metamorphic relationship between them. The fault is itself associated, further north, with a serpentinized dunnite pipe.

Oikocryst layers

Oikocrysts are extremely large pyroxene crystals (as much as 20cm across) that grow round the other minerals. These have been observed to occur in

certain layers about 1,5m into the hangingwall at several places where fall outs have occurred, The weak cleavage of these oikocrysts is moreover parallel to the stratification. These layers of oikocrysts provide potential coplanar weaknesses.

2.2 The structural components of the facies

Structurally the area investigated is characterised by the abundance of joints predominantly belonging to two sets, a laterally persistent strike set and a generally less persistent dip set. A third, infrequent set strikes about 20°- 30° left (anti-clockwise) of the strike set. This is termed the oblique set. Also present are patchy joints parallel to the stratification, the bedding set.

Stress-induced fracturing at a low-inclination to, or parallel to, the bedding has been observed in a few instances. The [EQN "sigma sub max"] in the hangingwall causing this fracture is aligned on dip, suggesting that it might be due to the ride effect of the hangingwall of the very extensively mined-out area updip of the site. It is to be seen immediately updip of some strike pillars and occasionally where, by linking adjacent convergent joints, falls have been possible. It clearly plays a role in completing the fracturing between groups of oikocryst cleavages. Because such fracturing plays a similar role to the jointing of the bedding set in causing instability, it is considered as if it was a joint set, the fracture set.

A joint configuration that occurs sporadically consists of a number of joints distributed in a roughly circular or elliptical grouping. These joints converge towards the centre of the circle or ellipse, feathering away from the bedding, steepening curvilinearly and then flattening towards the bedding at the centre. Several joints commonly occur together, concentricaly arranged and with a progressively smaller amplitude inward. They constitute a domical set. The instability of these domical structures is often aggravated by the strike set and dip set joints that cross them.

The strike set occurs as four subsets;

i.   a subset normal to bedding (and therefore dipping updip), the (normal subset),

ii.   a subset dipping about 70°-80° downdip, (down-dipping subset)

iii. a cymoid-curved subset (cymoid subset) that steepens downwards off hangingwall bedding joints to about 70° then flattens again towards the reef dip, always downdip and

iv.   a subset dipping at about 40° downdip. This subset could be a cross-bedding phenomenon (cross-bed subset) that coincidentaly has a similar strike to the other three subsets.

The cymoid curve joints have been seen to vary in amplitude along strike from almost 2m to 0,5m.

All subsets except the cymoid curve joints occur commonly as swarms of a number of joints. Swarm numbers vary but seldom exceed 20 joints with swarm widths mostly between 1m and 5m and swarm spacings occasionally up to 15m

The dip set occurs as a single subset with a minor range of dips: mostly dips are steeply to the north less commonly ranging around vertical. In most instances these joints terminate against or "jog" on joints of the strike set. Less frequently they transect the strike set and have a lateral persistence of tens of metres.

The oblique set occurs mainly as single joints that have a lateral persistence of several metres. Their dip is commonly around 70° updip.
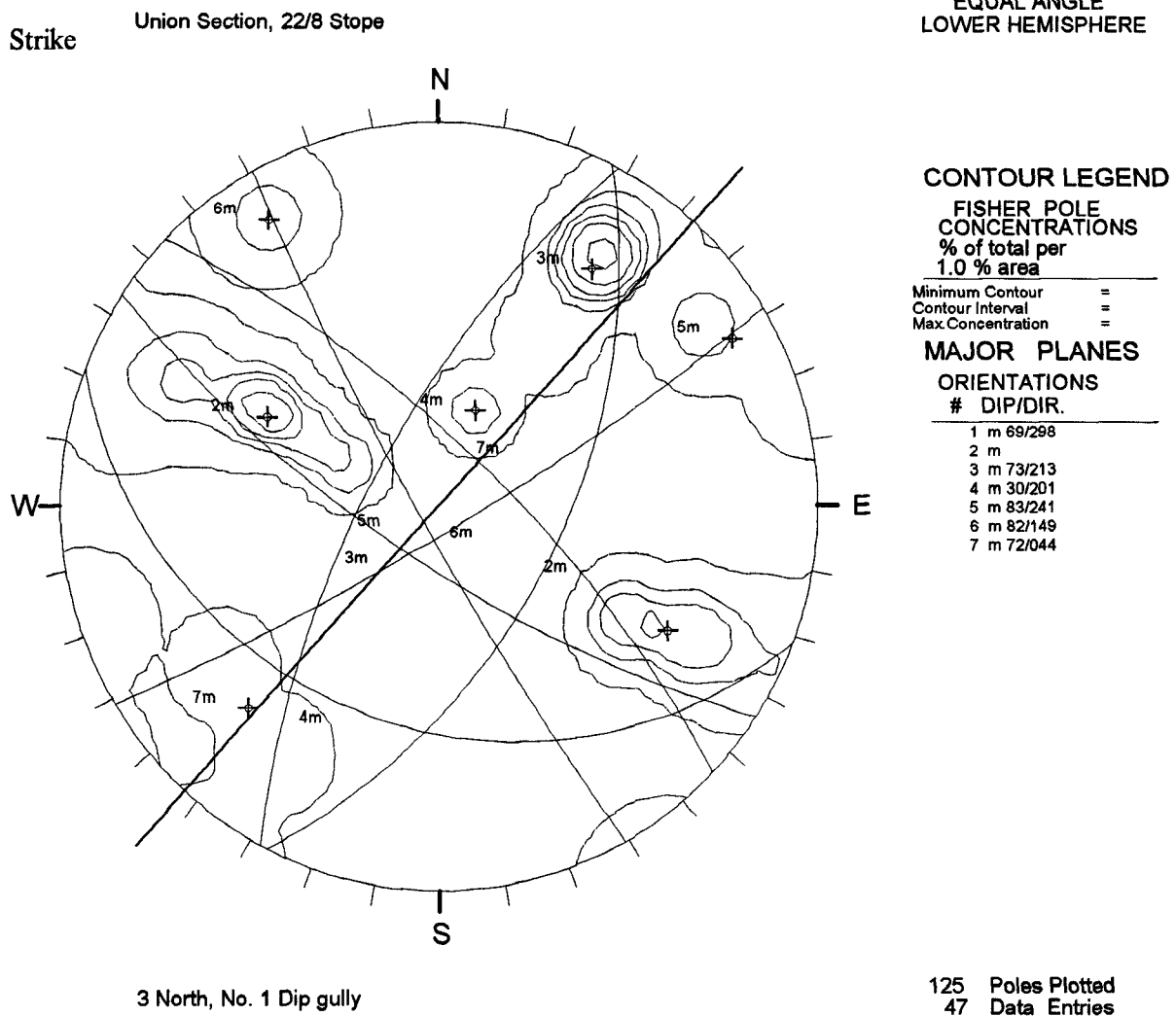
Figure 1. Typical stereographic plot of the joint poles

The grouping of the poles of the strike set as two and sometimes three sub-sets can be seen in any joint stereogram of the site (Figure 1 is a typical stereographic plot of the joint poles encountered in a typical raise). The frequency maxima of these sub-set poles are about 40° apart, i.e. their dips converge at about 40°. That numbers of adjacent and semi-adjacent (close enough to be linked by patches of bedding-parallel joints/ oikocryst cleavage/fracture) joints do in fact converge upward at such angles is illustrated in Figures 2a and 2b. The upward convergence between joints, whose strikes are not parallel but semi-

orthogonal or oblique, also contributes significantly to the instability of blocks in the hangingwall. The incidence of upward-convergence angles of such joints is illustrated in Figures 2a and 2c.

Frequency of Parallel Joint Convergence Angles

Frequency of Orthogonal Joint Convergence Angles
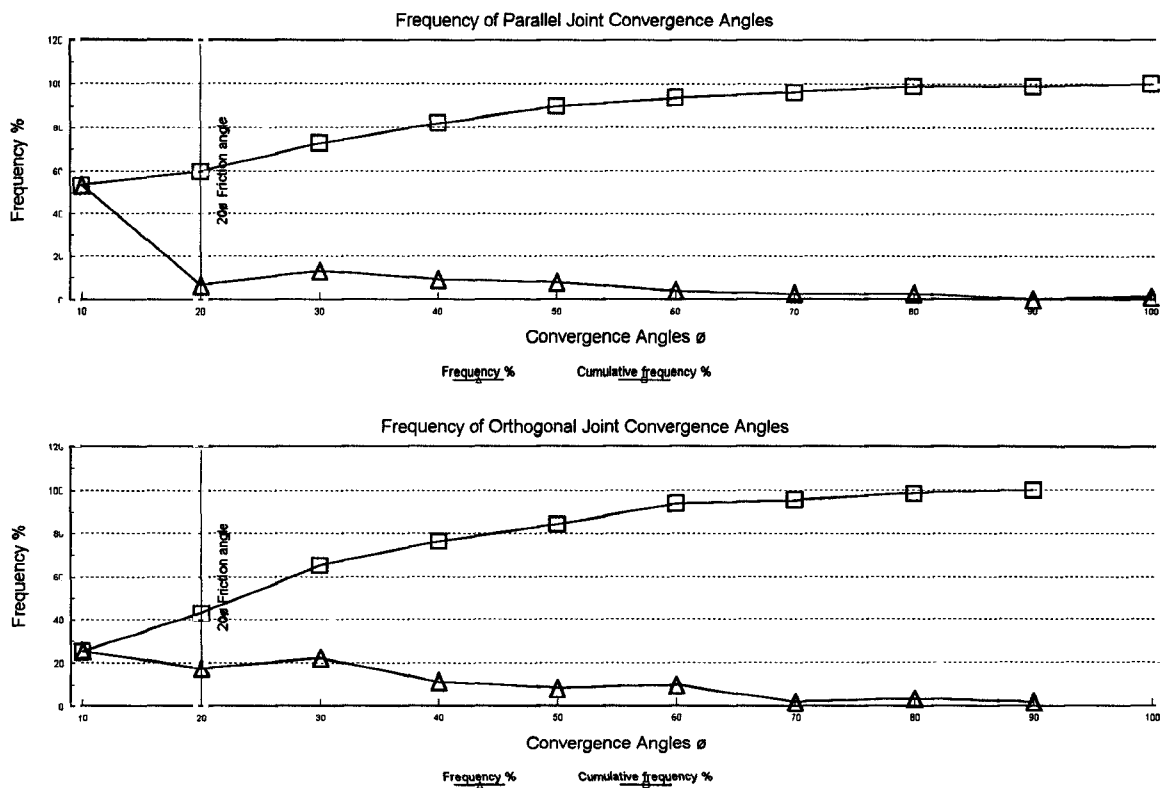
Figure 2a. The frequency of upward convergence between joints whose strikes parallel and whose strikes are semi-orthogonal or oblique

UNION SECTION, RUSTENBERG PLATINUM MINES

Key-block Apex Angles and Width, Parallel Joints

22/8 Stope, 3 North, No. 1 Dip Gully
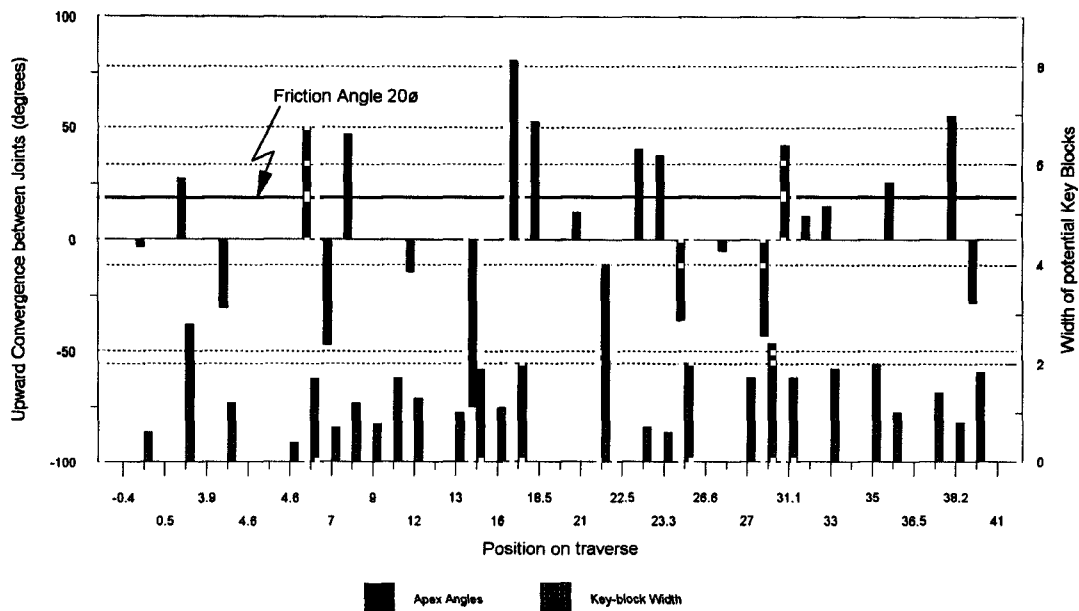
Figure 2b. The upward convergence between joints whose strikes are parallel

UNION SECTION, RUSTENBERG PLATINUM MINES

Key-block Apex Angles, Orthogonal Joints

22/8 Stope, 3 North No. 1 Dip Gully
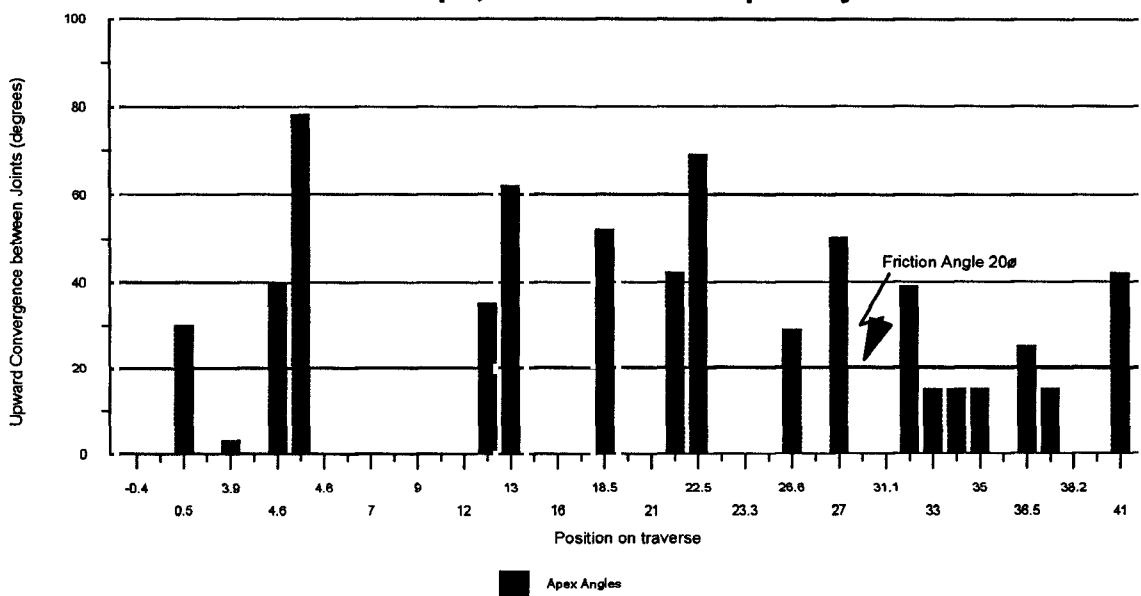
Figure 2c.The upward convergence between joints whose strikes are not parallel but are semi-orthogonal or oblique

2.3 The litho-structural facies of the site defined

This facies can be termed the serpentinised, pyroxenitic multiple-jointed facies. This summarises the main characteristics of the facies, namely:

a. Pyroxene-rich crystalline rocks

b. Serpentinisation along the numerous joints

c. Intensely jointed with multiple joint sets

3 The manner in which the characteristics of the litho-structural facies influence hangingwall stability.

It has been found that all the observed falls could be attributed to the fall of at least one clearly definable kinetically feasible block, of which there are many. The frictional resistance on the joints is particularly low: the serpentine that coats the joints has a naturally "soapy" feel to it and tilt tests indicated the angle of friction to be low, about 20°.

Falls occurred due to several factors, sometimes acting together:

a. the initial wedge block was bounded by joints that converge upwards and intersect with convergence or apical angles wider than 20°.

b. the initial block was bounded by a bed-normal strike joint and a cymoid curve joint

c. the initial fall was bounded laterally by joints converging upward at more than 20° and an overlying bedding-parallel joint

d. the initial fall was bounded laterally by joints converging upward at more than 20° and an overlying bedding-parallel fracture surface incorporating numbers of oikocryst cleavage planes; the geometry is similar to c above.

e. the lateral continuity of the strike joints and their dips creates "wedge-block beams" that allow the growth forward on strike of falls that are enabled to fall as segments due to the cross-cutting by the dip set joints

f. the bedding-parallel joints allow falls to spread laterally on dip and strike

g.   the occasional low-inclination fracture allows falls between non-intersecting upward-convergent joints.

g.   the domical joint sets seem unpredictable and unprojectable in locality or size, the margins of the set being readily overlooked as the face advances past it. Falls occur to progressively higher members of the set extending upward to as much as two metres.

It is inferred from the presence of numbers of the oikocryst cleavage planes as part of the smooth fracture surface from which rock has fallen in some major falls that the cleavage planes weakened the rock sufficiently for it to fracture and allow the fall. There are indications that some of the oikocryst cleavages may have been serpentinized, further weakening them.

4 The structural associations, their projectability and the predictability of ground instability

The property of all the joint sets to be laterally continuous along their strike as well as in their dips means that they can be projected from their exposures in the pre-developed dip and strike gullies. Even in the case of the dip-set, although the individual joints commonly truncate against strike-set joints, the swarms themselves have a lateral continuity.

The elements have been found to occur associated in a number of ways, the structural associations too being projectable. These structural associations have block stability and areal stability characteristics that can be used to define certain support requirements, most that are standard but several that seem likely to require innovative measures.

The first and most general structural association causing ground instability is the proximity and coexistence of the bedding-normal subset of the strike-set of joints with one other subset of the strike-set. The down-dip-dipping subset is the most common associate, joints of the cymoid curve subset and the cross-bed subset are less common. If the joints of the two subsets converge upwards at more than 20° (in the case of the cymoid curve subset this angle is that between the steepest portion of the joint and the adjacent bedding-normal subset), potential instability is created. Should a bedding-set joint or a layer of oikocrysts be present and/or a fracture set develop in the hangingwall between the two joint sets, they do not have to intersect to create a potentially unstable wedge-block beam but need merely to intersect the bedding joint or fracture.

These laterally-continuous wedge-block beams are in themselves semi-stable due to the inherent rock strength (the length of stable unsupported beams is likely to be a proportionality function of the beam thickness) until they are cut by joints of the dip-set or the oblique set. The lateral continuity of these or their swarms makes possible the projection of likely intersection zones: even if falls are not present in the pre-developed gullies likely instability zones seem to be projectable.

The influence of the oblique joints seems most often to be to help initiate falls.

The structural associations and their relation to instability can be summarised:

Structural Components (those in brackets assumed to be present; cannot be seen prior to fall)	Comment
A. bedding-normal subset + down-dip-dipping subset + dip set + (bedding set/ fracture set)	Most common. Moves forward with breast face dip set swarm wide or swarms closely spaced
B. bedding-normal subset + cymoid curve subset + dip set + (bedding set/fracture set)	Rare to fairly common, good lateral continuity; may change on strike with changing amplitude
C. bedding-normal subset + crossbed subset + dip set +(bedding set/fracture set)	Often limited but repetitive giving saw-tooth hangingwall profile. Height may be s to be a face-area problem on downdipping face laterally continuous in breasting faces
D. bedding-normal subset + down- dip-dipping subset + dip set + oblique set +(bedding set/fracture set)	Has a strong possibility of initiating a fall of semi-stable wedge-block beam. isolated oblique set joints should be pro stopes as cautionary zones
E. bedding-normal subset + dip set + (bedding set/fracture set)	Fairly common, seems generally stable
F. bedding-normal subset + oblique set + dip set + (bedding set/fracture set)	May cause localised fall which may extend if b wide-spread

Because the localities of the various structural components can be mapped in the pre-developed raises and gullies, the potential seems good to predict the hangingwall instability localities likely to be encountered and forecast the support requirements or mining procedures required to minimise falls

The apparently random occurrence of the domical joint sets has the implication that instability due to these cannot be predicted. When encountered by an advancing face, falls to these curved serpentinous joints will probably occur unexpectedly ahead of the front row of face support. If remedial support can be devised it should be available on an "on call" basis.

5 Support implication of the hangingwall instability structures at the Union Site.

The segmented nature of the Wedge - block beams created by both (a) the normal + down-dip dipping subsets and (b) the normal + cymoid curve subsets of the strike joint set coupled with their low cohesion and friction angles allow these to fall ahead of the conventional face support, as the face is advanced on breast.

Conceptually several approaches to catching and holding these wedge block beams seem possible. Each necessitates the use of blast on hydraulic props with large-area headboards set as close to the face as practicable.

Approach I (Figure I)

Faces should be mined 45° under hand. The face would thereby cross both strike and dip joint stets diagonally (Figure I). A corner of most prismatic segments of the Wedge blocks would be supported by the face and a corner would be available for support by a blast on
prop.

Plan view of stope face advancing at 45ø to strike

Joints, strike set

Stope face

Direction of advance

Joints, dip set

Props catch block while it is supported by face

Wedge block between

Joints A and B

B

A
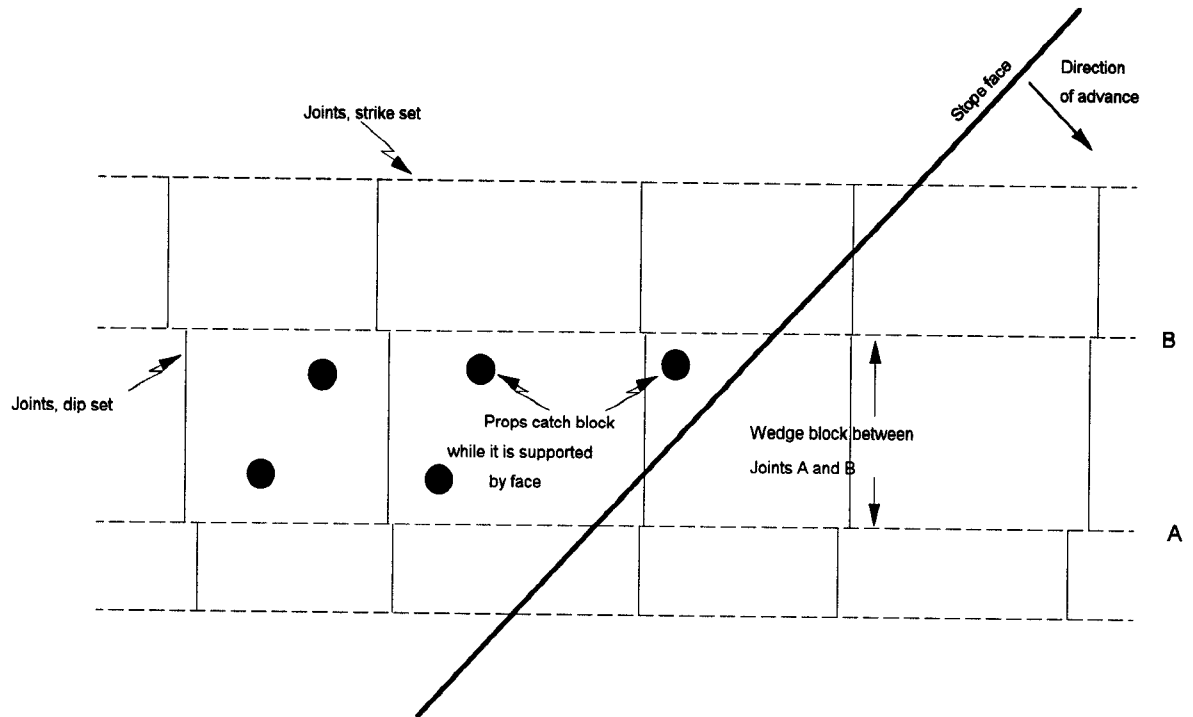
Approach II (Figure IIa and b)

Where a breasting face has encountered a previously undetected wedge block that has fallen ahead of the face support the face would be blasted in two phases . In the first phase (Figure IIa) the face would be drilled normally to within

1 m of the down-dip edge of the wedge. The drilling angle would be widened to about 45° to the face with the last two holes of this phase being drilled as "stub" holes, one above the other, collared about 2/3 of the way across the wedge block. This should provide a corner of the Wedge-block prism under which a blast on prop would be set. (Figure IIb). During the second phase of the blasting the first 3 or 4 pairs of holes up-dip of the prop would be drilled with a small burden and light charge to reduce impact on the prop and reduce concussion on the hangingwall that might dislodge it. The prop would not be removed until its support foundation had been taken over by load bearing permanent support. Close to the face blast on props would probably continue to be required forward along the wedge beam as the face advanced

Plan view of stope face advancing on breast

FIRST PHASE

Direction
of advance

Stope face

Joints, strike set

Joints, dip set

B

Wedge block between
Joints A and B

A

Wedge block fallen
ahead of support

Shot-holes at 45s

Supports

Normal shot-holes

Plan view of stope face advancing on breast

SECOND PHASE

Direction
of advance

Stope face

Joints, strike set

Normal shot-holes

Joints, dip set

Shot-holes at 45°

B

Wedge block between
Joints A and B

A

Props catch block
while it is supported
by face

Wedge block fallen
ahead of support

Supports

Approach III

A breasting or diagonally down dipping face encounters a wedge - block beam which falls out at the face. Jack hammer holes would be collared at the face within the wedge block, inclined slightly up and aligned diagonally outward across the joints that flank the falls (Figure III). Long shepherds crook rebar would be installed with resin grout for quick setting, with the protruding crook extending outside the fall Blast on prop would be set so as to clamp the crook ends against the hangingwall. Two factors would resist the fall; the truss-like effect of the bars and the shear strength of the bar where is crosses a joint. The problems of water-lubrication of serpentinous joints might necessitate dry drilling of some of the holes.

Plan view of stope face advancing on breast
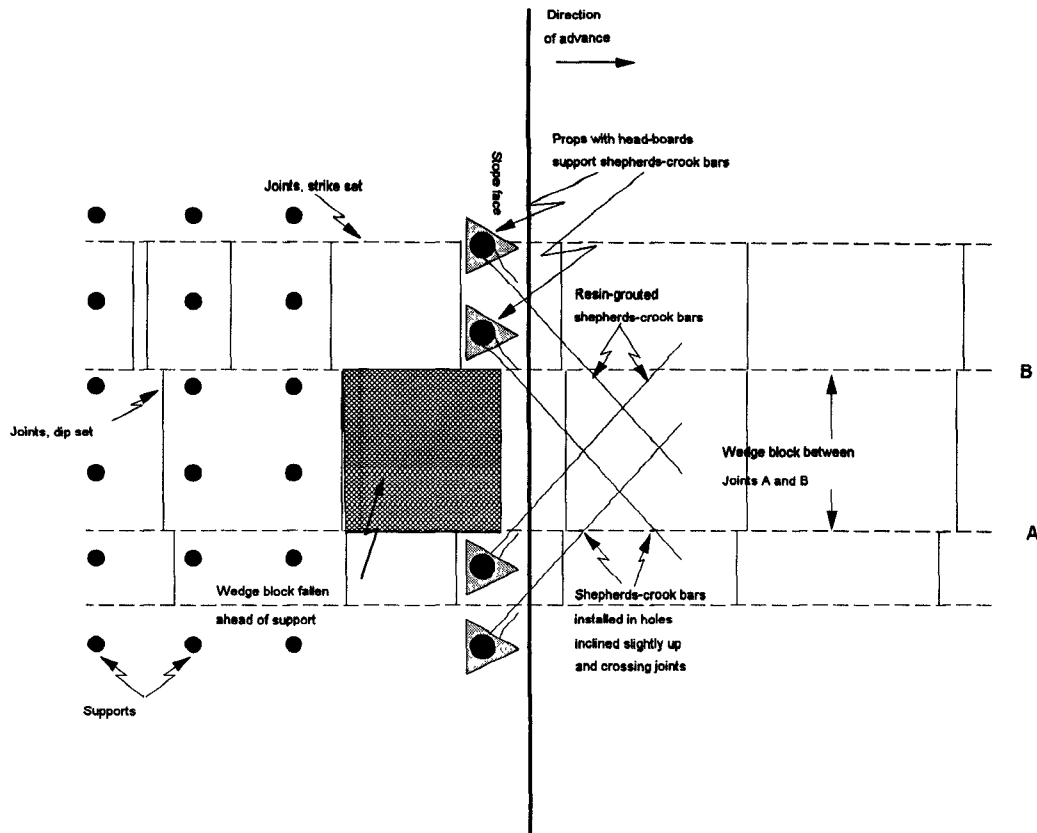
6 The applicability of litho-structural facies at other sites

Other localities on the Merensky horizon at Union Section and a number on the UG2 horizon at Eastern and Western Platinum have been visited and examined from the point of view of identifying the factors that influence the hangingwall stability. These factors and the geological environment in which they occur were assessed to ascertain whether the litho-structural facies concept could be usefully employed here as well.

It seems that it can.

The 7/22 stopes at Union can also be categorised as the serpentinised, pyroxenitic, multiple-jointed facies. The character of the hangingwall instability is very similar to that at the investigation site.

In the 12 and 13/22 stopes the rock is fresh and unaltered. Joints have a calcitic fill sometimes with a chloritic veneer. The same joint sets are prevalent as at the 8/22 site but they occur as occasional joints or limited swarms. Two of the subsets of the strike set, the normal and the down-dipping subsets are present. Instability and falls occur and are joint-related. The structural associations seem also to define the relative stability of the hangingwall.

On the UG2 horizon on Eastern and Western Platinum a significant structural component of the hangingwall is the presence of a thin (a few mm or a cm or two) weakly cohesive chromitite layer. The spacing between the top of the reef and this layer ranges from 0,5m to 3m in the area. It is laterally persistent over both Eastern and Western Platinum, moving further from the reef to the east.

The main lithological variants present are:

i. Fresh competent rock

ii. Weathering along joints at shallow depths

iii. Rock alteration in the vicinity of Replacement Pegmatoid bodies

The main structural variants present are:

i.   The position of the chromitite plane of weakness in the hangingwall

ii.   The joint density and orientations
iii. The presence in certain areas of high horizontal stress that causes hangingwall-parallel fracture

Although this latter variant is not truly a structural feature the stress that causes it is a geological feature and the fractures it creates are effectively the same as bedding set or low-inclination joints.

The differing separation between the hangingwall chromitite layer and the reef leads to a gradual transition from narrow to wide spacing: facies components in many fields are transitional.

The intensity of jointing , the joint set multiplicity, abundance and swarm width are other gradational facies components.

The facies that are tentatively definable are:

A.   Weathered, multiple-jointed facies with kaolinite/clay/sericite joint
        fillings and a facies variation of chromitite-reef separation from narrow spacing to wide spacing.

B.   Fresh rock sparsely-jointed facies with a facies variation of
        chromitite-reef separation from narrow spacing to wide spacing.

C.   Fresh rock intensely-jointed facies with a facies variation of
        chromitite-reef separation from narrow spacing to wide spacing.

D. Replacement pegmatoid moderately jointed.

E. Fresh rock, high horizontal stress jointed facies.

The structural associations of instability are clearly applicable in each of these facies environments. There projectability seems also to be good. As at Union Section some shallowly-inclined curved jointing was seen and would be likely not to be projectable; this did not seem to be true domical set jointing.

The weathered, multiple-jointed facies is very similar in its instability characteristics to the serpentinised, pyroxenitic multiple-jointed facies with the general occurrence of the weak chromitic layer being an exacerbating factor.

7 Conclusions

It appears that the two concepts of litho-structural facies and projectable structural associations are potentially useful in predicting the hangingwall stability conditions and support requirements of the platinum reef mining in the Bushveld.

The application and utilization of the concepts seems worthy of further investigation.

Joint Mapping Program and Characterization

Program description Purpose and goal

Weak hangingwall conditions associated with the geological alteration zones that are encountered in some sections of R.P.M. Union Section led to an investigation into the current mining method and support strategies. Particular attention was directed towards the behavior of the hangingwall, how to predict falls of ground and how to control them.

It is commonly understood that the stability of stoping excavations is dependent upon the structure, strength and competence of the immediate stope hangingwall; the extent of unsupported spans, both at the face and between individual support units; the rate of face advance; and the degree of hangingwall blast damage. The most important of these is undoubtedly the unsupported span.

Geology

22/8 Stope in the lower levels of Richard shaft is in a pothole reef that has a span of 4,4 km and is open ended downdip where it increases in size. The Pothole type reef is an olivine-bearing, pegmatoidal, feldspathic pyroxenite. The footwall is a feldspathic harzburgite (tarentaal). The hangingwall is a laminated and disturbed pyroxinite which is broken up by a predominant NE/SW striking, steeply dipping joint set (Strike set). A second joint set orientated about 10 degrees right of dip truncates against the above set and brakes the hangingwall up into a continuum of blocks (Dip set). The orthopyroxene and olivine crystals which make up the dark component of the pyroxinite hangingwall are commonly partially or completely serpentinized and all joints in the immediate hangingwall are hence well lubricated. A 1-5 mm calcite infill is often present on the strike set and less often on the dip joints Consequently the rock bisected by dip joints is more continuous and they are not as obvious as strike joints when joint surveys are undertaken in newly developed areas.

Structural mapping of the stope

As 22/8 stope was pre-developed, joint mapping of the hangingwall was undertaken in the dip and strike gullies prior to stoping commencing. Particular attention was given to mapping the frequency dip and direction of the joints, but also smoothness, the amount of fill and the continuity was carefully noted.This information was then captured on a spread sheet, mapped on a plan and stereo plotted. It was thus possible to identify potentially unstable joint patterns in the hangingwall at this stage. As strike

Diagram 1
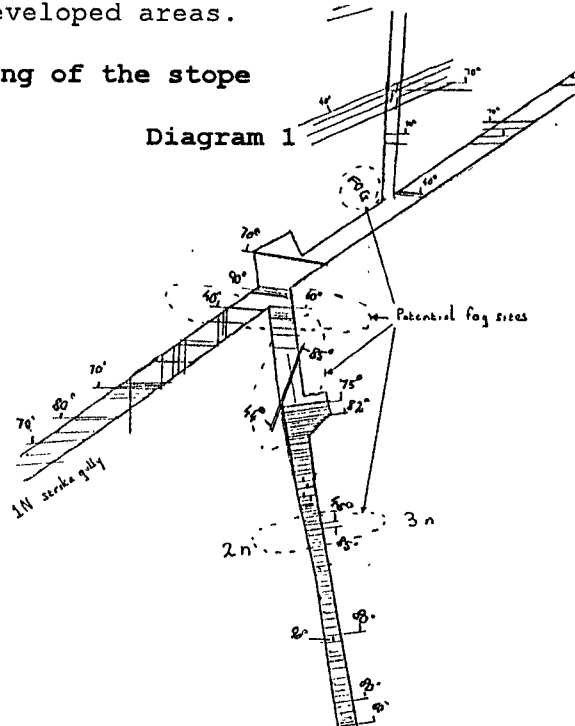
Jointing in 1N strike & 2n dip gullies showing potential foα confiαurations

continuous, these
unstable conditions were
assumed to persist into
neighbouring panels and
would be exposed as they
are mined.
This was verified by
continuing the joint
mapping into the panels
as they were mined.
Throughout the stope
strike joints were found
to be dominant,
continuous steep dipping,
highly serpentinized and
occasionally found to
contain a 1-5mm calcite
infill (photo 1). The
strike set joint spacing
was found to be variable
with swarms of 1 to 3 m
containing 50 j/m. Areas
in 3n panel and 3N strike
gully had joint spacing
of less than 1 j/m.
Dip orientated joints
which comprise later
steeply dipping joint
sets typically striking
10 degrees right of dip,
truncate up against the
strike joints and break
the hangingwall up into a
series of blocks.

Photo 1
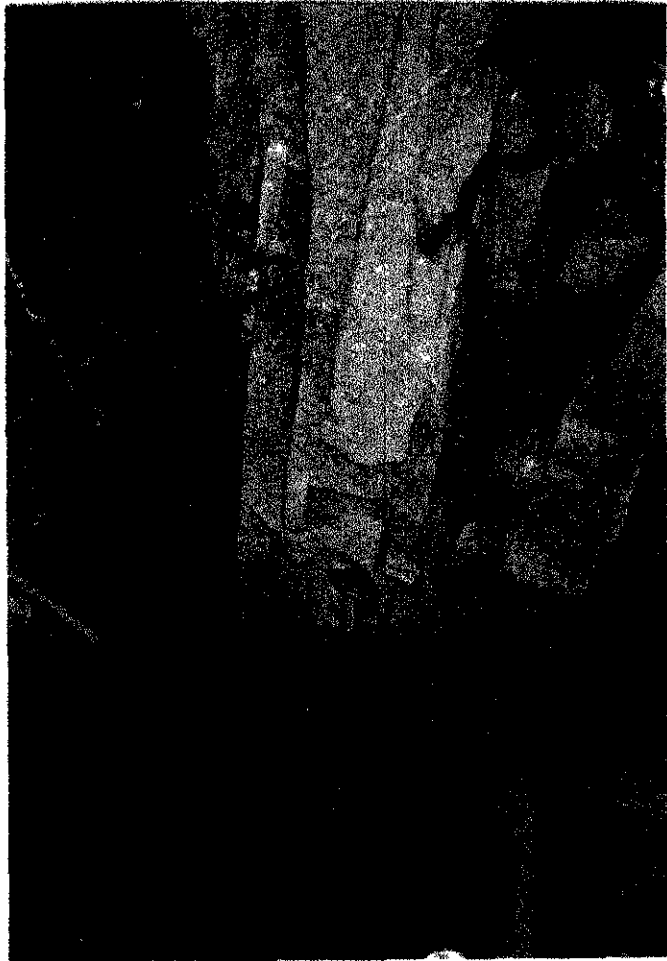
Strike & Dip Joints 22/8 Stope

Mechanism of key block fallout

Joint mapping following pre-development in this area always shows
the predominance of strike joints and less frequently the presence
of dip joints. Irregular joints with a variety of dip and
directions break up these joints but typically occur only every 10
to 20m.
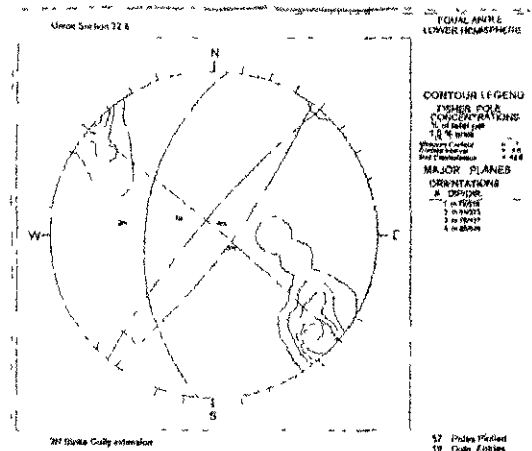
Photo 2
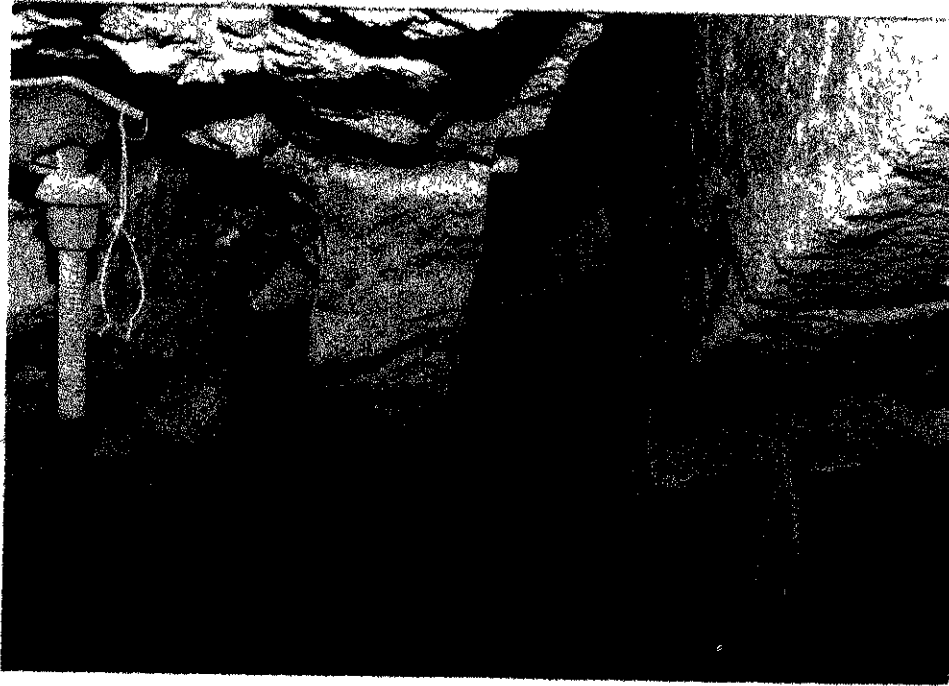
Key blocks between adjecent divergent joints

Two main types of dip joints are present in this stope, Those that
are continuous and those that truncate up against the strike
joints. The continuous dip joints, which are not common, and occur
mainly in the dip gully area, are generally steep dipping,
serpentinized easily visible and are responsible for blocky ground
conditions in their vacinity. The more common dip joints are those
that appear at first as only hair line cracks between strike
joints. As the mining spans increase and the hangin gwall begins
to buckle under closure, these dip joints become far more visible.
They, along with the more serpentinised strike joints are largely
responsible for falls of ground as they break up the hanging into
a continium of unstable blocks.

With pre-development it is possible to map the joints, predict
wedge fallout's and hence support accordingly (photo 2).

Dykes

Union section is home to a number of doleritic Dykes trending in
up to 4 different directions. The largest and most consistent are
25 to 60 m wide, vertical medium grained and dark grey and are
part of the Pilanesberg alkaline province. The remaining dykes
trend in a variety of directions, and are generally thinner (8-10
m), are dark fine-grained, doloritic varieties that post date the
Pilanesberg swarm. The vertical dyke that bisects 22/8 stope
(diagram 1) also cuts across the joints which are not present
inside the dyke but otherwise are seemingly unaffected by it's
presence. There is no evidence from measurements taken in 22/8
stope that ground conditions are worse close to the dyke then they
are further away.

Faults

Large faults are rare at Union Section, except in the south-
western part of the mine. A large number of smaller faults with
throws of a few centimeters to several meters are associated with

Domes

A sub-horizontal joint set that overlays the reef varies in dip from 0 to 40 degrees. Some of these joints take on a curved profile creating a dome feature. The size of these domes vary from 1 to 50 m. Domes represent an area of bad hangingwall as the rock within the outer curved surface is usually highly jointed with little cohesion to the surrounding rock mass (Photo 3).

Photo 3
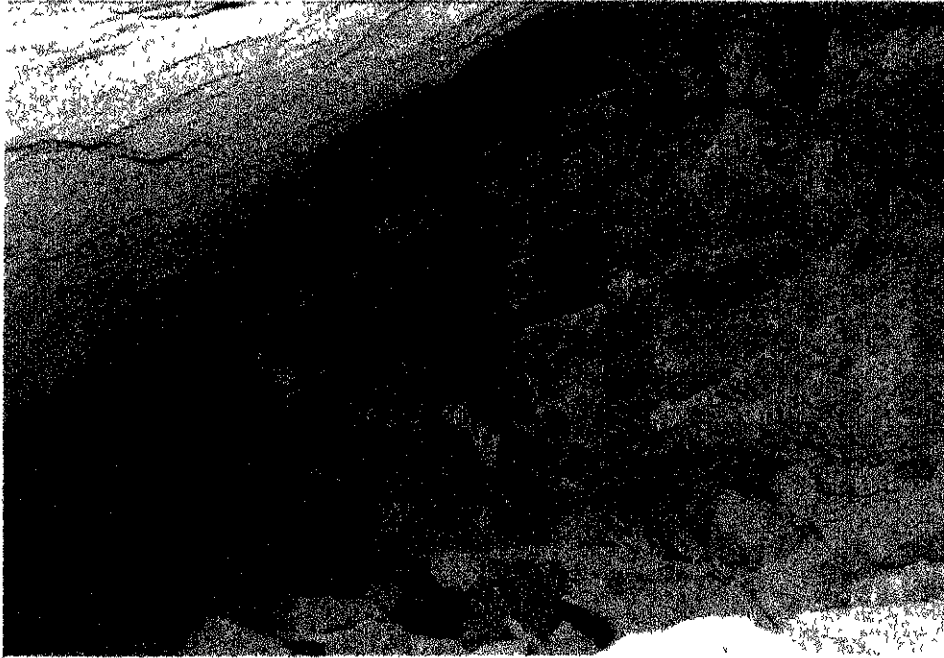
A half mined dome

As this presents a large dead weight situation, known domes in 22/8 stope have been left unmined (Photo 1).Attempts to predict the location of domes in advance have so far proved unsuccessful. However where a sub-horizontal serpentinized joint set occurs in the near hangingwall when mining in known disturbed ground, dome structures should be anticipated. Domes encountered in 22/8 stope typically increased the planned stoping width from 0,9 m to approximately 2 m over a typical diameter of 5 m.

Predicting falls of ground in 22/8 Stope

Six joint configurations have been identified as contributing to hangingwall instability.

These are:

A. Steep, planar, upward convergent joints that either intersect each other or intersect reef-parallel joints
(typical of strike joints).

B. Upward flattening (commonly cymoid curved) Strike joints with considerable lateral persistence (photo 4).

Photo 4

Cymoid Joint

C. Swarms of joints approximately on the reef strike with a dip of about 50 degrees (30 degrees to the plane of the reef) in a down-dip direction; these are thought likely to be serpentinised pyroxenitic cross-beds.

D. Occasional diagonal joints within Strike set swarms aligned 20 – 30 degrees to the main set and dipping more shallowly than the joints that they transect.

E. Clusters of upwards-flattening, semi-concentrically arranged, outward-dipping, low-inclination joints that form domical structures. Successive joints outward and upward are progressively more steeply dipping.

F. Occasional upward convergent pairs of dip joints that may cross through several Strike joints.

Pre-development allows for early inspection of these conditions. The joint configuration of categories A C D and F can be identified in advance . As most strike joints show considerable lateral persistence, any of the above configurations found to exist in the gullies are likely to persist throughout the adjacent panels.

Where key-blocks and shallow dipping weak joints are encountered good active support and good aerial coverage installed close to the face can contain collapses.

Configurations B and E remain unpredictable and are detected only when falls occur. Undermining a dome has proved to be difficult and dangerous with production personnel preferring to by-pass them and re-establish beyond their limits or alternately tarring them down. Cymoid curving joints, once evident, are usually successfully contained using stiff support.

Diagram 3
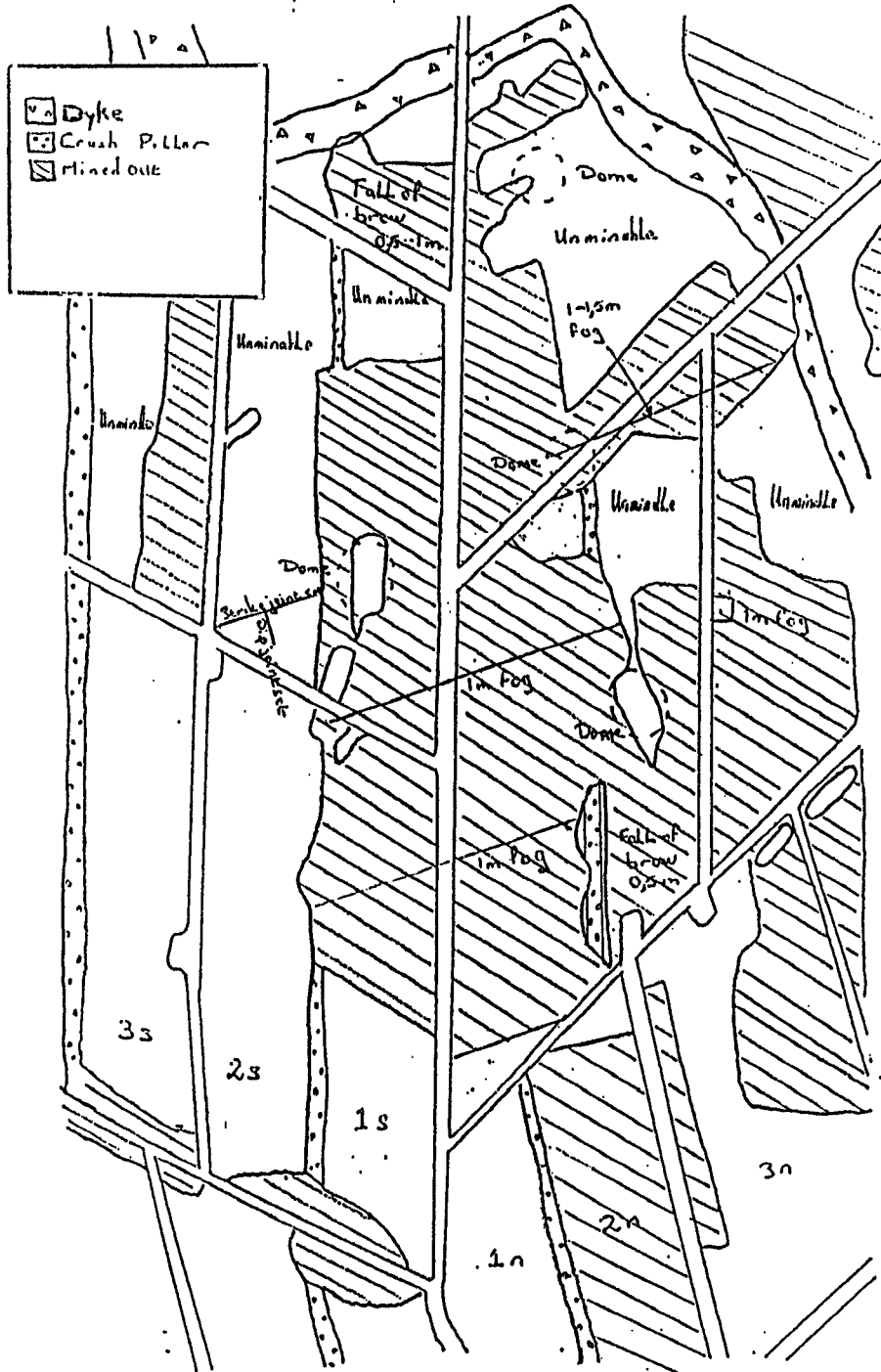
Appendix E2

Hangingwall Deformation Instrumentation Programme at RPM Union Section

PROJECT REPORT - GAP 024

Instrumentation

Introduction

The instrumentation programme was aimed at developing an understanding of the mining induced rock-mass behaviour, on the Bushveld Complex. Three different geotechnical categories have been proposed, mainly from visual observations, namely:
1) Good conditions
2) Intermediate conditions
3) Bad conditions

The first instrumentation site was located at Rustenburg Platinum Mine, Union Section. This site was identified as being in "Bad ground conditions". Work has progressed at the site from July 1994 and is due to be completed by the end of December 1995. During this time 160 closure and closure ride stations, 23 crack-meter stations, 7 stick loadcells and 8 extensometers were installed and 8 boreholes were geotechnically logged and 6 borehole camera surveys were performed. Interesting stope behaviour, not recorded by the instruments was also noted. An automated instrumentation system will be installed at the beginning of 1996 to verify some of our results. This system will only require limited supervision.

This report deals mainly with an analysis of the results of this first site and some appropriate deductions. The results of each instrument type is discussed under appropriate headings and a final overview is given in the conclusions. Graphs of the results may be viewed in the appendices.

Discussion

Stope sheets showing the instrumentation site and positions of all instruments are included in the Appendix.

Mining took place in the following sequences.:
1) Two breast panels immediately updip of the panels named Stope 3&4 were attempted.
2) The ledging and down-dip faces immediately updip of the panels Stope 1 & 2.
3) Panels marked Stope 1& 2 were mined on a Breast configuration.
4) The panel to the left of Stope 4 was attempted.
5) Stope 3& 4 were mined in a breast configuration.
6) Stope 5 & 6 were mined on a down-dip configuration simultaneously to the panels down-dip of stope 1& 2.

Panel Support

Temporary Support
Sticks were installed at the face in such a way as to ensure removal in the blast.

Permanent Support
Generally about 5 m was ledged before a row of grout packs was placed along the gully edge at a spacing of 2 m. After mining a further two or three metres a row of sticks was installed in Stope 1,2,3 & 4 but another row of packs in Stope 5 & 6. In Stope 1,2,3 & 4 lines of packs were alternated with sticks. The final configuration was support elements spaced skin to skin on a 2 m grid, dip and strike. Therefore in Stope 1,2,3 & 4 the spacing of the grout packs was 2 m on dip and 4 m on strike and in Stope 5 & 6, 2 m on dip and strike. However once the packs began to fail in Stope 3 & 4, other packs were installed.

Stoping width

There was a great variation due to "fallouts", however, generally the stoping width was about 1.2 m.

Mining history on panels Stope 3 & 4
Mining commenced on Stope 3 on the 14th December 1994. By 21st December 1994 the total span was 5.6m (including the width of the centre gully) and the first blast took place on Stope 4. Stope 3 & 4 were mined simultaneously until 6th January 1995, the full span was 12.9m. After this only the Stope 3 face was advanced to a total span of about 19m before mining commenced again on Stope 4. Although mining advance rates were initially relatively rapid, they later slowed and the final blast took place on Stope 4 about 100 days after the first blast. During the latter part of this time down-dip mining had been taking place on Stope 5.

Extensometer
These instruments were used to determine hangingwall movement and the depths at which this movement took place.

Extensometers were installed in three cubbies prior to mining:
   1) Cubby 1, where two holes were drilled: one to 50m and the other to 35m.
   2) Cubby 2, one hole to 35m.
   3) Cubby 4, one hole to 30m.
Two holes were drilled in Cubby 3, one to 50m and the other to 35m, and installation took place after Stope 4 had been partially mined. At this stage both holes were blocked at about 25m. Unfortunately the automated system used in this cubby covered the second hole so that only one could be used for reading.

From the results of Cubby 1 it was decided that short 10m holes would provide good information. Therefore 3 extensometers were installed in gullies at positions I2, I4 and I5 (see A1 in the appendix). I5 was installed 5m ahead of the mining down-dip face.

Most of the extensometers ended up being in pillars or unminable ground. The only exception was Ext1 & 2 located in Cubby 1. Therefore most of the information discussed below was based on the results of these two instruments. The information shown in the following graphs are based on movement between the anchor points and the collar of the hole.

Ext 1a

Ext 1b

EXTENSOMETER RESULTS - RPM UNION SECTION
CUBBY 1B - 22/8s/CENTRE GULLY

Legend:
- ■ 35.0 m
- ◆ 24.0 m
- ▲ 20.0 m
- ⊟ 7.5 m
- ◇ 1.0 m

Y-axis: MOVEMENT (mm) — 0, 20, 40, 60, 80
X-axis: TIME (DAYS) — 0, 100, 200, 300, 400
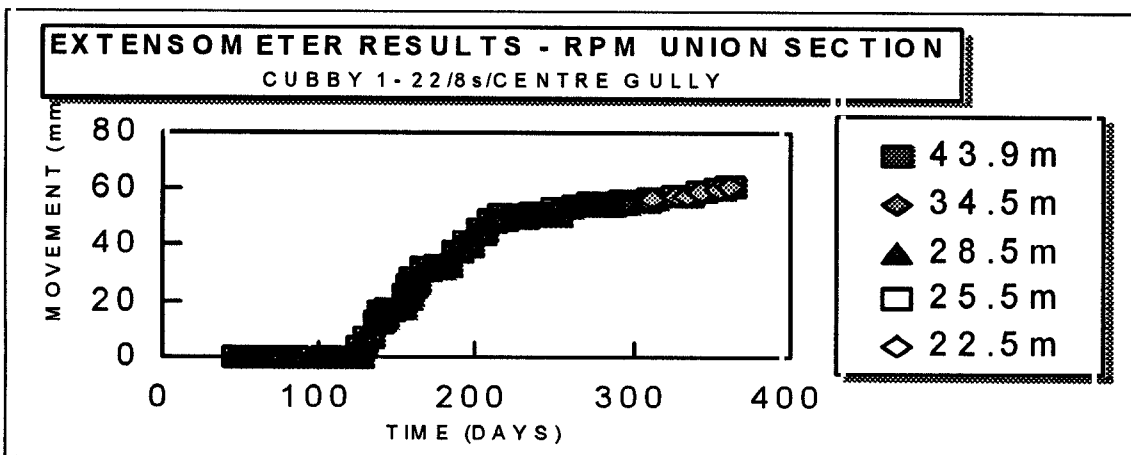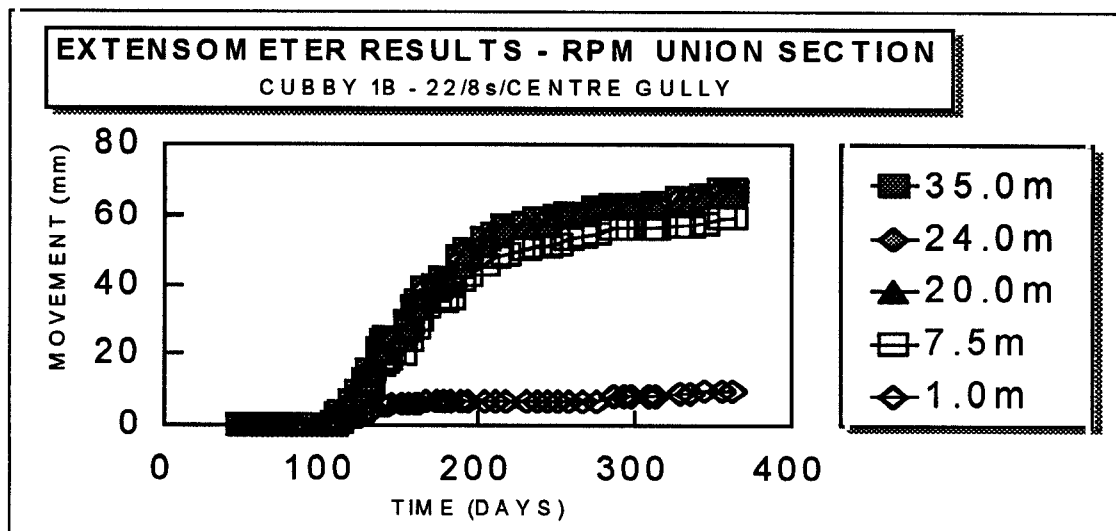
*NOTE

The total movement measured in the shorter hole is more than in the longer hole because of blast damage to EXT 1a, thus the initial movement was not recorded in that hole. However the results of EXT 1b were unaffected.

No movement was detected above 24.0m in either of the two holes and only 1 mm between 20.0 m and 24.0m. This indicates that little or no opening took place on the Bastard Reef contact, located about 25 m above the panel. Most movement took place between 1.0 m and 7.5 m with a relatively smaller movement below 1.0 m and between 7.5 m and 20.0 m., see appendix for details.

Movement was first detected when the mining face was in line with the extensometers. The span at this point was about 3.5 m including the centre gully. Between a span of 3.5 m and 19 m, movement occurred mainly below a depth of 1 m with a smaller amount between 1 m and 7.5 m. However once the span exceeded 19 m, at which stage a total of 22 mm hangingwall movement had occurred, very little further deformation occurred below 1 m indicating that the grout packs were generating a large enough support reaction to carry and confine a 1 m thickness of hangingwall.

The rate of movement decreased only about six days after mining of the panels was stopped, indicating strong creep behaviour. The creep behaviour was also observed during periods when no face advance occurred.

Extensometer located in Cubby 3

The extensometer in Cubby 3 off 3S drive, was located in the same "problematic" joint zone as the Closure Ride Meter stations discussed below (under "Problematic" Joints). Although there were problems with "fall outs", the depth of movement within the hangingwall was not shown to be significantly different to the results of Cubby 1. A graphical representation of the movement measured by the lower anchor points is shown below. A more comprehensive diagram of the total movement is located in the appendix, figure A29. Essentially openings in the hangingwall were confined to the lowest 4 m.

Initially a slight compression was measured in the hangingwall strata, as mining proceeded adjacent to the proposed crush pillar (surrounding the north side of the cubby). When stress fracturing was first detected in this pillar, downward movement of the loosened hangingwall was measured with the extensometer. The face had advanced 5.1 m down dip from the 3s drive.

After Stope 4 and Stope 6 had reached the positions indicated on the plans in the appendix figure A1, the extensometer equipment had to be removed because conditions around the site had deteriorate to such a degree that it was no longer safe to operate. The total movements measured between anchors was calculated and graphically presented in the appendix (figure A23). Downward movement, indicating tensile failure, was detected up to 10 m. Above this depth, a slight compressive closure was detected. This was probably as a result of the "Remnant" pillar located immediately to the south of the cubby.

Since the instrument was located in a pillar, face advance was not applicable and therefore a time base was used in the graph below.

EXTENSOMETER RESULTS

22/8d/3S DRIVE - CUBBY 3
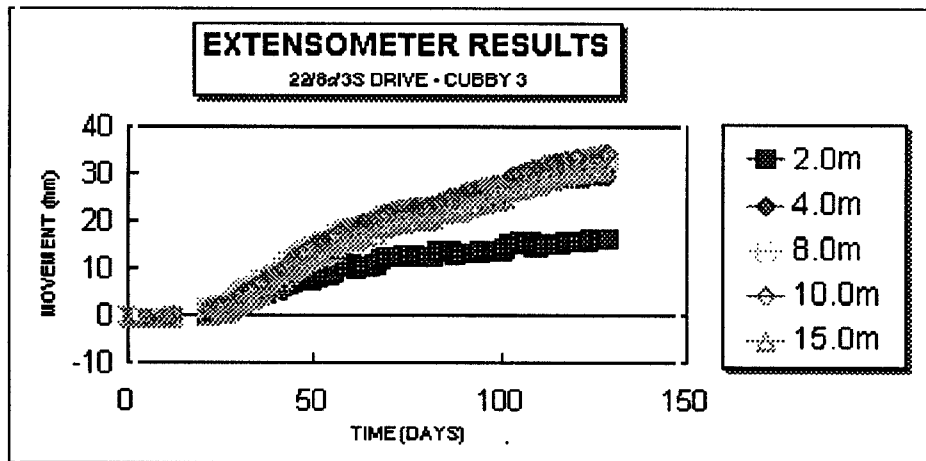
Closure-ride meter stations

The instruments were used to record closure and ride both prior to mining, in the pre-developed cubbies, and during mining, in the stopes.

For the purposes of this report only the following closure-ride meter stations are discussed:
1) The highlighted regions in plan 2 (figure A2 and A4 appendix).
2) A comparison between the highlighted regions on plan 3 (figure A3 appendix).
3) The results of Cubby 2 ahead of Stope 3 (figure A4 appendix).

1a) Closure in Stope 3 and 4

The graph below shows the closure results of stations in a line on dip parallel and close to the centre gully. Initially the closure rate was around 9 mm per metre of face advance. At about a span of 15 m the closure rate decreased to 6 mm per metre advance indicating that the grout packs were beginning to generate an effective support reaction. Comparing these findings with the extensometer Ext 1a & b results, indicates that the effective support reaction begins at a span of 15m and at a span of 19 m approximately 1 m depth of hangingwall is supported and confined. The measured closure at a span of 15 m was 82 mm and the extensometer results show about 10 mm of hangingwall opening. At this small span and relatively shallow depth (1200 m) this movement could be considered largely inelastic. In other words the hangingwall was significantly disturbed/loosened before a support reaction was generated.
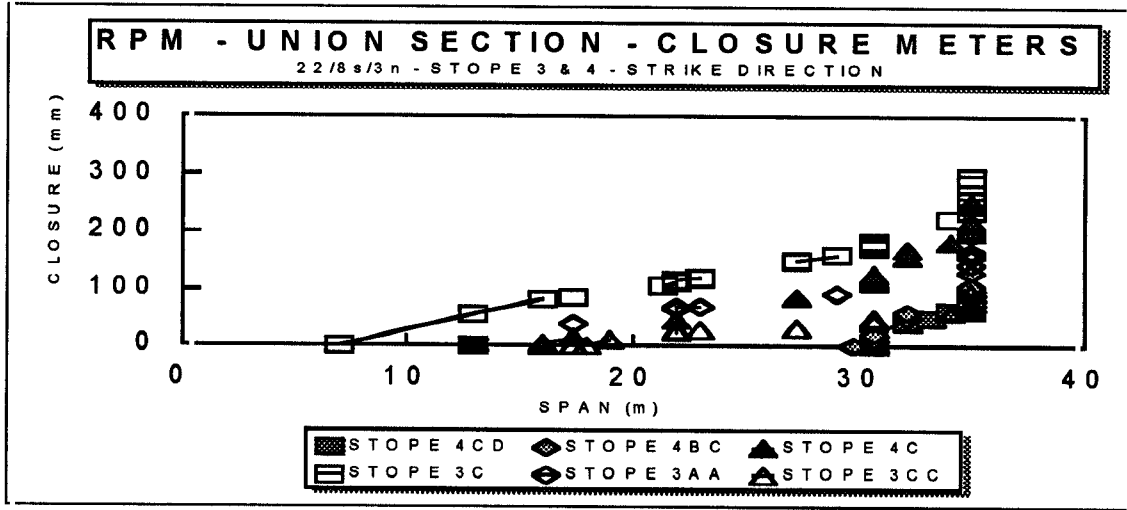
An increase in the closure rate to about 14 mm/m of face advance, was observed once the span exceeded 30 m. Although there was no evidence of an immanent back-break from the extensometer data, the possibly should not be ruled out.

Closure/span data is depicted below for stations 3A which was located at the top of Stope 3, to 3E towards the bottom of the panel. 3E did not show the same trends as 3A because down-dip mining of the panel below (Stope 5) started before the completion of Stope 4 (see figure A1).
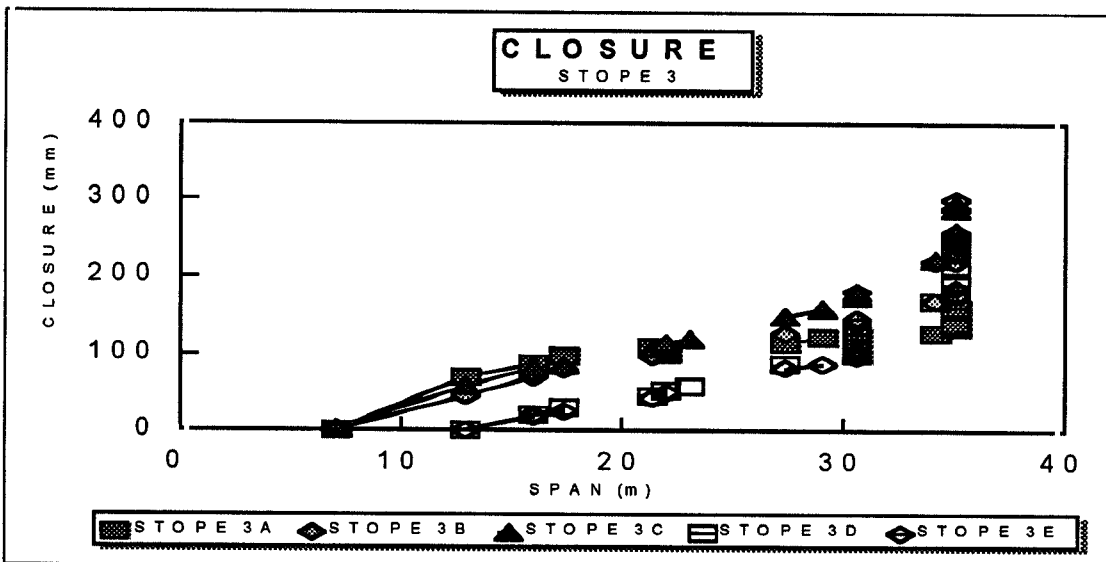

The following graph shows the closure results of closure-ride metre stations in a line on strike i.e. perpendicular to the faces. Station 4DC was located 3 m from the south face (left of Stope 4 figure 1A) and 3CC from the North face (right of Stope 3 figure 1A) when mining was stopped. The centre gully was located between 4C and 3C.

Note that closure rates for the stations located towards the centre of the panel show a similar trend to the previous graph. However the stations installed when a relatively large span already existed show a much higher initial closure rate of about 17 mm/m advance.

RPM - UNION SECTION - CLOSURE METERS
2 2 /8 s /3 n - STOPE 3 & 4 - STRIKE DIRECTION

Legend:
- STOPE 4CD
- STOPE 3C
- STOPE 4BC
- STOPE 3AA
- STOPE 4C
- STOPE 3CC

1b) Ride in Stope 3 and 4

If it is assumed that the footwall was moving relative to a static hangingwall, then the dip ride was down-dip by about 70 mm and strike ride was towards the centre gully averaging 35 mm. The graph below shows an example of the average ride measured on all the stations. Note the creep behaviour particularly shown at the end of the graph by the vertical lines.

DIP AND STRIKE RIDE
UNION SECTION - 22/8s/3N/1n - STOPE 3

Legend:
- DIP RIDE
- STRIKE RIDE
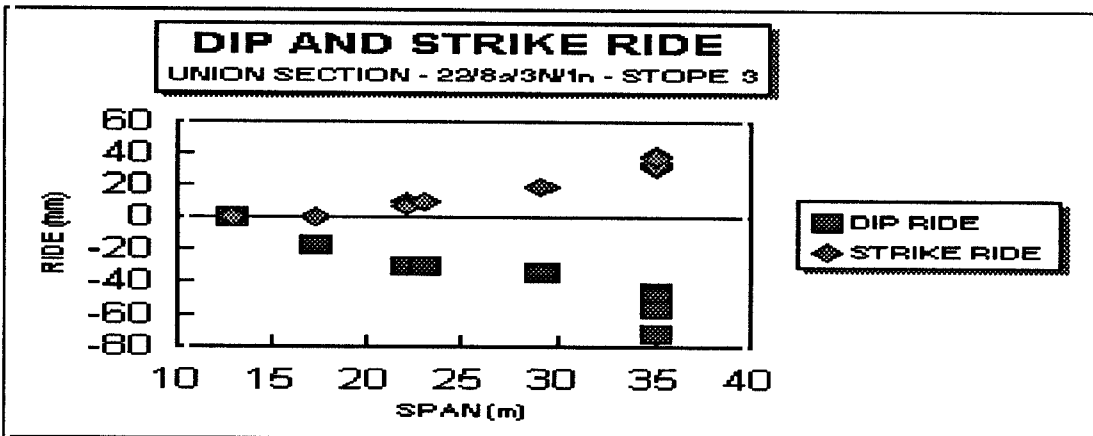
1c) Closure across "problematic" discontinuities

Prior to mining, several discontinuities were identified as being "problematic" due to their dip and strike orientations and fillings. One such discontinuity was traced from Stope 1 & 2 and cut through Stopes 5 & 4 and through Cubby 3. The trace of this discontinuity can be seen on the plan in figure A4 (appendix) indicated by the red line ending in Cubby 3. Large fallout's were associated in Stope 5 and Cubby 3. In Stope 4 however, where breast mining took place, it was possible to install support before a fallout. Closuremeter stations were also installed across this discontinuity in Stope 4, some results of which are displayed in the graph below. The relative positions of these stations are highlighted on the plan in figure A4 (appendix).
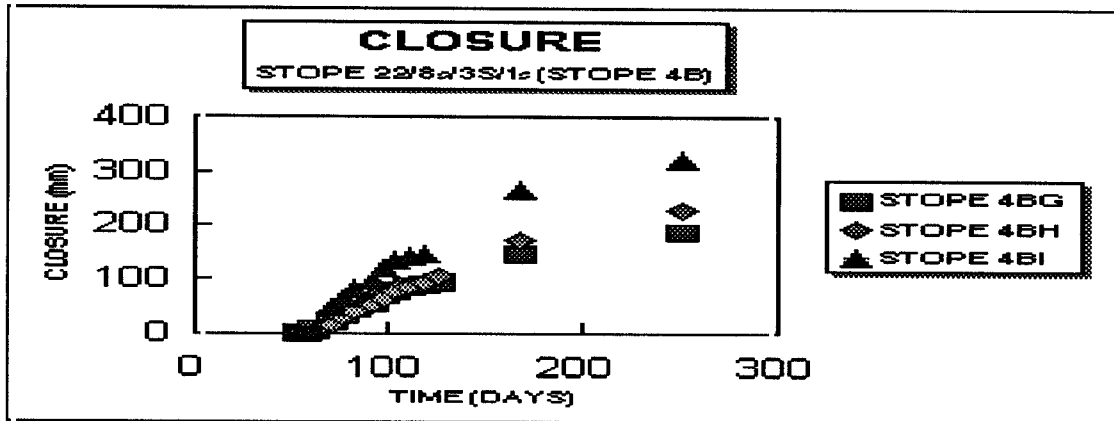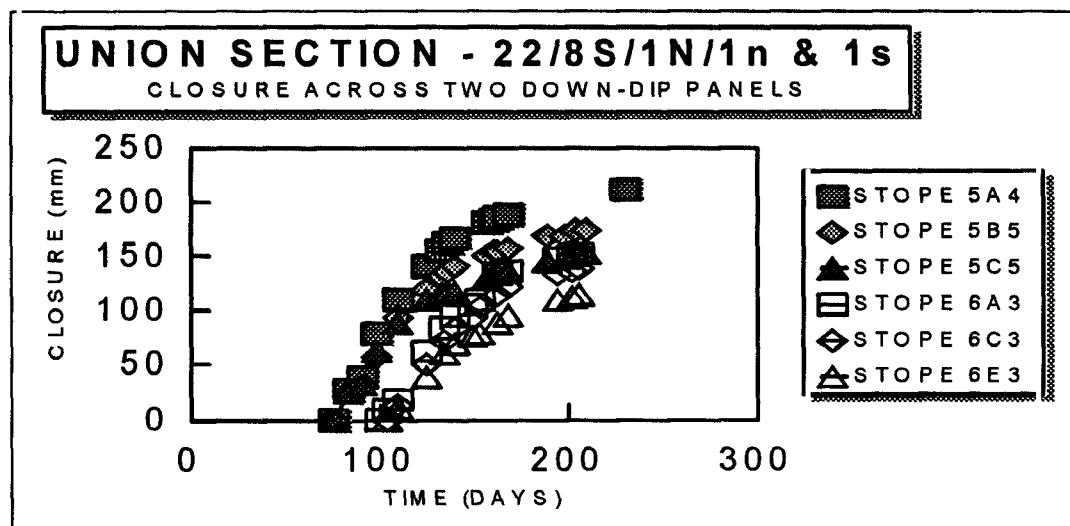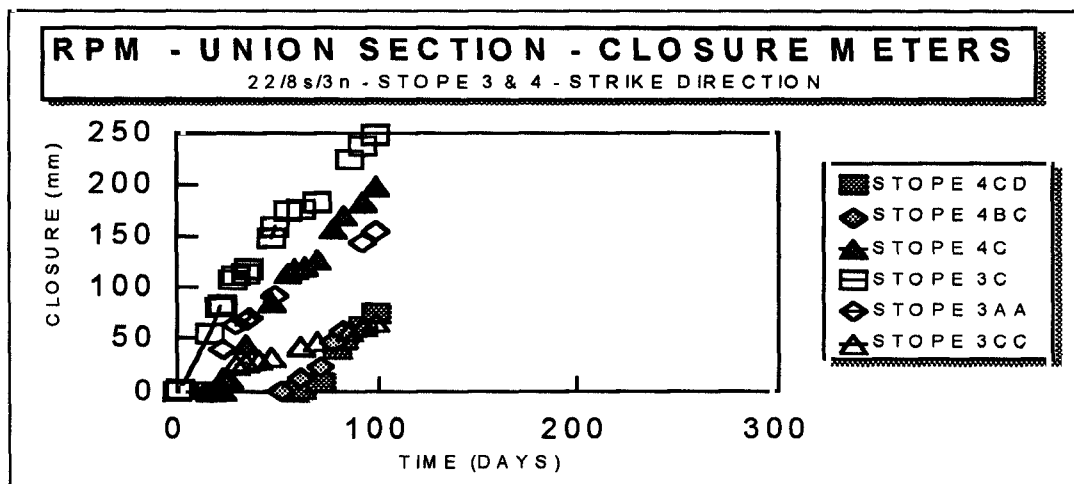

Closuremeter station 4BI was located below the discontinuity and the other two stations up-dip.
Note that the closure rate on 4BI was greater throughout the measured period, although similar trends occurred. Since the support resistance closure relationship was the same on either side of the discontinuity, it can be supposed that a greater force was involved on support elements immediately down-dip of the discontinuity. The extensometer installed in Cubby 3 however, did not show a greater depth of hangingwall movement. It is therefore assumed that the "extra" closure measured was associated with footwall movements. Since the joint persisted into the footwall, its trace was observed carefully once the panel was cleaned. Clear evidence of heave could be seen in Stope 4 but there was also an effect of tearing apart. Greater evidence of heave was observed in Stope 5, see observations below.

The observed "fallout's" associated with this discontinuity were about 1.5 m in depth.

2) Comparison between closure on Stopes 3 and 4 and Stopes 5 and 6

For the purposes of comparison a long time base was used in the graphs below to minimise such discriminating effects as face advance. The first of the two graphs shows the closure on Stopes 3 and 4 which were breast panels and the second, Stopes 5 and 6, were down-dip panels. Stopes 3 and 4 were mined before Stopes 5 and 6 and have a smaller span. Therefore it would be expected to have a smaller total closure than Stopes 5 and 6. However the graphs show the reverse to be true even although Stopes 5 and 6 was measured on a slightly longer time base.

RPM - UNION SECTION - CLOSURE METERS
22/8s/3n - STOPE 3 & 4 - STRIKE DIRECTION

STOPE 4CD
STOPE 4BC
STOPE 4C
STOPE 3C
STOPE 3AA
STOPE 3CC

UNION SECTION - 22/8S/1N/1n & 1s
CLOSURE ACROSS TWO DOWN-DIP PANELS

STOPE 5A4
STOPE 5B5
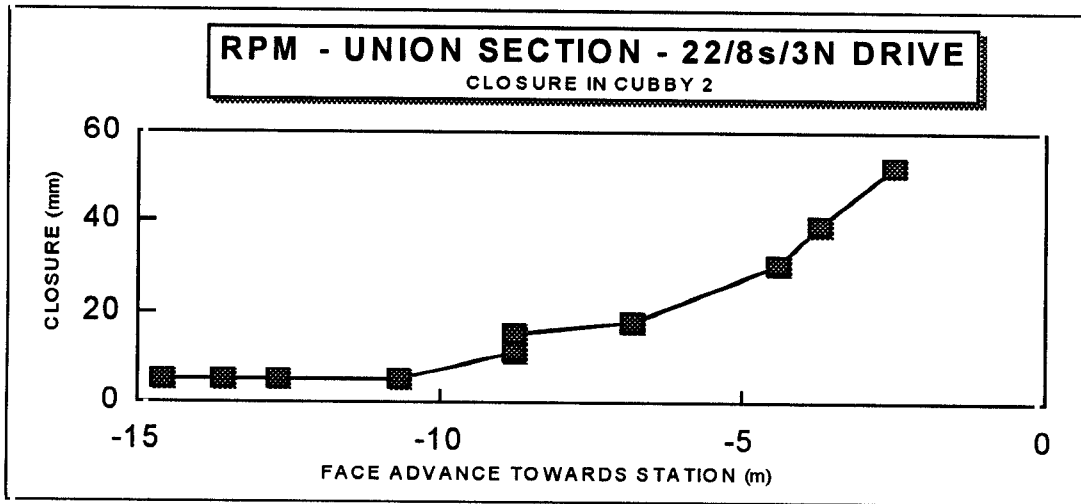STOPE 5C5
STOPE 6A3
STOPE 6C3
STOPE 6E3

) shows that, on the north side (right hand side) of Stope 5, relatively small pillars were cut. These pillars were intended to be crush pillars, however the average width of about 5m was too large and no crushing was observed. Stopes 3 and 4 were bounded on both the North and South sides by large, remnant, pillars.

Considering the relatively small spans in both Stopes 3 and 4 and Stopes 5 and 6 and the relatively shallow depth (approximately 1200 m below surface) the measured closure and closure rate is large. However if a mechanism of pillar punching and footwall heave is assumed then both the high closure rate and the difference in closure between the panels can be explained.
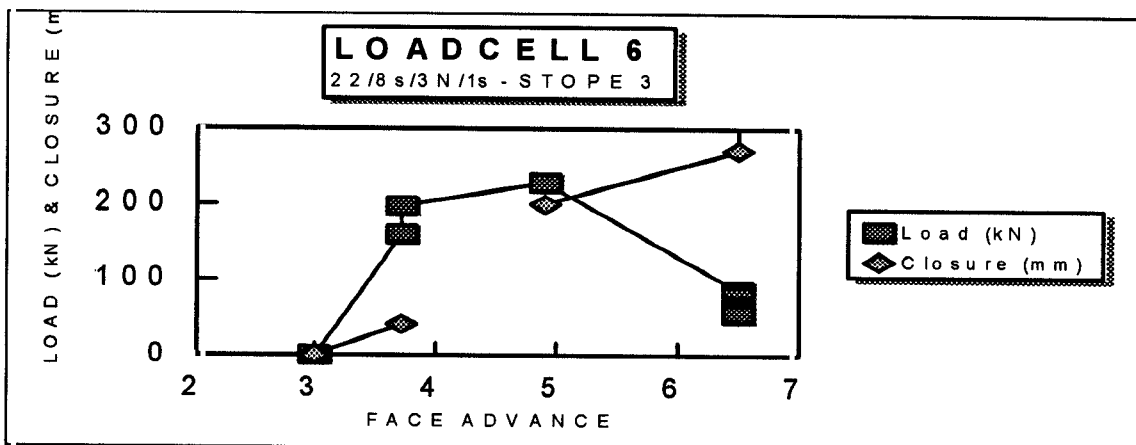
3) Closure ahead of the Stope 3 face

The results of Cubby 2, shown below, tend to confirm the pillar punching theory. As the mining face of Stope 3 advanced towards the station, closure was first observed when the face was about 10 m behind the station.

RPM - UNION SECTION - 22/8s/3N DRIVE
CLOSURE IN CUBBY 2

Graph: CLOSURE (mm) vs FACE ADVANCE TOWARDS STATION (m)

Stick load-cells

Referring to figure A1 (appendix), load-cells were installed at the positions marked by a small black circle (generally enclosing a closure meter red dot) in Stopes 1,2,3 and 4. Various positions within the panels were chosen i.e. near to the centre of a panel, close to a large pillar and close to the centre gully. The position did not appear to make a difference to the rate of loading.

The graph below is a typical example of most of the stations. Permanent support was usually installed 3 m from the face. Failure of the 200 mm diameter sticks generally took place after a 2 m face advance i.e. the face was 5 m from the stick. At this position the next row of permanent support was installed and the failed sticks replaced. Closure measured at the load-cell positions indicated about 25 mm deformation at failure i.e. 12 mm of closure per metre of face advance. This fast closure rate can be explained by pillar punching.

LOADCELL 6
22/8s/3N/1s - STOPE 3

Graph: LOAD (kN) & CLOSURE (mm) vs FACE ADVANCE
Legend: Load (kN), Closure (mm)

Deviations from the typical curve shown above were caused by the way in which the support elements were installed i.e. at an angle to the footwall or hangingwall where slipping or brushing occurred. One stick which had obviously not been turned in a lathe, was very much stronger than the typical stick.

Crack-meter stations

Two major joint sets were identified:

> 1) The set striking parallel to the strike of the reef and dipping towards the west i.e. up-dip of reef.
> 2) The set striking parallel to the dip of the reef.

For the purposes of this report the first set will be named "the strike set" and the second "the dip set." The strike set was the more continuous set, generally extending across the whole panel. The dip set was discontinuous often butting up against the strike set.

19 stations were installed at the positions marked by the circled numbers in figure A1 (appendix) to measure the lateral opening up of joints. Each station comprised two crack-meters, one on each of the two joint directions. At each of these positions plaster-of -paris was also installed.

No reliable information was derived from the crack-meter for two reasons:

> 1) The first blast on a panel bent and in many cases removed the pegs.
> 2) Subsequent movements were so small before the block fell out that it was not possible to measure using the available apparatus.

The plaster-of-paris was more successful, particularly when placed well away from the face. An interesting observation was made at a position just up-dip of Stope 1 and in Stope 1 where the monitored strike joint was dipping slightly down-dip. The section of hangingwall just up-dip of the joint moved down-dip, indicating a possible small horizontal force in the hangingwall. A diagram to illustrate this is included in figure A11 (appendix).

Plaster-of-paris installed ahead of the Stope 3 face did not show consistent results. At position 5 no detection of movement was observed even when the face was 1 m behind the station. However a fairly large fallout occurred 18 m ahead of the face seven days later. Plaster-of-paris in the region also showed movement at this time, but some positions indicated movement on the strike joints and others on the dip joints, without any apparent pattern. Considering that down-dip mining had been attempted in the region, it is possible that the joints had been loosened (perhaps without much movement) at that time. The repetitive vibrating action of the blasts could cause these loosened blocks to fall out even when blocks closer to the face, are unaffected.

Geological and Geotechnical logging

The cores from each of the diamond drilled boreholes drilled for the purposes of extensometers and borehole camera surveys were logged geologically and geotechnically. The geological logs and some parameters of the geotechnical logs are provided in the appendix, figures A5 to A10. Photographs of the cores are also located in the appendix, figures A22 to A28. Most of the joints, right up to 50 m above the stope, were infilled with serpentine which is a soapy type mineral, acting to lubricate the joints. It was therefore assumed that joint roughness on a micro scale would probably not be as significant as parameters such as joint density and has therefore not been included in the histograms in appendix 4. High angle joints were much more prevalent than the lower angle joints. RQD (Rock Quality Designation) is highly dependant on the driller and the speed he drills. It is therefore a useful tool to compare changes within a hole (provided one driller is involved) but when trying to compare different holes it can be confusing. However "joints per metre" is less dependant on the driller and is therefore more useful to compare holes.

Ext 1a and 1b were drilled in cubby 1 which was located in relatively good ground conditions. However the holes drilled in cubby 2 and cubby 3 were drilled in unminable ground conditions. Cubby 2 happened to be in a dome structure and cubby 3 in a "problematic" discontinuity zone. There does appear to be a slightly higher density of jointing, right up to the Bastard Reef, in the hole located in the dome structure. This hole also showed a higher density of low angle jointing especially in the first two metres. Analyses performed on the "joints per metre" may be compared in the appendix (figures A16 and A17).

Borehole camera surveys

The surveys were performed for several reasons:
        1) To observe exactly where the recorded movement was taking place in an extensometer hole
        2) To understand and prove the component of closure attributed to the hangingwall.
        3) To observe the state of a borehole prior to installing an extensometer.

Some of the observations are represented graphically in the appendix (figures A18 - A20).

Survey 1
This survey was performed in the same borehole as the long extensometer in Cubby 1, three months after mining of Stope 4 was completed. The lowest extensometer anchor was pushed upwards in an attempt to view the Bastard Reef contact. Unfortunately it was not possible to force the anchor above 25.44 m, which was just below this point. Some of the interesting observances are described below and a graphical representation may be viewed in figure A18.

At a point about 3.2 m above the stope two low angle fractures were open to about 30 mm each. Open flat dipping fractures were observed up to about 4.4 m and this was also the point where the highest, widely open, fracture was observed. Above this depth only steeply dipping joints were seen to be open. Comparing the number of fractures and joints observed in the immediate hangingwall, to the geotechnical log (which was performed prior to mining) there were many more low angle fractures/joints in the survey. It is therefore assumed that these planes are fractures induced by mining rather than naturally occurring discontinuities.

Comparing the depth of 4.4 m with the geological log, it appears that parting was taking place up to the base of the Norite. However it appears that the support reaction was probably only effective up to 3.2 m. Using the tributary area theory each pack should be carrying the load of rock with surface area of fifteen square metres. This works out to a load of about 144 t. Laboratory results indicate a pack strength of about 218 t. The difference could be attributed to the loading rates, loading before the grout had cured (which has not been tested in the laboratory) or the fact that the span where the survey was performed was larger than average, considering the fact that the hole was located in a cubby on the edge of a gully. The true in situ strength of these grout packs will be tested at the automated site, due to start early in 1996.

No evidence of lateral shear movement was observed in the survey. Rods were also pushed up to 50 m without giving any evidence of lateral movement. Therefore the following is assumed:

      1) The creep behaviour observed in the Closure-Ride Meter stations was associated with the footwall.
      2) No lateral movement took place on the Bastard Reef contact at this station.

Survey 2

At the time when the extensometer was installed in Cubby 3, mining was progressing towards the sight in the panel just up-dip of the gully (Stope 4). No mining had taken place down-dip or to the immediate south. This survey was performed to observe the state of the hole before installing the extensometer.

As shown in figure A19 (appendix), open joints/fractures were observed to a height of 14 m, however the high density zone was mainly confined to the first metre. The hole was blocked at 25 m preventing any further observation. The second hole in this cubby was also blocked but in this case at 22 m.

Comparing these results to the geological logs it appears that lateral movement took place at or near the Bastard Reef contact.

Survey 3

In order to understand the mechanisms involved with the footwall movements, it was decided to drill a hole up from the cross-cut into Stope 4 well after mining had been completed. The observations made in this hole are described below.

A marked increase of open fractures/joints was observed 9 m below the stope. From this point the joints were also more widely open. At a point 3.3 m below the stope, the widest open joint was observed. This joint was open to 15 mm and also showed signs of shear movement. A zone of high density fracturing (open fractures/joints) was observed for 1 m on either side of this discontinuity. Comparing these results to the geologists log showed that this position was close to the base of the Course Pseudo zone figure A20 (appendix).

Geomechanical Testing

Uniaxial compressive, Triaxial compressive, Brazilian tensile and Uniaxial tensile tests were performed on the cores from hangingwall holes in cubbies 1,2 and 3 and the footwall hole. These cores were also geotechnically logged. The results of the uniaxial tests, presented in the form of a histogram, may be compared to the Geotechnical logs in the appendix (figures A12 to A15). For comparison the extensometer anchor positions and results are also included. A report on the geomechanical testing including tables of results is included in appendix 2.

Generally one rock-type graded into another and it was therefore difficult to assess exactly where one rock ended and another started. Bearing this in mind the plotted change in strength will also probably be gradational. The pyroxenite found in the immediate hangingwall and the melanorite located immediately above that were the weakest rocks in the tested succession. The first notable increase in strength occurred from the base of the norite located immediately above the melanorite. This was also close to the highest point at which low angle fracturing was observed in the borehole camera survey.

The brazilian tensile tests and uniaxial tensile tests were performed at regular intervals within the first 10 m of hangingwall to verify any weak zones which could account for the observed partings in the borehole camera survey. No definite increase in tensile strength was observed in the region of 4.4 m but one specimen located 5.5 m above the hangingwall failed at a comparative very low value. The weak zone along which failure took place consisted of a higher density dark mineral, almost forming a lamina. Although the sample was pre-formed in the shape of a "dog-bone", failure preferred to occur on the "lamina" which was in the thicker portion of the specimen. The test was repeated three times on this specimen after glueing it together and in each case, failure took place on a different "lamina" at a low stress. If these weak zones persist at the top of the melanorite, they could be determining the height of parting and therefore support requirements.

The immediate footwall was not weaker than the immediate hangingwall and therefore did not provide confirmation for the pillar punching theory. However no geomechanical testing was performed in the Course Pseudo region, where most of the fracturing was observed. One uniaxial test at 19.24 m (3.11 m below the stope) showed a comparatively low strength of 99 MPa, however this result was influenced by a pre-existing discontinuity.

Observations

The following observations were made at the instrumentation sight:

1) Footwall heave was observed particularly along the "problematic joint zone" in Stope 5.

2) The depth to which most "fallouts" occurred was between 1 - 2 m.

3) Generally the blocks that fell out between discontinuities, in the hangingwall, appeared to come out as a unit and broke up on impact with the footwall.

4) "Fallouts" were usually associated with two phenomena: Joints cutting across the main joint direction, often these were "rogue" joints (with unusual dip and strike directions) and domes.

5) Most of the planes along which failure took place at the sight of a "fallout" were serpentinised.

6) Often the upper surface of a "fallout" appeared to fail on a zone equivalent to the 'lamina' observed in the uniaxial tensile tests.

7) One "fallout" was often followed by another in the same region, suggesting a "keyblock" mechanism of failure.

Photographs are located in the appendix (figure A21).

Conclusions

Comparing the extensometer results of Cubby 1 to the results of a closure ride meter station located immediately beneath (see graph below) the hangingwall openings constituted about a quarter of the total stope closure.

EXTENSOMETER AND CLOSURE RESULTS - RPM UNION
CUBBY 1b - 22/8s/CENTER GULLY
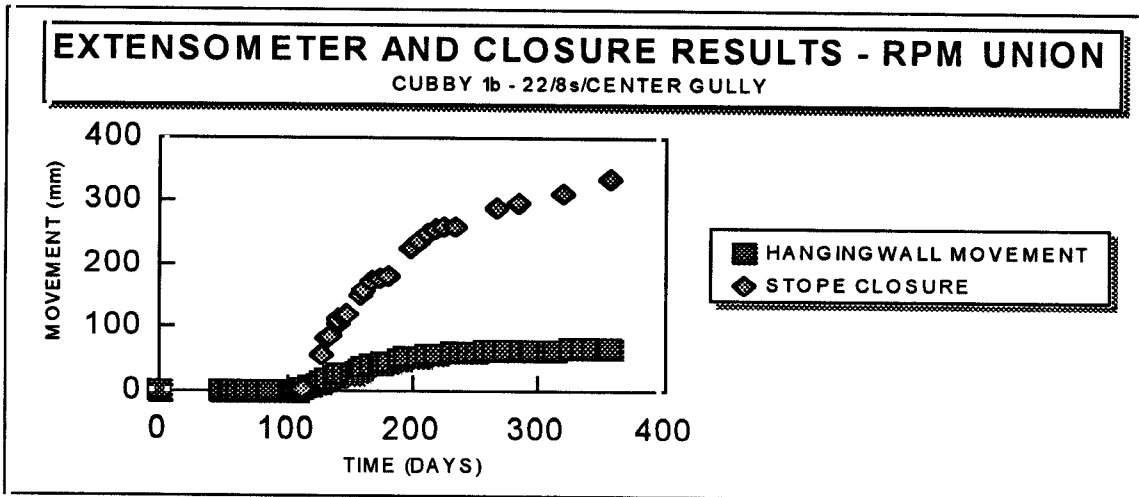
Based on the extensometer and Closure Ride Meter stations results in Stopes 3 and 4, a model of rock movement around the panel was formulated (see figure A29 appendix). Since there was only one extensometer result at the centre of the panel the footwall behaviour has been based on the total Closure Ride Meter station results. Therefore at the centre of the panel (where the hangingwall movement was known) the footwall component was around 200 mm. The Borehole Camera survey performed in the footwall indicated confirmation of this heave and also indicated that pillar punching could be a cause. Further evidence was attained by comparing the closure results in Stopes 5 and 6 with Stopes 3 and 4 and from the closure results in Cubby 2.

Based on the borehole camera survey performed in cubby 1, it appears that the induced failure due to mining, created a layer of relatively loose, broken rock, up to about 4.4 m in the hangingwall. Observations indicated that the immediate hangingwall was potentially divided into small blocks (often about shuebox size) by high angle surpentinised joints. It appears that in some cases vibrations caused by blasting were enough to loosen these planes. Removal of "keyblocks" often resulted in a much larger "fallout". Therefore the suggested qualities for effective support elements are listed below:
    1) Good areal coverage.
    2) Stiff or active support to ensure as little disturbance to the immediate hangingwall as possible.

Both the Extensometer and Closure Ride meter stations indicated a substantial stope movement before the Grout-Packs began to generate an effective support reaction. Although the sticks were stiff, failure occurred after a 2 m face advance. Therefore the system of support in this poor geotechnical domain was not adequate to prevent the many fallouts which occurred mainly at the time of blast. Further evidence was provided by the fact that large areas were considered unminable.

Closure rates in Stope 3 indicated a critical panel span of 30 m.

Appendix

Figures A1 - A4
Stope sheets showing the instrumentation sight at RPM Union Section and the instrumentation positions.

Figures A5 - A10
Histograms of some geotechnical parameters compared to the geological log of boreholes drilled in cubbies 1,2 & 3 and from the cross-cut.

Figure A11
Diagram of hangingwall movement along some "strike" joints, based on Crack-meter information.

Figures A12 - A15
Histograms of uniaxial compressive strengths compared to geotechnical logs and geological logs.

Figures A16 and A17
Analysis performed on the 'joints per meter' in two boreholes.

Figures A18 - A20
Histograms of the 'borehole camera survey' results.

Figure A21
Photographs of hangingwall "fallouts" and footwall heave

Figures A22 - A28
Photographs of the core from the extensometer holes and F/W1.

Figure A29
A model of movement around the stope based on extensometer and closure ride meter station results.
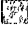
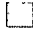## Appendix 2
Geomechanical testing report and results

.

Appendix
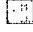
Stope sheets showing the instrumentation sight at RPM Union Section and the instrumentation positions.
Figures A1 - A4

RPM - UNION SECTION
22/8 STOPE SHEET
INSTRUMENTATION POSITIONS

RPM - UNION SECTION
22/8 STOPE SHEET
INSTRUMENTATION POSITIONS

Histograms of some geotechnical parameters compared to the geological log of boreholes drilled in cubbies 1,2 & 3 and from the cross-cut.
Figures A5 - A10

RUSTENBURG PLATINUM MINES
Union Section
Richard Shaft

Location: 22-8^S Raise (Peg F030 + 18 m) (Cuby 1a)
Attitude   + 90°

Location: R113/22
Date   10/8/94

Geological Log

Vertical scale

0   2   4   6 m

Extensometer
Results

RQD

Joints/m
≥45°

Core Recovery

Dip of joints

m

50,49

Mottled
Anorthosite:

45,26
44,43

Norite:

X

0
mm

39,54

37,17

Melanorite:

X

0
mm

Bastard
Reef:

X

0
mm

X

25,44   1
mm

Mottled
Anorthosite:

X

21,78

20,00

Spotted
Anorthosite:

15,50

55
mm

Leuconorite:

8,00

Norite:

4,44

Melanorite: 4,30

3,21   3,00

Pyroxenite:
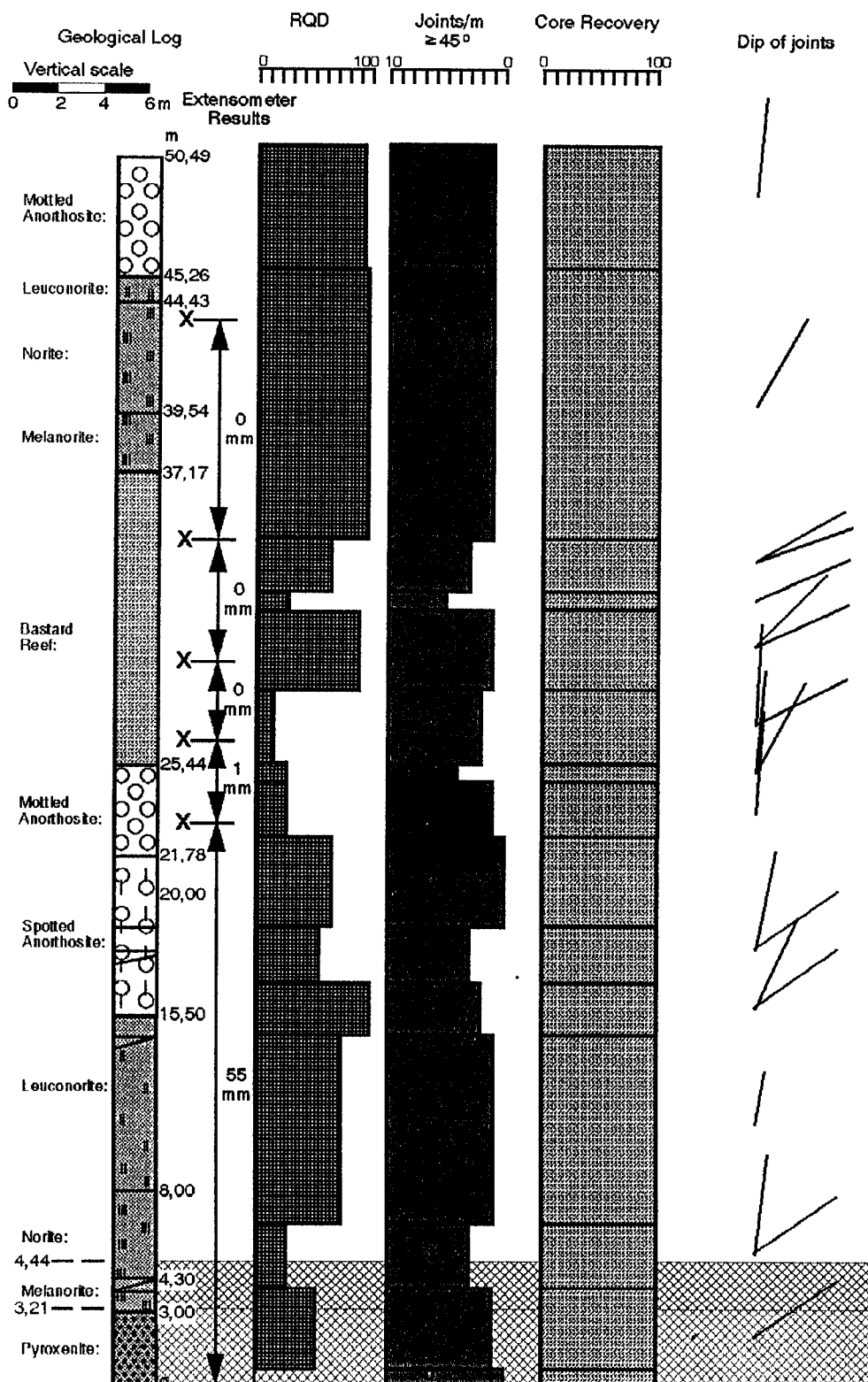
HOLE 1A

FIGURE A5

RUSTENBURG PLATINUM MINES
Union Section
Richard Shaft

Location: 22-8^S Raise (Peg F030 + 18 m) (Cuby 1b)
Attitude: + 90°

Borehole No.: R113A/22
Date: 31/08/94

FIGURE A6

RUSTENBURG PLATINUM MINES
Union Section
Richard Shaft

Location: 22-8^S Stope Drive 3N (Cubby 2)
Attitude: + 90°

Borehole No.: R113/22
Date: 25/10/94

Geological
Log

Geotechnical Log

RQD | Fracture/m | Core Recovery | Dip of Joints

FIGURE A7

RUSTENBURG PLATINUM MINES
Union Section
Richard Shaft

Location: 22-8^S Stope Drive 3^S(Cubby 3A)

Attitude + 90°

Borehole No.: R114A/22

Date: 28/10/94

Geological Log

Geotechnical Log

RQD   Fracture/m   Core Recovery   Dip of Joints

HangingwallLog

Vertical scale

0   2   4   6m
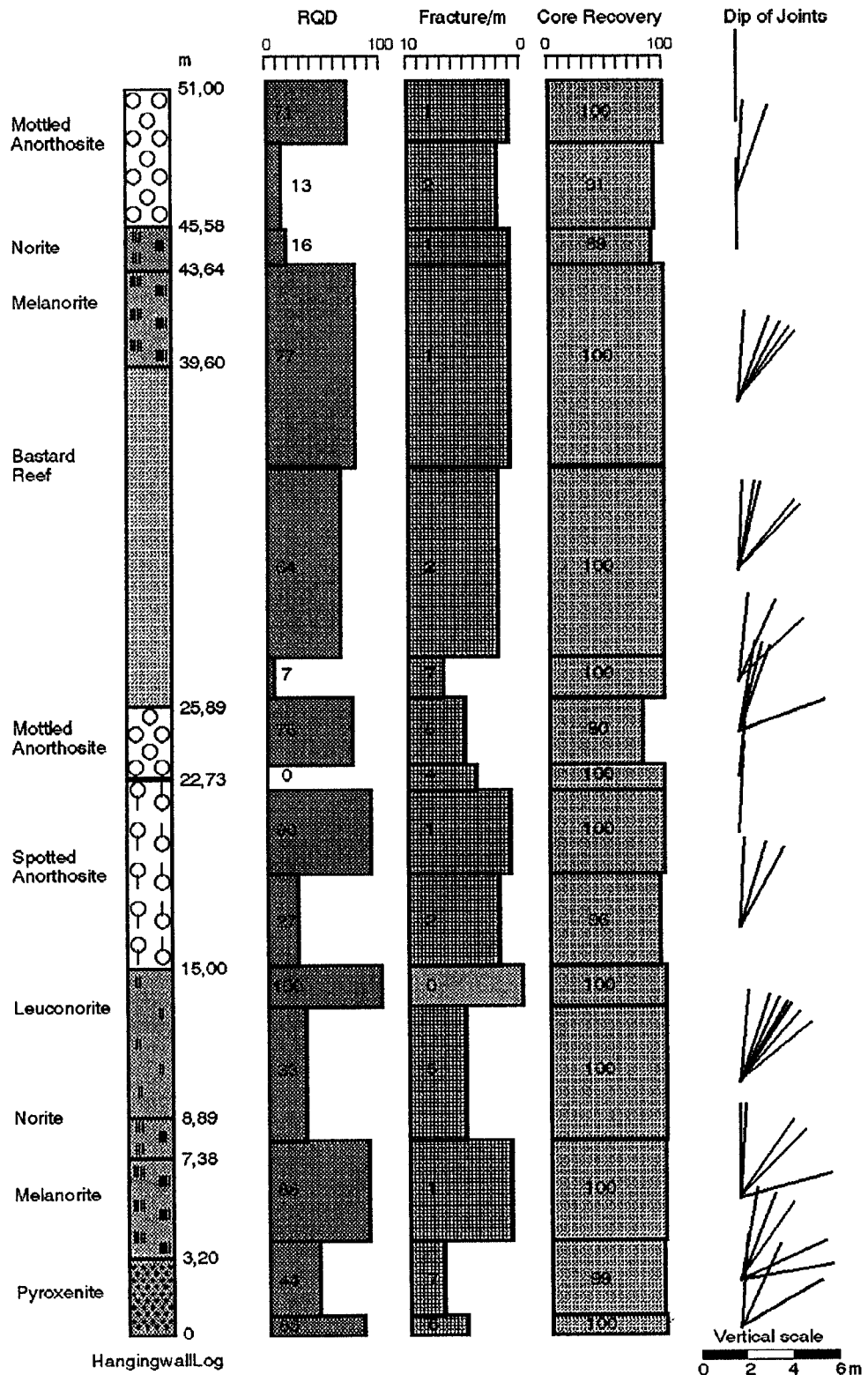
FIGURE A8

RUSTENBURG PLATINUM MINES
Union Section
Richard Shaft

Location: 22-8^S Stope Drive 3^S (Cubby 3B)   **Borehole No.:** R114/22

Attitude + 90°   **Date:** 28/10/94

Geological Log

Geotechnical Log

| | RQD | Fracture/m | Core Recovery | Dip of Joints |

| 0 | 100 | 10 | 0 | 0 | 100 |

	m	
Bastard Reef	27,90	
Mottled Anorthosite	25,63	
	23,10	
Spotted Anorthosite		16
		23
Leuconorite	15,25	
	10,17	
Norite		17
	7,45	
Melanorite		
	3,40	
Pyroxenite		
	0	

HangingwallLog

Vertical scale

0   2   4   6m
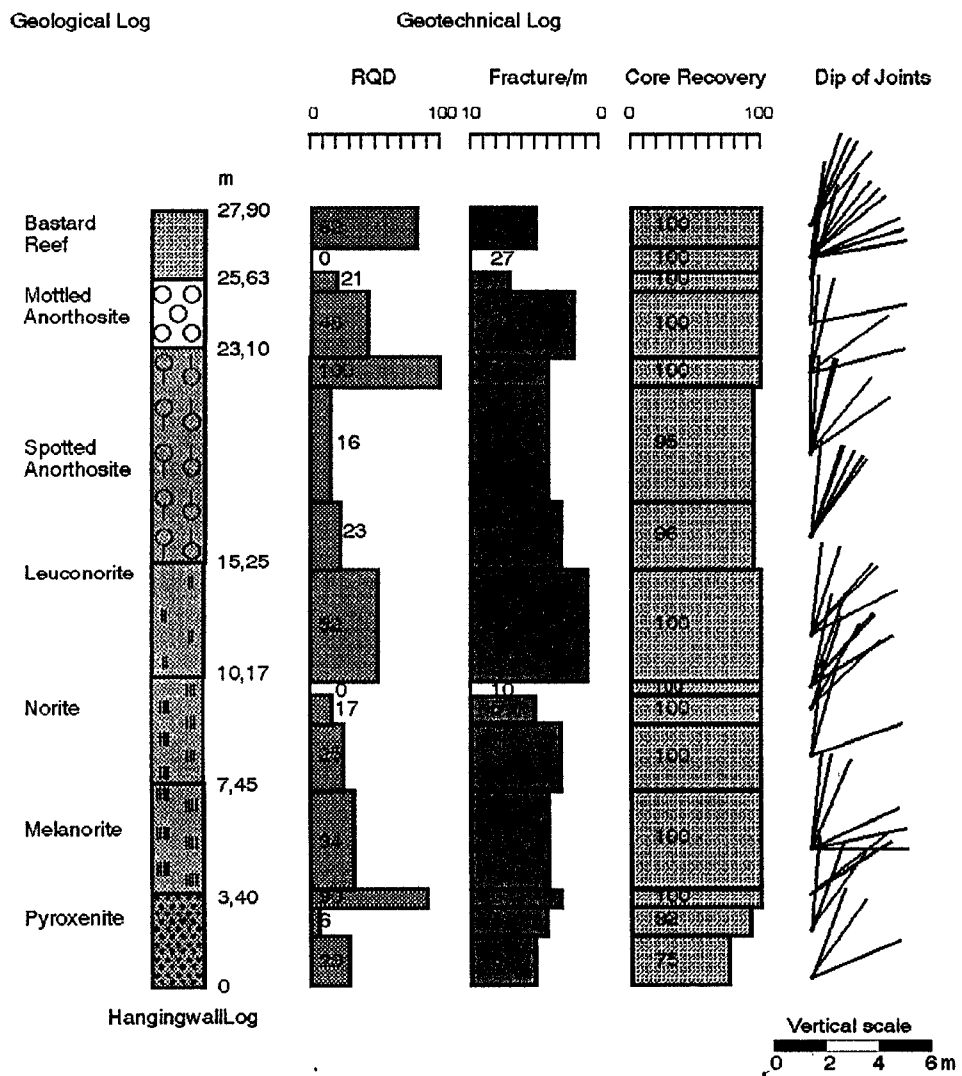
FIGURE A9

RUSTENBURG PLATINUM MINES- UNION SECTION

Borehole between cross-cut and 22/8s/3S/1S Stope - Drilled after Mining

Geology

Rocktype	Depth
Merensky	
Tarentaal	22,35 m
	20,85 m
Course Pseudo	19,60 m
Pyroxenite	
Harzburgite	5,32 m
	4,18 m
UG 2	2,89 m
Pyroxenite	2,09 m
Pyroxenite	

Geotechnical Log

RQD — 0 … 100

Joints/m — 10 … 0

Core Recovery — 0 … 100

Dip of joints

Mining Technology

Diagram of hangingwall movement along some "strike" joints, based on Crack-meter information.
Figure A11

320

SIDE-VIEW OF DOWN-DIP STOPE OF 3N DRIVE
SHOWING HANGINGWALL MOVEMENT ALONG
THE "A" JOINTS

"A" Joint

Hangingwall

Footwall

Face

Mining Technology

CSIR
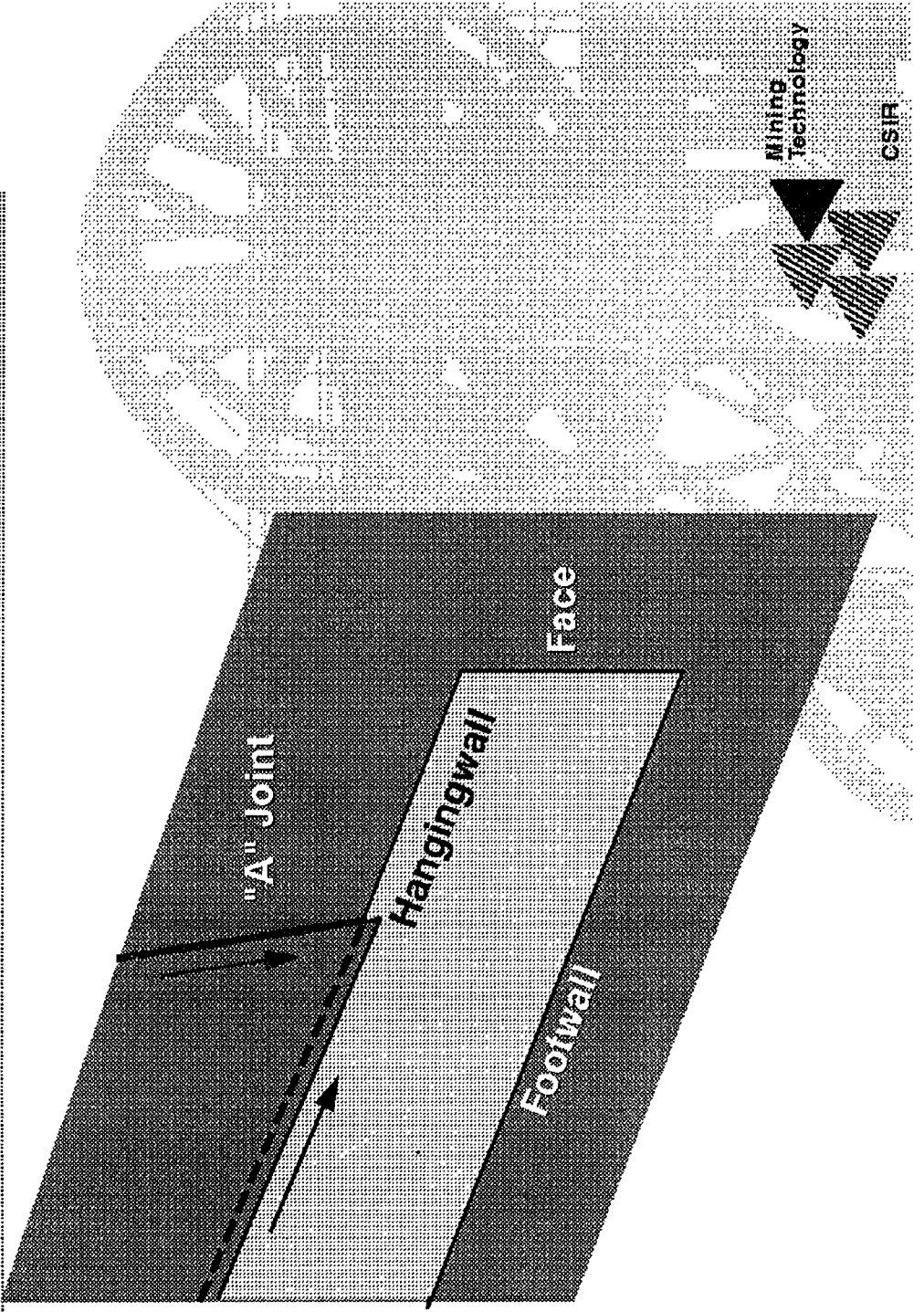
FIGURE A11

Histograms of uniaxial compressive strengths compared to geotechnical logs and geological logs.
Figures A12 - A15

RUSTENBURG PLATINUM MINES
Union Section
Richard Shaft

Location: 22-8^S Raise (Peg F030 + 18 m) (Cuby 1a)   Location: R113/22
Attitude + 90°   Date   10/8/94
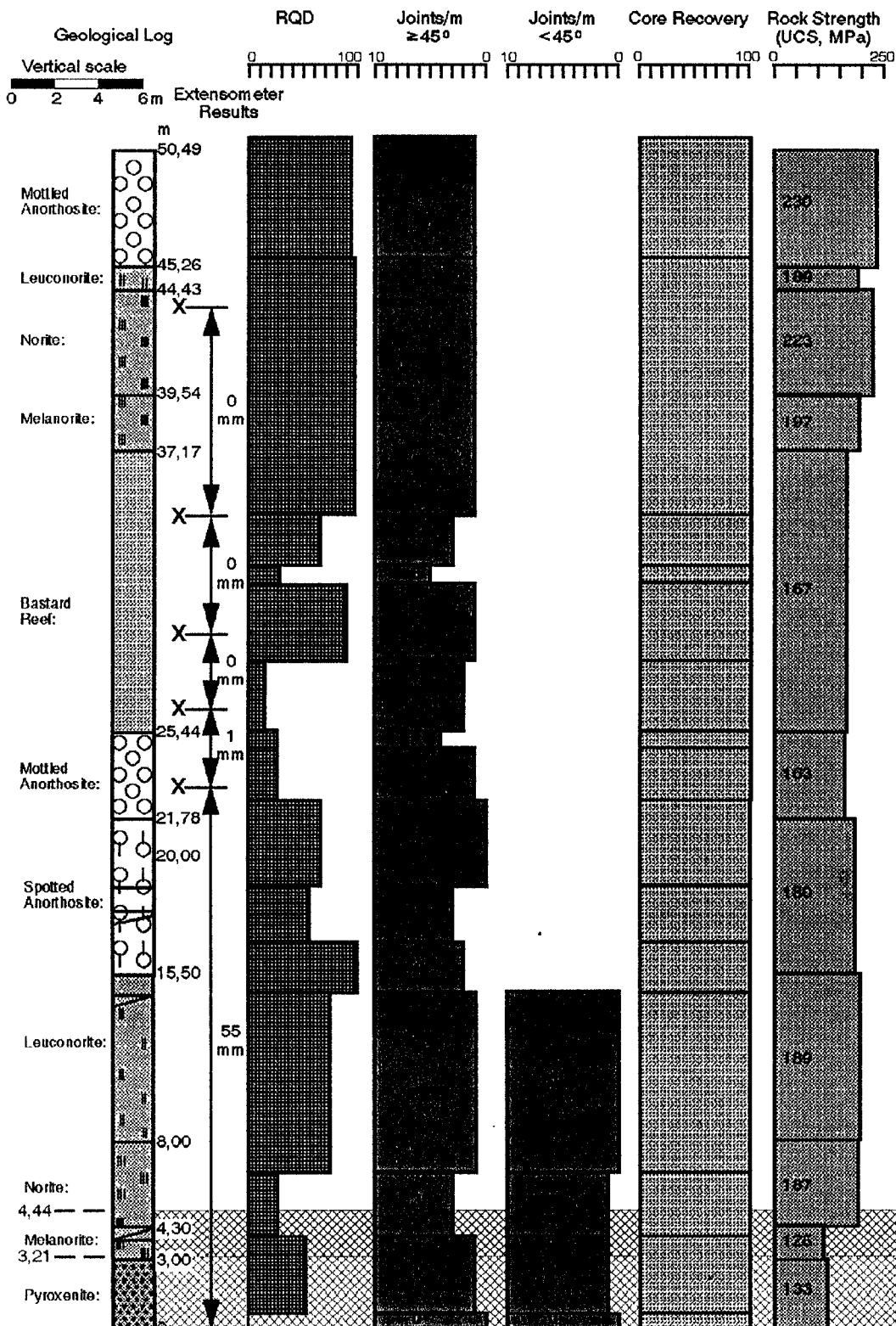
FIGURE A12

HOLE 1A

RUSTENBURG PLATINUM MINES
Union Section
Richard Shaft

Location: 22-8^S Raise (Peg F030 + 18 m) (Cuby 1b)

Attitude: + 90°

Borehole No.: R113A/22

Date: 31/08/94

Vertical scale

0 2 4 6 m

Geological
Log

Geotechnical Log

RQD	Joints/m ≥ 45°	Joints/m < 45°	Core Recovery	Rock strength (UCS, MPa)
0 100	10 0	10 0	0 100	0 250

Extensometer
Results

Bastard Reef:

Mottled Anorthosite:

Spotted Anorthosite:

Leuconorite:

Norite:

Melanorite:

Pyroxenite:

Hangingwall

36,00

25,24

22,24

14,90

8,13

6,00

4,44

3,21

3,20

0

mm

1 mm

7 mm

48 mm

9 mm

187

183

180

189

187

126

133
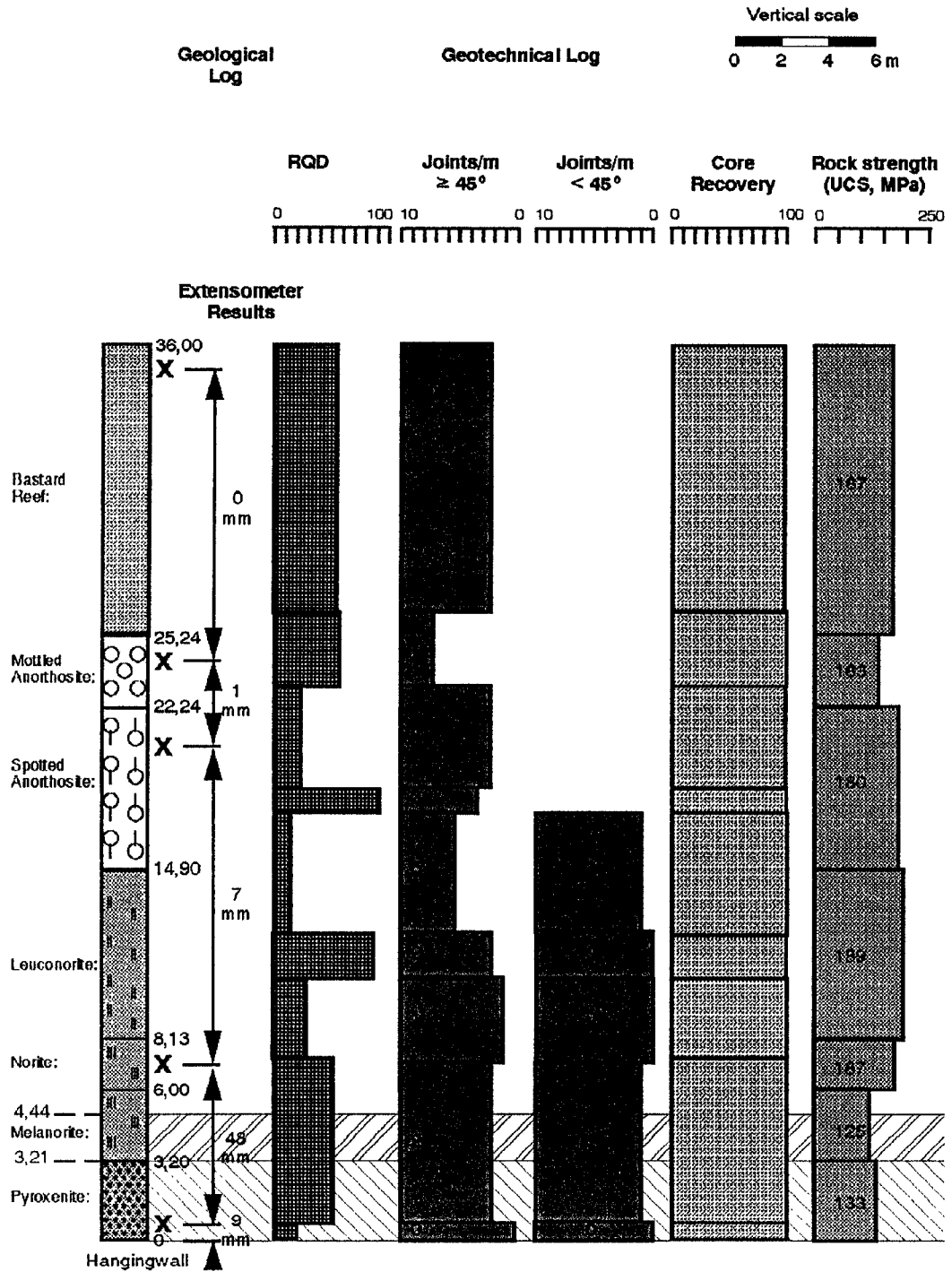
FIGURE A13

HOLE 1B

RUSTENBURG PLATINUM MINES
Union Section
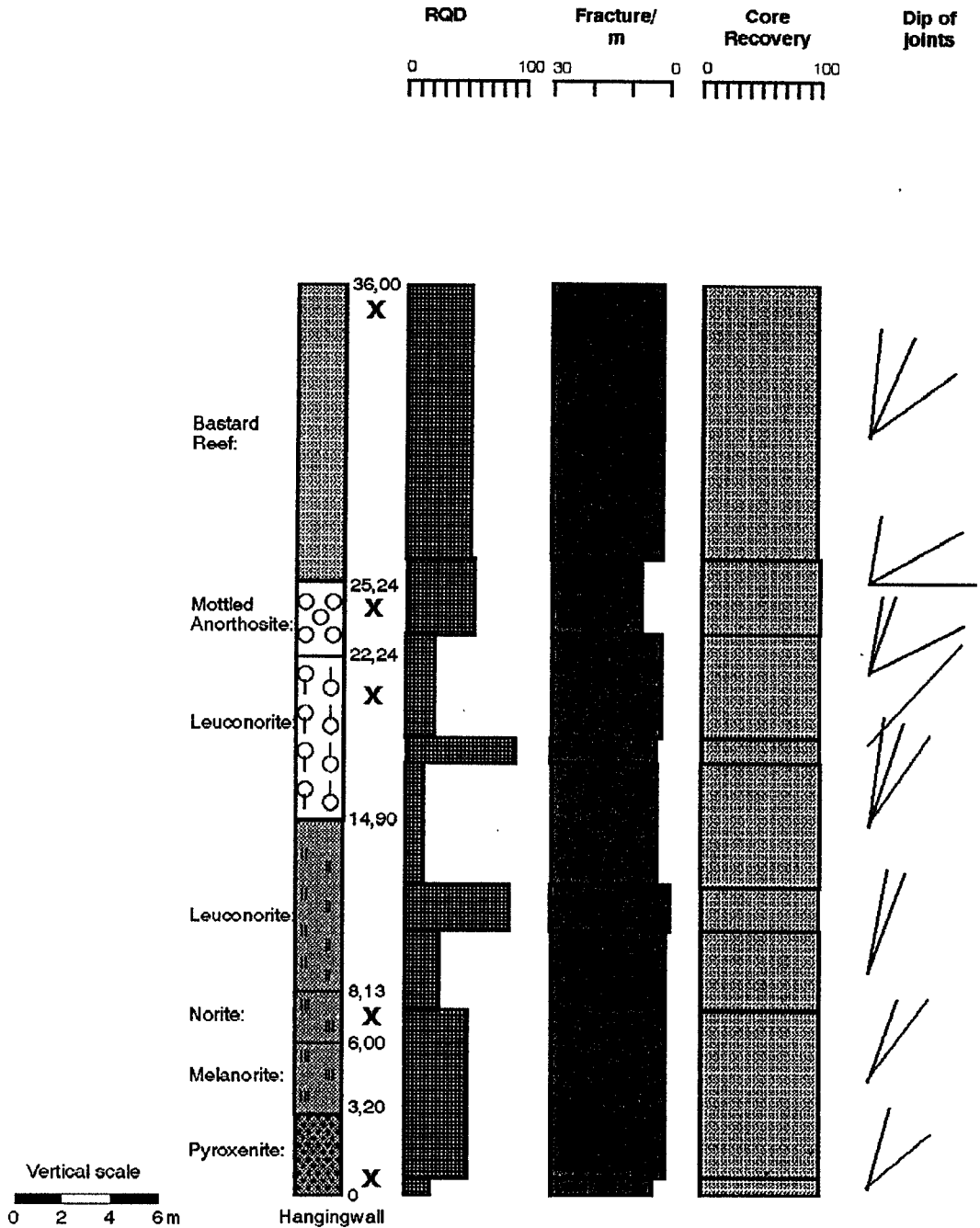### Richard Shaft

Location: 22-8^S Stope Drive 3^S Cubby 3A

Attitude + 90°

Borehole No.: R114A/22

Date: 28/10/94
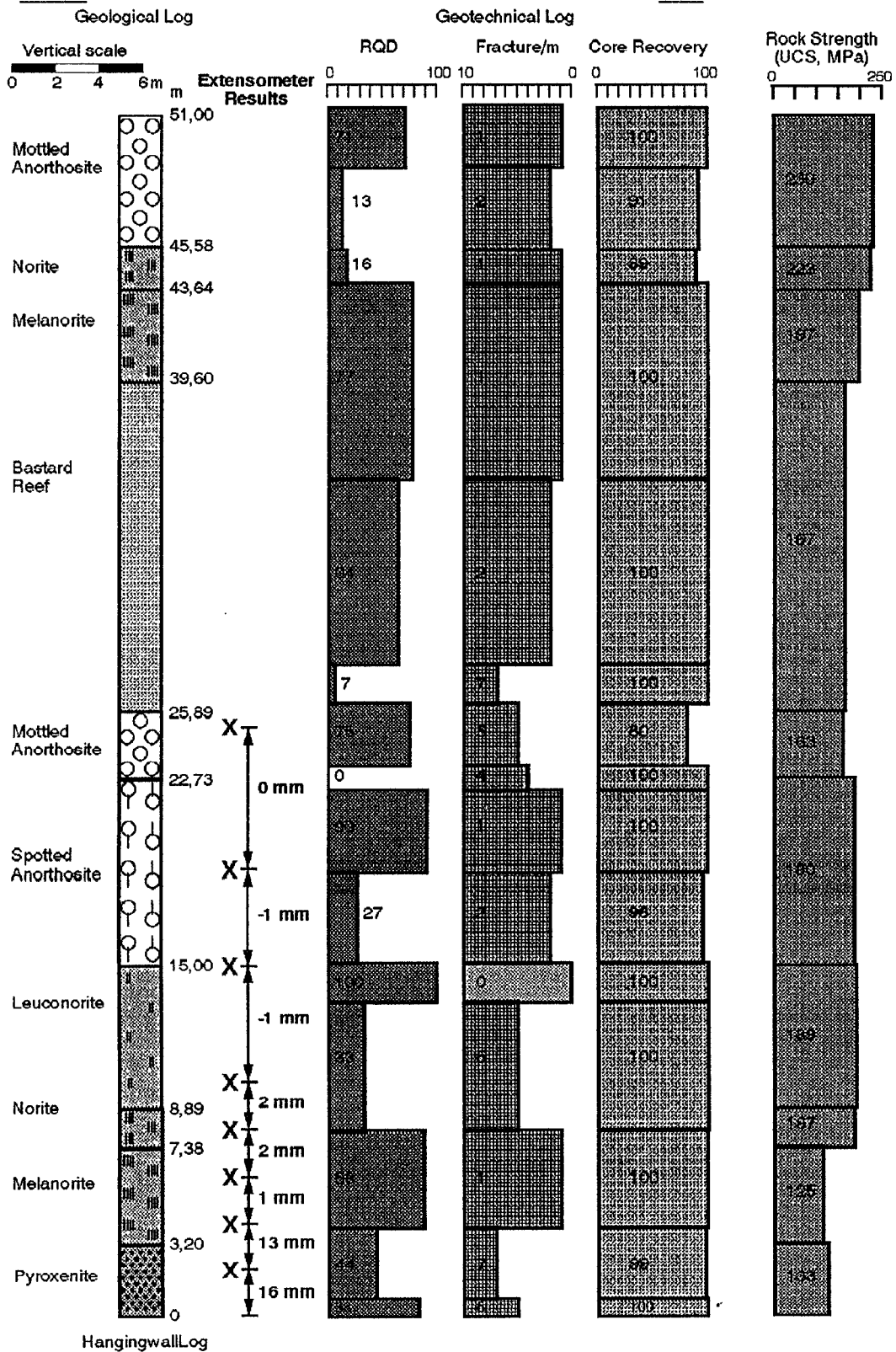
FIGURE A14

RUSTENBURG PLATINUM MINES- UNION SECTION

Borehole between cross-cut and 22/8s/3S/1S Stope -
Drilled after Mining

Geology		Geotechnical Log			
		RQD	Joints/m	Core Recovery	Rock Strength (UCS, MPa)
Rocktype	Depth	0 100	10 0	0 100	0 250

Merensky

Tarentaal — 22,35 m — 218

— 20,85 m — ?

Course Pseudo — 19,60 m

Pyroxenite — 167

Harzburgite — 5,32 m

— 4,18 m

UG 2 — 38

Pyroxenite — 2,89 m — 101

— 2,09 m

Pyroxenite

Cross-Cut

Analysis performed on the 'joints per meter' in two boreholes.
Figures A16 and A17

327

FIGURE A16

328
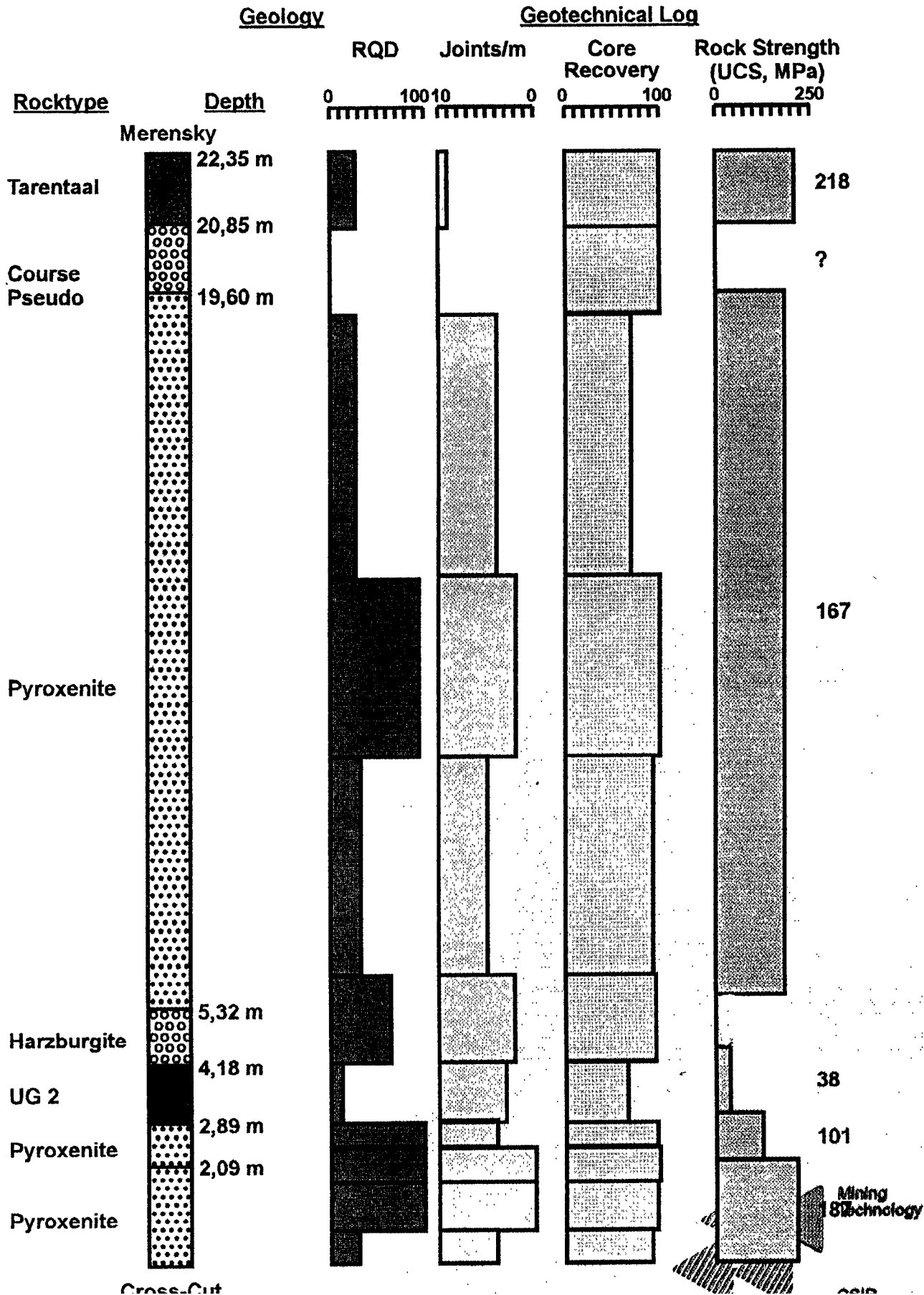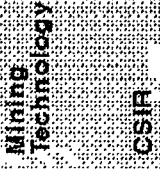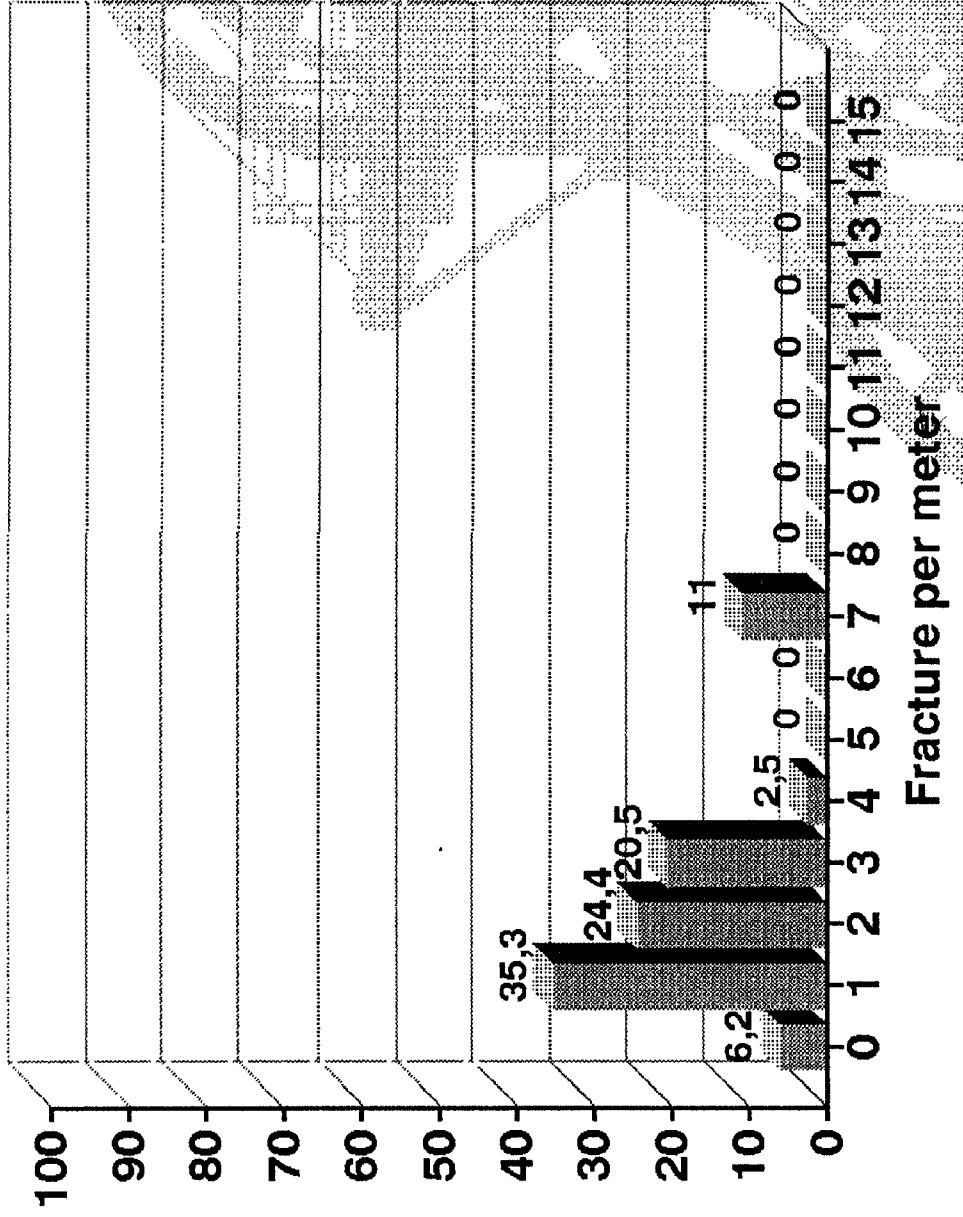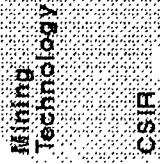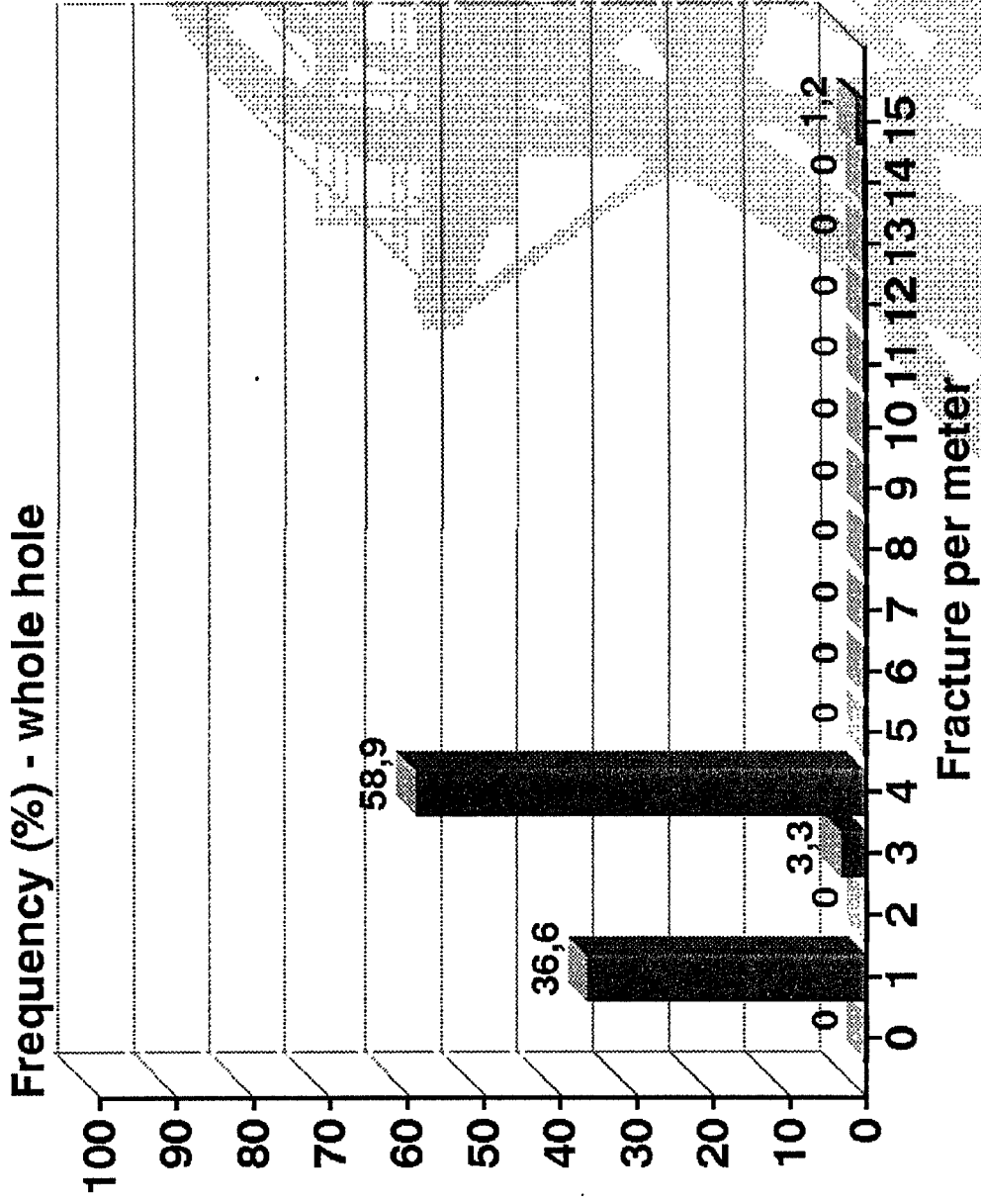
FIGURE A17

Histograms of the 'borehole camera survey' results.
Figures A18 - A20

RUSTENBURG PLATINUM MINES
Union Section
Richard Shaft

Location: 22-8^S Raise (Peg F030 + 18 m) (Cuby 1a)

Attitude + 90°

Location: R113/22

Date: 10/8/94

Geological Log
Vertical scale

0   2   4   6 m

Borehole Camera Survey

Depth (m)	Open	Angle (0)

25,44

Mottled Anorthosite:

X

21,78

24.30 m   **0.5 mm**

20,00

Spotted Anorthosite:

17.83 m   **0.5 mm**

15,50

Leuconorite:

8,00

7.99 m   **0.5 mm**

Norite:

5.57 m   **0.5 mm**

4.44 m   **3.0 mm**

Melanorite:

3.21 m   60.0 mm

3,00

2.28 m   10.0 mm

Pyroxenite:

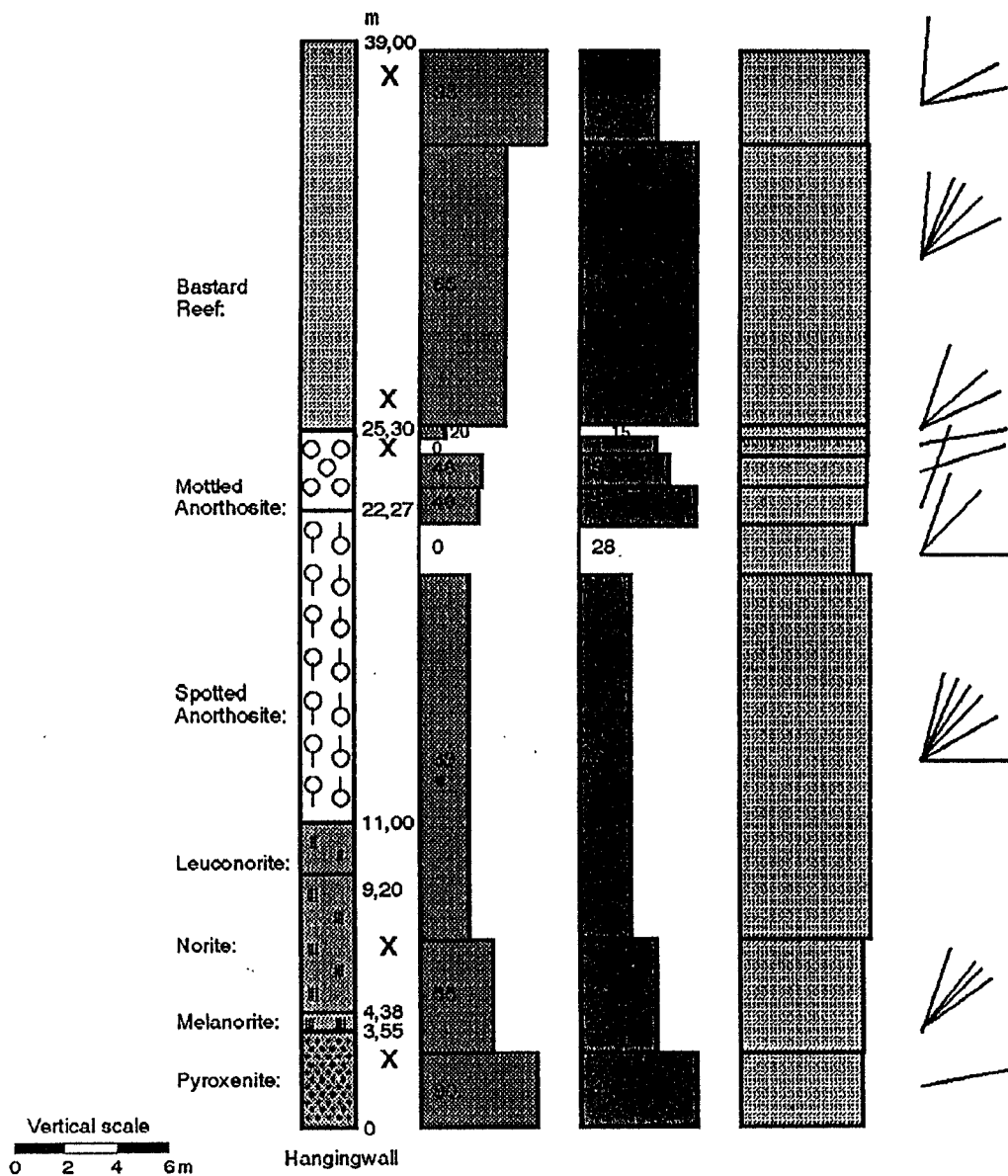**1.52 m   5.0 mm**

0.78 m   3.0 mm

0
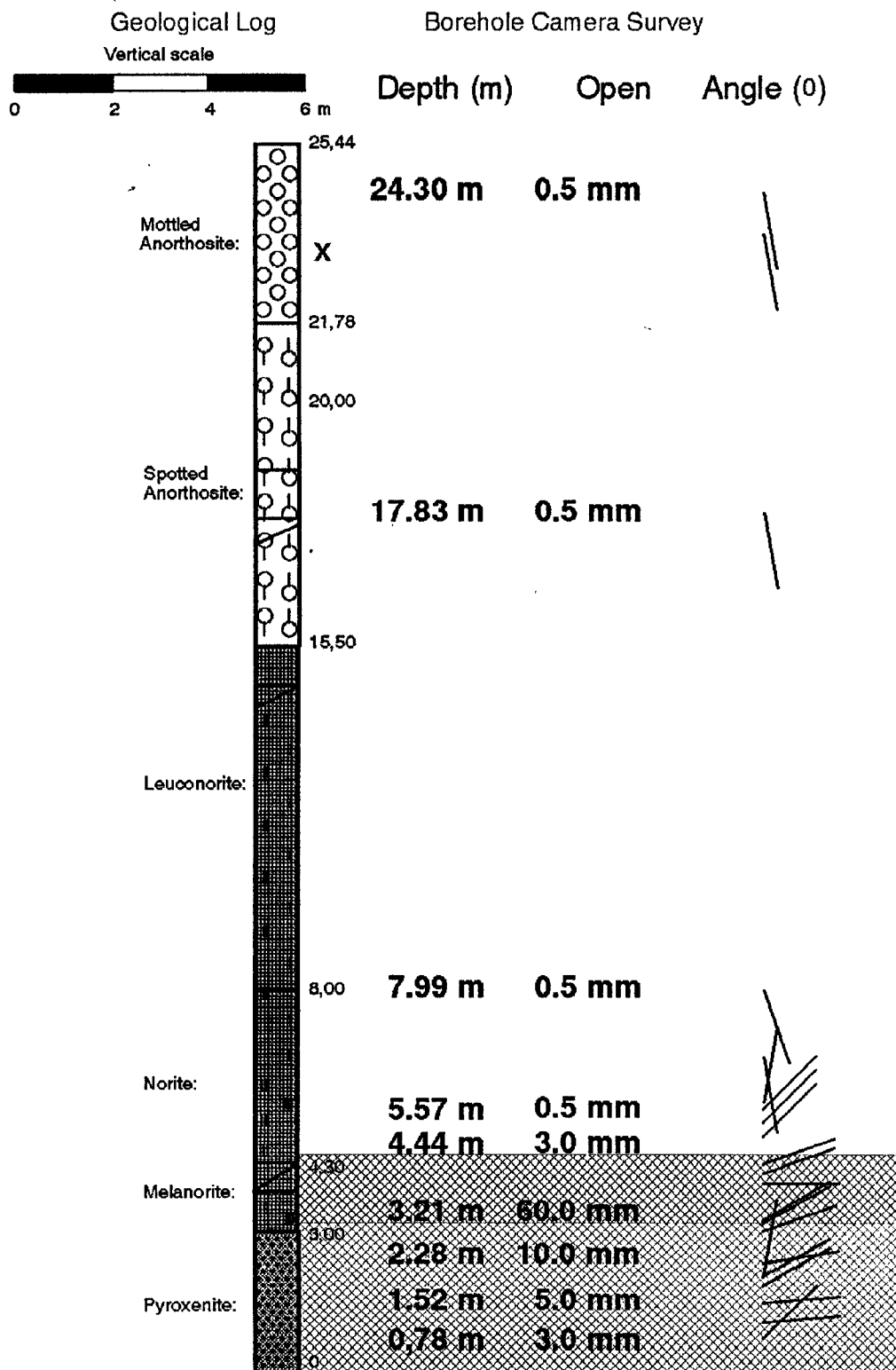
FIGURE A18

SURVEY 1

RUSTENBURG PLATINUM MINES
Union Section
Richard Shaft

Location: 22-8^S Stope Drive 3^S Cubby 3A

Attitude +90°

Borehole camera survey performed
before installing the extensometer

Borehole No.: R114A/22

Date: 28/10/94

Geological Log

Vertical scale

0   2   4   6m

Extensometer
Results

Number of open fractures

0   10

Rock Strength
(UCS, MPa)

0   250

25,89

Mottled
Anorthosite

22,73

0 mm

Spotted
Anorthosite

1 mm

15,00 X

1 mm

Leuconorite

2 mm

8,89

Norite

2 mm

7,38

Melanorite

1 mm

3,20

13 mm

Pyroxenite

16 mm

0

HangingwallLog
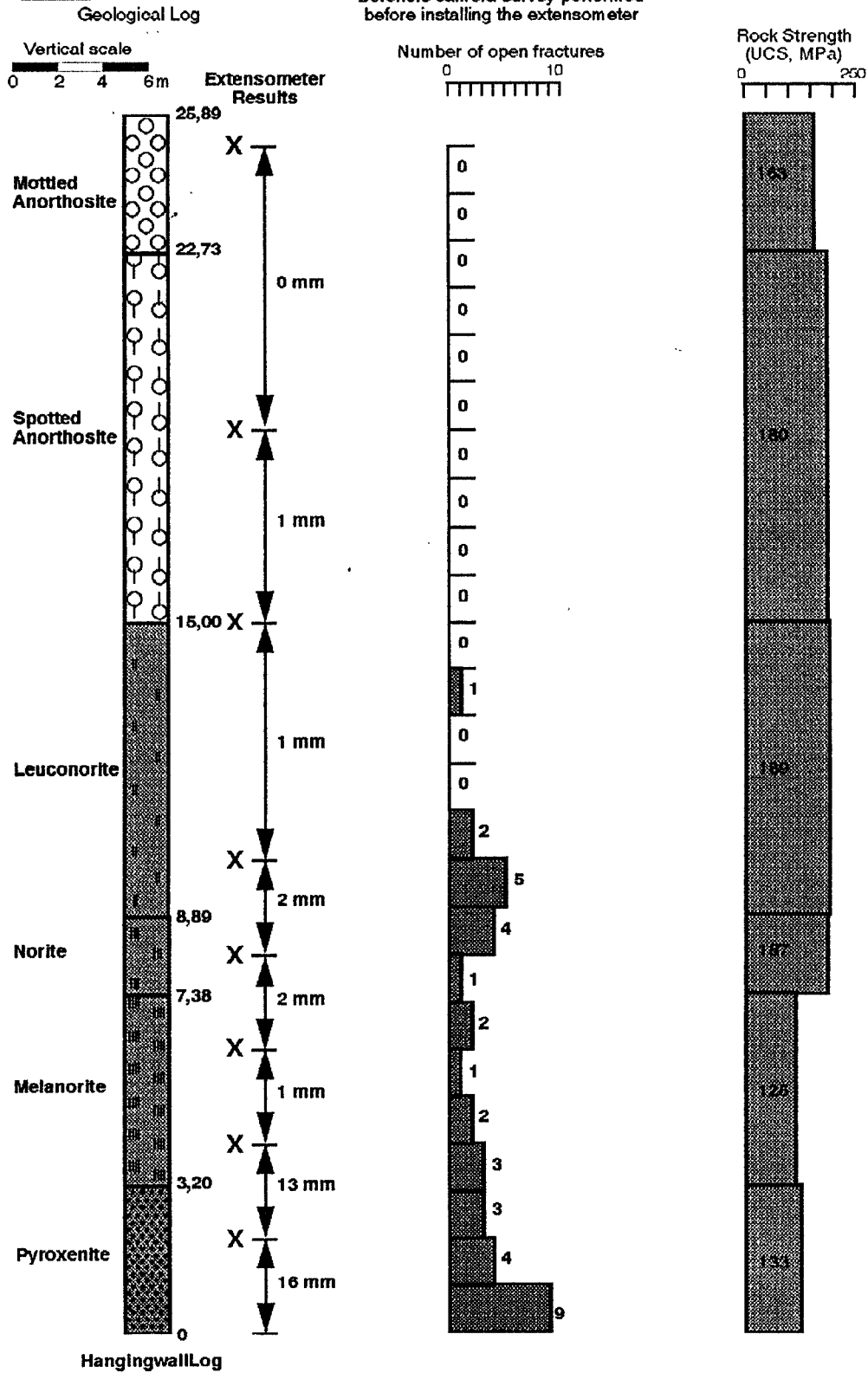
FIGURE A19

SURVEY 2

RUSTENBURG PLATINUM MINES- UNION SECTION

**Borehole between cross-cut and 22/8s/3S/1S Stope -
Drilled after Mining**

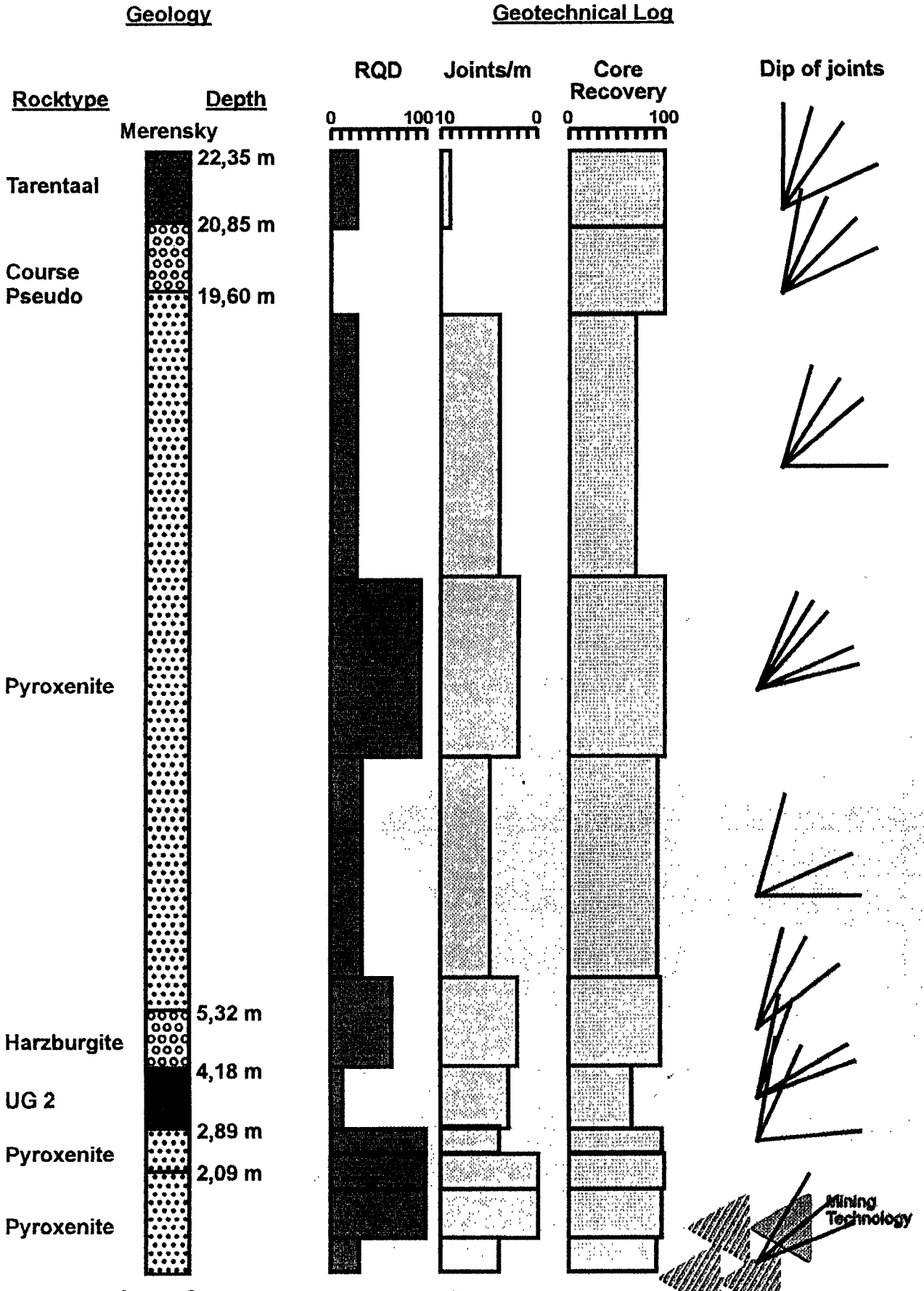| Geology		Borehole Camera Survey

Number of Open Joints/
Fractures per metre

Rocktype	Depth	0 5 10 15	
Merensky			
	22,35 m		5
Tarentaal			7
	20,85 m		6
Course Psuedo	19,60 m		12
			13
			8
			3
			4
			7
			6
			1
			0
Pyroxenite			2
			1
			0
			3
			1
	5,32 m		
Harzburgite	4,18 m		
UG 2			0
	2,89 m		1
Pyroxenite	2,09 m		
			2
Pyroxenite			4

15 mm open
3,3 m below

5 mm open
9,0 m below

Mining
Technology

CSIR

Cross-Cut
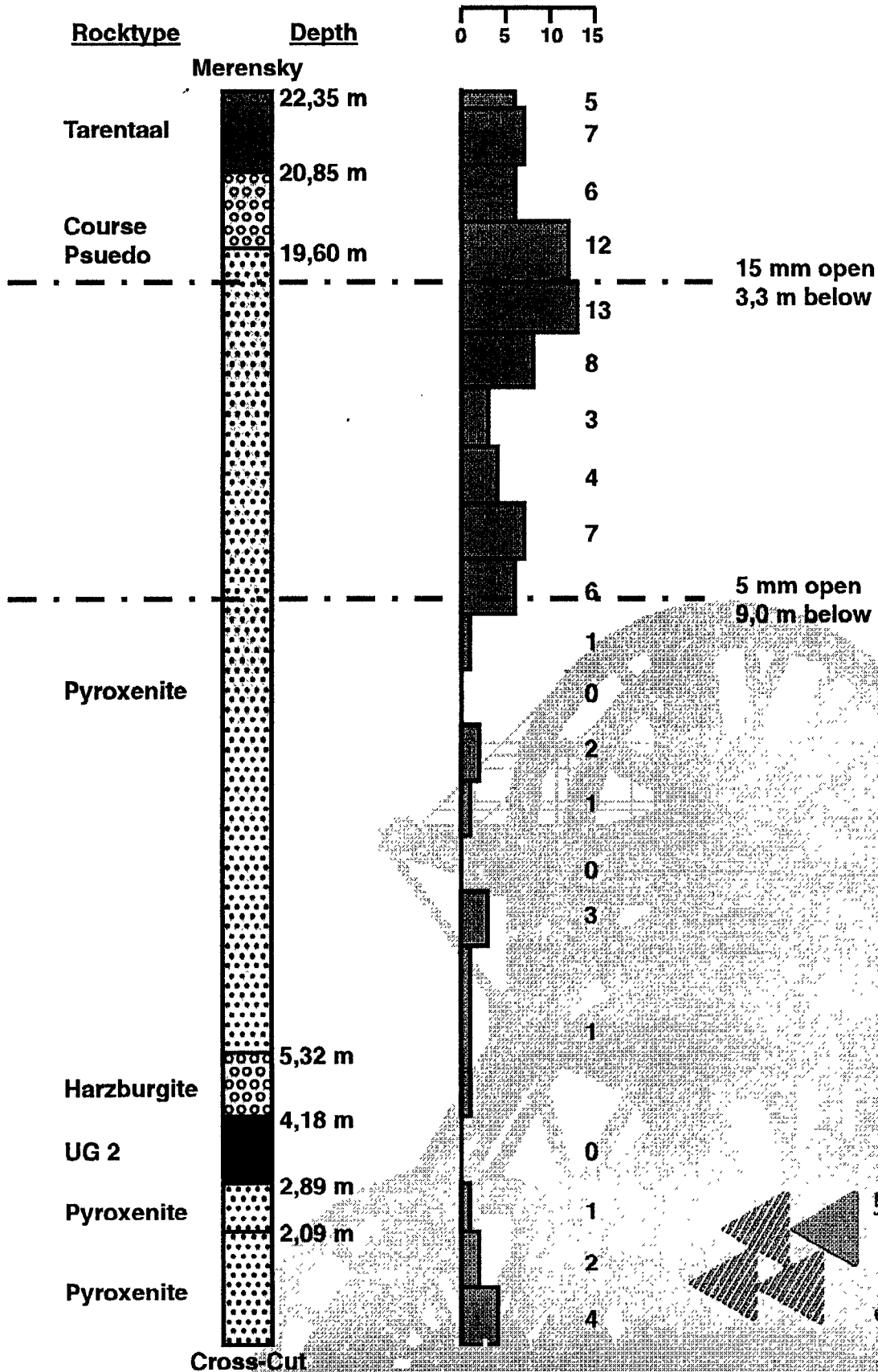
FIGURE A20

Photographs of hangingwall "fallouts" and footwall heave.
Figure A21

"Fallout" 1

"Fallout" 2

Footwall Heave

FIGURE A.31

Photographs of the core from the extensometer holes and F/W1.
Figures A22 - A28
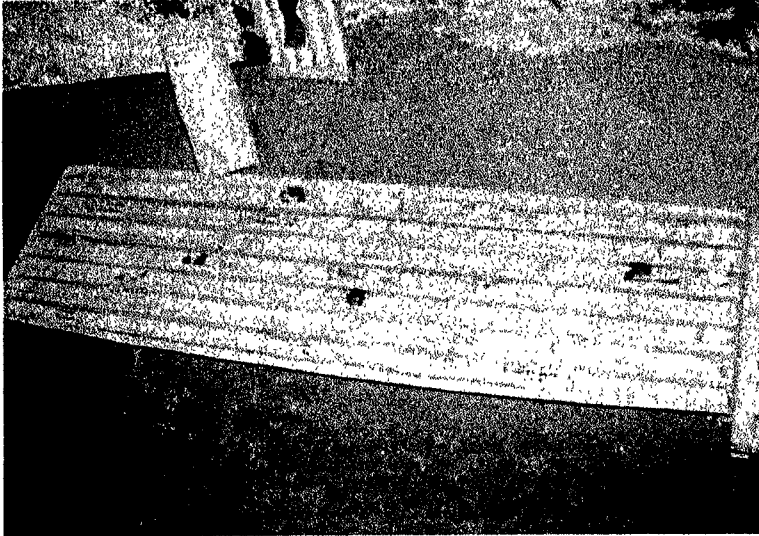
RPM - Union Section
22/8^S/Centre Gully
HOLE 1A
Tray 1
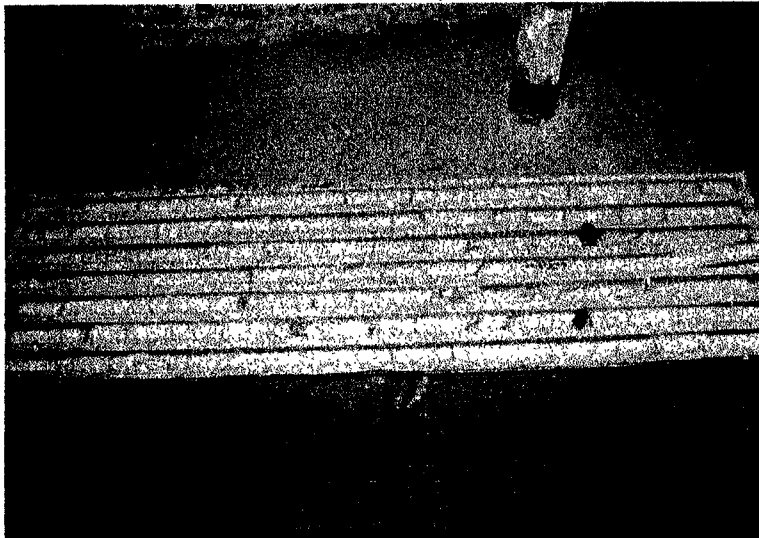
RPM - Union Section
22/8^S/Centre Gully
HOLE 1A
Tray 2
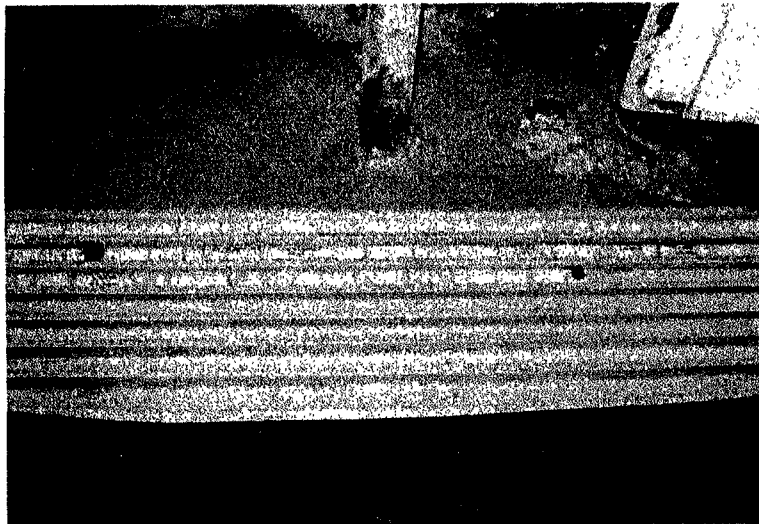
RPM - Union Section
22/8^S/Centre Gully
HOLE 1A
Tray 3

FIGURE A22
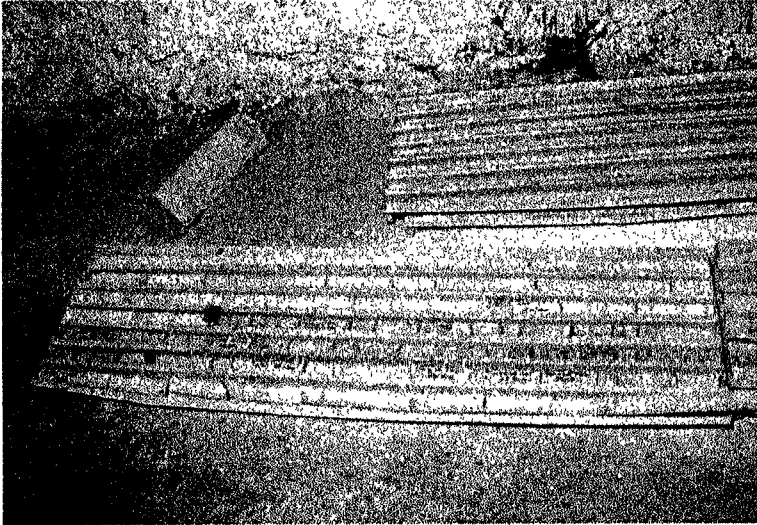
**RPM - Union Section
22/8^S/Centre Gully
HOLE 1A
Tray 3**
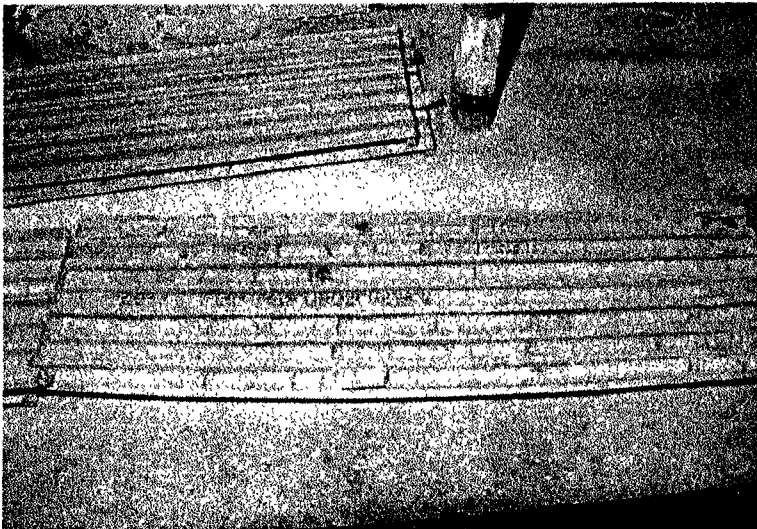
**RPM - Union Section
22/8^S/Centre Gully
HOLE 1A
Tray 4**
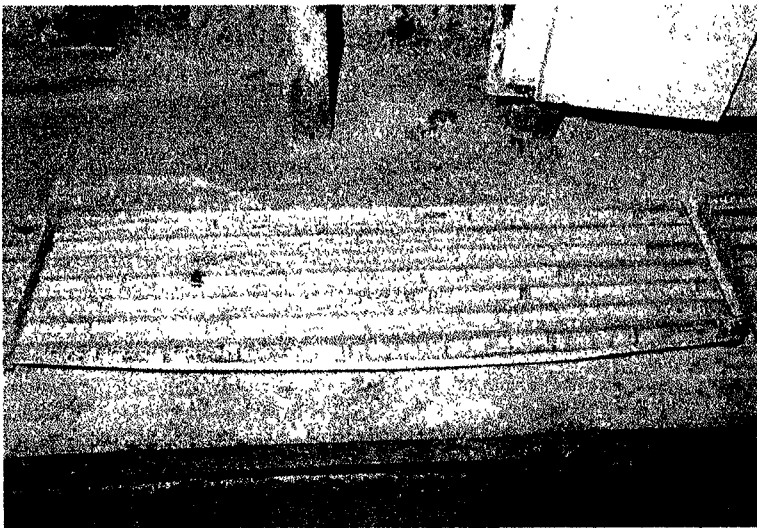
**RPM - Union Section
22/8^S/Centre Gully
HOLE 1A
Tray 5**

FIGURE A23
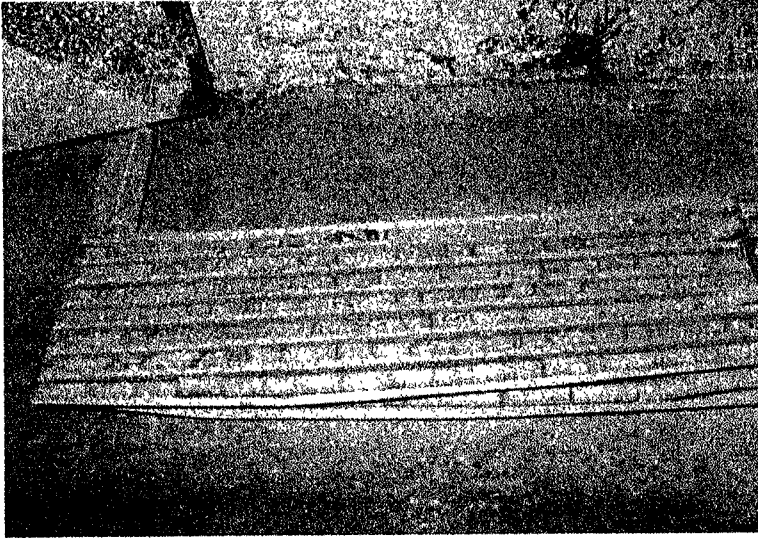
**RPM - Union Section
22/8^S/Centre Gully
HOLE 1B
Tray 1**
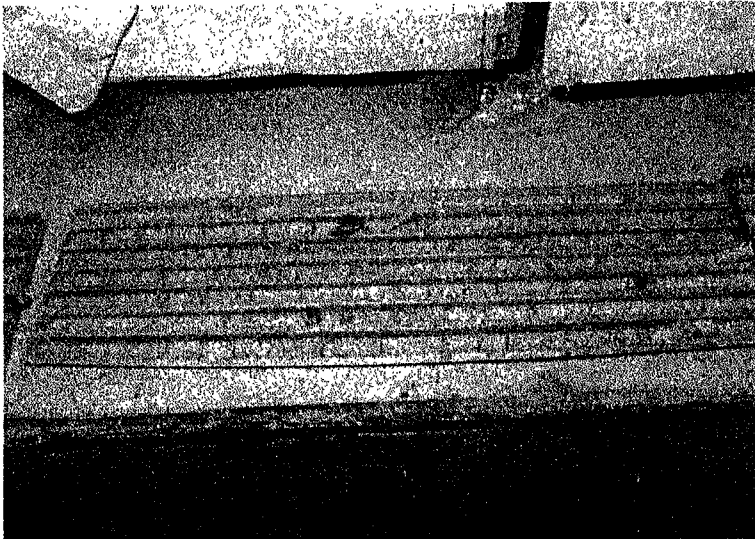
**RPM - Union Section
22/8^S/Centre Gully
HOLE 1B
Tray 2**
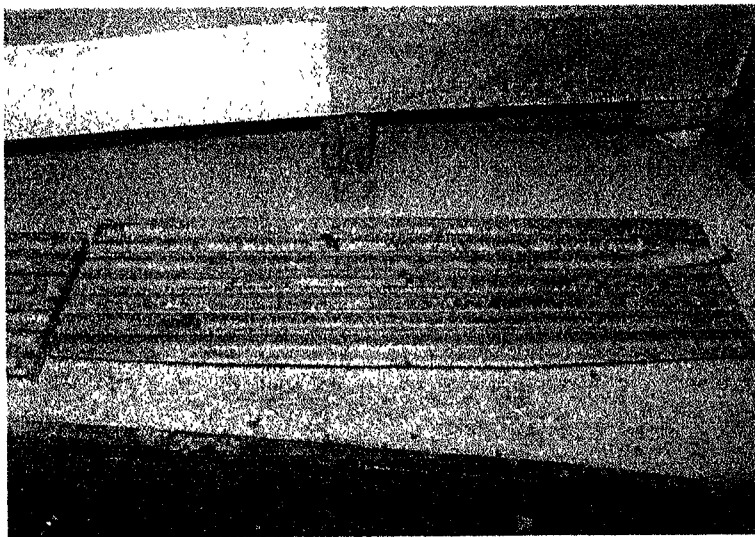
**RPM - Union Section
22/8^S/Centre Gully
HOLE 1B
Tray 3**

FIGURE A24

339

RPM - Union Section
22/8^S/3N
HOLE 2
Tray 1
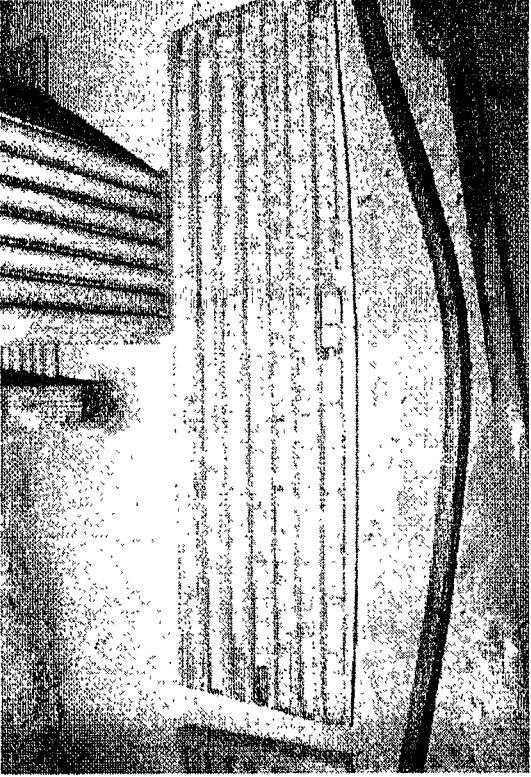
RPM - Union Section
22/8^S/3N
HOLE 2
Tray 2
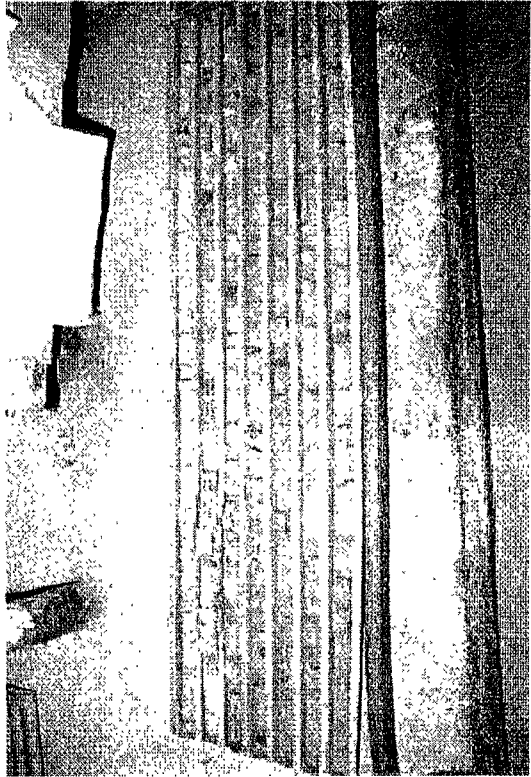
RPM - Union Section
22/8^S/3N
HOLE 2
Tray 3

RPM - Union Section
22/8^S/3N
HOLE 2
Tray 4

FIGURE A25
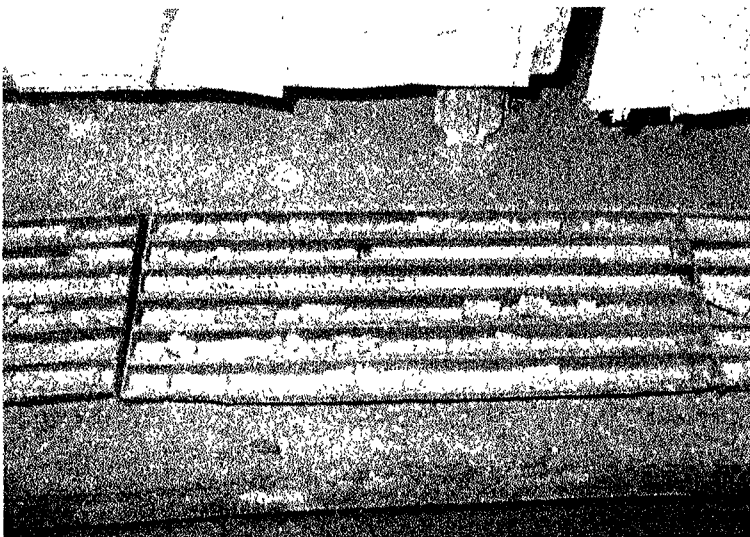
RPM - Union Section
22/8^S/3S
HOLE 3A
Tray 3
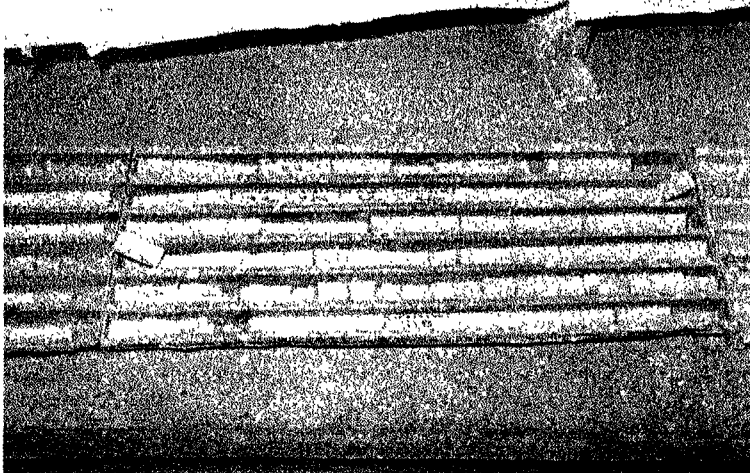
RPM - Union Section
22/8^S/3S
HOLE 3A
Tray 4

RPM - Union Section
22/8^S/3S
HOLE 3A
Tray 5

RPM - Union Section
22/8^S/3S
HOLE 3A
Tray 6
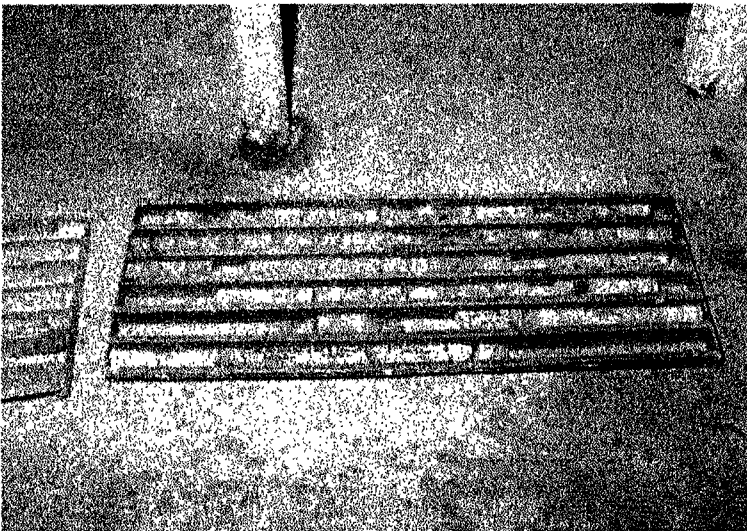
RPM - Union Section
22/8^S/3S
HOLE 3A
Tray 7

RPM - Union Section
22/8^S/3S
HOLE 3B
Tray 1
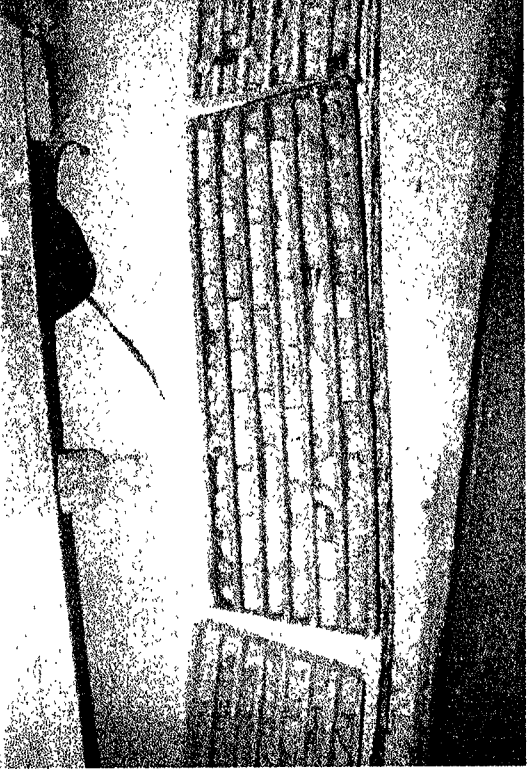
RPM - Union Section
22/8^S/3S
HOLE 3B
Tray 2
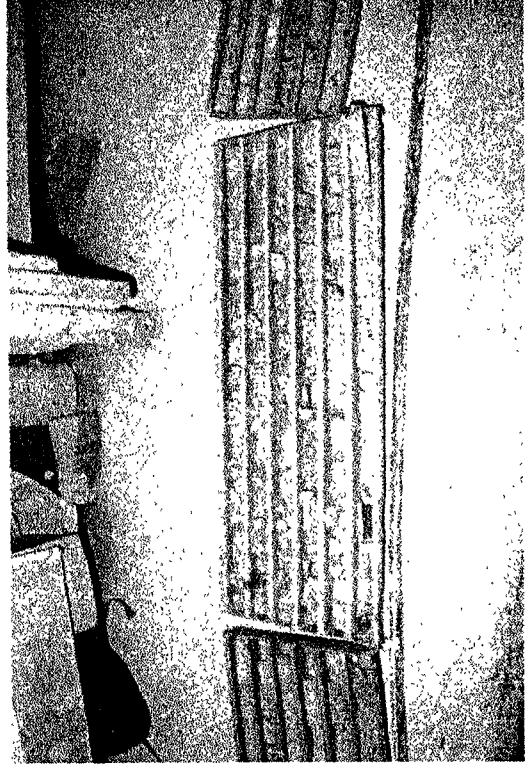
RPM - Union Section
22/8^S/3S
HOLE 3B
Tray 3
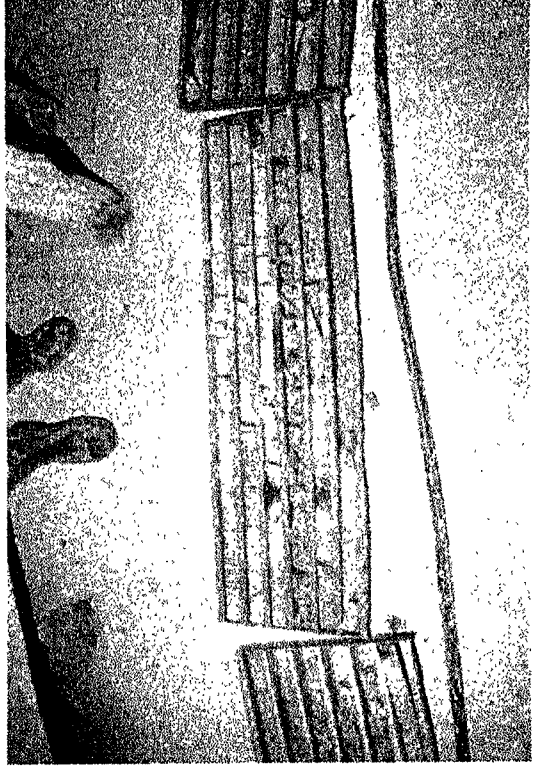
RPM - Union Section
22/8^S/3S
HOLE 3B
Tray 4

FIGURE A28

A model of movement around the stope based on extensometer and closure ride meter station results.
Figure A29

344

RPM - UNION SECTION - 22/8s/STOPE 1S & 1N
STOPE MOVEMENT

Hangingwall

Footwall

Mining Technology

CSIR

60 mm

71 mm

260-65 mm

248 mm

317 mm

80 mm

74 mm

18 mm

66 mm

65 mm
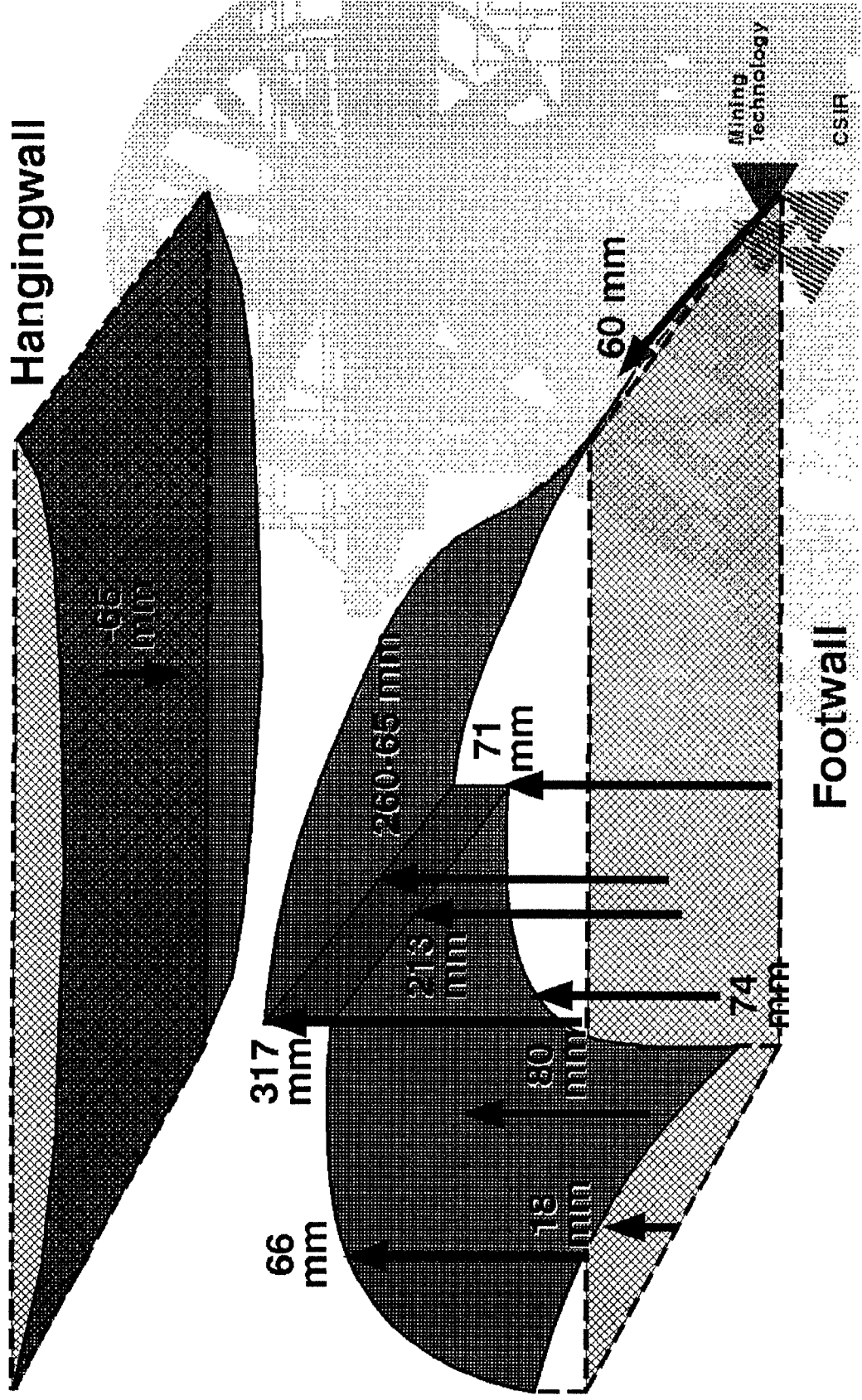
FIGURE A29

Appendix 2

GEOMECHANICAL TESTING PERFORMED ON VARIOUS HANGINGWALL AND FOOTWALL ROCKS FROM THE INSTRUMENTATION SITE AT RPM - UNION SECTION

INTRODUCTION

Uniaxial and triaxial compressive tests were performed on cores from boreholes in Cubbies 1,2 & 3 and borehole F/W1 to establish the geomechanical properties of the various lithological units in the hangingwall and footwall respectively.

Tensile Brazilian and uniaxial tensile tests were performed to determine the reason for the observed failure and loosening below 4.4 m in the hangingwall.

TEST PROCEDURE

Cylinders of 76.2 mm length and 25.4 mm diameter were used to perform the uniaxial and triaxial tests and discs of 12.7 mm length and 25.4 mm diameter for the brazilian tests. These tests were conducted individually in a stiff 2MN displacement controlled press at a displacement rate of 0.08 mm per minute. Failure took place in about 10 minutes in the case of the uniaxial tests, 30 to 45 minutes for the triaxial tests and about 3 minutes for the brazilians. The uniaxial tensile tests were performed under slightly different loading conditions at the Pretoria facility of the CSIR.

The uniaxial tests were performed by being deformed axially until failure took place. In the case of the triaxial tests, the samples were tested inside a pressure vessel and the lateral confinement was supplied by a fluid as follows:

     1) Initially the confinement was increased hydrostatically with the axial stress to a pre-determined confinement level (10 MPa, 20 MPa or 40 MPa).

     2) The confinement level was kept constant while the axial stress was increased until the sample failed.

The brazilian samples were recored, to enable the tensile stress to develop approximately parallel to the stratification. Unfortunately this resulted in small samples of 25.4 mm diameter and 12.7 mm length. Table 2 shows the results.

The uniaxial tensile tests were shaped in the form of a "dog bone" to ensure failure away from the ends. The dimensions of these samples were 35.1 mm at the ends and 29.6 mm at the centre. A summary of the results are shown in table 3.

Axial deformation and load were monitored during all the tests and volume change was monitored on the confinement tests. Poisson's Ratio was determined from the volume change measurements. Radial strain measurements were attempted on the uniaxial tensile tests however the strain gauges used for this purpose were not sensitive enough.

TABLE 1A

Sample No/	Borehole Depth	σ3 MPa	σ1 MPa	E Gpa	ν
Pyroxenite **(Bastard** **Reef)**					
UIA - 2	25,7	0	141	101,5	
UIA - 3	26,5	0	151	101,6	
UIA - 4	26,9	0	113	66,9	
UIA - 5	28,4	0	182	99,7	
UIA - 6	29,4	0	188	127,8	
UIA - 7	31,3	0	167	127,9	
UIA - 8	31,8	0	253	148,2	
UIA - 9	32,7	0	83*	61,6	
UIA - 10	33,2	0	186	113,7	
UIA - 11	35,3	0	121	100,9	
TAI - 2	35,7	10	240	126,7	0,17
TAI - 1	35,8	10	304	90,9	0,24
TAI - 3	28,0	20	343	118,2	0,18
TAI - 8	29,1	20	274	114,7	0,16
TAI - 7	28,9	40	514	94,3	0,23
TAI - 9	35,6	40	456	123,6	0,14
U3A - 10	28,6	0	128	75,3	
U3A - 15	35,5	0	188	113,8	
U3B - 1	27,8	0	80*	57,3	
U3B - 3	30,7	0	118	65,0	
U3B - 22	32,7	0	216	122,6	
U3B - 14	37,1	0	188	113,0	
U3B - 6	37,8	0	159	74,4	
T3B - 25	31,2	10	177	75,9	0,39
T3B - 24	30,8	20	312	107,3	0,20
T3B - 6	39,5	20	349	95,3	0,22
T3B - 7	31,1	40	419	109,8	0,19
Mean-S.D.			(15) 167-38	(25) 104-21	(10) 0,21-0,07
Pyroxenite **(Merensky)**					
U2 - 1	0,8	0	147	95,2	
U2 - 2	2,7	0	140	100,2	
U3A - 14	0,1	0	151	113,6	
U3A - 6	1,6	0	114	94,9	
U3A - 1	3,3	0	66*	59,1	
U3B - 7	0,8	0	113	90,7	
U3B - 24	1,8	0	83*	59,5	
T3B - 23	0,4	10	174	111,4	0,22
T3B - 9	0,5	20	239	116,4	0,19
T3B - 2	0,6	40	330	111,2	0,18
Mean-S.D.			(5) 133-16	(8) 104-9	(3) 0,20-0,02

* Failed on discontinuity - not included in averages.

TABLE 1B

Sample No/	Borehole Depth	σ3 Mpa	σ1 MPa	E Gpa	ν
Leuconorite					
U3A -4	7,8	0	100*	39,6	
U2 -5	10,3	0	180	78,3	
U3A - 9	13,8	0	192	84,0	
U3B - 17	11,5	0	87*	65,5	
U3B - 8	14,4	0	196	74,6	
T3B - 11	14,0	10	301	78,9	0,25
T3B - 13	14,1	20	391	82,1	0,21
T3B - 19	14,2	40	534	90,0	0,22
Mean-S.D.			(3) 189 - 7	(6) 81-5	(13) 0,23-0,02

Sample No /	Borehole Depth	σ3 MPa	σ1 MPa	E GPa	ν
Melanorite					
U2 - 3	4,0	0	131	81,1	
U3A - 3	5,7	0	112	52,9	
U3B - 5	3,4	0	75*	52,5	
U3B - 16	4,4	0	112	52,4	
U3B - 11	5,0	0	148	66,7	
U3B - 21	6,4	0	123	53,6	
U3B - 18	39,9	0	197	92,5	
T3B - 8	39,6	10	291	86,7	0,25
T3B - 22	4,6	10	224	70,1	0,23
T3B - 21	4,8	20	302	77,6	0,25
T3B - 20	4,7	40	420	84,2	0,21
T3B - 3	39,8	40	496	99,7	0,19
Mean-S.D			(6) 137-29	(11) 74-16	(5) 0,23-0,02

Sample No /	Borehole Depth	σ3	σ1	E	ν
Norite					
UIA - 12	44,0	0	206	102,6	
U2 - 4	7,0	0	175	93,2	
U3A - 5	9,5	0	199	101,0	
U3B - 9	44,7	0	250	89,0	
U3B - 4	45,4	0	215	95,8	
Mean-S.D.			(5) 209-24	(5) 96-5	

* Failed on discontinuity - not included in averages.

TABLE 1C

Laboratory Test Results. 22/8 stope Richard shaft

Sample No/	Borehole Depth	σ3 MPa	σ1 MPa	E Gpa	ν
Anorthosite (mottled)					
UI A -1	24,6	0	161	53,4	
UI A -13	46,9	0	168 *	78,4	
UI A - 14	49,5	0	243	90,6	
TAI - 6	49,1	10	252	115,5	0,13
TAI - 4	49,2	20	156 *	89,7	0,20
TAI - 5	49,4	40	462	121,1	0,16
U2 - 8	22,9	0	219	77,0	
U2 - 9	23,1	0	206	75,1	
U3A - 8	23,8	0	132	53,6	
U3A - 11	25,2	0	167	85,6	
U3B - 12	23,6	0	225	69,2	
U3B - 13	24,6	0	112	41,8	
U3B - 2	49,0	0	240	82,3	
U3B - 20	49,4	0	241	89,0	
U3B - 10	49,9	0	210	79,9	
T3B - 1	24,8	20	214 *	57,4	0,29
T3B - 4	25,1	40	311 ·	61,5	0,23
T3B - 5	50,2	10	297 ·	83,9	0,22
T3B - 16	50,7	10	353	80,6	0,24
T3B - 12	50,9	20	431	85,6	0,20
T3B - 15	50,6	40	569	89,3	0,20
Mean-S.D.			(11) 196-44	(18) 80-19	(7) 0,20-0,04
(Anorthosite (spotted)					
U2 - 6	14,2	0	175	71,9	
U2 - 7	18,5	0	149	58,9	
U3A - 2	17,0	0	198	74,5	
U3A - 7	20,1	0	167	81,0	
U3A - 12	22,6	0	173	61,1	
U3A - 13	22,1	0	127*	75,4	
U3B - 19	18,3	0	195	75,8	
U3B - 15	19,5	0	197	75,2	
U3B - 23	22,1	0	189	81,2	
T3B - 10	19,2	10	312	79,4	0,23
T3B - 14	22,0	10	195	55,7	0,25
T3B - 17	19,3	20	395	86,5	
T3B - 18	19,4	40	540	89,4	0,21
Mean-S.D.			(8) 180-16	(12) 74-12	(3) 0,23-0,02

RESULTS

Hangingwall

In the case of the uniaxial and triaxial compression tests specimens of 76.2 mm length and 25.4 mm diameter were used. The results of these tests have been summarised in table 1. Strength parameters derived from a straight line fit regression analysis, relating the axial stress at failure to the confining stress, are shown in figures 1 to 5. Stress-strain curves for all tests performed in the hangingwall rocks are in appendix A.

Table 2

BRAZILIAN TEST RESULTS

LOCATION: RPM - Union Section - 22/8s/centre gully, hole Cubby 1b.

Depth into Hangingwall (m)	Tensile Strength (MPa)	Rock Type
0.34	9.66	Pyroxenite
0.36	11.90 *	Pyroxenite
1.37	4.98	Pyroxenite
1.39	4.40	Pyroxenite
2.22	6.26	Pyroxenite
2.24	11.30 *	Pyroxenite
3.41	9.47	Melanorite
3.43	11.10 *	Melanorite
5.04	6.99	Melanorite
5.06	8.25	Melanorite
6.15	4.95	Norite
6.17	5.61	Norite
7.41	3.82	Norite
7.43	3.82	Norite
9.66	8.32	Leuconorite
9.68	10.10	Leuconorite

* Samples did not fail correctly.

TABLE 3A

TABLE : 1710-MC-1

RESULTS OF POST TEST MOISTURE CONTENT DETERMINATIONS

▲ CSIR

95-12-05

11:34

G:\GM\1710\1710-MC1.WQ1

EG 165.004

Sample Location : Rustenburg Platinum Mine, Union Section, 22/8s/Centre Gully, Hole 1B

SPECIMEN PARTICULARS			SPECIMEN DIMENSIONS		MOISTURE CONTENT DETERMINATION			
CSIR Specimen No 1710-	Rock Type	Depth (m)	Dia. at Failure (mm)	Height (mm)	Mass before drying (g)	Mass Oven dry 105 °C (g)	Moisture Content (%)	Notes
DTM-01	Pyroxenite	0.75	29.4	119.2	298.54	298.28	0.087	
DTM-02	Pyroxenite	2.70	29.9	119.4	305.07	304.82	0.082	
DTM-03	Melanorite	3.70	29.6	119.1	287.59	287.35	0.084	
DTM-04	Melanorite	5.55	35.1	119.4	269.09	268.80	0.108	
DTM-05	Leuconorite	8.55	26.0	93.4	150.67	150.48	0.126	

Revision 1

TABLE 3B

TABLE : 1710-DT1

RESULTS OF DIRECT TENSILE STRENGTH TESTS WITH DEFORMABILITY MEASUREMENTS

▲ CSIR

G:\GM\1710\1710-DT1.WQ1
EG 165.004

95-12-05
11:43

Sample Location : Rustenburg Platinum Mine, Union Section, 22/8s/Centre Gully, Hole 1B

SPECIMEN PARTICULARS			SPECIMEN DIMENSIONS				SPECIMEN TEST RESULTS			
CSIR Specimen No 1710 -	Rock Type	Depth (m)	Dia. at Failure (mm)	Height (mm)	Height to Dia Ratio	Density (kg/m^3)	Failure Load (kN)	Strength (UCS) (MPa)	Deformation Modulus @ tan 50 %	Notes
DTM-01	Pyroxenite	0.75	29.4	119.2	4.1	3218	3.02	4.45	94.6	
DTM-02	Pyroxenite	2.70	29.9	119.4	4.0	3231	6.24	8.89	132.3	
DTM-03	Melanorite	3.70	29.6	119.1	4.0	3140	3.20	4.66	30.0	
DTM-04	Melanorite	5.55	35.1	119.4	3.4	3026	3.16	3.27	30.6	1 & 3
DTM-04a	Melanorite	5.55	35.1	119.4		3026	2.08	2.15		1 & 2
DTM-04b	Melanorite	5.55	35.1	119.4		3026	2.27	2.35		1 & 2
DTM-05	Leuconorite	8.55	26.0	93.4	3.6	2890	3.34	6.30	40.2	

Revision 2

Specimens were machined to a "dog-bone" shape.

Notes :   1, 2 and 3 refer to specimen no 1710-DTM-04, -04a, -04b.

1. Failure in thicker part of specimen, close to one end: Dark bands; possibly igneous layering.
2. Retest after specimen was cemented together again.
3. At the minimum cross-sectional area (Dia=29.5) the equivalent stress was 4.63 MPa.

Footwall

No stress-strain curves were provided with the results but the average uniaxial strengths and regression analyses are shown below. Strength parameters derived from a straight line fit regression analysis, relating the axial stress at failure to the confining stress, are shown in figures 7 and 8 for the Pyroxenite below and above the UG2.

Depth into Footwall (m)	Uniaxial Compressive Strength (MPa)	Rock Type
0 to 1.5	218	Tarentaal
2.75 to 17.03	167	Pyroxenite
17.03 to 18.17	Approx. 170	Harzburgite
18.17 to 19.46	38	UG2
19.46 to 20.26	101	Upper Pyroxenite
20.26 to 22.35	187	Lower Pyroxenite

The core of the Course Pseudo was very broken and no tests were possible in this zone..

DISCUSSION

Hangingwall

Table 1 averages all tests performed on a particular rock type, some from a sequence below the Bastard Reef and some above. These results do not match averages taken from individual lithological units such as the uniaxial results displayed in Appendix 6, however it was necessary to mix lithological units to provide a good statistical analysis on a particular rock type. The true uniaxial results for each lithological unit are displayed in Appendix 6.

Strengths of the rocks in the immediate hangingwall were relatively weak, the Pyroxenite and Melanorite appearing to have a similar compressive strength. Above this zone was a considerably stronger Norite. This result was confirmed both by compressive and tensile testing. Physical observations revealed that the top of the failed or loosened rock was close to the point indicated to be the change from Melanorite to Norite in the hole Ext1, located in Cubby 1.

One of the uniaxial tensile tests, located at 5.55 m, failed on a unusually high density of dark minerals which formed an almost horizontal lamina. Even although the sample had been shaped in the form of a "dog bone", failure took place in the wider zone near one of the endpieces. The stress at the centre of the "dog-bone" was similar to other tests at failure, however dividing the result by the surface area where failure took place provided a very low stress. The sample was glued together and the test was repeated three times with the same results see table 2. Although this specimen was located higher than the observed upper point of failure, the hole was different to the one used for the observation and in this hole the test was located near the top of the Melanorite zone.

Since the length of the brazilian tests was smaller than ten times the largest Crystal, the results were unreliable and therefore not considered in the above discussion.

Footwall

The uniaxial compressive tests performed in the immediate footwall were stronger than the immediate hangingwall, however no tests were performed in the Course Pseudo zone because the core pieces were too small. It was also in this zone where the greatest number of open discontinuities were observed. One test located just below the Course Pseudo zone failed at a very low value (99 MPa). Unfortunately this test was influenced by a discontinuity.

General observations

The following observations were made during testing:

1) Generally the samples failed in a more controlled manner than tests performed on the Witwatersrand gold mines, even although the Young's Moduli were similar.

2) High degree of non-linear, plastic behaviour observed both at the beginning of the test and above the yield point. This was particularly noticeable in the triaxial tests.

3) An increase in confinement appears to have caused a increase in the Young's Modulus and a decrease in Poisson's Ratio. This observation has been confirmed by other tests performed on Bushveld Igneous rocks.

4) It was not possible to measure radial strain on the uniaxial tensile tests even although strain-gauges were used. The radial strains appear to have been very small.

CONCLUSIONS

The results of the testing is summarised in the table below:

Rock Type	Calculated Uniaxial Compres. Strength (MPa)	Average Uniaxial Compres. Strength (MPa)	Cohesion at Failure (MPa)	Average Young's Modulus (GPa)	Average Poisson's Ratio	Kc
Hanging						
Bastard	167	167	30.6	104	0.21	7.45
Mottled Anorthosite	196	196	40.2	80	0.20	5.96
Spotted Anorthosite	179	180	29.5	74	0.23	9.20
Leuconorite	202	189	34.3	81	0.23	8.62
Norite		209		96		
Melanorite	145	137	25.6	74	0.23	8.01
Merensky	132	133	29.7	104	0.20	4.79
Footwall						
Tarentaal		218				
Pyroxenite 2.75 m to 17.03 m	167	167	34.8			5.74
Harzburgite		Approx. 170				
UG2		38				
Upper Pyroxenite		101				
Lower Pyroxenite	187	187	50.2			2.59

Hangingwall

It is unclear whether the limiting factor for the failure zone was the change in rock strength or the presents of unusual bands or "laminae". However in Stope 3 & 4 it is evident that the zone extends up to the base of the Norite.

Footwall

The fact that no testing was possible in the Course Pseudo suggests that the rockmass was weaker at this point than for the rest of the hole. This could mean that the intact strength was weak or there was an unusual high intensity of adversely orientated discontinuities or both. It is possible that pillar punching was facilitated by adversely orientated discontinuities rather than intact compressive strength. If this is true then areas where adversely orientated discontinuities do not exist in the footwall, could result in pillar failure or hangingwall instabilities.

Pillars

Observations made during testing suggest that pillars should be less likely to fail violently and should deform more before failure, than for similar mining conditions on the gold mines.

Stiffness of a pillar could be increased by applying confinement.

Straight line regression analyses for the various hangingwall rock types.

357

R.P.M. - UNION SECTION

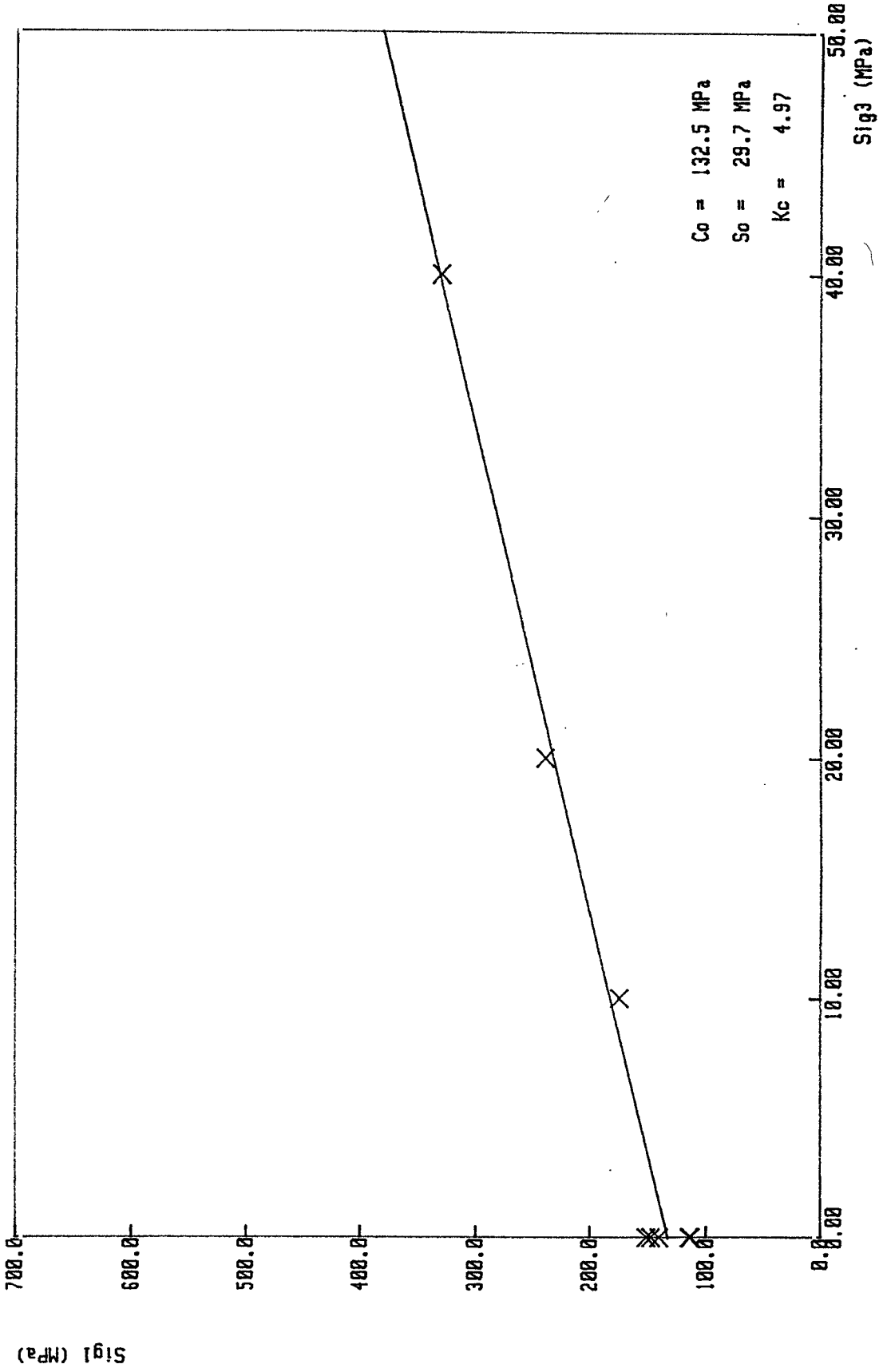ANGLE OF INT.FRIC. = 41.78   COEF. = .891
Line is Y = 132 + 4.97X   Fit : 98.1%

Co = 132.5 MPa
So = 29.7 MPa
Kc = 4.97

Sig1 (MPa)
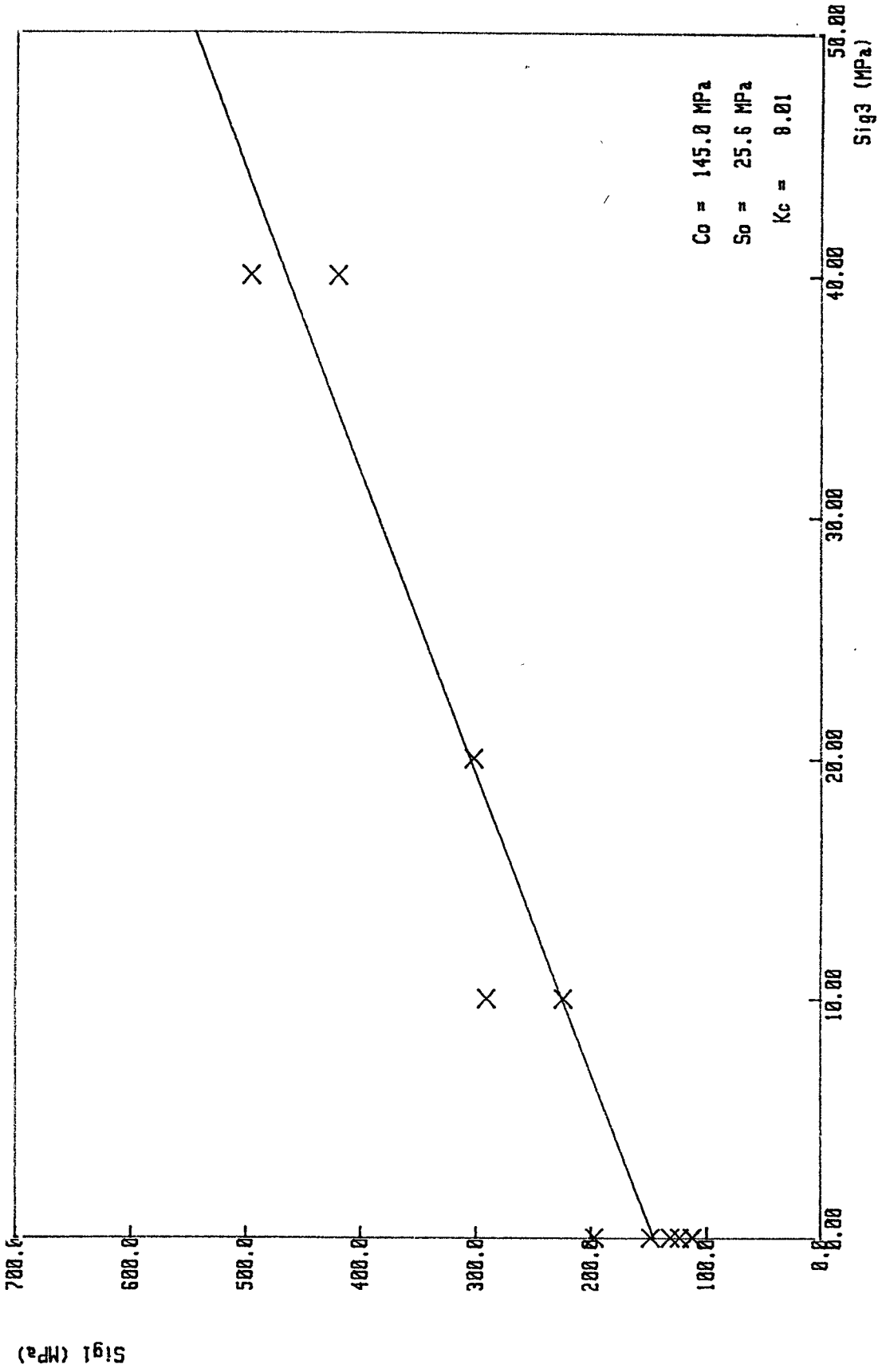
Sig3 (MPa)

File PYR MER on 9/12/95

FIGURE 1 - PYROXENITE (MERENSKY)

FIGURE 2 - MELANORITE

R.P.M. - UNION SECTION

ANGLE OF INT.FRIC. = 52.38   COEF. = 1.297
Line is Y = 202 + 8.62X   Fit : 99.4%

Co = 201.6 MPa
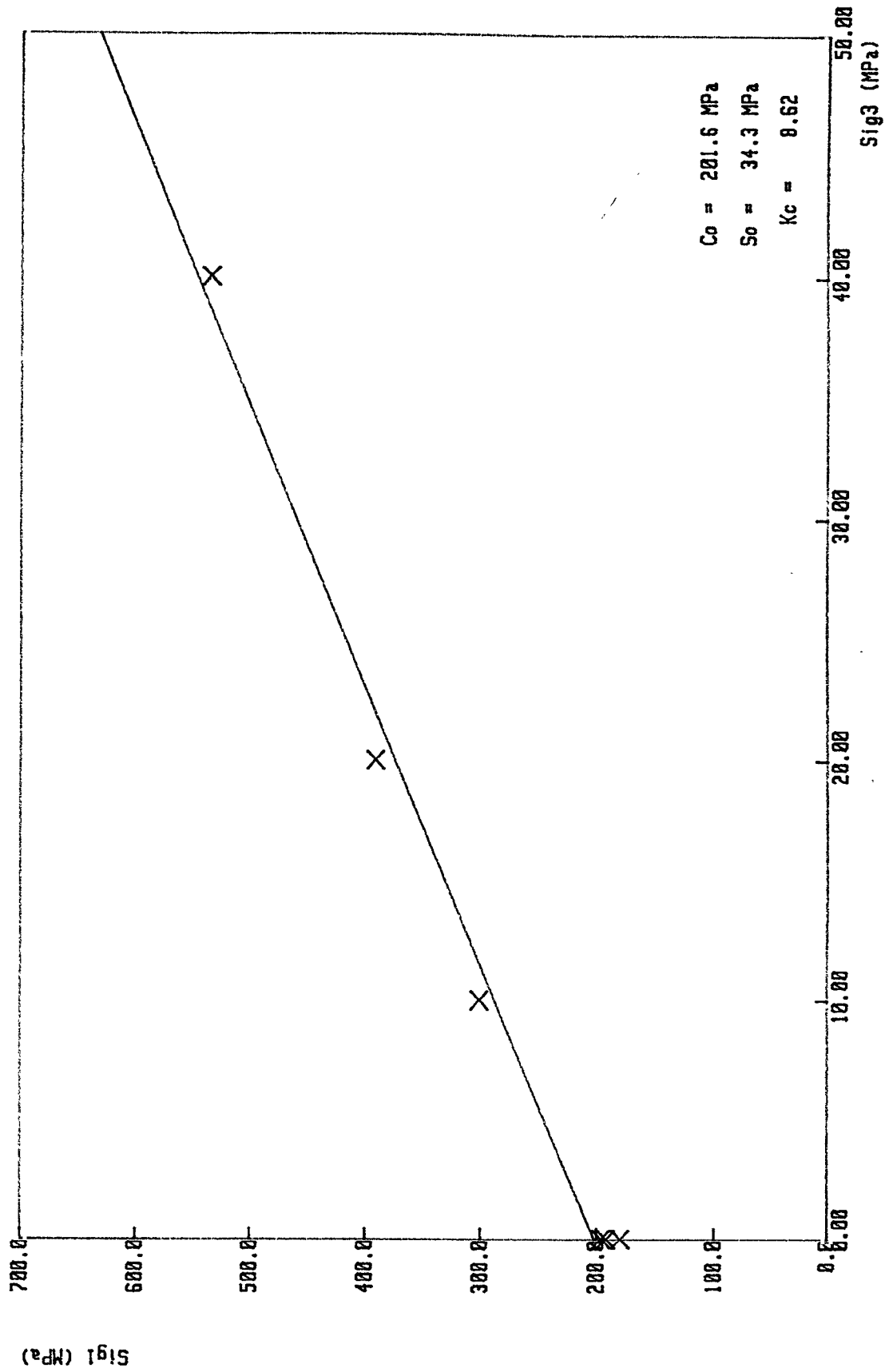So = 34.3 MPa
Kc = 8.62

Sig3 (MPa)

Sig1 (MPa)

FIGURE 3 - LEUCONORITE

File LEUC3 on 8/12/95

R.P.M. - UNION SECTION

ANGLE OF INT.FRIC. = 53.51 COEF. = 1.352

Line is Y = 179 + 9.2X   Fit : 96.4%

C_o = 179.1 MPa

S_o = 29.5 MPa

K_c = 9.20

Sig3 (MPa)

Sig1 (MPa)

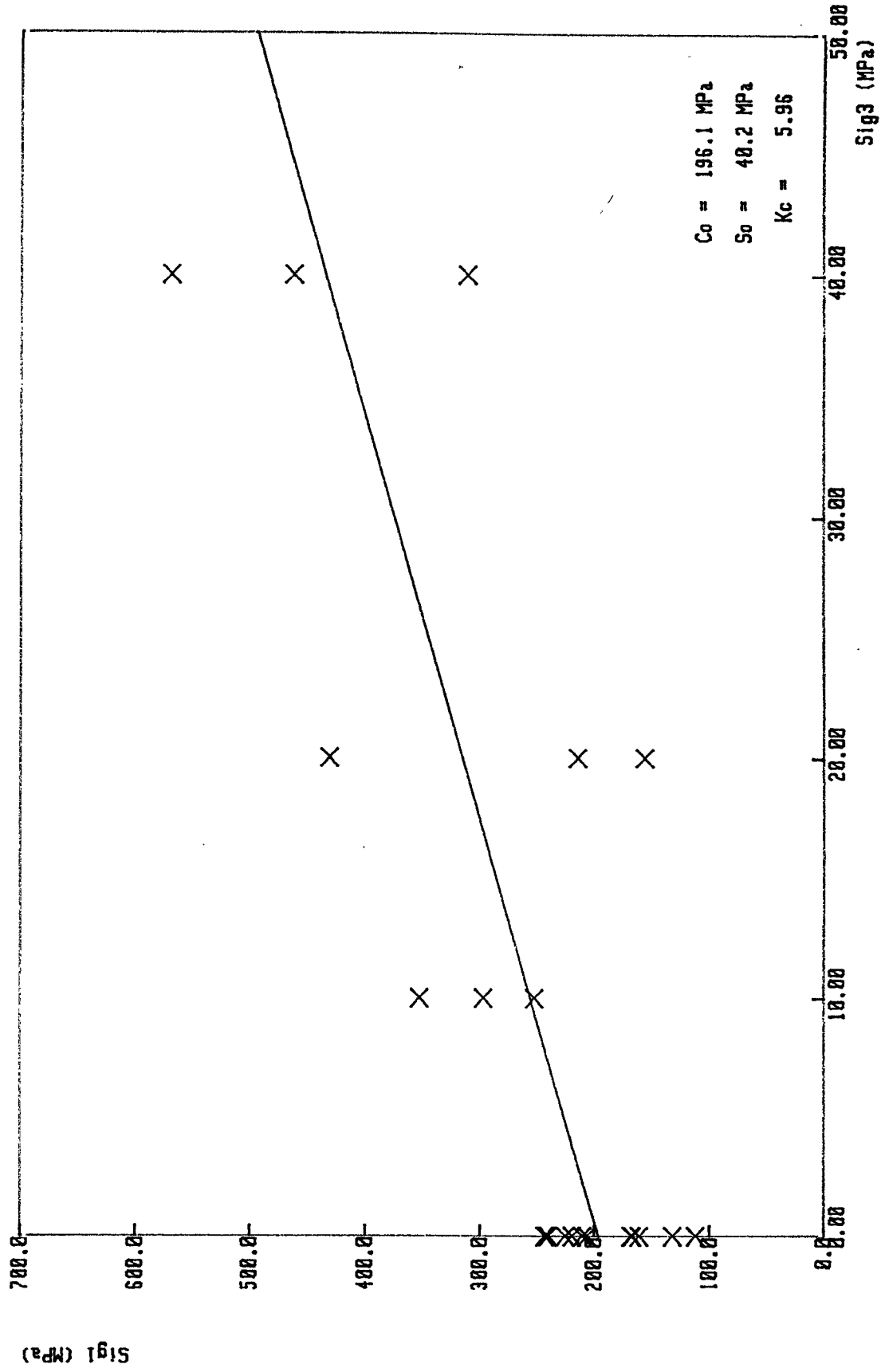FIGURE 4 - ANORTHOSITE (SPOTTED)

File SPOTM4 on 8/12/85
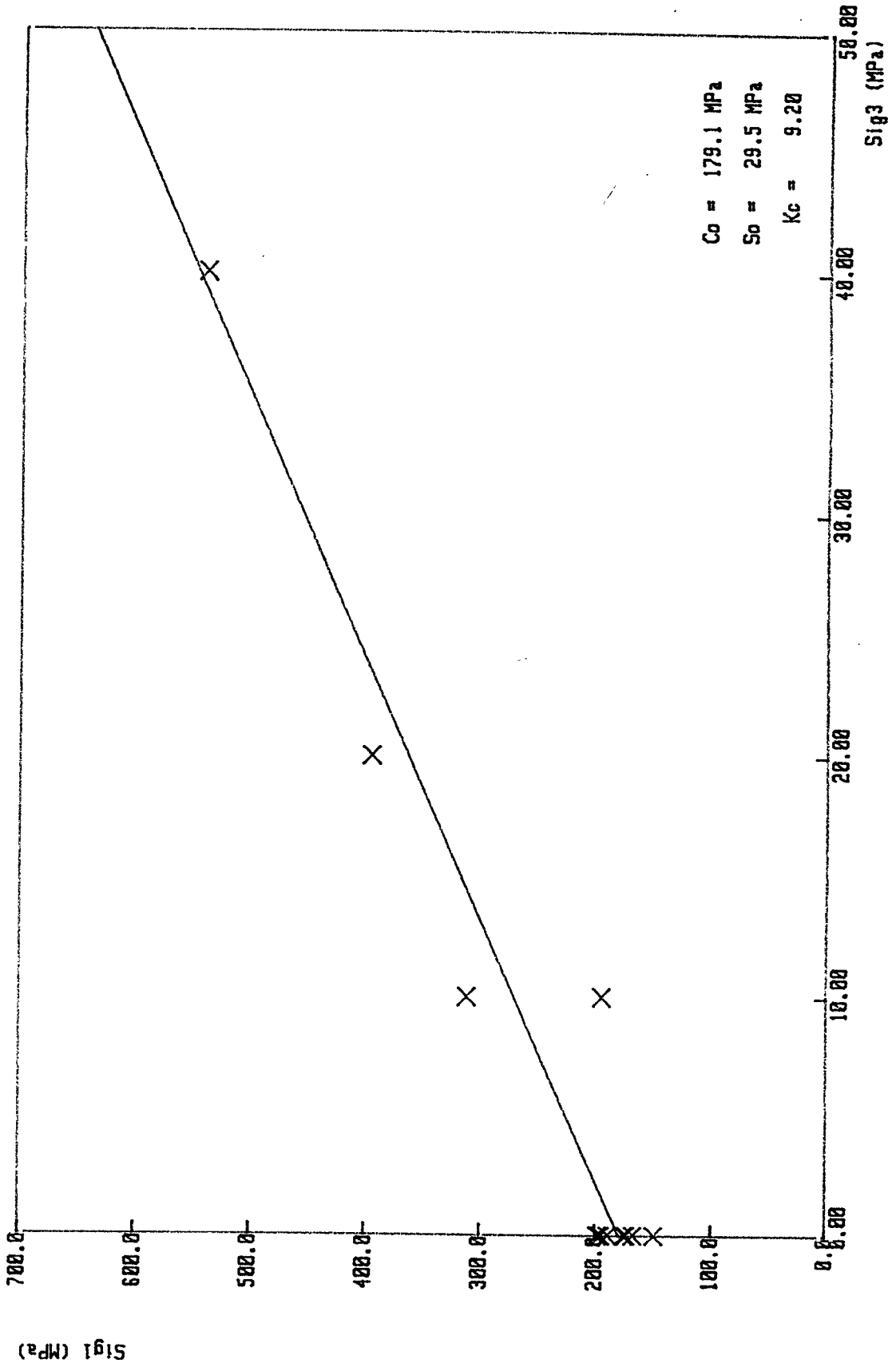
FIGURE 5 - ANORTHOSITE (MOTTLED)

R.P.M. - UNION SECTION

ANGLE OF INT.FRIC. = 49.77   COEF. = 1.182

Line is Y = 167 + 7.45X   Fit : 93.3%
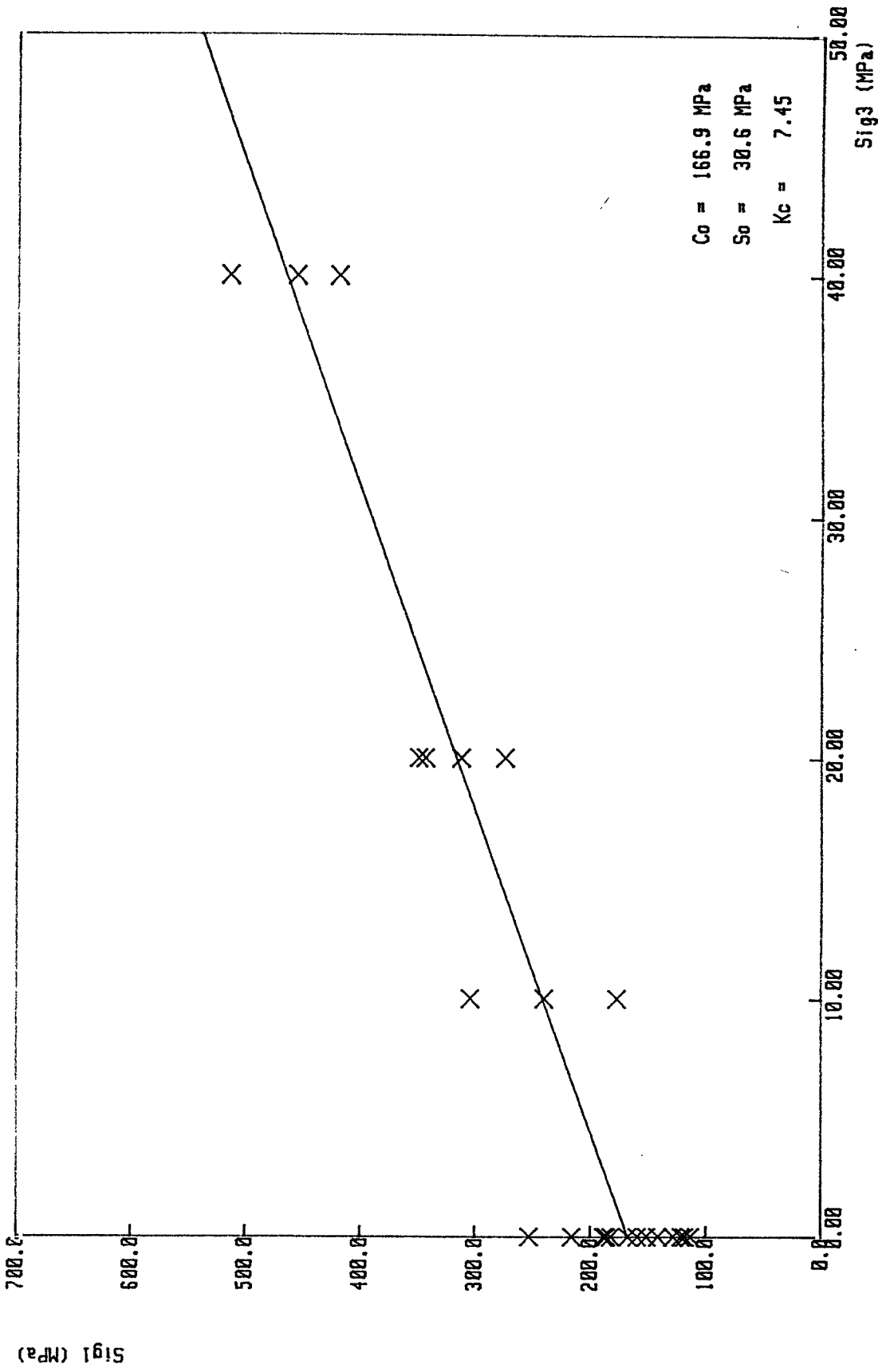

Co = 166.9 MPa

So = 30.6 MPa

Kc = 7.45

Sig3 (MPa)

Sig1 (MPa)

FIGURE 6 - PYROXENITE (BASTARD)

File PYR.DRS on 8/12/93

Straight line regression analyses for the various footwall rock types.

364

R.P.M. - UNION SECTION

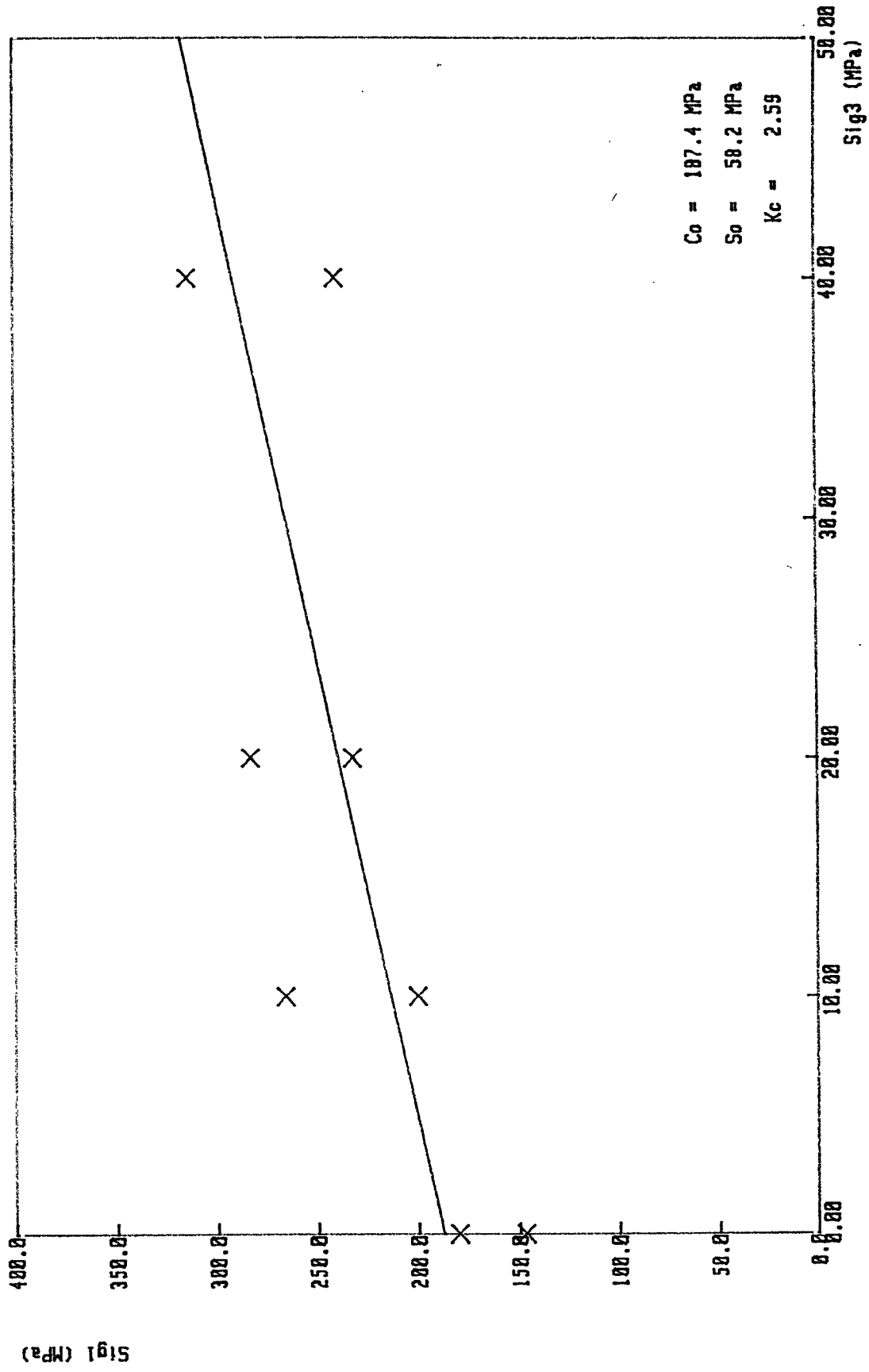ANGLE OF INT.FRIC. = 26.38   COEF. = .494
Line is Y = 187 + 2.59X   Fit : 73.9%

Co = 187.4 MPa
So = 58.2 MPa
Kc = 2.59

Sig3 (MPa)

Sig1 (MPa)

FIGURE 7 - PYROXENITE - 0 to 2.09 m

File PYROXE1 on 8/13/85

R.P.M. - UNION SECTION

ANGLE OF INT.FRIC. = 44.70   COEF. = .990

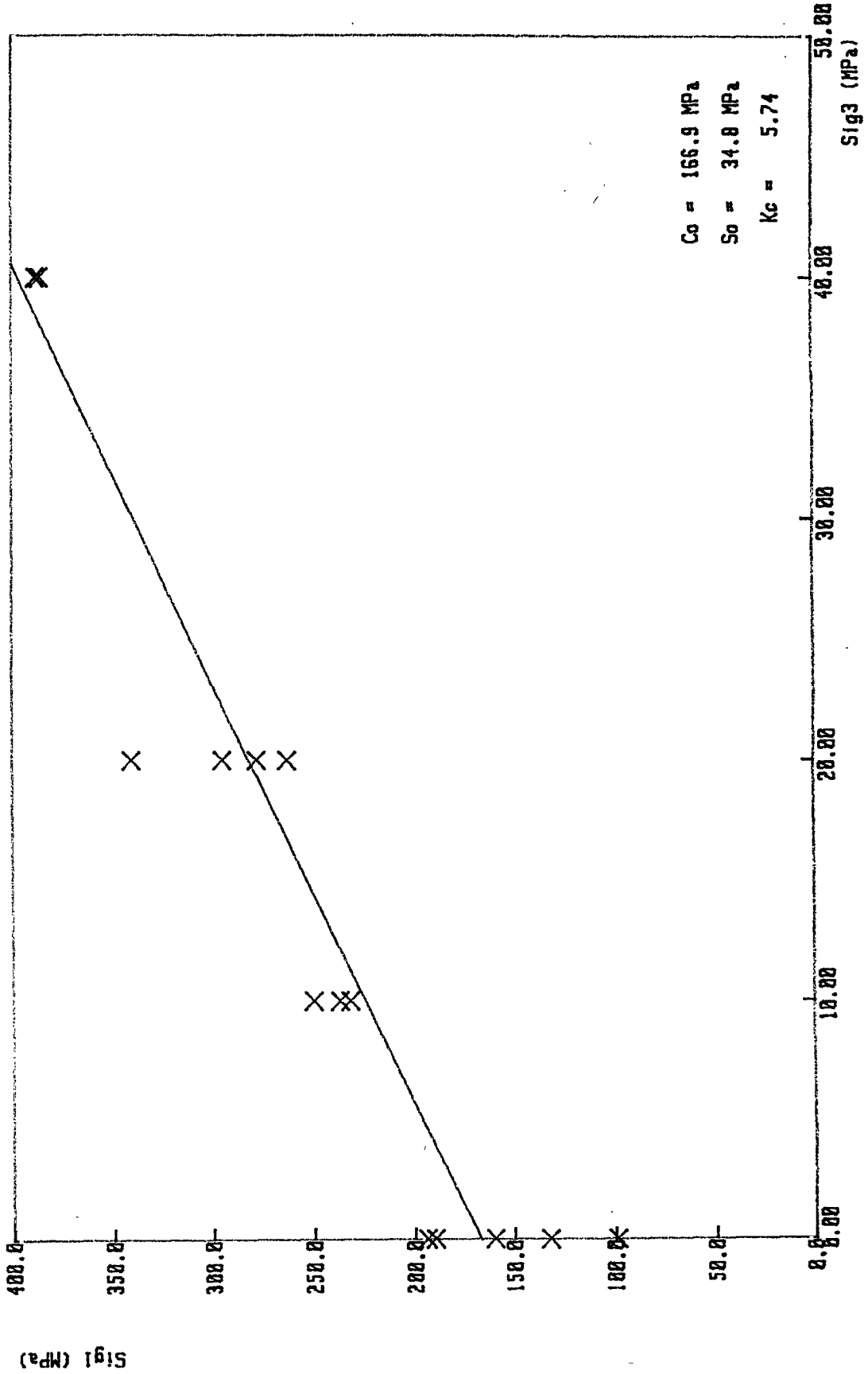Line is Y = 167 + 5.74X   Fit : 95.3%

Co = 166.9 MPa
So = 34.8 MPa
Kc = 5.74

Sig3 (MPa)

Sig1 (MPa)

FIGURE 8 - PYROXENITE - 5.32 to 19.6 m

File PYR4C3 on 9/12/95